

**A Biophysical and Biochemical Approach to Understanding the Interplay between
Quaternary Structure and Function of Human Calprotectin**

by

Jules Rabie Stephan

B.S. Biological Chemistry
The University of Chicago, 2013

Submitted to the Department of Chemistry in Partial Fulfillment of the Requirements of
the Degree of

DOCTOR OF PHILOSOPHY IN BIOLOGICAL CHEMISTRY

at the
Massachusetts Institute of Technology

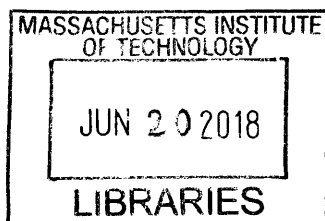
June 2018

©Massachusetts Institute of Technology, 2018
All Rights Reserved

Signature of Author: **Signature redacted**
Department of Chemistry
5/7/18

Signature redacted
Certified by: _____
Elizabeth M. Nolan
Associate Professor of Chemistry
Thesis Supervisor

Signature redacted
Accepted by: _____
Robert W. Field
Haslam and Dewey Professor of Chemistry
Chairman, Departmental Committee for Graduate Students



This doctoral thesis has been examined by a committee of the Department of Chemistry
as follows:

Signature redacted

Catherine L. Drennan
HHMI Professor and Investigator and Professor of Chemistry and Biology
Committee Chairperson

Signature redacted

Elizabeth M. Nolan
Associate Professor of Chemistry
Thesis Supervisor

Signature redacted

Alexander M. Klivanov
Novartis Professor of Chemistry and Bioengineering
Committee Member

A Biophysical and Biochemical Approach to Understanding the Interplay between Quaternary Structure and Function of Human Calprotectin

by

Jules Rabie Stephan

Submitted to the Department of Chemistry
on 5/7/18 in Partial Fulfillment of the
Requirements for the Degree of
Doctor of Philosophy in Biological Chemistry.

ABSTRACT

In response to an invading pathogen, the host organism initiates an immune response to fight infection. One component of the response involves metal-sequestering proteins that starve pathogens of essential metal nutrients. Humans release calprotectin (CP), a heterooligomer of S100A8 and S100A9, from neutrophils and epithelial cells to prevent microbes from accessing manganese, iron, nickel, and zinc. CP also binds Ca(II) ions, which increases the transition-metal affinity and antimicrobial activity of CP. In addition, Ca(II) causes the S100A8/S100A9 CP heterodimer to form a S100A8₂/S100A9₂ tetramer. When this dissertation research began, it was known that CP inhibited bacterial growth by sequestering transition metals, and that CP could transmit a proinflammatory signal; however, little was known about the fate of CP after release. The focus of this work was to better understand how the extracellular space may affect CP on biophysical and biochemical levels. Our approach was to study the molecular-level consequences of Ca(II) binding and tetramerization. We found that the heterotetramer exhibited significant resistance to enzymatic proteolysis compared to the heterodimer. Using NMR spectroscopy, we observed that the dynamics of CP change significantly upon Ca(II) binding small, yet notable, alterations in secondary structure. Finally, we discovered that methionine oxidation of CP inhibited Ca(II)-induced tetramerization, resulting in accelerated proteolysis. Taken together, our studies provided new insights into how CP survives the harsh conditions of the extracellular space, and a mechanism for clearing CP from the extracellular space.

Thesis Supervisor: Elizabeth M. Nolan
Title: Associate Professor of Chemistry

Chapter Abstracts

Chapter 1: Innate Immunity and the Fate of Calprotectin

Mammals have two branches of immunity that work in concert to protect the host. Innate immunity rapidly recognizes foreign organisms using germline-encoded receptors, and mounts an inflammatory response. The innate immune system also presents antigens to the adaptive immune system, which develops antibodies specifically tailored to pathogen-derived antigens. We discuss innate and adaptive immunity as well as their intersections, and review the current knowledge of processes that involve extracellular calprotectin. This Chapter concludes by discussing the contributions of this research to understanding the fate of extracellular human calprotectin.

Chapter 2: Calcium-Induced Tetramerization and Zinc Chelation Shield Human Calprotectin from Degradation by Host and Bacterial Extracellular Proteases

This Chapter describes our investigations into the relationship between the quaternary structure of CP and its protease stability. We describe two new variants of CP-Ser termed I60K and I60E that have the (A8)I60E or (A8)I60K mutations, respectively. These variants remain dimeric in the presence of Ca(II); however, a metal at this His₆ site causes I60E and I60K to tetramerize. We compare the protease stability of CP, I60E, and I60K against a panel of host proteases. In the presence of excess Ca(II) ions, CP-Ser is a poor substrate for all of the tested proteases, in contrast I60E and I60K are degraded over the course of the experiments. In the presence of excess Ca(II) ions and 1 equivalent of Mn(II), all of the proteins are resistant to degradation. We attribute the resistance of I60E and I60K to degradation in the presence of Mn(II) to tetramerization. We conclude that an unappreciated function of Ca(II)-induced tetramerization is to protect against proteolysis. In addition, the staphylococcal extracellular protease GluC cleaves the final

four residues from the S100A8 subunit, regardless of oligomeric state. This cleavage site is close to the His₃Asp site, and coordination of Zn(II) prevented cleavage by GluC.

Chapter 3: NMR Spectroscopy Reveals the Effect of Ca(II) on the Dynamics of the Calprotectin Dimer

In this Chapter, we report NMR spectroscopic studies of I60K in the absence and presence of Ca(II). In the absence of Ca(II), we were unable to assign the S100A8 backbone, and we assigned ≈94% of the S100A9 backbone. In the presence of Ca(II), we assigned ≈66% of the S100A8 backbone and ≈94% of the S100A9 backbone. We observe that Ca(II) causes nearly every peak to shift in the S100A8 and S100A9 [¹H-¹⁵N]-HSQC spectra; however, the amide resonances of the S100A9 C-terminal extension does not undergo changes in chemical shift with the addition of Ca(II). Using the secondary structure prediction program TALOS-N, we find that the secondary structure of the I60K heterodimer agrees well with reported crystal structures of the CP heterotetramer except for small key regions in the linker region and C-terminal section of helix IV. To investigate dynamics, we measure the T₁, T₂, hetNOE of the S100A8 subunit in the presence of Ca(II) and the S100A9 subunit in the presence and absence of Ca(II). We use T₁, T₂, and hetNOE data to perform model free analysis, which provides insight into the picosecond to nanosecond timescale dynamics of the polypeptide backbones. We find that the linker region and C-terminal section of helix IV display Ca(II)-induced changes in dynamics. We hypothesize that changing the dynamics of these regions promotes tetramerization by revealing residues involved in tetramerization and increases transition-metal affinity by preorganizing the binding sites.

Chapter 4: Oxidative Post-Translational Modifications Accelerate Proteolysis of Calprotectin

In this Chapter, we study the biochemical consequences of post-translational oxidation of CP, specifically methionine oxidation and disulfide bond formation. By performing mass spectrometry of human nasal mucus and pimple pus, we observe that CP can be oxidized *in vivo*, and we use ^{15}N -labeled protein as an internal standard to demonstrate that the observed oxidation did not occur after harvesting the samples. We find that oxidation of (A9)M81 inhibits Ca(II)-induced tetramerization. In contrast, metal coordination at the His₆ site causes CP to form a tetramer after methionine oxidation. We find that the loss of tetramerization caused by methionine oxidation results in accelerated proteolysis of CP that is prevented when the methionine-oxidized CP is bound to Ca(II) and Mn(II). Despite inhibition of Ca(II)-induced tetramerization, methionine-oxidized CP displays antimicrobial activity at physiological concentrations. In addition, both full-length CP subunits contain a single cysteine residue, and we find that CP is capable of forming disulfide bonds within a heterodimer and between heterodimers. We find that both of these disulfide-linked species, particularly the “intradimer” disulfide species, are degraded more rapidly than unmodified CP by trypsin in the presence of Ca(II). We propose an extension to the working model of CP where reactive oxygen species generated during the immune response oxidize CP resulting in accelerated proteolysis. We reason that clearance of CP in this manner is important for avoiding excessive CP-mediated proinflammatory signaling that has been observed by other research groups.

Appendix 1: Protease Activity Controls

When studying the protease resistance of CP variants, we employed conditions that contained different transition-metal ions. It was necessary to assess the activity of the employed proteases under the various conditions to determine whether or not the metal ions were responsible for the observed differences in protease resistance. This

Appendix contains activity assays with small-molecule-protease substrates. We find that our experimental conditions did not have a significant effect on activity of the employed proteases, which confirms our conclusion that changing the oligomeric state of CP with transition-metal ions is responsible for the observed differences in protease stability.

Appendix 2: Additional Characterization of CP Variants and Oxidized Species

This Appendix contains characterization of new CP variants that were prepared for this dissertation. The characterization includes SDS-PAGE, circular dichroism spectra, Mn(II) competition titrations, size-exclusion chromatograms, sedimentation profiles, full HPLC chromatograms from protease digestion experiments, and antimicrobial activity assays.

Appendix 3: Additional Spectra and Parameters for NMR Spectroscopy

This Appendix contains the details for the settings and field strengths that were used for all NMR spectroscopy experiments for each protein. Additionally, the parameters for processing all of the raw FIDs is included. Supporting spectra are also included.

Appendix 4: Several Dimer-Dimer Interface Variants of CP Exhibit Ca(II)-Induced Tetramerization

When we were screening CP variants in search of mutations that prevent tetramerization, we found variants that showed some degree of tetramer deficiency as well as no perturbation to tetramerization. This Appendix contains size-exclusion chromatograms of these variants and sedimentation profiles of a select of variants. These results suggest that there are residues at the tetramer interface in addition to (A8)I60 that contribute to tetramerization as well as others that appear to be nonessential for tetramerization.

For Mom and Dad

Acknowledgements

Graduate school has been an important time for me. Over five years much has changed. I cannot help but cringe when I look at my first notebook or the first figures that I prepared. I think it is a similar feeling to looking back at old pictures, and laughing at the clothes you once wore. Outside of the laboratory, I sometimes realize that the way I make plans or organize priorities is far more efficient and thoughtful than I would have done five years ago. All of this is to say that I have grown immensely as a scientist and the benefits have extended into the rest of my life.

Professor Elizabeth M. Nolan is responsible for those developments, and for that I am deeply grateful. Liz has created an environment that challenges her group members, and I believe that real growth happens when a person is challenged. Liz expects excellence from her group members. I do not know whether or not I ever truly met her expectations; however, I am certain that my attempts lifted me beyond anything I would have achieved on my own. Whenever prospective graduate students or post-docs ask me what I like about working for Liz, I answer with the same two answers (i) she respects the people that work for her and (ii) she is fully engaged with her science. Whenever I spoke with Liz, I felt that she listened, and the evidence is in this dissertation. My work is a significant departure from the bioinorganic chemistry that my S100 predecessors studied. Liz allowed me to follow my interests even though they drew us into unfamiliar territory. All along the way, Liz provided feedback and insight to make my science the best it could. To the second point, Liz's enthusiasm for science, commitment to excellence, and level of engagement are an inspiration for everyone who works with her.

I would like to thank my thesis chair Professor Catherine Drennan. Each of our annual meetings have been helpful and her career advice has given me much to think about. Professor Alexander Klibanov has served as my other committee member, and I am grateful for his support and career guidance. I am grateful to Professor Bradley Pentelute. He has been a friendly face since I first arrived for visiting weekend, and his

generosity in allowing me to use his mass spectrometers enabled me to perform what is perhaps my favorite set of experiments. I am indebted to Professor Robert Griffin and Dr. Robert Silvers, a post-doctoral fellow in his laboratory, for making the NMR studies we imagined a reality. I have learned much from both of you, and we have learned a great deal about calprotectin through our collaboration. We also collaborated with Professor Michael Gross at Washington University at St. Louis and Dr. Jagat Adhikari, a post-doctoral fellow in his laboratory, and I am excited to report their insightful discoveries soon. I am deeply appreciative of Dr. Benjamin Bleier and Angela Nocera for being so accommodating, which allowed me to obtain extremely important samples.

I have been privileged to work alongside great scientists in the laboratory. Dr. Megan Brophy and Dr. Toshiki Nakashige got me started in the lab. Before coming to MIT, I had never worked with proteins or bacteria, and their mentorship made my transition go smoothly. Dr. Andrew Wommack and Ms. Deborah Pheasant showed me the ropes of analytical ultracentrifugation, which may be my favorite experiment, and has proven extremely useful. Everyone else (Phoom, Lisa, Rose, Simone, Tim, Julie, Fangting, Fabien, Claire, Wilma, Lisa, Emily, Anmol, and Haritha) made the laboratory a great place to do science. I was always enjoyed sharing exciting results, disappointing results, and stories with you guys. You provided feedback on my presentations, papers, science, and exams that were crucial to my success. Many of you were subjected to my particular brand of humor, which is really only funny to me. You handled it with a confused chuckle and an eye roll, and I cannot ask for much more than that. I am fortunate to have worked with three fantastic undergraduates Christine, Sherlene, and Rebekah. Working with you has been among the most rewarding experiences in graduate school. I hope that I have given you an experience like I had as an undergraduate. I know that no matter where the future takes me I want mentorship to be part among my responsibilities. Our neighbors in the Shoulders lab have been a great help too. Andrew walked me through

western blotting, and I think just about every graduate student in the Shoulders lab scanned a blot for me before I was trained.

The final group of people to thank is my friends and family. I have been fortunate see Eric, a close high school friend, once every few months. Every visit has been a pleasure. John was one of my first friends in college. Our phone calls and gaming sessions have been welcome distractions from the stresses of graduate school. Zak was a fantastic mentor while I was an undergraduate, and working with him inspired me to go to graduate school. Since coming to MIT, he has served a similar mentor role while being a fantastic friend. I am going to miss our regular lunch meetups. I do not think that I can properly thank my parents and sister because I cannot imagine living without them. It is their support that has brought me to this point, and will continue to propel me forward. For those reasons, I dedicate my dissertation to them. Lastly, there is one major thing that has changed during graduate school. I was not married five years ago, and I am now. I have shared everything with Kat, and I would not want to spend my life with anyone else.

Table of Contents

Abstract.....	3
Dedication.....	8
Acknowledgements.....	9
Table of Contents.....	12
List of Figures.....	16
List of Tables.....	19
Abbreviations.....	21
Chapter 1: Innate Immunity and the Fate of Calprotectin.....	25
1.1. Innate Immunity.....	26
1.1.1. Innate vs. Adaptive Immunity.....	26
1.1.2. Connections between Innate and Adaptive Immunity.....	29
1.1.3. The Neutrophil.....	36
1.2. Calprotectin in Innate Immunity.....	39
1.2.1. Nutritional Immunity.....	39
1.2.2. CP is a Metal-Sequestering Protein.....	40
1.2.3. Structure of CP.....	43
1.3. The Fate of Calprotectin is an Emerging Topic.....	45
1.3.1. Limitations of the Working Model.....	45
1.3.2. Metal Piracy.....	47
1.3.3. Proinflammatory Signaling.....	48
1.4. Summary of Thesis.....	49
1.5. References.....	52
Chapter 2: Calcium-Induced Tetramerization and Zinc Chelation Shield Human Calprotectin from Host and Bacterial Extracellular Proteases.....	69
2.1. Introduction.....	70
2.2. Experimental.....	72
2.2.1. General Materials and Methods.....	72
2.2.2. Instrumentation.....	73
2.2.3. Protein Purification.....	74
2.2.4. Site-Directed Mutagenesis.....	75
2.2.5. Analytical Size-Exclusion Chromatography.....	76
2.2.6. Sedimentation Velocity Experiments.....	77
2.2.7. Protease Digestion Assays.....	78
2.2.8. Protease Activity Assays.....	79
2.2.9. Antimicrobial Activity Assays.....	80
2.2.10. Antimicrobial Activity Assays with Trypsin.....	80
2.2.11. Mn(II) Competition Experiments with ZP1.....	82
2.2.12. Circular Dichroism Spectroscopy.....	82
2.3. Results and Discussion.....	82

2.3.1. Design and Preparation of Tetramer-Deficient Variants of Calprotectin.....	82
2.3.2. (A8)I60E and (A8)I60K Mutations Disrupt Ca(II)-Induced Tetramerization.....	85
2.3.3. I60E and I60K Variants Form Heterotetramers in the Presence of Mn(II) or Fe(II).....	87
2.3.4. Tetramerization Protects Calprotectin against Host Proteases..	93
2.3.5. Proteolysis by Trypsin Abolishes Antibacterial Activity.....	97
2.3.6. The Staphylococcal Protease GluC Cleaves the S100A8 Subunit in the Absence of Zn(II).....	98
2.3.7. The GluC Degradation Product Exhibits <i>in vitro</i> Antibacterial Activity.....	101
2.3.8. Biological Implications and Outlook.....	103
2.4. Acknowledgements.....	104
2.5. References.....	104

Chapter 3: NMR Spectroscopy Reveals the Effect of Ca(II) on the Dynamics of the Calprotectin Dimer.....	113
3.1. Contributions.....	114
3.2. Introduction.....	114
3.3. Experimental.....	117
3.3.1. General Materials and Methods.....	117
3.3.2. Site-Directed Mutagenesis.....	117
3.3.3. Protein Expression and Purification – General Protocol.....	118
3.3.4. Protein Overexpression and Purification – Selective ¹⁵ N Labeling of Phe, Leu, Ile, or Val.....	112
3.3.5. Mass Spectrometry.....	123
3.3.6 Analytical Size-Exclusion Chromatography.....	125
3.3.7. NMR Sample Preparation.....	125
3.3.8. General NMR Spectroscopy Methods.....	126
3.3.9. Backbone Resonance Assignment.....	126
3.3.10. NMR Spectroscopy of I60K Variants.....	127
3.3.11. Estimation of Molecular Weight from Magnetic Relaxation Rates	127
3.3.12. Chemical Shift Perturbations.....	128
3.3.13. Relaxation and Model-Free Analysis.....	128
3.4. Results and Discussion.....	128
3.4.1. Prior Structures of CP.....	128
3.4.2. Assignment of the I60K Subunits in the Presence and Absence of Ca(II).....	131
3.4.3. CSP Analysis Reveals Regions that Respond to the (A8)I60K Mutation and Ca(II).....	137
3.4.4. TALOS-N Highlights Regions that Rearrange with Ca(II).....	142
3.4.5. Relaxation Analysis Uncovers Ca(II)-Induced Changes in Dynamics.....	149
3.4.6. Conclusions and Outlook.....	153

3.5. Acknowledgements	157
3.6. References	158

Chapter 4: Oxidative Post-Translation Modification Accelerates Proteolysis of Calprotectin.....

4.1. Contributions	166
4.2. Introduction	166
4.3. Experimental	169
4.3.1. General Materials and Methods.....	169
4.3.2. General Instrumentation.....	171
4.3.3. Site-Directed Mutagenesis.....	172
4.3.4. Preparation and Purification of CP and Variants.....	173
4.3.5. Preparation and Purification of Oxidized CP-Ser Variants.....	174
4.3.6. Oxidation of CP.....	175
4.3.7. Collection of Human Nasal Mucus.....	176
4.3.8. Collection of Human Pus.....	176
4.3.9. Preparation of Human Mucus and for LC-MS.....	177
4.3.10. Antimicrobial Activity Assays.....	178
4.3.11. Metal Competition Experiments with ZP1.....	178
4.3.12. Analytical Size-Exclusion Chromatography.....	179
4.3.13. Anion-Exchange Chromatography.....	180
4.3.14. Analytical Ultracentrifugation (Sedimentation Velocity).....	181
4.3.15. Protease Digestion of Oxidized CP-Ser.....	182
4.3.16. Protease Digestion of Oxidized CP.....	183
4.3.17. SDS-PAGE and Western Blots.....	183
4.4. Results	184
4.4.1. Oxidized CP Subunits are Observed in Human Mucus and Pus.....	184
4.4.2. Methionine Oxidation of CP-Ser Causes Heterotetramer Dissociation.....	190
4.4.3. (A9)MetO81 Serves as the Determinant for Heterotetramer Dissociation.....	191
4.4.4. Preparation of Oxidized CP-Ser.....	193
4.4.5. CP-Ser O ₄ and CP-Ser O ₅ Exhibit Defective Ca(II)-Induced Tetramerization.....	195
4.4.6. CP-Ser O ₄ and CP-Ser O ₅ Interconvert between Heterodimers and Heterotetramers.....	196
4.4.7. CP-Ser Retains Antimicrobial Activity after Methionine Oxidation.....	202
4.4.8. Oxidized CP-Ser Binds Transition Metals with High Affinity.....	202
4.4.9. Oxidized CP-Ser is Protease Sensitive.....	203
4.4.10. Oxidation of CP Yields Disulfide-Linked Oligomers.....	207
4.4.11. dsl-CP is Protease Sensitive.....	212
4.4.12. dsl-CP and MetO-dsl-CP are Degraded by at Comparable Rates.....	214
4.5. Discussion	214
4.6. Acknowledgments	222

4.7. References.....	222
Appendix 1: Protease Activity Assays.....	232
Appendix 2: Additional Characterization of CP Variants and Oxidized Species.....	238
A2.1. Additional Characterization for Chapter 2.....	239
A2.2. Additional Characterization for Chapter 3.....	253
A2.3. Additional Characterization for Chapter 4.....	256
Appendix 3: NMR Spectra and Parameters for Acquisition and Processing of NMR Spectra.....	267
Appendix 4: Several Dimer-Dimer Interface Variants of CP Exhibit Ca(II)-Induced Tetramerization.....	310
A4.1. Introduction.....	311
A4.2. Generation of DNA for Variant Proteins.....	311
A4.3. Analytical Size-Exclusion Chromatography.....	313
A4.4. Results.....	315
A4.5. References.....	319
Biographical Note.....	321
CV.....	322

List of Figures

Chapter 1

Figure 1.1. Summary of the immune cells discussed in Chapter 1.....	28
Figure 1.2. A simplified depiction of the process to develop antibodies.....	31
Figure 1.3. Diagram of the C1 complex.....	33
Figure 1.4. Diagram of mannose-binding lectin in complex with MASPs.....	34
Figure 1.5. Initiation of the alternative complement pathway.....	35
Figure 1.6. Maturation process for the human neutrophil.....	37
Figure 1.7. Crystal structure of Ni(II)-Ca(II)-Na(I)-CP-Ser.....	44
Figure 1.8. Diagram of possible fates of CP.....	46

Chapter 2

Figure 2.1. Tetramer interface of CP in complex with Mn(II), Ca(II), and Na(I).....	84
Figure 2.2. Analytical SEC of CP-Ser, I60E, and I60K.....	86
Figure 2.3. AUC of I60E and I60K fitted with Sedfit.....	88
Figure 2.4. AUC of I60E and I60K fitted with DCDT+.....	88
Figure 2.5. Susceptibility of Ca(II)-bound CP-Ser, I60E, and I60K to trypsin.....	95
Figure 2.6. Susceptibility of Ca(II)-bound CP-Ser, I60E, and I60K to HNE.....	96
Figure 2.7. AMA assays performed with untreated and trypsin-treated CP-Ser, I60E, and I60K.....	98
Figure 2.8. Susceptibility of Ca(II)-bound CP-Ser, I60E, and I60K to GluC.....	100
Figure 2.9. Growth inhibition of bacteria by CP-Ser and Δ SHKE.....	102

Chapter 3

Figure 3.1. Crystal structure and sequence alignment of CP-Ser.....	130
Figure 3.2. TROSY spectra of A9-I60K.....	133
Figure 3.3. Assigned residues shown on the primary structure of I60K.....	134
Figure 3.4. TROSY spectra of A8-I60K.....	136
Figure 3.5. Overlay of A9-I60K and A9-CP-Ser [^1H - ^{15}N]-HSQC spectra.....	139
Figure 3.6. Overlay of A8-I60K and A8-CP-Ser [^1H - ^{15}N]-HSQC spectra.....	140
Figure 3.7. Ca(II)-induced chemical shift perturbations of I60K.....	142
Figure 3.8. TALOS-N analysis of A8-I60K-Ca(II).....	144
Figure 3.9. TALOS-N analysis of A8-I60K+Ca(II).....	145
Figure 3.10. TALOS-N analysis of A9-I60K-Ca(II).....	146
Figure 3.11. TALOS-N analysis of A9-I60K+Ca(II).....	147
Figure 3.12. Relaxation analysis of A9-I60K-Ca(II).....	151
Figure 3.13. Relaxation analysis of A9-I60K+Ca(II).....	152
Figure 3.14. Comparisons of S100A11-Ca(II) and S100A11+Ca(II) crystal structures.....	154
Figure 3.15. Crystal structure of Mn(II)-Ca(II)-CP-Ser tetramer.....	155
Figure 3.16. Comparison of Ni(II)-Ca(II)-CP-Ser and Ni(II)-CP-Ser crystal structures.....	157

Chapter 4

Figure 4.1. Mass spectra of mucus.....	187
---	-----

Figure 4.2. Mass spectrometry of additional mucus.....	188
Figure 4.3. Mass spectra of pus.....	189
Figure 4.4. SEC and mass spec of H ₂ O ₂ -treated CP-Ser.....	192
Figure 4.5. SEC of H ₂ O ₂ -treated Met→Ala variants.....	194
Figure 4.6. SEC of CP-Ser O ₄ and CP-Ser O ₅	196
Figure 4.7. AUC of CP-Ser O ₄ and CP-Ser O ₅ fitted with Sedfit.....	198
Figure 4.8. AUC of CP-Ser O ₄ and CP-Ser O ₅ fitted with DCDT+.....	200
Figure 4.9. AMA assays with CP-Ser O ₄ and CP-Ser O ₅	203
Figure 4.10. ZP1 competition titrations with CP-Ser O ₄ and CP-Ser O ₅	204
Figure 4.12. HPLC analysis of trypsin-treated CP-Ser and oxidized CP-Ser.....	206
Figure 4.12. HPLC analysis of HNE-treated CP-Ser and oxidized CP-Ser.....	207
Figure 4.13. Western blot of H ₂ O ₂ -treated CP.....	208
Figure 4.14. SDS-PAGE of H ₂ O ₂ -treated CP(A9-C3S).....	209
Figure 4.15. SEC and SDS-PAGE of H ₂ O ₂ -treated CP.....	210
Figure 4.16. HPLC analysis of trypsin-treated dsl-CP.....	213
Figure 4.17. HPLC analysis of trypsin-treated MetO-dsl-CP.....	215
Figure 4.18. Alignments of S100A8 proteins from various organisms.....	221
 Appendix 1	
Figure A1.1. Trypsin activity assay.....	233
Figure A1.2. Chymotrypsin activity assay.....	234
Figure A1.3. HNE activity assay.....	235
Figure A1.4. GluC activity assay.....	236
 Appendix 2	
Figure A2.1. SDS-PAGE analysis of CP-Ser, I60K, I60E, and ΔSHKE.....	239
Figure A2.2. CD spectra of CP-Ser, I60K, I60E, and ΔSHKE.....	240
Figure A2.3. ZP1 competition for Mn(II) with CP-Ser and variants.....	241
Figure A2.4. CP-Ser and variants Ca(II) activation titration with ZP1 and Mn(II)..	242
Figure A2.5. SEC of CP-Ser and variants ±Ca(II)±Mn(II).....	243
Figure A2.6. SEC of CP-Ser and variants ±Ca(II)±Fe(II).....	244
Figure A2.7. Sedfit sedimentation distributions of tetramer-deficient variants.....	245
Figure A2.8. Full HPLC traces of trypsin digestions with tetramer-deficient variants.....	246
Figure A2.9. Susceptibility of Ca(II)-bound tetramer-deficient variants to chymotrypsin with full HPLC traces.....	247
Figure A2.10. Susceptibility of Mn(II)-Ca(II)-bound tetramer-deficient variants to HNE with full HPLC traces.....	248
Figure A2.11. Growth inhibition of <i>E. coli</i> by tetramer-deficient variants.....	249
Figure A2.12. HPLC analysis of proteins prior to AMA assay.....	250
Figure A2.13. Full HPLC traces GluC digestions with tetramer-deficient variants	251
Figure A2.14. SEC of CP-Ser and ΔSHKE.....	252
Figure A2.15. SDS-PAGE analysis of I60K with uniform isotopic labeling.....	253
Figure A2.16. SDS-PAGE analysis of I60K with random fractional deuteration and uniform carbon and nitrogen isotopic labeling.....	254
Figure A2.17. SDS-PAGE analysis of I60K with selective ¹⁵ N labeling.....	254

Figure A2.18. SDS-PAGE of CP-Ser with uniform ¹⁵ N labeling.....	255
Figure A2.19. SEC with 500 μM I60K and CP-Ser.....	255
Figure A2.20. SDS-PAGE analysis of Met→Ala variants and oxidized CP-Ser....	256
Figure A2.21. CD spectra of Met→Ala variants, CP-Ser O ₄ , and CP-Ser O ₅	257
Figure A2.22. Mass spectra of CP-Ser O ₄ and CP-Ser O ₅	258
Figure A2.23. Locations of Met residues in the CP-Ser tetramer.....	258
Figure A2.24. Anion-exchange chromatograms of CP-Ser and Oxidized CP-Ser	259
Figure A2.25. HPLC traces of chymotrypsin digestions with oxidized CP-Ser.....	260
Figure A2.26. HPLC traces of proteinase K digestions with oxidized CP-Ser.....	261
Figure A2.27. HPLC traces of HNE digestions with oxidized CP-Ser.....	262
Figure A2.28. Peak area plots from HNE digestions of oxidized CP-Ser.....	263
Figure A2.29. Mass spectra of dsl-CP and MetO-dsl-CP.....	264
Figure A2.30. SDS-PAGE analysis of MetO-dsl-CP reaction.....	265

Appendix 3

Figure A3.1. Calculated molecular weight based on magnetic relaxation rates... 299	299
Figure A3.2. [¹ H- ¹⁵ N]-HSQCs of selectively labeled A8-I60K-Ca(II).....	300
Figure A3.3. [¹ H- ¹⁵ N]-HSQCs of selectively labeled A8-I60K+Ca(II).....	301
Figure A3.4. [¹ H- ¹⁵ N]-HSQCs of selectively labeled A9-I60K-Ca(II).....	302
Figure A3.5. [¹ H- ¹⁵ N]-HSQCs of selectively labeled A9-I60K+Ca(II).....	303
Figure A3.6. [¹ H- ¹⁵ N]-HSQCs of A9-I60K, A9-I60K(H103A), and A9 I60K(H105A)-Ca(II).....	304
Figure A3.7. [¹ H- ¹⁵ N]-HSQCs of A9-I60K, A9-I60K(H103A), and A9 I60K(H105A)+Ca(II).....	305
Figure A3.8. [¹ H- ¹⁵ N]-HSQCs of A9-I60K, A9-I60K(P107A), and A9 I60K(P114A)-Ca(II).....	306
Figure A3.9. [¹ H- ¹⁵ N]-HSQCs of A9-I60K, A9-I60K(P107A), and A9 I60K(P114A)+Ca(II).....	307
Figure A3.10. Relaxation and model-free analysis of A8-I60K+Ca(II).....	308

Appendix 4

Figure A4.1. SDS-PAGE of variant proteins.....	315
Figure A4.2. Analytical SEC of I60K and I73R.....	316
Figure A4.3. Analytical SEC of CP-Ser(E57A)(I73R) and CP-Ser(E57K)(I73R)...	317
Figure A4.4. Analytical SE of CP-Ser(ΔHb) and CP-Ser(ΔHb)(Q69A).....	318
Figure A4.5. Analytical SEC of CP-Ser(W88R).....	318
Figure A4.6. AUC of I73R and I73S.....	319

List of Tables

Chapter 2

Table 2.1. Molecular weights and extinction coefficients.....	73
Table 2.2. Mass spectrometry of CP-Ser and variant proteins.....	75
Table 2.3. Primers employed for site-directed mutagenesis.....	76
Table 2.4. Calculated sedimentation coefficients and molecular weights using Sedfit.....	89
Table 2.5. Calculated sedimentation coefficients and molecular weights using DCDT+.....	90

Chapter 3

Table 3.1. Primers used for mutagenesis.....	118
Table 3.2. Protein nomenclature and examples of isotopic labeling nomenclature.....	119
Table 3.3. Mass spectrometry of proteins with nonspecific labeling.....	121
Table 3.4. Mass spectrometry of proteins with selective ¹⁵ N labeling.....	122
Table 3.5. Components for selective labeling medium.....	124

Chapter 4

Table 4.1. Molecular weights and extinction coefficients for the S100A8 and S100A9 subunits.....	170
Table 4.2. Molecular weights and extinction coefficients for commercial proteins.....	171
Table 4.3. Primers employed for site-directed mutagenesis.....	173
Table 4.4. Mass spectrometric analysis of CP and variants.....	175
Table 4.5. Summary of mucus samples analyzed.....	186
Table 4.6. Calculated sedimentation coefficients and molecular weights using Sedfit.....	199
Table 4.7. Calculated sedimentation coefficients and molecular weights using DCDT+.....	201

Appendix 3

Table A3.1. NMR acquisition parameters for A8-I60K-Ca(II).....	268
Table A3.2. NMR processing parameters for A8-I60K-Ca(II).....	268
Table A3.3. NMR acquisition parameters for A8-I60K+Ca(II).....	269
Table A3.4. NMR processing parameters for A8-I60K+Ca(II).....	270
Table A3.5. NMR acquisition parameters for variant proteins.....	271
Table A3.6. NMR processing parameters for variant proteins.....	271
Table A3.7. NMR acquisition parameters for CP-Ser.....	272
Table A3.8. NMR processing parameters for CP-Ser.....	272
Table A3.9. Chemical shifts of assigned A8-I60K-Ca(II) resonances.....	273
Table A3.10. Chemical shifts of assigned A8-I60K+Ca(II) resonances.....	276
Table A3.11. Chemical shifts of assigned A9-I60K-Ca(II) resonances.....	279
Table A3.12. Chemical shifts of assigned A9-I60K+Ca(II) resonances.....	272
Table A3.13. Model-free analysis parameters for A8-I60K-Ca(II).....	285
Table A3.14. Model-free analysis parameters for A9-I60K-Ca(II).....	289
Table A3.15. Model-free analysis parameters for A9-I60K+Ca(II).....	294

Appendix 4

Table A4.1. Primers employed for site-directed mutagenesis..... 313

Abbreviations

ABC	ATP-binding cassette
Ala	alanine
AMA	antimicrobial activity
Amp	ampicillin
Asp	aspartate
ATCC	American Type Culture Collection
AUC	analytical ultracentrifugation
AXC	analytical ultracentrifugation
BCR	B cell receptor
BME	β -mercaptoethanol
<i>C. albicans</i>	<i>Candida albicans</i>
CbpA	calprotectin binding protein A
CD	circular dichroism
CP	calprotectin
CP-Ser	calprotectin with both cysteines mutated to serine
Cys	cysteine
Da	dalton
DC	dendritic cell
DMSO	dimethylsulfoxide
DNA	deoxyribonucleic acid
dsl	disulfide-linked
DSS	4,4-dimethyl-4-silapentane-1-sulfonic acid
<i>E. coli</i>	<i>Escherichia coli</i>
EDTA	ethylenediaminetetraacetic acid
ESI	electrospray ionization
<i>F. magna</i>	<i>Finogoldia magna</i>
Glu	glutamate
GluC	glutamyl endopeptidase C
HEPES	4-(2-hydroxyethyl)-1-piperazineethanesulfonic acid
His	histidine
HNE	human neutrophil elastase
HPLC	high performance liquid chromatography
HSQC	heteronuclear single quantum coherence
Hz	hertz
Ig	immunoglobulin
IgG	immunoglobulin G
IgM	immunoglobulin M
IPTG	Isopropyl- β -D-1-thiogalactopyranoside
Kan	kanamycin
K_d	dissociation constant
<i>L. plantarum</i>	<i>Lactobacillus plantarum</i>

LB	Luria Bertani
LC-MS	liquid chromatography-mass spectrometry
Leu	leucine
LPS	lipopolysaccharide
Lys	lysine
MASP	mannose-binding protein associated serine proteases
MeCN	acetonitrile
Met	methionine
MetO	methionine sulfoxide
MHC	major histocompatibility complex
MRS	Man Rogosa Sharpe
MWCO	molecular-weight cutoff
<i>N. gonorrhoeae</i>	<i>Neisseria gonorrhoeae</i>
<i>N. meningitidis</i>	<i>Neisseria meningitidis</i>
NET	neutrophil extracellular trap
NIH	National Institutes of Health
NMR	nuclear magnetic resonance
NRAMP	natural resistance macrophage protein
NSF	National Science Foundation
OD	optical density
PAMP	pathogen-associated molecular pattern
PCR	polymerase chain reaction
PDB	Protein Data Bank
Phe	phenylalanine
PMSF	phenylmethylsulfonyl fluoride
PRR	pattern recognition receptor
PVDF	polyvinylidene fluoride
ROS	reactive oxygen species
rpm	revolutions per minute
<i>S. aureus</i>	<i>Staphylococcus aureus</i>
<i>S. pneumoniae</i>	<i>Streptococcus pneumoniae</i>
<i>S. Typhimurium</i>	<i>Salmonella enterica</i> serovar Typhimurium
SDM	standard deviation from the mean
SDS-PAGE	sodium dodecyl sulfate-polyacrylamide gel electrophoresis
SEC	size-exclusion chromatography
SEM	standard error from the mean
T1	longitudinal relaxation time
T2	transverse relaxation time
TCEP	tris(2-carboxyethyl)phosphine
TCR	T cell receptor
TPEN	<i>N,N,N',N'</i> -tetrakis(2-pyridylmethyl)ethylenediamine
TFA	trifluoroacetic acid
TLR4	toll-like receptor 4

TRIS	tris(hydroxymethyl)aminomethane
TROSY	transverse relaxation optimized spectroscopy
TSB	tryptic soy broth
Val	valine
ZP1	Zinpyr-1

Chapter 1: Innate Immunity and the Fate of Calprotectin

1.1 Innate Immunity

1.1.1. *Innate vs. Adaptive Immunity*

In order to survive and flourish, an organism must have the ability to protect itself from environmental dangers and rival organisms. Unicellular and multicellular organisms have developed sophisticated systems to recognize and exterminate threats to their survival. The innate immune system represents an ancient host-defense strategy that is conserved between animals and plants.¹ More recently, vertebrates developed a second arm of defense termed adaptive immunity. Adaptive immunity is exclusive to vertebrates, and there is a major distinction between the adaptive immune systems of jawless and jawed vertebrates.^{2,3} Innate and adaptive immunity work together in vertebrates to form a bastion that is stronger than either working in isolation. Innate immunity serves as the first line of defense, and provides the adaptive immune system with antigens used to program a response specific to the invader at hand.

The hallmarks of innate immunity are recognition of specific pathogen-associated molecular patterns (PAMPs) and subsequent deployment of broad-spectrum antimicrobial agents in response.^{1,4} PAMPs are molecules produced by foreign organisms that the host recognizes using pattern-recognition receptors (PRRs). For example, the host is alerted to the presence of Gram-negative or Gram-positive bacteria through PRRs that bind bacterial membrane/cell-wall components such as lipopolysaccharide (LPS) or lipoteichoic acid, respectively.¹ The PRRs are germline encoded; therefore, they are passed from one generation to the next. The utility of the innate immune system lies in its ability to easily identify foreign organisms.

The earliest identified PRRs were the Toll-like receptors. The indication that Toll proteins were mediators of innate immunity came from studies with *Drosophila melanogaster*. It was found that mutation of the *Toll* gene in *D. melanogaster* grievously

weakened the fly's immune response to fungal infection; however, the antibacterial response remained robust.⁵ The authors found that Toll was a membrane protein that bound a product from a proteolytic cascade that was initiated by microbial invasion. They also discovered that the signal transduction pathway activated by Toll led to release of antifungal proteins. By searching for human homologs to *D. melanogaster* Toll, it was demonstrated that a protein, later named Toll-like receptor 4 (TLR4), was responsible for transducing a proinflammatory signal.⁶ The discovery that Toll-like receptors serve as receptors for PAMPs in mammals came from studies of mice that did not mount an inflammatory response upon LPS stimulation.^{7,8} It was found that these mice were homozygous for a point mutation in the *Tlr4* gene or lacked the gene entirely. The mice lacking functional TLR4 were specifically more susceptible to infection by Gram-negative organisms. Humans encode 10 TLR proteins, enabling rapid detection of a diverse set of foreign organisms and activation of cells that contribute to innate immunity, which will be discussed in greater detail in subsection 1.1.2.

In contrast to the innate immune system, which identifies invaders by molecules common to many pathogens, adaptive immunity is celebrated for its highly specific nature. The adaptive immune system generates antibodies that specifically bind to a pathogen, marking them for destruction. Antibodies also neutralize toxins by binding to them. Similar to the innate immune system, cellular receptors initiate the adaptive immune response. The receptors are expressed on the cell surface of specialized lymphocytes termed T cells and B cells, and the receptors are named T cell receptors (TCR) and B cell receptors (BCR), respectively (Figure 1.1). The TCRs and BCRs are not germline encoded; rather, they continuously change through controlled randomization, a process termed somatic hypermutation.⁹ Each T cell and B cell expresses a single TCR or BCR isoform. T cells and B cells are activated after an antigen binds the TCRs or BCRs.

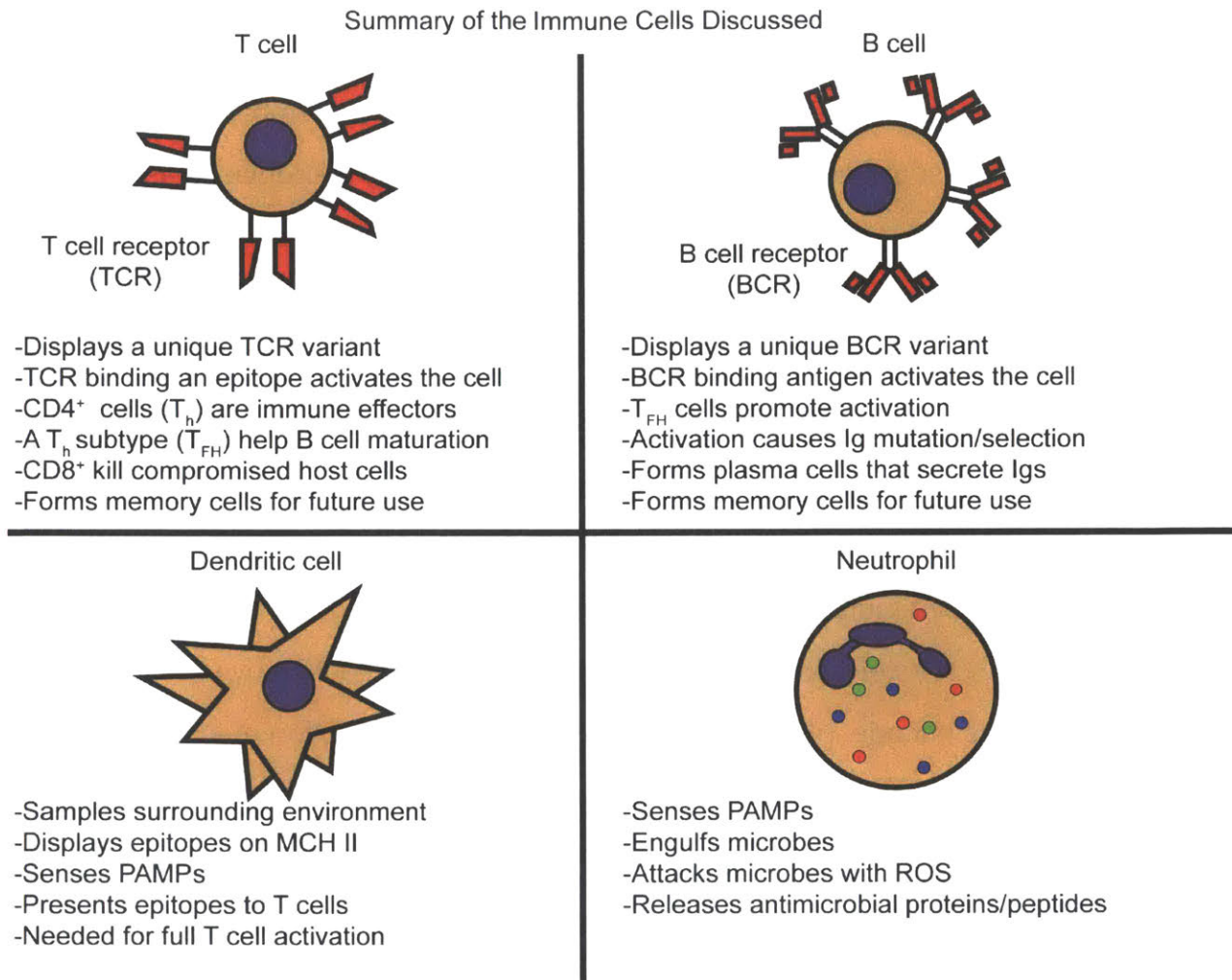


Figure 1.1. A summary of the immune cells discussed in this chapter. The T cell and B cell receptors are simplified to only show representations of the extracellular domains involved in epitope and antigen recognition, respectively.

T cells can be grouped into two broad classes: CD4⁺ T cells and CD8⁺ T cells.^{10,11} CD8⁺ positive cells are also called cytotoxic T cells. Their TCRs engage the major histocompatibility complex (MHC) I of host cells. MCH I displays antigens derived from intracellular molecules. If a cell is cancerous or is infected with a virus, it will display non-self antigens that activate CD8⁺ T cells. Onnon4⁺ T cells by the MHC II of antigen-presenting cells (Figure 1.2). After activation, a CD4⁺ T cell will proliferate into many different subtypes, each of which fulfills an important role in guiding the immune response,

which is the basis for naming them helper T cells. Activated CD4⁺ cells were historically classified as either Th1 or Th2 cells, and it had been shown that Th2 cells are necessary for B cells to produce antibodies.^{12,13} Later studies demonstrated that there are many subtypes of activated CD4⁺ cells, and that follicular helper T cells (T_{FH}) provide cytokines necessary for B cells to generate antibodies.^{10,14}

The production of antibodies begins with stimulation of a BCR, causing the B cell to internalize the bound molecule, degrade it, and present the fragments on the MHC II (Figure 1.2). A T_{FH} cell that recognizes a peptide presented on a B cell will interact with the activated B cell (Figure 1.2). The interaction stimulates the B cell in a number of ways that promotes proliferation, affinity maturation of the antibody, switching from production of IgM to other another isotype, and survival.¹⁴ Eventually, B cell clones that efficiently recognize the parent antigen are selected, and become plasma cells or memory B cells. The plasma cells secrete antibodies that are used to fight the infection, whereas memory B cells remain dormant until stimulated by their antigen, causing rapid proliferation of plasma cells and release of antibodies. Likewise, this process creates memory T cells that will recognize future encounters with the pathogen. The time between infection and production of high-affinity immunoglobulins requires several days. By retaining memory cells, the organism can dramatically reduce the time required for a strong response by the adaptive immune system.

1.1.2. *Connections between Innate and Adaptive Immunity*

Though the innate and adaptive immune systems were presented as operating independently, there are intersections that are critical for robust host defense; however, they were not always appreciated. Beginning with the discovery of the adaptive immune system, the prevailing notion had been that strong activation of TCRs and BCRs were the only signals needed to mount an adaptive immune response. At a symposium in 1989, Dr. Charles Janeway presented a new hypothesis to counter what he termed “the

immunologist's dirty little secret," which was that antibody generation at the time relied on administration of the antigen with complete Freund's adjuvant (a mixture of dead *Mycobacterium tuberculosis* or *Bordetella pertussis*).¹⁵ The adjuvant was necessary because it had been observed that stimulation of T cells with an antigen was insufficient to induce a response, and that an adjuvant of heat-killed pathogens was essential for raising antibodies.^{15,16} These observations led to Janeway's hypothesis that a second signal alongside the match between a TCR/BCR and an epitope/antigen was necessary for stimulating an immune response. Janeway proposed that dendritic cells (DCs) provide the second signal.¹⁵ Dendritic cells are part of the innate immune system and are considered to be antigen-presenting cells (Figures 1.1 and 1.2).^{17,18} DCs express many PRRs, and continually present fragments of endocytosed molecules on their MCH II. The importance of DCs was illustrated in a series of studies using DCs and mice in which MyD88, a protein essential for transducing the signal from a TLR-ligand interaction, was knocked out.^{6,19-21} It was found that MyD88 and PAMPs were essential for enabling DCs to productively present antigens to T cells. It is thought that the need for PRR activation and TCR activation serves to avoid generating an autoimmune response because PRR activation confirms that a pathogen is present.^{15,22}

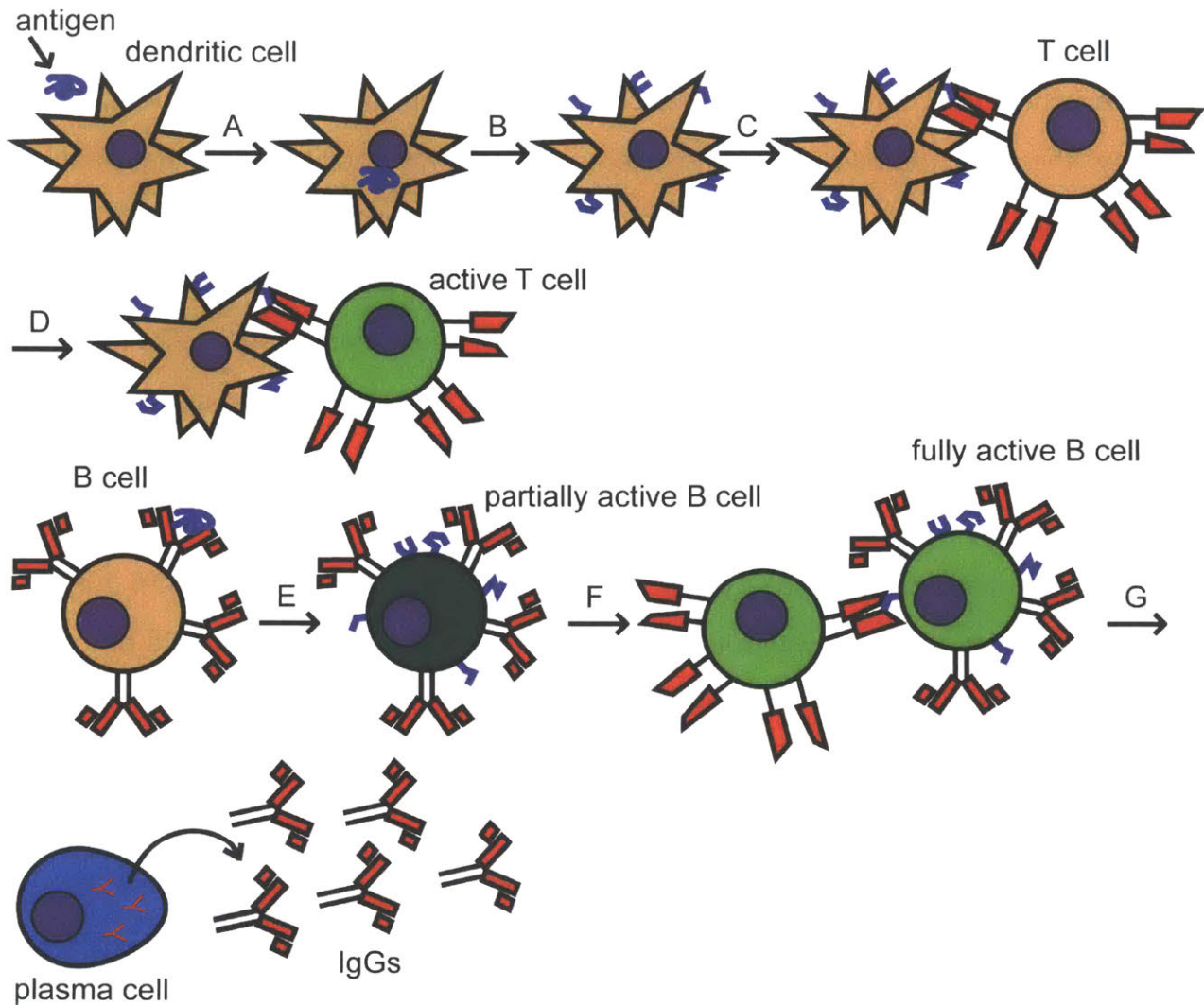


Figure 1.2. A simplified depiction of the process by which the adaptive immune system develops antibodies against an antigen. (A) A dendritic cell endocytoses an antigen and is stimulated by a PAMP (not shown). (B) The dendritic cell proteolyzes the antigen and displays the fragments on its MHC II. (C) A CD4⁺ T cell binds a presented epitope through its TCR. (D) The T cell becomes activated by the TCR-epitope interaction and factors secreted by the dendritic cells that are not shown. (E) A B cell binds an antigen through its BCR causing the cell to endocytose the antigen and become activated. The antigen is proteolyzed, and the fragments are displayed on its MHC II. (F) An activated T cell binds the epitope, now displayed on a B cell, that was recognized earlier. T cell further activates the B cell by secreting effector molecules (not shown) and forming protein-protein interactions between T cell and B cell surface proteins. (G) The B cell proliferates, differentiates, and mutates its BCR; this process is not illustrated. Eventually high affinity BCRs are selected, and those clones become plasma cells that secrete Igs based on their BCRs (IgGs shown). Memory T cells and B cells form to provide a rapid response to future infection (not shown).

The complement system represents another connection between innate and adaptive immunity. There are three branches of the complement system: the classical pathway, the lectin pathway, and the alternative pathway. Activation of the classical pathway begins with the soluble C1 protein complex, which is an oligomer of C1q, C1r, and C1s. The C1q component of the complex is a hexamer of collagen-like triple helices comprising 18 polypeptide chains (Figure 1.3).^{23,24} The hexamerization occurs at the N-terminal ends of the proteins. The complex splits to form six trimeric coiled-coils, and each polypeptide terminates with a globular domain that binds IgG and IgM (Figure 1.3).^{25,26} The Ig domains from a single coil trimerize. A tetramer of C1r₂C1s₂, the monomers of which are proteases secreted as zymogens, forms on the triple helices (Figure 1.3).^{24,27} Once the complex engages with multiple IgGs and/or IgMs, the C1r subunits of the C1 complex activate themselves by self-cleavage, enabling them to activate C1s by proteolytic cleavage.²⁸ The C1s subunits go on to initiate the complement cascade (Figure 1.3).²⁷

Lectin pathway initiation is a combination of PRR activation and the classical complement pathway. Collectins and ficolins form soluble collagen-like triple helices that can associate into oligomers ranging from dimers to hexamers. The preferred oligomer may differ among collectins and ficolins (Figure 1.4).^{29,30} The C-terminal domain of each polypeptide is globular, and is used for binding sugars displayed on microbial, viral, or Ig surfaces.^{29,31,32} Collectins use lectin domains, and ficolins use fibrinogen-like domains for binding carbohydrates.³⁰ Similar to the C1 complex, multivalent interactions between a collectin or ficolin and target carbohydrates cause activation of mannose-binding protein-associated serine proteases (MASPs) that are complexed to the collectin or ficolin (Figure 1.4).³¹ The MASPs prefer to form homodimers. It has been shown that MASP-1 cleaves MASP-2, which initiates the complement cascade (Figure 1.4).³⁰

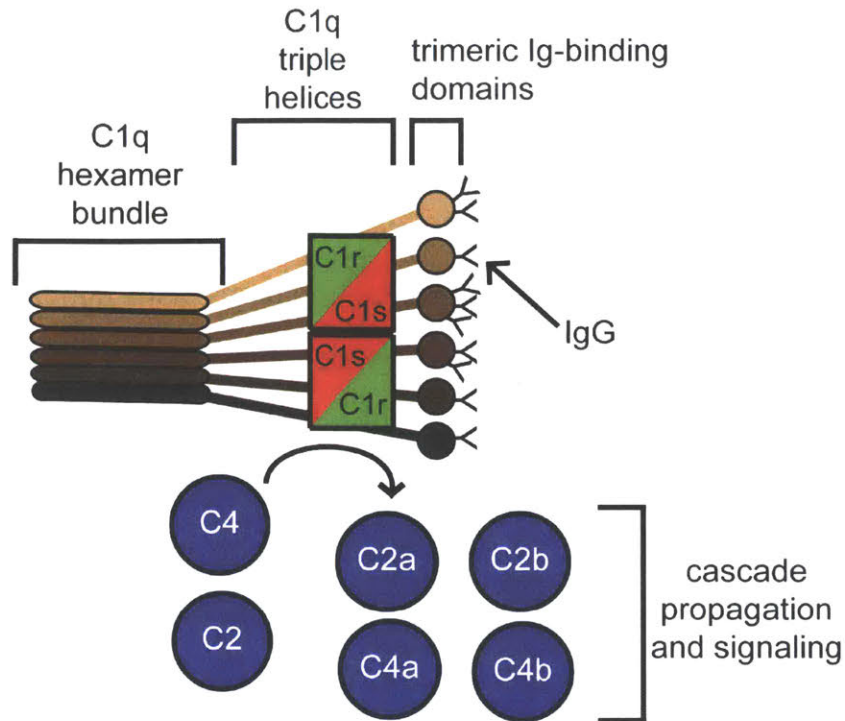


Figure 1.3. Diagram of the C1 complex. Each C1q subunit is a trimer, and six C1q subunits (shown in shades of brown) form a hexamer bundle. Triple helices branch out from the C-terminal region of the hexamer and terminate with globular Ig-binding domains. The trimeric Ig-binding domains are represented as a single sphere. Each bundle of globular Ig-binding domains can bind up to three Igs (IgGs shown). The C1s and C1r zymogens form a tetramer on the triple helices. Once a sufficient number of Igs have been bound, C1s is activated, which cleaves C1r. Once active, C1r cleaves C2 and C4 into C2a, C2b, C4a, and C4b. The C4a fragment is an anaphlytoxin and the other fragments form multi-protein complexes that participate in propagation of the complement cascade.

Lastly, the alternative pathway requires no specific receptor-ligand interaction for pathway initiation (Figure 1.5).^{33,34} The C3 protein is a central element of the complement cascade common to the propagation of all three pathways, and it is capable of slow spontaneous activation by hydrolysis of an internal thioester.³⁵ After hydrolysis, C3 associates with factor B, a zymogen protease. The complex, C3B, is a substrate for factor D, which activates factor B by cleaving it. Activated factor B cleaves new molecules of C3 to form C3a and C3b. C3b can associate with a new molecule of factor B, which can be activated by proteolytic cleavage, further increasing the amount of active factor B. The

complex of C3b and cleaved factor B (C3bBb) can then cleave new molecules of C3 to create a positive feedback loop as well as propagate the complement cascade (Figure 1.5). Cleavage of C3 to form C3b also greatly increases the reactivity of the internal thioester, allowing C3b to acylate amines and alcohols on cell surfaces. Accumulated C3b is a strong opsonin, as are downstream proteolytic fragments of the complement cascade, which marks an entity for destruction. To prevent opsonization of host cells, C3b can be intercepted by factor H or homologs that are displayed on the surface of host cells to prevent amplification.³⁶ Further dampening of the alternative pathway is caused by the protease factor I, which inactivates C3b after sequestration, by cleaving it. By taking stock of the three complement pathways, one can appreciate the spectrum of immunity that ranges from the highly non-specific alternative pathway to the antibody-targeted classical pathway, and the PRR-like system of the lectin pathway lying in the middle.

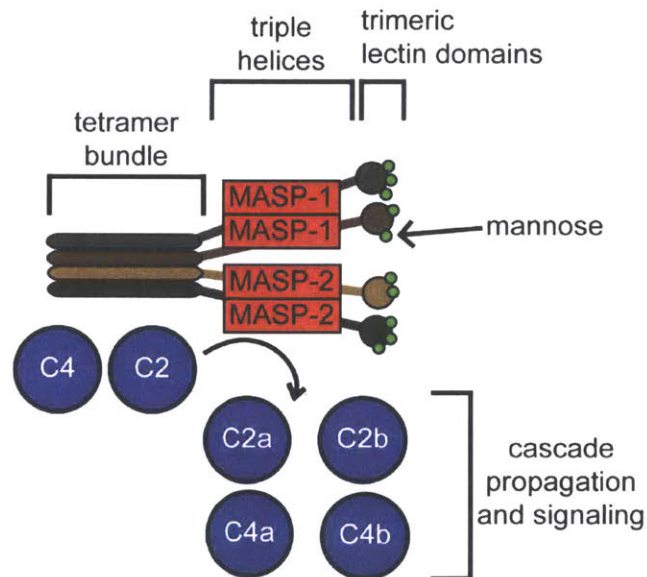


Figure 1.4. A diagram of mannose-binding lectin (MBL) complexed with MASP-1 and MASP-2. MBL trimerizes by forming a triple helix. Trimeric units of MBL tetramerize through their N-terminal domains. The C-terminal domains are lectins. Each bundle of three lectins is shown as a single sphere. After a sufficient number of sugars have been bound, MASP-1 becomes active allowing it to cleave MASP-2, which cleaves C4 and C2 to produce C2a, C2b, C4a, C4b. The C4a fragment is an anaphlytoxin and the other fragments form multi-protein complexes that participate in propagation of the complement cascade.

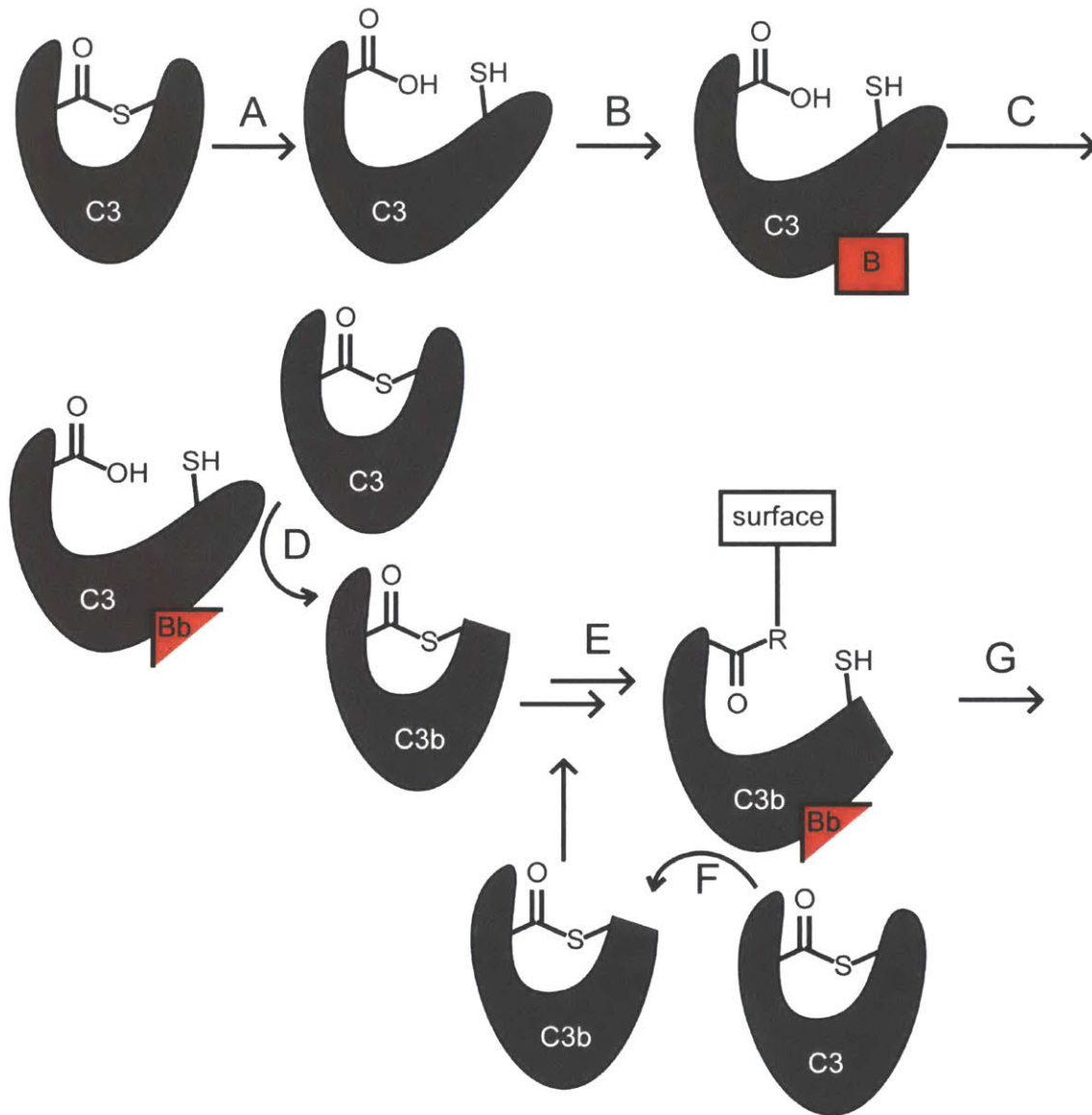


Figure 1.5. Initiation of the alternative pathway. Regulatory proteins (e.g. factor H and factor I) are not depicted. (A) Initiation begins with the slow spontaneous hydrolysis the internal thioester of C3. (B) After hydrolysis, C3 can associate with the zymogen protease factor B. (C) After complexation, factor B is cleaved by factor D (not depicted). The proteolytically active fragment Bb remains bound to C3. (D) The C3Bb complex cleaves new molecules of C3 to form C3b (E) The thioester of C3b is reactive, and can acylate solvent exposed amines and alcohols. After acylation, C3b can bind a new molecule of factor B, which is activated by factor D in a manner analogous to steps B and C. (F) The complex C3bBb can cleave more C3 to create a positive feedback loop and/or propagate the complex cascade. (G) The complex C3bBb can propagate the complement cascade.

1.1.3. *The Neutrophil*

The neutrophil is the most common white blood cell in humans, and is a central player in innate immunity. Under basal conditions, humans produce approximately 10^{11} neutrophils per day through the process of granulopoiesis.³⁷ The high production of neutrophils is matched by their rapid turnover. Neutrophils have been estimated to have a half-life of approximately 7 h; however, there is variability in reported half-lives, and neutrophils that are not in circulation can live considerably longer.^{37,38} In order to support such high production of neutrophils, it has been estimated that two thirds of bone marrow is dedicated to generating neutrophils and closely-related monocytes.³⁹ The genesis of a neutrophil begins with a hemopoietic stem cell that differentiates into a lymphoid-primed multipotent progenitor cell.^{39,40} Subsequently, the cell differentiates into a granulocyte-monocyte progenitor cell in a process controlled by many transcription factors.⁴¹ Once the granulocyte-monocyte progenitor cell differentiates into a myeloblast, it is no longer considered a stem cell because it is destined to become a granulocyte, and instead is classified in the mitotic pool.^{42,43} The mitotic pool also includes further differentiated cells: myeloblasts, promyelocytes, and myelocytes (Figure 1.6).⁴³ The post-mitotic pool encompasses metamyelocytes, and band neutrophils (Figure 1.6).⁴³ Maturation terminates with the band cell becoming a segmented neutrophil that is ready for release into circulation (Figure 1.6).

As a cell matures into a neutrophil, the nucleus of the cell undergoes major changes, and its resulting shape varies between organisms.⁴⁴ The details of nuclear morphology that follow are specific to human neutrophils (Figure 1.6). While in the stem cell pool, the nucleus is round, similar to other cells. The nucleus takes on a “horseshoe” shape in the mitotic pool. The horseshoe becomes more exaggerated, and the ends bulge as the cell becomes a banded neutrophil. A fully mature neutrophil has a signature segmented nucleus where narrow sections separate bulging sections. Neutrophil nuclei commonly have three segments; however, cells with more segments have been

observed, and they are termed hyper-segmented neutrophils. Despite the fact that segmentation correlates with neutrophil development, it has been reported that hyper-segmented and segmented cells have comparable age.⁴⁵

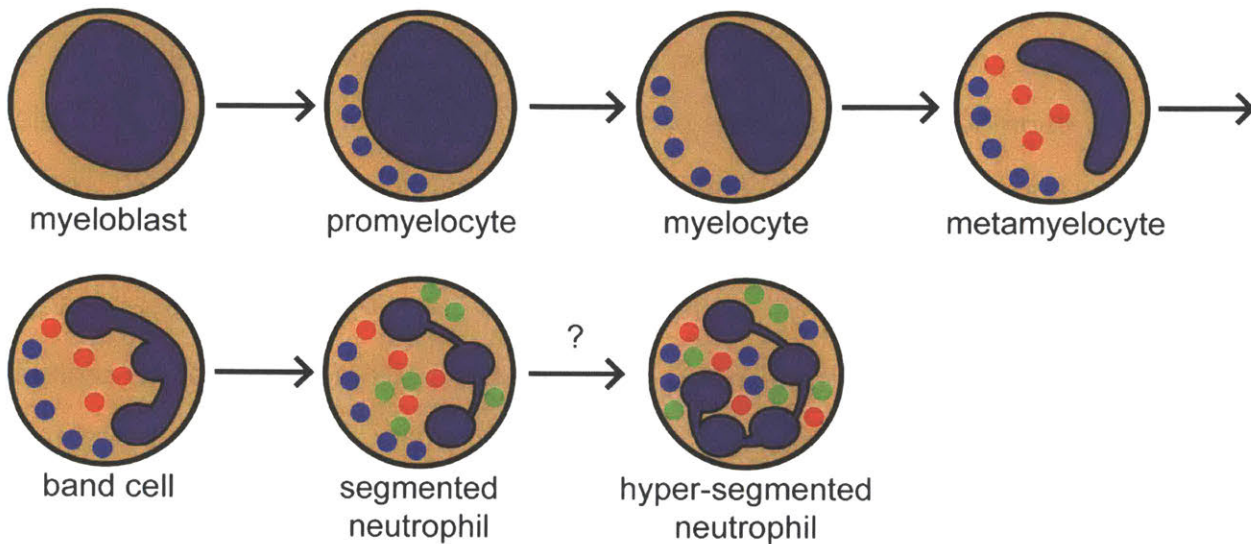


Figure 1.6. The maturation process of a neutrophil beginning with the myeloblast.^{43,44} The blue circles represent azurophilic granules. The red circles represent secondary granules. The green circles represent tertiary granules. The granules carry antimicrobial proteins and peptides. The transition from segmented neutrophil to hyper-segmented neutrophil has a question mark because it is unclear whether hyper-segmented neutrophils are more mature than segmented neutrophils.

Granules also follow a defined formation pathway as a neutrophil matures (Figure 1.6). During the process of becoming a promyelocyte, the primary granules begin to form. Primary granules are also known as azurophilic granules because of their high myeloperoxidase content that gives these granules a distinct blue color when stained with the Romanowski stain.^{46,47} Primary granules also contain other antibacterial molecules including proteinase 3, cathepsin G, neutrophil elastase, azurocidin, α -defensins (human neutrophil peptides 1-4), and bactericidal permeability-increasing protein.^{46,47} The secondary granules form as the cell differentiates from a myelocyte to a metamyelocyte. During the transition from a band cell to a segmented neutrophil, the tertiary granules

form.^{46,47} The secondary and tertiary granules contain similar batteries of antimicrobials including lactoferrin, lipocalin-2, lysozyme, and LL37.^{46,47} Many of these proteins/peptides (e.g. α -defensins, azurocidin, and LL37) kill by damaging microbial cell membranes.⁴⁸⁻⁵⁰ Alternative mechanisms of action of α -defensins and related peptides are areas of current interest.⁵¹ Other proteins (e.g. lysozyme, neutrophil elastase, and cathepsin G) enzymatically degrade bacterial proteins or cell walls.^{52,53} In addition to the antimicrobials, the secondary and tertiary granules contain matrix metalloproteinases 8, 9, and 25. These enzymes degrade nearby tissue to promote immune cell entry and swelling.⁴⁶ Other antimicrobial proteins are stored in the cytosol of neutrophils. Calprotectin (CP, S100A8/S100A9 oligomer, calgranulin A/B oligomer, MRP8/MRP14 oligomer, L1 protein, cystic fibrosis antigen) accounts for approximately 40% of cytosolic protein in neutrophils.⁵⁴ Other antimicrobial proteins stored in the cytosol include S100A12 (Calgranulin C) and phospholipases that attack bacterial membranes.^{55,56}

In addition to the soluble antimicrobial proteins, neutrophils store NOX-2 (a NADPH oxidase) in the plasma membrane. NOX-2 is composed of many different proteins that associate after the neutrophil has engulfed a microbe.^{46,57} The microbe is quarantined to the phagosome, and the NOX-2 complexes are delivered to the phagosomal membrane. NOX-2 is oriented such that it receives electrons from the cytosol, which are used to reduce O_2 to superoxide ($O_2^{\cdot-}$) in the phagosome. The superoxide anion can dismutate to form oxygen and hydrogen peroxide (H_2O_2). The activity of NOX-2 is prodigious; it has been found that NOX-2 activation caused neutrophils to consume oxygen at approximately a 10-fold faster rate than resting cells,⁵⁸ giving rise to a phenomenon known as the "oxidative burst." When measuring the oxidative burst using an ensemble of cells, the burst was sustained between 20 and 30 min. In contrast, a study using single cells found that the burst duration was between 2 and 3 min before subsiding to a rate of oxygen consumption slightly higher than basal levels.^{59,60} In addition, merging of the phagosome and granules causes the granule

proteins to enter the phagosome. Fusion of the primary granules with the phagosome releases myeloperoxidase, which catalyzes the reaction of H_2O_2 with Cl^- to generate the extremely potent oxidant HOCl.⁵⁷ The combination of oxidants ($\text{O}_2^{\cdot-}$, H_2O_2 , and HOCl) and antimicrobial agents is thought to effectively kill microbes. Granules may also fuse with the plasma membrane to deliver their contents to the extracellular space. Once a neutrophil has phagocytosed and bombarded a pathogen, neutrophils can undergo apoptosis, and be cleared by a macrophage or form a neutrophil extracellular trap (NET).^{61,62} When forming a NET, the nucleus grows and eventually disintegrates as the chromatin unwinds. Simultaneously, leftover granules also dissolve. The cell forms a NET by releasing its entire intracellular contents including cytosolic proteins, granule proteins, DNA and histones.⁶² NETs have been found to exert antimicrobial activity against several microbes. Mice unable to form nets due to a peptidylarginine deaminase 4 knockout were more susceptible to staphylococcal necrotizing fasciitis than wild-type mice.⁶³ It has been shown that generation of ROS is critical for NET formation.⁶² The factors that lead to NETosis remain poorly understood; however, it is apparent that NETs are an important facet of neutrophil function.

1.2 Calprotectin in Innate Immunity

1.2.1. Nutritional Immunity

In addition to the active destruction of pathogens described in the previous section, the host has mechanisms to starve invading pathogens of essential nutrients. Transition metals are essential nutrients for all life, and serve as catalytic, structural cofactors, and signaling agents. When fighting infection, the host lowers the availability of nutrient transition metals through a process termed “nutritional immunity.”⁶⁴⁻⁶⁷ Sequestration of metal ions constitutes an important strategy to defend against microbial invasion. Limitation of iron was the first example of nutritional immunity; however, in recent years

the importance of limiting manganese and zinc has emerged.^{64,65,68} The neutrophil contributes to nutritional immunity by releasing lactoferrin, lipocalin-2, CP, and S100A12. Lactoferrin chelates Fe(III) to inhibit iron uptake by bacteria.⁶⁹ In response to iron restriction, bacteria secrete siderophores, which are capable of extracting Fe(III) from lactoferrin and related proteins. The prototypical example of a siderophore acquiring Fe(III) from host proteins is enterobactin, a siderophore used by many Gram-negative organisms.⁷⁰ To combat the siderophores, the host releases lipocalin-2 to sequester ferric siderophores, especially enterobactin.⁷¹ In addition to metal-chelating proteins, neutrophils express metal-transport proteins that remove transition metals from the phagosome. Namely, neutrophils localize natural resistance-associated macrophage protein (NRAMP1) to the membrane of tertiary granules.⁷² NRAMP1 is a divalent metal-ion transporter that pumps nutrient metals out of the phagosome.⁷³ Though this discussion focused on acquisition of uncomplexed metal ions, a similar tug-of-war over occurs for heme.⁷⁴

1.2.2. CP is a Metal-Sequestering Protein

The importance of manganese and zinc limitation became widely appreciated when it was observed that *Staphylococcus aureus* abscesses were depleted of Mn and Zn.⁷⁵ In particular, Mn was depleted in a CP-dependent manner, and mice lacking the S100A9 gene (knocking out S100A9 prevents S100A8 production)⁷⁶ suffered from a more serious infection. This discovery motivated efforts to understand the metal-binding properties of CP and the effects of CP-mediated metal sequestration on microbial metal-ion homeostasis.

Early studies using protein obtained from neutrophils had established that CP displayed Zn(II)-reversible antimicrobial activity.⁷⁷⁻⁷⁹ Later studies that employed recombinant protein demonstrated that CP could inhibit the growth of bacteria, which was attributed to depriving the microbes of Mn(II) or Zn(II).^{75,80-83} Observations that bacteria

upregulated Mn(II) and Zn(II) transport machinery in response to CP treatment provided further credibility to metal-sequestration model of CP activity.^{84,85} It was hypothesized that sequestration of Mn(II) by CP prevented activation of superoxide dismutase in *S. aureus*, which weakened the cells to the ROS generated by neutrophils.⁸⁶ Subsequent studies with mouse models of infection and bacteria in culture found that knocking out genes for Mn(II) transport reduced infectivity and superoxide dismutase activity in *S. aureus*, and that the presence of CP gave rise to similar phenotypes, leading to the conclusion that CP deprived the bacteria of Mn(II).^{84,86} Recently, it was found that *S. aureus* relies on a cambialistic superoxide dismutase named SodM under manganese-limiting conditions.⁸⁷ This enzyme can use iron in place manganese when the bacteria are treated with CP; however, it has a much lower catalytic activity than SodA, which requires a Mn(II) cofactor for activity.

In addition to the protective effects of CP, perturbing metal homeostasis can increase infectivity. One study addressed the interplay between *Salmonella enterica* serovar Typhimurium virulence and CP.⁸⁸ In a mouse model of *S. Typhimurium* colitis, robust infiltration of neutrophils into the cecum and an increase in fecal calprotectin occur. When ZnuABC, a Zn(II)-uptake system of *S. Typhimurium*, was disrupted by knocking out *znuA*, the bacteria displayed markedly lower colonization, which indicated that virulence was linked to the ability to acquire Zn(II). The colonization could be rescued by feeding the mice extra Zn(II), which presumably counteracted Zn(II) sequestration by CP. The surprising result was that wild-type *S. Typhimurium* colonization was decreased when the mice were unable to produce CP. It had been shown that *S. Typhimurium* thrives in inflammatory environments where many other microbes struggle to survive.⁸⁹ At least part of the success of *S. Typhimurium* under inflammatory conditions can be ascribed to ZnuABC enabling the pathogen to acquire Zn(II) when challenged with CP.

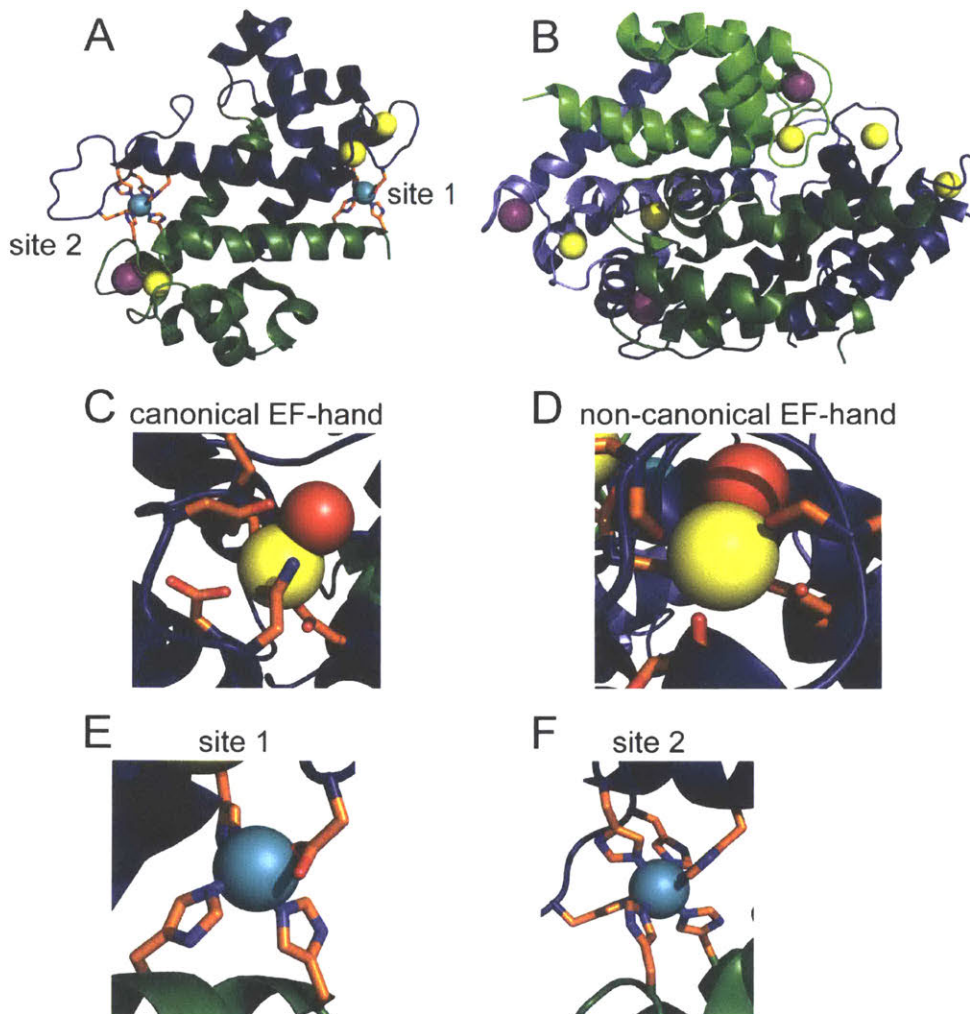
Other work has addressed how CP impacted metal-ion homeostasis of *Streptococcus pneumoniae*. This pathogen has a relatively high requirement for Mn,⁹⁰

and it had been shown that Mn was necessary for *S. pneumoniae* to survive oxidative stress.^{91,92} Transport of Mn(II) in *S. pneumoniae* is mediated by the ABC transporter PsaABC; however, the transporter can be poisoned by high concentrations of Zn(II), and bombardment of *S. pneumoniae* with Zn(II) during infection protected the host.⁹³ It was found that preventing expression of CP in mice led to delayed death and less dissemination of *S. pneumoniae* in a model of pneumococcal pneumonia.⁹⁴ Preventing CP expression did not alter neutrophil infiltration or cytokine production, indicating that loss of CP did not alter the innate immune response. Using recombinant CP, it was demonstrated that CP could rescue the growth of *S. pneumoniae* in the presence of high Zn(II) concentrations, presumably by sequestering Zn(II) and allowing PsaABC to transport Mn(II). The authors concluded that CP alters the ratio of Mn(II):Zn(II) during infection such that *S. pneumoniae* can acquire Mn(II) and spread the infection.

Many studies have investigated the consequences of Mn(II) and Zn(II) sequestration by CP; however, recently it has been established that CP also binds Fe(II) and Ni(II).^{95,96} Bacteria grown in medium treated with CP exhibited marked growth defects unless Fe was replenished into the medium, and recombinant CP inhibited Fe uptake into *Escherichia coli* and *Pseudomonas aeruginosa*. Recently, CP was reported to bind Ni(II).⁹⁶ Though nickel is used as a protein cofactor less frequently than manganese, iron, and zinc, Ni(II) is employed in urease by *Helicobacter pylori*, *Klebsiella pneumoniae*, and *Staphylococcus* spp. to detoxify their environments by increasing the pH.⁹⁷⁻⁹⁹ CP was found to bind Ni(II) and decrease Ni acquisition by *S. aureus*.⁹⁶ Additionally, CP inhibited the ability of *S. aureus* to increase the pH of growth media and urease activity was decreased in *S. aureus* lysates. Lastly, recombinant CP has been shown to inhibit Cu uptake by *Candida albicans*, and induce a Cu starvation response that was also observed in a murine model kidney invasion by *C. albicans*.¹⁰⁰

1.2.3. Structure of CP

CP is a heterooligomer of two S100 proteins, S100A8 (α subunit, 10.8 kDa) and S100A9 (β subunit, 13.2 kDa).^{101,102} The apo protein is an $\alpha\beta$ heterodimer (Figure 1.7A). The identifying characteristics of the S100 family are their small size (≈ 12 kDa), α -helical fold, and two EF-hand domains connected by a linker.^{103,104} The C-terminal EF-hand of S100 proteins resembles that of calmodulin, and is termed a canonical EF-hand (Figure 1.7C). These EF-hands have been shown to have highly tunable dissociation constants. For instance, the EF-hands of calbindin proteins have been shown to have dissociation constants on the order of 10 nM for Ca(II), whereas other proteins have dissociation constants on the order of 10 μ M.¹⁰⁵⁻¹⁰⁸ The N-terminal EF-hand has been termed a non-canonical or pseudo EF-hand, and is exclusive to S100 proteins (Figure 1.7D).^{109,110} The pseudo EF-hand forms a larger loop than the canonical EF-hand, it exhibits a lower coordination number, and contains fewer negatively charged residues. Due to their unique features, pseudo EF-hands have weaker Ca(II) affinities than canonical EF-hands.¹⁰⁹ The EF-hands of CP are important sensors that provide a signal for significant biochemical changes. In the presence of excess Ca(II), CP tetramerizes to form an $\alpha_2\beta_2$ heterotetramer (Figure 1.7B).^{81,111} In the presence of Ca(II), the protein exhibits orders of magnitude higher transition-metal affinity, enhanced antimicrobial activity, and increased thermal stability.^{81,95,96,111,112} These observations provided the basis for the working model of CP function (Figure 1.8). Due to the low resting intracellular Ca(II) concentration (≈ 100 nM),¹¹³ CP is presumed to be Ca(II)-free in the cytosol, which keeps the protein in the low affinity state. As CP is released, it will be exposed to the high concentration of Ca(II) in the extracellular space (≈ 2 mM),¹¹³ causing the protein to Ca(II) and tetramerize, which activates the high transition-metal affinity for competing with bacteria.



A8 ---MLTELEKALNSIIDVY**HKYSLIKGNFHAVYRDDLKKLLETESPOYIRKK**---- 49
A9 MTSKMSQLERNIETIINTF**HQYSVKLGHPDTLNQGEFKELVRKDLQNFLKKNKNE** 56

A8 -GADVWFKELDINTDGAVNFQEFLLILVIKMGVAA**HKKSH**EESHKE----- 93
A9 KVIEHIMEDLDTNADKQLSFEEFIMLMARLTWAS**HEKMHEGDEGPGHHHKPGLGEGTP** 114

Figure 1.7. Crystal structure of CP with Ni(II), Ca(II), and Na(I) bound, PDB: 5W1F.⁹⁶ (A) A dimer shown with Na(I), Ca(II), and Ni(II) bound. (B) Structure of the CP tetramer without the transition metals. One dimer is in light colors, and the other is in dark colors. (C) C-terminal canonical EF-hand of S100A9 with Ca(II) bound. (D) N-terminal pseudo EF-hand of S100A9 with Ca(II) bound. (E) Site 1 with Ni(II) bound. (F) Site 2 with Ni(II) bound. S100A8 is green. S100A9 is blue. The purple spheres are Na(I) ions. The yellow spheres are Ca(II) ions. The red spheres are water molecules. The teal spheres are Ni(II) ions. (G) Sequence alignment of S100A8 and S100A9 with transition-metal-binding residues in red.

In addition to the Ca(II)-binding sites, there are two sites at the dimer interface that coordinate transition metals. “Site 1” is a His₃Asp motif composed of (A8)His83, (A8)His87, (A9)His20, and (A9)Asp30 (Figure 1.7E), and “site 2” is a His₆ motif composed of (A8)His17, (A8)His27, (A9)His91, (A9)His95, (A9)His103, and (A9)His105 (Figure 1.7F).^{82,83,114,115} Site 1 binds Zn(II) with high affinity, and the biologically unprecedented His₆ motif of site 2 binds Mn(II), Fe(II), Zn(II), and Ni(II) with high affinity. No solution structures of CP have been published, and the available crystal structures are of CP in the tetramer state; thus, a description of the molecular-level events that occur upon Ca(II) binding are lacking. Structures of the S100A8 and S100A9 homodimers are available; however, these structures provide limited insight into the process of tetramerization aside from the observation that the CP tetramer buries more hydrophobic surface area than the S100A8 and S100A9 homodimers.^{114,116-119} With structural information on the CP heterodimer, it should be possible to understand the tetramerization process and rigorously to attribute the relative contributions of Ca(II) binding and tetramerization to the increase in transition-metal affinity.

1.3 The Fate of CP is an Emerging Topic

1.3.1. Limitations of the Working Model

The scientific community’s understanding of CP has greatly advanced since the protein was discovered approximately 30 years ago. Despite considerable advances, the working model for CP lacks important details. On a molecular level, we do not understand how Ca(II) causes the CP tetramer to form. Although it is widely accepted that the Ca(II)-bound tetramer has increased transition metal affinities, the structural/dynamic factors responsible for this feature are unknown. Another gap in our knowledge is fate of CP after release because the working model ends with coordination of transition metals by CP. It is important to recognize that we generally expect that the concentration of CP during

infection far exceeds the concentration of bioavailable metals. As a result, the working model only applies to a fraction of extracellular CP. Studies that address the fate of CP are necessary to understand how the fight for transition metals evolves over time and to understand progression of processes that CP mediates. Research groups are beginning to explore the fate of CP, and the following subsections describe several important discoveries.

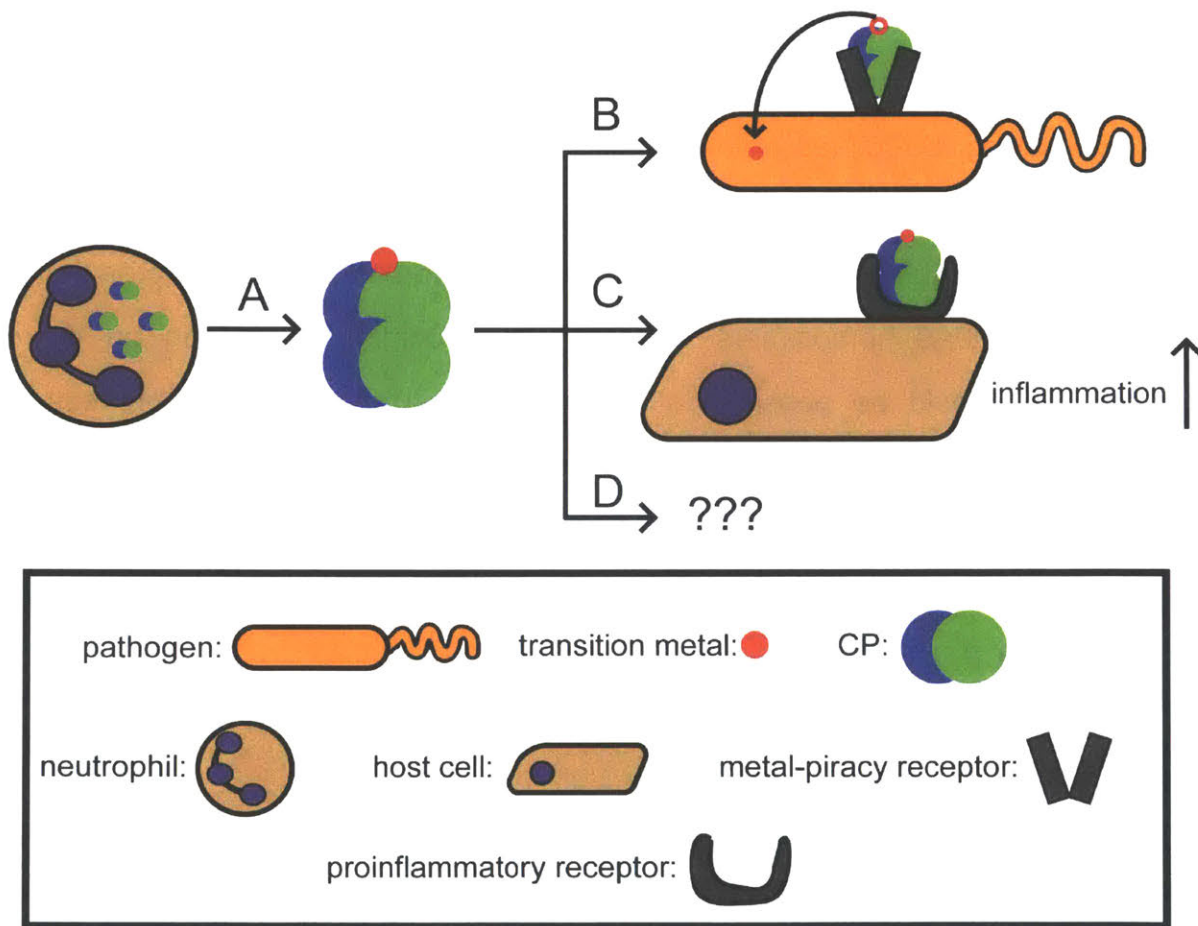


Figure 1.8. Possible fates of CP based on literature precedence. (A) CP is stored as a dimer in the cytosol of a neutrophil. As CP is released into the extracellular space it binds Ca(II) and tetramerizes. It may bind a transition metal. (B) A receptor on a pathogen binds CP, and removes the transition metal, which is imported into the cytosol. (C) A receptor on a host cell, perhaps TLR4, binds CP causing secretion of proinflammatory factors. (D) CP is modified in some way, marking it for an as of yet undetermined fate.

1.3.2. Metal Piracy

Events that follow CP coordinating transition metals are beginning to be unraveled. One possible avenue for investigation is how microbes defeat CP (Figure 1.8). One group reported that *Fingoldia magna*, a common opportunistic anaerobic pathogen, uses protein L to bind and inactivate CP.¹²⁰ Human neutrophil lysate and placental extract were subjected to affinity chromatography with immobilized fragments of protein L, and the eluent was analyzed SDS-PAGE and western blot. Two bands were identified as S100A8 and S100A9, indicating that the A domain of protein L bound CP. The protein L–CP interaction was inhibited by EDTA, suggesting that protein L was specific for the Ca(II)-bound CP tetramer. Interaction between protein L and CP was further supported by surface plasmon resonance. Cells expressing protein L were found to bind CP by immunofluorescence microscopy. *F. magna* with protein L knocked out displayed a growth inhibition phenotype when treated with CP compared to wild-type cells, which grew at a rate comparable to untreated cells. The molecular nature of the protein L resistance was not described, and may be a fruitful avenue for future study.

Another group reported that *Neisseria meningitidis* expresses a TonB-dependent transporter that pirates Zn(II) from CP.¹²¹ The authors named the protein CbpA (calprotectin binding protein A). CbpA is in the same class as TbpA, which is known to pirate Fe(III) from transferrin.¹²²⁻¹²⁵ CbpA was upregulated in the presence of CP, and the upregulation could be reversed by Zn(II) and not Mn(II), MoO₄²⁻, Co(II), Cu(II), or Fe(III). *N. meningitidis* was grown on plates supplemented with the metal chelator *N,N,N',N'*-tetrakis(2-pyridylmethyl)ethylenediamine (TPEN) to induce Zn(II) limitation, and grown with Zn(II)-loaded CP supplied on a filter disc. Only cells expressing CbpA were able to proliferate in both experiments. In a complementary experiment, cells were grown on a plate that contained a filter disc loaded with apo CP. When CbpA or TonB was knocked out, a zone of clearance was observed around the disc. When a variant of CP lacking site 2 was used, the wild-type, $\Delta cbpA$, $\Delta tonB$ cells grew without a defect, which indicated the

CbpA was necessary to extract metal from site 2 of CP. A more recent report described similar findings with the TonB-dependent transporter TdfH in *Neisseria gonorrhoeae*.¹²⁶ These studies are thought-provoking; however, more detailed analyses of these piracy systems are warranted. In particular, the scope of metal that can be pirated has not been explored and specificity of the CbpA and TdfH for site 2 versus site 1 is unknown. Both studies used TPEN, which chelates many metals with high affinity, and they did not perform ICP-MS to quantify the metals in the growth media, which would shed light on the metal speciation. Using the site 2 variant prevents CP from coordinating Zn(II) as well as other metals at the His₆ site; therefore, there is uncertainty in the metal(s) responsible for growth recovery. Of note, the more recent study used ICP-OES to show that TdfH caused the cells to accumulate Zn(II), which support the notion of Zn(II) piracy.

1.3.3. Proinflammatory Signaling

It has been reported that CP is a ligand for TLR4.^{127,128} The evidence for a CP–TLR4 interaction was largely indirect, and some of the data are summarized below. Experiments with bone marrow cells isolated from wild-type or *S100A9*^{-/-} knockout mice demonstrated that expression of CP potentiated TNF- α secretion, which is a product of TLR4 activation. Likewise, injection of recombinant CP to *S100A9*^{-/-} knockout mice increased TNF- α secretion. The authors observed that LPS stimulation resulted in secretion of CP, and that S100A8 alone was sufficient for stimulation. The stimulation of mouse bone marrow cells and human monocytes by LPS and S100A8 could be disrupted with inhibitors of three different kinases. These observations led the authors to suggest that CP acts in an autocrine fashion to create a positive feedback proinflammatory signal. The direct evidence for an interaction between CP and TLR4 was a plot of two sensorgrams from a surface plasmon resonance experiment using immobilized TLR4-MD2 (MD2 is a necessary protein co-factor for signal transduction)^{129,130} that demonstrated association and dissociation of S100A8. The most interesting findings were

that *S100A9*^{-/-} knockout mice exhibited increased survival in models of LPS-induced shock and *E. coli*-induced abdominal sepsis compared to wild-type mice. The increased survival of the *S100A9*^{-/-} knockout mice could be reversed by co-administration of CP. The authors concluded that CP caused excessive activation of TLR4, leading to increased mortality. This report was followed by findings that CP was necessary for development of autoreactive cytotoxic T cells, and that CP induced a refractory period during which LPS could not elicit an inflammatory response through TLR4.^{131,132} It should be noted that TNF- α secretion can be induced by pathways of other than TLR4 activation and that the kinase inhibitors were not specific to the TLR4 signaling pathway.

A common theme in biology is homeostasis: there is generally a mechanism to dampen an upregulation signal. A body of work suggests that CP is a signaling molecule that can cause damage to the host.^{128,131,132} The deleterious outcomes caused by CP signaling may arise from dysregulation of CP. We posit that further understanding the fate of CP after release will elucidate the forces that attempt to keep CP signaling within a healthy regime. Additionally, there are examples of bacteria that have developed mechanisms to defeat CP, and it is likely that there are other as-yet unidentified strategies to overcome this host-defense protein.

1.4 Summary of Thesis

The aim of this research was to understand tetramerization of CP on a molecular-level in order to formulate new hypotheses for the fate of CP after release *in vivo*. Chapter 2 describes our discovery that tetramerization of CP confers protease resistance. In this work, we report characterization of new CP variants, termed tetramer-deficient variants, that are unable to tetramerize in the presence of Ca(II). These variants allowed us to compare the proteolytic stability of the CP dimer and tetramer in the presence of Ca(II). We observed that the tetramer-deficient variants were rapidly degraded by trypsin,

chymotrypsin and human neutrophil elastase, whereas the CP tetramer was a poor substrate for all of these proteases. Endoproteinase GluC, which is a staphylococcal extracellular protease, was an exception because it only cleaved the final four residues of S100A8 regardless of the CP oligomeric state. When the protease digestion assays were performed in the presence of Ca(II) and Mn(II), the tetramer-deficient variants recovered protease stability, which we attributed to the Mn(II) converting them to the tetrameric form. We demonstrated the importance of protease resistance with an experiment where CP and the tetramer-deficient variants were treated with trypsin in the presence of Ca(II) prior to an antimicrobial activity assay. In this experiment, the tetramer-deficient variants failed to inhibit the growth of *E. coli* after trypsin treatment, however, CP retained full activity.

In Chapter 3, we further study one tetramer-deficient variant using NMR spectroscopy in order to gain insight into how Ca(II) binding affects the structure and dynamics of the CP heterodimer. Our hypothesis was that studying a tetramer-deficient variant in the presence of Ca(II) would enable us to observe and understand the Ca(II)-bound dimer. Results from such studies would enable us to describe how Ca(II) prepares CP to tetramerize and potentially how Ca(II) causes CP to bind transition metals with higher affinity. Using secondary structure prediction software, we found that the secondary structure of the dimer, for assignable residues, strongly agreed with the experimental data from crystal structures of the tetramer; however, there were small notable areas that became more helical with the addition of Ca(II). Due to the difficulty of assigning the protein, we investigated the dynamics of the protein using NMR spectroscopy because the problematic relaxation properties that we observed likely arose from the protein experiencing exchange on the NMR timescale. We measured the amide T1, T2, and hetNOE of both I60K subunits in the presence and absence of Ca(II), and used these parameters to fit models of dynamics for each assigned residue. We found that both subunits experienced significant exchange. We were able to compare the effect

of Ca(II) on the S100A9 subunit. By analyzing the regions of altered exchange and chemical shift perturbation due to Ca(II), we found evidence for helices III and IV of the S100A9 subunit alternating between open and closed conformations, which was suggested by previous work on other S100 proteins. Our data are consistent with a hypothesis where Ca(II) biases the helices to open, which exposes residues involved in tetramerization. We reason that tetramerization further stabilizes the open conformation. In addition, we obtained evidence that Ca(II) causes the transition metal binding residues in helix IV to become more ordered, which may contribute to increasing the transition-metal affinity.

In Chapter 4, we provide evidence for ROS marking CP for destruction. We performed mass spectrometry of human nasal mucus and pimple pus, and observed species of CP bearing additional oxygen atoms, which is consistent with conversion of methionine to Met sulfoxide (MetO). In a subset of those samples, we added ^{15}N -labeled CP to serve as an internal control for adventitious Met oxidation, which confirmed that the oxidation occurred before sample extraction. We generated MetO-containing CP *in situ* using H_2O_2 , and found that the CP tetramer was converted to a dimer over time in the presence of Ca(II). When we performed the same reaction in the presence of Mn(II), we observed a comparable oxidation by mass spectrometry; however, the tetramer remained intact. Studies of single Met \rightarrow Ala variants revealed that mutation of (A9)Met81 to Ala prevented H_2O_2 -induced dissociation, leading us to conclude that oxidation of this residue triggered dissociation. Examining the crystal structure revealed that (A9)Met81 was the only Met residue at the dimer-dimer interface. We reasoned that conversion of hydrophobic Met to hydrophilic MetO decreased the driving force for tetramerization. Using analytical ultracentrifugation, we found that Met oxidation of CP did not wholly prevent tetramerization, but rather the MetO-CP proteins were rapidly interconverting between the dimer and tetramer oligomeric states in the presence of Ca(II). We used these proteins in antimicrobial activity assays, in which we found that MetO modifications

resulted in minor attenuation of the proteins' antimicrobial activity. When we compared the proteolytic stability of the MetO-CP to CP in the presence of Ca(II), we found that the oxidized protein was degraded more quickly by several proteases. We attributed the increased protease stability to the incomplete tetramerization, and protease digestions in the presence of Ca(II) and Mn(II) were consistent with this hypothesis.

The experiments described above were performed with a CP variant where the two native Cys residues were mutated to Ser. In order to address how the wild-type protein is affected by ROS, we treated wild-type CP with H₂O₂, and we observed species with disulfide bonds within and between CP heterodimers. We assayed the protease stability of the disulfide-linked CP in the presence of Ca(II), and found that the disulfide bonds resulted in faster degradation. Taken together, we demonstrated that the MetO is a physiologically relevant post-translational modification of CP, and that it can cause the protein to lose its protease resistance by causing the protein to convert from the tetramer to the dimer, resulting in accelerated proteolysis. The protease stability and tetramerization could be rescued by Mn(II) coordination. We hypothesize that Met oxidation of CP by ROS generated during the immune response serves as a mechanism to regulate the concentration of CP in the extracellular space. Furthermore, we propose that the protection afforded by transition-metal coordination enables the host to prevent releasing metals that CP has sequestered. Our preliminary experiments with wild-type CP suggest another mode to regulate CP using ROS that deserves further investigation in the future. More broadly, our results inform the effect of MetO on protein-protein interactions, the signaling functions of ROS, and the role of Met during the oxidative burst.

1.5 References

1. Janeway, C. A.; Medzhitov, R., Innate immune recognition. *Annu. Rev. Immunol.* **2002**, *20* (1), 197.

2. Boehm, T., Design principles of adaptive immune systems. *Nat. Rev. Immunol.* **2011**, *11* (5), 307-317.
3. Litman, G. W.; Rast, J. P.; Fugmann, S. D., The origins of vertebrate adaptive immunity. *Nat. Rev. Immunol.* **2010**, *10* (8), 543-553.
4. Medzhitov, R.; Janeway, C., Innate immunity. *NEJM* **2000**, *343* (5), 338-344.
5. Lemaitre, B.; Nicolas, E.; Michaut, L.; Reichhart, J.-M.; Hoffmann, J. A., The dorsoventral regulatory gene cassette *spätzle/Toll/cactus* controls the potent antifungal response in *Drosophila* adults. *Cell* **1996**, *86* (6), 973-983.
6. Medzhitov, R.; Preston-Hurlburt, P.; Janeway Jr, C. A., A human homologue of the *Drosophila* Toll protein signals activation of adaptive immunity. *Nature* **1997**, *388* (6640), 394-397.
7. Hoshino, K.; Takeuchi, O.; Kawai, T.; Sanjo, H.; Ogawa, T.; Takeda, Y.; Takeda, K.; Akira, S., Cutting edge: toll-like receptor 4 (TLR4)-deficient mice are hyporesponsive to lipopolysaccharide: evidence for TLR4 as the LPS gene product. *J. Immunol.* **1999**, *162* (7), 3749-3752.
8. Poltorak, A.; He, X.; Smirnova, I.; Liu, M.-Y.; Huffel, C. V.; Du, X.; Birdwell, D.; Alejos, E.; Silva, M.; Galanos, C.; Freudenberg, M.; Ricciardi-Castagnoli, P.; Layton, B.; Beutler, B., Defective LPS signaling in C3H/HeJ and C57BL/10ScCr mice: mutations in *Tlr4* gene. *Science* **1998**, *282* (5396), 2085-2088.
9. Early, P.; Huang, H.; Davis, M.; Calame, K.; Hood, L., An immunoglobulin heavy chain variable region gene is generated from three segments of DNA: VH, D and JH. *Cell* **1980**, *19* (4), 981-992.
10. Pennock, N. D.; White, J. T.; Cross, E. W.; Cheney, E. E.; Tamburini, B. A.; Kedl, R. M., T cell responses: naïve to memory and everything in between. *Adv. Physiol. Educ.* **2013**, *37* (4), 273-283.
11. Smith-Garvin, J. E.; Koretzky, G. A.; Jordan, M. S., T cell activation. *Annu. Rev. Immunol.* **2009**, *27* (1), 591-619.

12. Cooper, M. D.; Peterson, R. D. A.; Good, R. A., Delineation of the thymic and bursal lymphoid systems in the chicken. *Nature* **1965**, *205* (4967), 143-146.
13. Mosmann, T. R.; Coffman, R. L., TH1 and TH2 cells: different patterns of lymphokine secretion lead to different functional properties. *Annu. Rev. Immunol.* **1989**, *7* (1), 145-173.
14. Crotty, S., A brief history of T cell help to B cells. *Nat. Rev. Immunol.* **2015**, *15* (3), 185-189.
15. Janeway, C. A., Approaching the asymptote? evolution and revolution in immunology. *Cold Spring Harb. Symp. Quant. Biol.* **1989**, *54*, 1-13.
16. Jenkins, M.; Pardoll, D.; Mizuguchi, J.; Quill, H.; Schwartz, R., T-Cell unresponsiveness in vivo and in vitro: fine specificity of induction and molecular characterization of the inresponsive state. *Immunol. Rev.* **1987**, *95* (1), 113-135.
17. Banchereau, J.; Steinman, R. M., Dendritic cells and the control of immunity. *Nature* **1998**, *392* (6673), 245-252.
18. Gallucci, S.; Lolkema, M.; Matzinger, P., Natural adjuvants: endogenous activators of dendritic cells. *Nat. Med.* **1999**, *5* (11), 1249-1255.
19. Kaisho, T.; Takeuchi, O.; Kawai, T.; Hoshino, K.; Akira, S., Endotoxin-induced maturation of MyD88-deficient dendritic cells. *J. Immunol.* **2001**, *166* (9), 5688-5694.
20. Kawai, T.; Adachi, O.; Ogawa, T.; Takeda, K.; Akira, S., Unresponsiveness of MyD88-deficient mice to endotoxin. *Immunity* **1999**, *11* (1), 115-122.
21. Adachi, O.; Kawai, T.; Takeda, K.; Matsumoto, M.; Tsutsui, H.; Sakagami, M.; Nakanishi, K.; Akira, S., Targeted disruption of the MyD88 gene results in loss of IL-1- and IL-18-mediated function. *Immunity* **1998**, *9* (1), 143-150.
22. Iwasaki, A.; Medzhitov, R., Control of adaptive immunity by the innate immune system. *Nat. Immunol.* **2015**, *16* (4), 343-353.
23. Lu, J.; Kishore, U., C1 complex: an adaptable proteolytic module for complement and non-complement functions. *Front. Immunol.* **2017**, *8*.

24. Mortensen, S. A.; Sander, B.; Jensen, R. K.; Pedersen, J. S.; Golas, M. M.; Jensenius, J. C.; Hansen, A. G.; Thiel, S.; Andersen, G. R., Structure and activation of C1, the complex initiating the classical pathway of the complement cascade. *Proc. Natl. Acad. Sci. U. S. A.* **2017**, *114* (5), 986-991.
25. Gaboriaud, C.; Juanhuix, J.; Gruez, A.; Lacroix, M.; Darnault, C.; Pignol, D.; Verger, D.; Fontecilla-Camps, J. C.; Arlaud, G. J., The crystal dtructure of the globular head of complement protein C1q provides a basis for its versatile recognition properties. *J. Biol. Chem.* **2003**, *278* (47), 46974-46982.
26. Cooper, N. R., The classical complement pathway: activation and regulation of the first complement component. In *Advances in Immunology*, Dixon, F. J., Ed. Academic Press: 1985; Vol. 37, pp 151-216.
27. Sim, R. B.; Tsiftoglou, S. A., Proteases of the complement system. *Biochem. Soc. Trans.* **2004**, *32* (1), 21-27.
28. Fey, P. D.; Endres, J. L.; Yajjala, V. K.; Widhelm, T. J.; Boissy, R. J.; Bose, J. L.; Bayles, K. W., A genetic resource for rapid and comprehensive phenotype screening of nonessential *Staphylococcus aureus* genes. *MBio* **2013**, *4* (1), e00537-00512.
29. Holmskov, U.; Thiel, S.; Jensenius, J. C., Collectins and ficolins: humoral lectins of the innate immune defense. *Annu. Rev. Immunol.* **2003**, *21* (1), 547-578.
30. Garred, P.; Genster, N.; Pilely, K.; Bayarri-Olmos, R.; Rosbjerg, A.; Ma, Y. J.; Skjoedt, M.-O., A journey through the lectin pathway of complement—MBL and beyond. *Immunol. Rev.* **2016**, *274* (1), 74-97.
31. Presanis, J. S.; Kojima, M.; Sim, R. B., Biochemistry and genetics of mannan-binding lectin (MBL). *Biochem. Soc. Trans.* **2003**, *31* (4), 748-752.
32. Weis, W. I.; Drickamer, K.; Hendrickson, W. A., Structure of a C-type mannose-binding protein complexed with an oligosaccharide. *Nature* **1992**, *360* (6400), 127-134.
33. Thurman, J. M.; Holers, V. M., The central role of the alternative complement pathway in human disease. *J. Immunol.* **2006**, *176* (3), 1305-1310.

34. Maves, K. K.; Weiler, J. M., Properdin: approaching four decades of research. *Immunol. Res.* **1993**, *12* (3), 233.
35. Müller-Eberhard, H. J., Molecular organization and function of the complement system. *Annu. Rev. Biochem.* **1988**, *57* (1), 321-347.
36. Ferreira, V. P.; Pangburn, M. K.; Cortés, C., Complement control protein factor H: The good, the bad, and the inadequate. *Mol. Immunol.* **2010**, *47* (13), 2187-2197.
37. Dancey, J. T.; Deubelbeiss, K. A.; Harker, L. A.; Finch, C. A., Neutrophil kinetics in man. *J. Clin. Invest.* **1976**, *58* (3), 705-715.
38. Tak, T.; Tesselaar, K.; Pillay, J.; Borghans, J. A. M.; Koenderman, L., What's your age again? Determination of human neutrophil half-lives revisited. *J. Leukoc. Biol.* **2013**, *94* (4), 595-601.
39. Borregaard, N., Neutrophils, from marrow to microbes. *Immunity* **2010**, *33* (5), 657-670.
40. Coffelt, S. B.; Wellenstein, M. D.; de Visser, K. E., Neutrophils in cancer: neutral no more. *Nat. Rev. Cancer* **2016**, *16* (7), 431-446.
41. Friedman, A. D., Transcriptional control of granulocyte and monocyte development. *Oncogene* **2007**, *26* (47), 6816-6828.
42. Görgens, A.; Radtke, S.; Möllmann, M.; Cross, M.; Dürig, J.; Horn, Peter A.; Giebel, B., Revision of the human hematopoietic tree: granulocyte subtypes derive from distinct hematopoietic lineages. *Cell Reports* **2013**, *3* (5), 1539-1552.
43. Hong, C.-W., Current understanding in neutrophil differentiation and heterogeneity. *Immune Netw.* **2017**, *17* (5), 298-306.
44. Pillay, J.; Tak, T.; Kamp, V. M.; Koenderman, L., Immune suppression by neutrophils and granulocytic myeloid-derived suppressor cells: similarities and differences. *Cell. Mol. Life Sci.* **2013**, *70* (20), 3813-3827.

45. Fliedner, T. M.; Cronkite, E. P.; Killmann, S. Å.; Bond, V. P., Granulocytopoiesis. II. emergence and pattern of labeling of neutrophilic granulocytes in humans. *Blood* **1964**, *24* (6), 683-700.
46. Nathan, C., Neutrophils and immunity: challenges and opportunities. *Nat. Rev. Immunol.* **2006**, *6* (3), 173-182.
47. Cowland, J. B.; Borregaard, N., Granulopoiesis and granules of human neutrophils. *Immunol. Rev.* **2016**, *273* (1), 11-28.
48. Lehrer, R. I.; Lu, W., α -Defensins in human innate immunity. *Immunol. Rev.* **2012**, *245* (1), 84-112.
49. Gennaro, R.; Zanetti, M., Structural features and biological activities of the cathelicidin-derived antimicrobial peptides. *Biopolymers* **2000**, *55* (1), 31-49.
50. Gabay, J. E.; Scott, R. W.; Campanelli, D.; Griffith, J.; Wilde, C.; Marra, M. N.; Seeger, M.; Nathan, C. F., Antibiotic proteins of human polymorphonuclear leukocytes. *Proc. Natl. Acad. Sci. U. S. A.* **1989**, *86* (14), 5610-5614.
51. Brogden, K. A., Antimicrobial peptides: pore formers or metabolic inhibitors in bacteria? *Nat. Rev. Micro.* **2005**, *3* (3), 238-250.
52. Pham, C. T. N., Neutrophil serine proteases: specific regulators of inflammation. *Nat. Rev. Immunol.* **2006**, *6* (7), 541-550.
53. Fleming, A.; B, M.; S, F. R. C., On a remarkable bacteriolytic element found in tissues and secretions. *Proc. R. Soc. Lond. B* **1922**, *93* (653), 306-317.
54. Edgeworth, J.; Gorman, M.; Bennett, R.; Freemont, P.; Hogg, N., Identification of p8,14 as a highly abundant heterodimeric calcium binding protein complex of myeloid cells. *J. Biol. Chem.* **1991**, *266* (12), 7706-7713.
55. Wright, G. W.; Ooi, C. E.; Weiss, J.; Elsbach, P., Purification of a cellular (granulocyte) and an extracellular (serum) phospholipase A2 that participate in the destruction of *Escherichia coli* in a rabbit inflammatory exudate. *J. Biol. Chem.* **1990**, *265* (12), 6675-6681.

56. Tardif, M.; Chapeton-Montes, J. A.; Posvanzic, A.; Nathalie, P.; Gilbert, C.; Tessier, P. A., Secretion of S100A8, S100A9, and S100A12 by neutrophils involves reactive oxygen species and potassium efflux. *J. Immunol. Res.* **2015**, *2015*, e296149.
57. Hurst, J. K., What really happens in the neutrophil phagosome? *Free Radic. Biol. Med.* **2012**, *53* (3), 508-520.
58. DeLeo, F. R.; Allen, L.-A. H.; Apicella, M.; Nauseef, W. M., NADPH oxidase activation and assembly during phagocytosis. *J. Immunol.* **1999**, *163* (12), 6732-6740.
59. Jiang, Q.; Griffin, D. A.; Barofsky, D. F.; Hurst, J. K., Intraphagosomal chlorination dynamics and yields determined using unique fluorescent bacterial mimics. *Chem. Res. Toxicol.* **1997**, *10* (10), 1080-1089.
60. Pan, L.; Zhang, X.; Song, K.; Tang, B.; Cai, W.; Wu, X.; Rupp, R. A.; Xu, J., Real-time imaging of autofluorescence NAD(P)H in single human neutrophils. *Appl. Opt.* **2009**, *48* (6), 1042-1046.
61. Brinkmann, V.; Reichard, U.; Goosmann, C.; Fauler, B.; Uhlemann, Y.; Weiss, D. S.; Weinrauch, Y.; Zychlinsky, A., Neutrophil extracellular traps kill bacteria. *Science* **2004**, *303* (5663), 1532-1535.
62. Brinkmann, V.; Zychlinsky, A., Beneficial suicide: Why neutrophils die to make NETs. *Nat. Rev. Micro.* **2007**, *5* (8), 577-582.
63. Li, P.; Li, M.; Lindberg, M. R.; Kennett, M. J.; Xiong, N.; Wang, Y., PAD4 is essential for antibacterial innate immunity mediated by neutrophil extracellular traps. *J. Exp. Med.* **2010**, *207* (9), 1853-1862.
64. Hood, M. I.; Skaar, E. P., Nutritional immunity: transition metals at the pathogen-host interface. *Nat. Rev. Microbiol.* **2012**, *10* (8).
65. Kehl-Fie, T. E.; Skaar, E. P., Nutritional immunity beyond iron: a role for manganese and zinc. *Curr. Opin. Chem. Biol.* **2010**, *14* (2), 218-224.
66. Weinberg, E. D., Nutritional immunity. Host's attempt to withhold iron from microbial invaders. *JAMA* **1975**, *231* (1), 39-41.

67. Cassat, James E.; Skaar, Eric P., Iron in infection and immunity. *Cell Host & Microbe* **2013**, *13* (5), 509-519.
68. Brophy, M. B.; Nolan, E. M., Manganese and microbial pathogenesis: sequestration by the mammalian immune system and utilization by microorganisms. *ACS Chem. Biol.* **2015**, *10* (3), 641-651.
69. Baker, H. M.; Baker, E. N., A structural perspective on lactoferrin function. *Biochem. Cell Biol.* **2012**, *90* (3), 320-328.
70. Loomis, L. D.; Raymond, K. N., Solution equilibria of enterobactin and metal-enterobactin complexes. *Inorg. Chem.* **1991**, *30* (5), 906-911.
71. Goetz, D. H.; Holmes, M. A.; Borregaard, N.; Bluhm, M. E.; Raymond, K. N.; Strong, R. K., The neutrophil lipocalin NGAL Is a bacteriostatic agent that interferes with siderophore-mediated iron acquisition. *Mol. Cell* **2002**, *10* (5), 1033-1043.
72. Canonne-Hergaux, F.; Calafat, J.; Richer, E.; Cellier, M.; Grinstein, S.; Borregaard, N.; Gros, P., Expression and subcellular localization of NRAMP1 in human neutrophil granules. *Blood* **2002**, *100* (1), 268-275.
73. Courville, P.; Chaloupka, R.; Cellier, M. F. M., Recent progress in structure–function analyses of Nramp proton-dependent metal-ion transporters This paper is one of a selection of papers published in this Special Issue, entitled CSBMCB — Membrane Proteins in Health and Disease. *Biochem. Cell Biol.* **2006**, *84* (6), 960-978.
74. Choby, J. E.; Skaar, E. P., Heme synthesis and acquisition in bacterial pathogens. *J. Mol. Bio.* **2016**, *428* (17), 3408-3428.
75. Corbin, B. D.; Seeley, E. H.; Raab, A.; Feldmann, J.; Miller, M. R.; Torres, V. J.; Anderson, K. L.; Dattilo, B. M.; Dunman, P. M.; Gerads, R.; Caprioli, R. M.; Nacken, W.; Chazin, W. J.; Skaar, E. P., Metal chelation and inhibition of bacterial growth in tissue abscesses. *Science* **2008**, *319* (5865), 962-965.

76. Hobbs, J. A.; May, R.; Tanousis, K.; McNeill, E.; Mathies, M.; Gebhardt, C.; Henderson, R.; Robinson, M. J.; Hogg, N., Myeloid cell function in MRP-14 (S100A9) null mice. *Mol. Cell. Biol.* **2003**, *23* (7), 2564-2576.
77. Sohnle, P.; Collinslech, C.; Wiessner, J., The zinc-reversible antimicrobial activity of neutrophil lysates and abscess fluid supernatants. *J. Infect. Dis.* **1991**, *164* (1), 137-142.
78. Murthy, A.; Lehrer, R.; Harwig, S.; Miyasaki, K., In-vitro candidastatic properties of the human neutrophil calprotectin complex. *J. Immunol.* **1993**, *151* (11), 6291-6301.
79. Loomans, H. J.; Hahn, B. L.; Li, Q.-Q.; Phadnis, S. H.; Sohnle, P. G., Histidine-based zinc-binding sequences and the antimicrobial activity of calprotectin. *J. Infect. Dis.* **1998**, *177* (3), 812-814.
80. Sohnle, P. G.; Hunter, M. J.; Hahn, B.; Chazin, W. J., Zinc-reversible antimicrobial activity of recombinant calprotectin (migration inhibitory factor—related proteins 8 and 14). *J. Infect. Dis.* **2000**, *182* (4), 1272-1275.
81. Brophy, M. B.; Hayden, J. A.; Nolan, E. M., Calcium ion gradients modulate the zinc affinity and antibacterial activity of human calprotectin. *J. Am. Chem. Soc.* **2012**, *134* (43), 18089-18100.
82. Damo, S. M.; Kehl-Fie, T. E.; Sugitani, N.; Holt, M. E.; Rathi, S.; Murphy, W. J.; Zhang, Y.; Betz, C.; Hench, L.; Fritz, G.; Skaar, E. P.; Chazin, W. J., Molecular basis for manganese sequestration by calprotectin and roles in the innate immune response to invading bacterial pathogens. *Proc. Natl. Acad. Sci. U. S. A.* **2013**, *110* (10), 3841-3846.
83. Brophy, M. B.; Nakashige, T. G.; Gaillard, A.; Nolan, E. M., Contributions of the S100A9 C-terminal tail to high-affinity Mn(II) chelation by the host-defense protein human calprotectin. *J. Am. Chem. Soc.* **2013**, *135* (47), 17804-17817.
84. Kehl-Fie, T. E.; Zhang, Y.; Moore, J. L.; Farrand, A. J.; Hood, M. I.; Rathi, S.; Chazin, W. J.; Caprioli, R. M.; Skaar, E. P., MntABC and MntH contribute to systemic

Staphylococcus aureus infection by competing with calprotectin for nutrient manganese. *Infect. Immun.* **2013**, *81* (9), 3395-3405.

85. Hood, M. I.; Mortensen, B. L.; Moore, J. L.; Zhang, Y.; Kehl-Fie, T. E.; Sugitani, N.; Chazin, W. J.; Caprioli, R. M.; Skaar, E. P., Identification of an *Acinetobacter baumannii* zinc acquisition system that facilitates resistance to calprotectin-mediated zinc sequestration. *PLOS Pathog.* **2012**, *8* (12), e1003068-e1003068.

86. Kehl-Fie, Thomas E.; Chitayat, S.; Hood, M. I.; Damo, S.; Restrepo, N.; Garcia, C.; Munro, Kim A.; Chazin, Walter J.; Skaar, Eric P., Nutrient metal sequestration by calprotectin inhibits bacterial superoxide defense, enhancing neutrophil killing of *Staphylococcus aureus*. *Cell Host & Microbe* **2011**, *10* (2), 158-164.

87. Garcia, Y. M.; Barwinska-Sendra, A.; Tarrant, E.; Skaar, E. P.; Waldron, K. J.; Kehl-Fie, T. E., A superoxide dismutase capable of functioning with iron or manganese promotes the resistance of *Staphylococcus aureus* to calprotectin and nutritional immunity. *PLOS Pathog.* **2017**, *13* (1), e1006125.

88. Liu, Janet Z.; Jellbauer, S.; Poe, A. J.; Ton, V.; Pesciaroli, M.; Kehl-Fie, T. E.; Restrepo, Nicole A.; Hosking, M. P.; Edwards, Robert A.; Battistoni, A.; Pasquali, P.; Lane, Thomas E.; Chazin, Walter J.; Vogl, T.; Roth, J.; Skaar, Eric P.; Raffatellu, M., Zinc sequestration by the neutrophil protein calprotectin enhances *Salmonella* growth in the inflamed gut. *Cell Host & Microbe* **2012**, *11* (3), 227-239.

89. Lupp, C.; Robertson, M. L.; Wickham, M. E.; Sekirov, I.; Champion, O. L.; Gaynor, E. C.; Finlay, B. B., Host-mediated inflammation disrupts the intestinal microbiota and promotes the overgrowth of Enterobacteriaceae. *Cell Host & Microbe* **2007**, *2* (2), 119-129.

90. Lisher, J. P.; Giedroc, D. P., Manganese acquisition and homeostasis at the host-pathogen interface. *Front. Cell. Infect. Microbiol.* **2013**, *3*.

91. Berry, A. M.; Paton, J. C., Sequence heterogeneity of PsaA, a 37-kilodalton putative adhesin essential for virulence of *Streptococcus pneumoniae*. *Infect. Immun.* **1996**, *64* (12), 5255-5262.
92. Coady, A.; Xu, M.; Phung, Q.; Cheung, T. K.; Bakalarski, C.; Alexander, M. K.; Lehar, S. M.; Kim, J.; Park, S.; Tan, M.-W.; Nishiyama, M., The *Staphylococcus aureus* ABC-type manganese transporter MntABC is critical for reinitiation of bacterial replication following exposure to phagocytic oxidative burst. *PLOS ONE* **2015**, *10* (9), e0138350.
93. McDevitt, C. A.; Ogunniyi, A. D.; Valkov, E.; Lawrence, M. C.; Kobe, B.; McEwan, A. G.; Paton, J. C., A molecular mechanism for bacterial susceptibility to zinc. *PLOS Pathog.* **2011**, *7* (11), e1002357.
94. Achouiti, A.; Vogl, T.; Endeman, H.; Mortensen, B. L.; Laterre, P.-F.; Wittebole, X.; Zoelen, M. A. D. v.; Zhang, Y.; Hoogerwerf, J. J.; Florquin, S.; Schultz, M. J.; Grutters, J. C.; Biesma, D. H.; Roth, J.; Skaar, E. P.; Veer, C. v. t.; Vos, A. F. d.; Poll, T. v. d., Myeloid-related protein-8/14 facilitates bacterial growth during pneumococcal pneumonia. *Thorax* **2014**, *69* (11), 1034-1042.
95. Nakashige, T. G.; Zhang, B.; Krebs, C.; Nolan, E. M., Human calprotectin is an iron-sequestering host-defense protein. *Nat. Chem. Biol.* **2015**, *11* (10), 765-771.
96. Nakashige, T. G.; Zygiel, E. M.; Drennan, C. L.; Nolan, E. M., Nickel sequestration by the host-defense protein human calprotectin. *J. Am. Chem. Soc.* **2017**, *139* (26), 8828-8836.
97. Benoit, S. L.; Miller, E. F.; Maier, R. J., *Helicobacter pylori* stores nickel to aid its host colonization. *Infect. Immun.* **2013**, *81* (2), 580-584.
98. Maroncle, N.; Rich, C.; Forestier, C., The role of *Klebsiella pneumoniae* urease in intestinal colonization and resistance to gastrointestinal stress. *Res. Microbiol.* **2006**, *157* (2), 184-193.

99. Gatermann, S.; John, J.; Marre, R., *Staphylococcus saprophyticus* urease: characterization and contribution to uropathogenicity in unobstructed urinary tract infection of rats. *Infect. Immun.* **1989**, *57* (1), 110-116.
100. Besold, A. N.; Gilston, B. A.; Radin, J. N.; Ramsoomair, C.; Culbertson, E. M.; Li, C. X.; Cormack, B. P.; Chazin, W. J.; Kehl-Fie, T. E.; Culotta, V. C., Role of Calprotectin in Withholding Zinc and Copper from *Candida albicans*. *Infect. Immun.* **2018**, *86* (2), e00779-17.
101. Steinbakk, M.; Naess-Andresen, C. F.; Lingaas, E.; Dale, I.; Brandtzaeg, P.; Fagerhol, M. K., Antimicrobial actions of calcium-binding leukocyte L1 protein, calprotectin. *Lancet* **1990**, *336* (8718), 763-765.
102. Pröpper, C.; Huang, X.; Roth, J.; Sorg, C.; Nacken, W., Analysis of the MRP8-MRP14 protein-protein interaction by the two-hybrid system suggests a prominent role of the C-terminal domain of S100 proteins in dimer formation. *J. Biol. Chem.* **1999**, *274* (1), 183-188.
103. Donato, R., Functional roles of S100 proteins, calcium-binding proteins of the EF-hand type. *Biochim. Biophys. Acta* **1999**, *1450* (3), 191-231.
104. Donato, R., S100: a multigenic family of calcium-modulated proteins of the EF-hand type with intracellular and extracellular functional roles. *Int. J. Biochem. Cell Biol.* **2001**, *33* (7), 637-668.
105. Linse, S.; Brodin, P.; Drakenberg, T.; Thulin, E.; Sellers, P.; Elmden, K.; Grundstroem, T.; Forsen, S., Structure-function relationships in EF-hand calcium-binding proteins. Protein engineering and biophysical studies of calbindin D9k. *Biochemistry* **1987**, *26* (21), 6723-6735.
106. Baudier, J.; Glasser, N.; Gerard, D., Ions binding to S100 proteins. I. Calcium- and zinc-binding properties of bovine brain S100 alpha alpha, S100a (alpha beta), and S100b (beta beta) protein: Zn²⁺ regulates Ca²⁺ binding on S100b protein. *J. Biol. Chem.* **1986**, *261* (18), 8192-8203.

107. Lee, Y.-H.; Tanner, J. J.; Larson, J. D.; Henzl, M. T., Crystal structure of a high-affinity variant of rat alpha-parvalbumin. *Biochemistry* **2004**, *43* (31), 10008-10017.
108. Yamniuk, A. P.; Nguyen, L. T.; Hoang, T. T.; Vogel, H. J., Metal ion binding properties and conformational states of calcium- and integrin-binding protein. *Biochemistry* **2004**, *43* (9), 2558-2568.
109. Gifford, Jessica L.; Walsh, Michael P.; Vogel, Hans J., Structures and metal-ion-binding properties of the Ca²⁺-binding helix-loop-helix EF-hand motifs. *Biochem. J.* **2007**, *405* (2), 199.
110. Kawasaki, H.; Nakayama, S.; Kretsinger, R. H., Classification and evolution of EF-hand proteins. *Biometals* **1998**, *11* (4), 277-295.
111. Vogl, T.; Roth, J.; Sorg, C.; Hillenkamp, F.; Strupat, K., Calcium-induced noncovalently linked tetramers of MRP8 and MRP14 detected by ultraviolet matrix-assisted laser desorption/ionization mass spectrometry. *J. Am. Soc. Mass Spectrom.* **1999**, *10* (11), 1124-1130.
112. Hayden, J. A.; Brophy, M. B.; Cunden, L. S.; Nolan, E. M., High-affinity manganese coordination by human calprotectin is calcium-dependent and requires the histidine-rich site formed at the dimer interface. *J. Am. Chem. Soc.* **2013**, *135* (2), 775-787.
113. Brini, M.; Ottolini, D.; Cali, T.; Carafoli, E., Calcium in health and disease. *Met. Ions Life Sci.* **2013**, *13*, 81-137.
114. Korndörfer, I. P.; Brueckner, F.; Skerra, A., The Crystal structure of the human (S100A8/S100A9)₂ heterotetramer, calprotectin, illustrates how conformational changes of interacting α -Helices can determine specific association of two EF-hand proteins. *J. Mol. Bio.* **2007**, *370* (5), 887-898.
115. Nakashige, T. G.; Stephan, J. R.; Cunden, L. S.; Brophy, M. B.; Wommack, A. J.; Keegan, B. C.; Shearer, J. M.; Nolan, E. M., The hexahistidine motif of host-defense protein human calprotectin contributes to zinc withholding and its functional versatility. *J. Am. Chem. Soc.* **2016**, *138* (37), 12243-12251.

116. Itou, H.; Yao, M.; Fujita, I.; Watanabe, N.; Suzuki, M.; Nishihira, J.; Tanaka, I., The crystal structure of human MRP14 (S100A9), a Ca²⁺-dependent regulator protein in inflammatory process¹¹Edited by R. Huber. *J. Mol. Bio.* **2002**, *316* (2), 265-276.
117. Ishikawa, K.; Nakagawa, A.; Tanaka, I.; Suzuki, M.; Nishihira, J., The structure of human MRP8, a member of the S100 calcium-binding protein family, by MAD phasing at 1.9 Å resolution. *Acta Cryst.* **2000**, *56* (5), 559-566.
118. Lin, H.; Andersen, G. R.; Yatime, L., Crystal structure of human S100A8 in complex with zinc and calcium. *BMC Struct. Biol.* **2016**, *16*, 8.
119. Chang, C.-C.; Khan, I.; Tsai, K.-L.; Li, H.; Yang, L.-W.; Chou, R.-H.; Yu, C., Blocking the interaction between S100A9 and RAGE V domain using CHAPS molecule: A novel route to drug development against cell proliferation. *Biochim. Biophys. Acta* **2016**, *1864* (11), 1558-1569.
120. Åkerström, B.; Björck, L., Bacterial surface protein L binds and inactivates neutrophil proteins S100A8/A9. *J. Immunol.* **2009**, *183* (7), 4583-4592.
121. Stork, M.; Grijpstra, J.; Bos, M. P.; Mañas Torres, C.; Devos, N.; Poolman, J. T.; Chazin, W. J.; Tommassen, J., Zinc piracy as a mechanism of *Neisseria meningitidis* for evasion of nutritional immunity. *PLoS Pathog.* **2013**, *9* (10), e1003733.
122. Anderson, J. E.; Sparling, P. F.; Cornelissen, C. N., Gonococcal transferrin-binding protein 2 facilitates but is not essential for transferrin utilization. *J. Bacteriol.* **1994**, *176* (11), 3162-3170.
123. Boulton, I. C.; Gorrings, A. R.; Allison, N.; Robinson, A.; Gorinsky, B.; Joannou, C. L.; Evans, R. W., Transferrin-binding protein B isolated from *Neisseria meningitidis* discriminates between apo and diferric human transferrin. *Biochem. J.* **1998**, *334* (Pt 1), 269-273.
124. Calmettes, C.; Alcantara, J.; Yu, R.-H.; Schryvers, A. B.; Moraes, T. F., The structural basis of transferrin sequestration by transferrin-binding protein B. *Nat. Struct. Mol. Biol.* **2012**, *19* (3), 358-360.

125. Cornelissen, C. N.; Kelley, M.; Hobbs, M. M.; Anderson, J. E.; Cannon, J. G.; Cohen, M. S.; Sparling, P. F., The transferrin receptor expressed by gonococcal strain FA1090 is required for the experimental infection of human male volunteers. *Mol. Microbiol.* **1998**, *27* (3), 611-616.
126. Jean, S.; Juneau, R. A.; Criss, A. K.; Cornelissen, C. N., *Neisseria gonorrhoeae* evades calprotectin-mediated nutritional immunity and survives neutrophil extracellular traps by production of TdfH. *Infect. Immun.* **2016**, *84* (10), 2982-2994.
127. Ehrchen, J. M.; Sunderkötter, C.; Foell, D.; Vogl, T.; Roth, J., The endogenous Toll-like receptor 4 agonist S100A8/S100A9 (calprotectin) as innate amplifier of infection, autoimmunity, and cancer. *J. Leukoc. Biol.* **2009**, *86* (3), 557-566.
128. Vogl, T.; Tenbrock, K.; Ludwig, S.; Leukert, N.; Ehrhardt, C.; van Zoelen, M. A. D.; Nacken, W.; Foell, D.; van der Poll, T.; Sorg, C.; Roth, J., Mrp8 and Mrp14 are endogenous activators of Toll-like receptor 4, promoting lethal, endotoxin-induced shock. *Nat. Med.* **2007**, *13* (9), 1042-1049.
129. Pålsson-McDermott, E. M.; O'Neill, L. A. J., Signal transduction by the lipopolysaccharide receptor, Toll-like receptor-4. *Immunology* **2004**, *113* (2), 153-162.
130. Giannini, T. L.; Teghanemt, A.; Zhang, D.; Esparza, G.; Yu, L.; Weiss, J., Purified monomeric ligand MD-2 complexes reveal molecular and structural requirements for activation and antagonism of TLR4 by Gram-negative bacterial endotoxins. *Immunol. Res.* **2014**, *59* (1-3), 3-11.
131. Loser, K.; Vogl, T.; Voskort, M.; Lueken, A.; Kupas, V.; Nacken, W.; Klenner, L.; Kuhn, A.; Foell, D.; Sorokin, L.; Luger, T. A.; Roth, J.; Beissert, S., The Toll-like receptor 4 ligands Mrp8 and Mrp14 are crucial in the development of autoreactive CD8+ T cells. *Nat. Med.* **2010**, *16* (6), 713-717.
132. Austermann, J.; Friesenhagen, J.; Fassl, S. K.; Ortkras, T.; Burgmann, J.; Barczyk-Kahlert, K.; Faist, E.; Zedler, S.; Pirr, S.; Rohde, C.; Müller-Tidow, C.; von Köckritz-Blickwede, M.; von Kaysenberg, C. S.; Flohé, S. B.; Ulas, T.; Schultze, J. L.; Roth, J.;

Vogl, T.; Viemann, D., Alarmins MRP8 and MRP14 induce stress tolerance in phagocytes under sterile inflammatory conditions. *Cell Reports* **2014**, 9 (6), 2112-2123.

Chapter 2: Calcium-Induced Tetramerization and Zinc Chelation Shield Human Calprotectin from Host and Bacterial Extracellular Proteases

This Chapter is adapted from *Chem. Sci.* **2016**, 7 (3), 1962-1975.

2.1. Introduction

Calprotectin (CP, S100A8/S100A9 oligomer, MRP-8/14 oligomer, calgranulins A and B) is an antimicrobial protein and important player in the human innate immune response and inflammation.¹⁻⁷ Neutrophils and epithelial cells express CP and release the protein into the extracellular space where it functions as an antimicrobial factor and a mediator of inflammation.⁸⁻¹³ Because of its remarkable biophysical properties and coordination chemistry, CP sequesters transition metal ions at sites of infection and thereby participates in the host metal-ion withholding response.¹³⁻²⁴ In addition, CP is reported to be an endogenous ligand of toll-like receptor 4 (TLR4) and thereby contributes to the host inflammatory response.^{11,25} Despite these established roles, little is known about the fate of CP following its release into the extracellular space. In considering the extracellular functions and fate of CP, we questioned how CP copes with the harsh environments that it encounters at sites of infection, inflammation, and in the intestinal lumen. These locales harbor a number of factors that pose challenges for the host-defense machinery, which include proteases as well as reactive oxygen and nitrogen species. Protease resistance is a hallmark of host-defense peptides, such as the defensins,^{26,27} that are abundant in these environments, and we reasoned that CP must resist attack by extracellular proteases. Indeed, full-length murine S100A8 and S100A9 subunits have been detected in murine tissue abscesses infected with *Staphylococcus aureus*.¹⁶ We hypothesized that changes in the quaternary structure of CP resulting from metal chelation contribute to protease resistance as described below. This notion is inspired by the defensins, which utilize disulfide bonds to achieve a three-stranded β -sheet fold that stabilizes the peptide backbone against proteolytic degradation,^{28,29} and metal-chelating proteins such as lactoferrin, which exhibits enhanced resistance to degradation by trypsin and chymotrypsin in its Fe(III)-bound form.^{30,31}

Human CP exhibits complex oligomerization³²⁻³⁷ and metal-binding properties.¹⁹⁻²⁴ It is a heterooligomer of the Ca(II)-binding S100 proteins S100A8 (93 amino acids, 10.8

kDa, α -subunit) and S100A9 (114 amino acids, 13.2 kDa, β -subunit).^{32,34,35} Apo human CP exists as a heterodimer ($\alpha\beta$).³² Each CP subunit exhibits two EF-hand domains, and Ca(II) ion binding results in formation of the CP heterotetramer ($\alpha_2\beta_2$).³⁴⁻³⁷ Each heterodimer also harbors two sites that form at the S100A8/S100A9 interface for chelating transition metal ions.^{17,19-24,36} In addition to affecting quaternary structure, Ca(II) ions also modulate the transition metal binding properties and antimicrobial activity of CP.^{19-22,24} Because extracellular Ca(II) levels are high, the CP heterotetramer is expected to be a relevant and abundant extracellular form.^{19,38} We therefore questioned whether Ca(II) binding to CP and consequent formation of the heterotetramer protects the scaffold against degradation by host and bacterial proteases. The proteolytic stability of CP is largely unexplored, and some of the results from published studies appear to be conflicting. Two independent studies demonstrated that the CP heterooligomer is more protease resistant than the S100A8 and S100A9 homodimers.^{39,40} One of these reports also found that CP in human leukocyte cell lysate was a poor substrate for trypsin and proteinase K in both the absence and presence of a Ca(II) and Zn(II) supplement.³⁹ A recent investigation evaluated the susceptibility of CP collected from human fecal matter to trypsin hydrolysis, and concluded that CP in fecal samples is susceptible to trypsin degradation.⁴¹ A complicating factor in evaluating and comparing the outcomes of these studies is that the speciation of the CP substrate is unknown and likely multifaceted (i.e. oligomeric state, metal-free versus metal-bound). To clarify whether CP resists protease attack and test our hypothesis that speciation plays a role, we sought to systematically evaluate how metal ions and quaternary structure influence proteolytic stability.

In this work, we report that Ca(II)-induced tetramerization protects CP from host serine proteases. Moreover, we establish that Zn(II) complexation protects the S100A8 C-terminus from the staphylococcal serine protease GluC. These data support a new dimension to how Ca(II) ions and transition metals modulate the function and fate of

extracellular CP, indicating that Ca(II) binding allows CP to sequester transition metals and resist attack by host proteases.

2.2. Experimental

2.2.1. General Materials and Methods

All solvents, reagents, and chemicals were obtained from commercial suppliers and used as received. All buffers and metal solutions were prepared using Milli-Q water (18.2 M Ω ·cm, 0.22- μ m filter, Millipore). For metal-binding experiments, HEPES buffer was prepared with Ultrol grade HEPES (free acid, Calbiochem) and TraceSELECT NaCl (Fluka), and aqueous TraceSELECT NaOH (Sigma) was used for pH adjustments. Disposable polypropylene spatulas were used to transfer buffer components. Buffers were treated with Chelex 100 resin (Biorad, 10 g/L) by stirring each buffer/Chelex mixture in a polypropylene beaker for at least 1 h, and the Chelex was removed by filtration through a 0.22- μ m filter. All buffers were stored in polypropylene bottles. A Tris buffer (1 mM Tris, 0.5 mM EDTA, pH 8.5) was prepared from Tris base (J. T. Baker) and EDTA disodium dihydrate (Mallinckrodt) and used for circular dichroism spectroscopy. The highest available purity of calcium chloride (99.99%) and manganese chloride (99.99%) were purchased from Alfa Aesar, and anhydrous zinc chloride (99.999%) and (NH₄)₂Fe(SO₄)₂·6H₂O (99.997%) were purchased from Sigma. Stock solutions of Ca(II) (370 mM), Mn(II) (1 M), Zn(II) (1 M) were prepared by using Milli-Q water and acid-washed volumetric glassware, and were stored in polypropylene tubes. The Fe(II) salt was weighed on the bench top, and then transferred to a polypropylene tube, and then brought into a Vacuum Atmospheres Company nitrogen glove box. The iron salt was dissolved to give a 100-mM stock solution using water that had been degassed with Ar. All iron-containing samples were prepared in the glove box using buffers that had been degassed with Ar. Working solutions of metals were prepared fresh for each experiment by diluting

the stock solution into buffer (75 mM HEPES, 100 mM NaCl, pH 7.5) or Milli-Q water. Protein concentration was determined by optical absorbance at 280 nm using a BioTek Synergy HT plate reader outfitted with a calibrated Take3 Micro-Volume plate, and the appropriate extinction coefficient (Table 2.1).

Table 2.1. Molecular weights and extinction coefficients for proteins used in this study.

Protein	Molecular Weight (Da)^a	ϵ_{280} (M⁻¹ cm⁻¹)^b
A8(C42S)	10 818.5	11 460
A8(C42S)(I60K)	10 833.5	11 460
A8(C42S)(I60E)	10 834.5	11 460
A8(C42S)(S90Stop)	10 336.9	11 460
A9(C3S)	13 094.7 ^c	6 990
Trypsin	23 300	30 000 ⁴⁶
Chymotrypsin	25 000	50 000 ⁴⁷
Glutamyl endopeptidase (GluC)	30 000	-
Human neutrophil elastase (HNE)	28 500	-

^a Molecular weights were calculated by using the ProtParam tool available on the ExPASy server (<http://web.expasy.org/protparam>). ^b Extinction coefficients (280 nm) were calculated by using the ProtParam tool. ^c In all preparations, LCMS revealed that the dominant purified species lacked the N-terminal methionine. The peptide molecular weight is the theoretical value for S100A9(C3S) lacking the N-terminal Met residue.

2.2.2. Instrumentation

An Agilent 1200 series instrument equipped with a thermostatted column compartment set to 20 °C, and a multi-wavelength detector set at 220 and 280 nm (500 nm reference wavelength with 100 nm bandwidth), was used to perform analytical high-performance liquid chromatography (HPLC). A Proto C4 column (5- μ m pore, 4.6 x 250 mm, Higgins Analytical Inc.) set at a flow rate of 1 mL/min was employed for all analytical

HPLC experiments. HPLC-grade acetonitrile (MeCN) and trifluoroacetic acid (TFA) were routinely purchased from EMD and Alfa Aesar, respectively. For all HPLC runs, solvent A was 0.1% TFA/H₂O and solvent B was 0.1% TFA/MeCN.

An Agilent 1260 series LC system equipped with an Agilent 6230 TOF system housing an Agilent Jetstream ESI source was employed to perform high-resolution mass spectrometry. An Agilent Poroshell 300SB-C18 (5- μ m pore) and denaturing protocol were utilized for all LC-MS analyses. Solvent A was 0.1% formic acid/H₂O. Solvent B was 0.1% formic acid/MeCN. Protein samples (5 μ M) were prepared in water and 1 μ L was injected for each analysis. The S100A8 and S100A9 subunits were eluted by using a gradient of 0-65% over 30 min. The resulting mass spectra were deconvoluted using the maximum entropy algorithm in MassHunter BioConfirm (Agilent).

Measurements of optical density (OD₆₀₀) of bacterial cultures and optical absorption spectroscopy were carried out with a Beckman Coulter DU 800 spectrophotometer thermostatted at 25 °C with a Peltier temperature controller. Fluorescence spectra were collected on a Photon Technologies International QuantaMaster 40 fluorimeter outfitted with a continuous xenon source for excitation, autocalibrated QuadraScopic monochrometers, a multimode PMT detector, and a circulating water bath maintained at 25 °C. This instrument was controlled by the FelixGX software package. FelixGX was used to integrate the emission spectra.

2.2.3. Protein Purification

Variants of human CP were overexpressed and purified as described previously.⁴² All variants are based on CP-Ser, which is composed of S100A8(C42S) and S100A9(C3S), and the protocol affords the S100A8/S100A9 heterodimer form of each variant. Protein yields for the variants I60E, I60K and Δ SHKE ranged from 12 to 35 mg/L of culture. The purified proteins were stored at -80 °C, and only thawed once immediately before use. Mass spectrometry analysis is presented in Table 2.2.

Table 2.2. Mass spectrometric analysis of CP-Ser and variants.

Protein	S100A8 Observed Mass (g/mol)	S100A9 Observed Mass ^a (g/mol)
CP-Ser	10 818.6	13 094.7
I60K	10 833.7	13 095.0
I60E	10 834.7	13 094.9
ΔSHKE	10 337.1	13 095.0

^a In all preparations, the dominant purified species of the S100A9 subunit lacked the N-terminal methionine. The masses reported here are the observed values for S100A9(C3S) lacking the N-terminal Met residue.

2.2.4. Site-Direction Mutagenesis

A modified Quick-Change site-directed mutagenesis protocol was employed to generate plasmids encoding S100A8(C42S)(I60K), S100A8(C42S)(I60E), and S100A8(C42S)(S90STOP). The *S100A8(C42S)* gene had been ligated into a vector pET41a vector using the *NdeI* and *XhoI* restriction sites. The mutagenesis primers are listed in Table 2.3. PCR amplification was carried out using PfuTurbo DNA polymerase. For the I60K and I60E variants, the PCR protocol was: 95 °C for 30 sec, 95 °C for 30 sec, 55 °C for 1 min, 68 °C for 15 min, (25 cycles), and 4 °C hold. For the ΔSHKE variant, the protocol was the same, but the annealing temperature was 51 °C. After PCR amplification, the template DNA was digested by *DpnI* (New England Biolabs) by adding 1 μL of the restriction enzyme to a 25-μL PCR reaction at t=0 and 1.5 h with incubation at 37 °C. The digestion products were transformed into chemically competent *E. coli* TOP10 cells. Overnight cultures (5 mL, 50 μg/mL kanamycin) were grown from single colonies. The plasmids were isolated using a miniprep kit (Qiagen). The presence of the mutations and fidelity of the protein coding sequences were verified by DNA sequencing (Quintara Biosciences).

Table 2.3. Primers employed for site-directed mutagenesis.

Primer	Sequence ^a
I60K-1	5'-GTTTAAGGAGTTGGAC <u>AAG</u> AACACGGATGGCGCTG-3'
I60K-2	5'-CAGCGCCATCCGTGTT <u>CTT</u> GTCCAACCTCCTTAAAC-3'
I60E-1	5'-GTTTAAGGAGTTGGAC <u>GAA</u> AACACGGATGGCGCTG-3'
I60E-2	5'-CAGCGCCATCCGTGTT <u>TTC</u> GTCCAACCTCCTTAAAC-3'
ΔSHKE-1	5'-GAAGAGCCACGAAGAG <u>TAA</u> CATAAAGAGTAACTC-3'
ΔSHKE-2	5'-GAGTTACTCTTTATG <u>TTA</u> CTCTTCGTGGCTCTTC-3'

^a The codons containing mutations are underlined and colored red.

2.2.4. Analytical Size-Exclusion Chromatography

An ÄKTA purifier (GE Lifesciences) housed in a 4 °C cold room and outfitted with a 100- μ L sample loop was used to perform all analytical size exclusion chromatography (SEC) experiments.¹⁹ A Superdex 75 10/300 GL column (GE Lifesciences) equilibrated in running buffer was calibrated with a low-molecular-weight calibration mixture (GE Lifesciences) as described previously.¹⁹ The protein of interest was thawed at room temperature and buffer exchanged from the storage buffer into the running buffer using a spin filter (0.5-mL, 10-kDa MWCO, Amicon), and the protein concentration was adjusted to 30 μ M by diluting with the running buffer. For the experiments with Ca(II), 600 μ M Ca(II) was included in the running buffer and protein sample. For experiments with Mn(II) or Fe(II) only, 300 μ M Mn(II) or Fe(II) was added to the sample only. For experiments with both Ca(II) and Mn(II) or both Ca(II) and Fe(II), the running buffer and sample contained 600 μ M Ca(II) and 33 μ M Mn(II) or 33 μ M Fe(II) was included in the sample only. Samples were incubated for 15 min at 4 °C after adding metals and then centrifuged at 13 000 rpm for 10 min. The entire volume of each sample (30 μ M protein, 300 μ L) was loaded onto the 100- μ L sample loop. The loop was emptied with 0.5 mL of running buffer, and the protein was eluted over one column volume at a flow rate of 0.5 mL/min at 4 °C. Iron-

containing samples were allowed to incubate for 50 min in the glove box before being centrifuged at 13 000 rpm for 10 min.

2.2.5. Sedimentation Velocity Experiments

A Beckman XL-I Analytical ultracentrifuge outfitted with an An-60 Ti rotor was employed for all sedimentation velocity (SV) experiments. The rotor housed conventional double-sector charcoal filled Epon centerpieces within the sample cells and contained quartz (absorption optics) or sapphire (interference optics) windows. The absorption wavelength for optical detection was 280 nm. The samples were centrifuged at 42 000 rpm and 20 °C until sedimentation was complete. SEDNTERP⁴³ was employed to calculate the buffer viscosity (η), buffer density (ρ), and protein partial specific volume (\bar{v}) at 20 °C. The sedimentation velocity data was analyzed using previously described methods,⁴⁴ and full details in Tables 2.4 and 2.5. Hydrodynamic modeling computations were performed with HYDROPRO⁴⁵ using the crystal structures of Ca(II)-bound CP-Ser (PDB 1XK4³⁶) and Ca(II)-, Na(I)- and Mn(II)-bound CP-Ser (PDB 4XJK²²) to obtain theoretical sedimentation coefficients for the CP-Ser heterodimer and heterotetramer. All modeling was carried out with buffer viscosity (η) and buffer density (ρ) of water at 20 °C and a protein partial specific volume (\bar{v}) of 0.7388 mL/g.

One day prior to an experiment, each protein sample was thawed and diluted to 27 μ M in 75 mM HEPES, 100 mM NaCl at pH 7.5. The resulting samples were dialyzed against 1 L of the same buffer containing 10 g of Chelex resin at 4 °C overnight. The dialyzed samples were transferred to 1.7-mL polypropylene tubes and centrifuged (13 000 rpm, 5 min, 4 °C) to sediment any Chelex resin. Aliquots of the dialysis buffer were centrifuged (3 000 rpm, 5 min, 4 °C) in 50-mL polypropylene tubes and the supernatant was used for the reference samples in the SV experiment. In select experiments, EDTA (1.35 mM), Ca(II) (540 μ M), and/or Mn(II) (30 μ M) were added to the reference and protein samples. The references and protein samples were allowed to incubate while the SV

window assemblies were constructed (≈ 1.5 h). The SV window assemblies were loaded with 410 μL of reference buffer and 400 μL of protein containing sample.

2.2.6. *Protease Digestion Assays*

Trypsin (Affymetrix) and chymotrypsin (Amresco) were obtained as lyophilized powders, stored at 4 $^{\circ}\text{C}$, and dissolved water to afford solutions of ≈ 50 -100 μM immediately before use. Reported extinction coefficients for trypsin and chymotrypsin were used to determine the protein concentrations (Table 2.1).^{46,47} Frozen stock solutions of glutamyl endopeptidase (GluC) (New England Biolabs), and human neutrophil elastase (HNE) (Enzo Life Sciences) were obtained as lyophilized powders. The entire portion of each protease was dissolved in assay buffer to afford solutions with concentrations of ≈ 0.1 mg/mL and ≈ 1 mg/mL for GluC and HNE, respectively. The solutions were stored at -20 $^{\circ}\text{C}$ (GluC) or -80 $^{\circ}\text{C}$ (HNE). Protease digestion assays were performed on a 350- μL scale at pH 7.5 (75 mM HEPES, 100 mM NaCl). Aliquots of CP-Ser, I60E, and I60K were thawed at room temperature and diluted to 30 μM using the assay buffer in 1.7-mL microcentrifuge tubes. To select samples, Ca(II) (1.5 mM), Mn(II) (30 μM), and Zn(II) (60 μM) were added, and the resulting solutions were incubated at room temperature for at least 15 min prior to the assay. To initiate each digestion assay, an aliquot (between 5 and 10 μL as appropriate) of protease was added to the 350- μL protein solution to bring the protease concentration to 0.45 μM (trypsin) or 0.3 μM (others). The resulting solution was immediately mixed with a pipet and incubated at 37 $^{\circ}\text{C}$. Aliquots (45 μL) of the reaction were quenched with 155 μL of aqueous 0.77% (v/v) TFA at $t = 0, 0.5$ min, 1, 2, 3, and 4 h. The quenched solutions were centrifuged (13 000 rpm, 10 min, 4 $^{\circ}\text{C}$), and the resulting samples were analyzed by analytical HPLC using a solvent gradient of 10–60% B over 50 min. S100A8 eluted at ≈ 38 min (depending on the variant) and S100A9 eluted at 39.8 min. Select peaks were collected manually and further analyzed by LC-MS. Controls without protease were prepared, quenched, and analyzed in an identical manner

except that ubiquitin (Sigma) was added to 0.3 μM because it was found to improve consistency in peak intensity between runs. Frozen stocks of ubiquitin (117 μM , 1 mg/mL) were prepared in water, stored at $-20\text{ }^{\circ}\text{C}$, and thawed before use.

2.2.7. Protease Activity Assays

To determine if the metals used in the digestion assays altered protease activity, enzymatic activity assays using small molecule substrates were performed in the absence and presence of metals. Protease stock solutions were prepared as described above. All experiments were carried out in triplicate and averaged. For trypsin, N_{α} -benzoyl-L-arginine ethyl ester HCl (BAEE, Santa Cruz Biotech) was dissolved to 10 mM in 75 mM HEPES, 100 mM NaCl, pH 7.5, and then diluted to 80 μM in the same buffer with 1.5 mM Ca(II) with or without 30 μM Mn(II). These solutions were dispensed into quartz cuvettes (Starna), 1 mL of solution per cuvette. The reaction was initiated by adding trypsin to 8.4 nM in a cuvette and briefly shaking. The reaction was monitored continuously at 253 nm. An analogous experiment was carried out to assay the activities of chymotrypsin and human neutrophil elastase (HNE). For chymotrypsin, the substrate N -succinyl-Ala-Ala-Pro-Phe p -nitroanilide (Enzo Life Sciences) was dissolved to 40 mM in dimethylformamide. In the experiment, the chymotrypsin was diluted to 2 nM and the substrate concentration was 0.4 mM. The chymotrypsin reactions were continuously monitored at 410 nm in quartz cuvettes. For HNE, the substrate N -succinyl-Ala-Ala-Val-Ala p -nitroanilide (Santa Cruz Biotech) was dissolved to 100 mM dimethylsulfoxide. In the assay, HNE was diluted to 10 nM, and the substrate was 0.5 mM. The HNE reactions were continuously monitored at 410 nm in polystyrene cuvettes.

The activity of glutamyl endopeptidase (GluC) was assayed with carboxybenzyl-Leu-Leu-Glu- β -naphthylamide. A 1-mM stock solution of the substrate was made in dimethylsulfoxide. The reactions were carried out on a 1-mL scale in quartz cuvettes (Starna), and monitored by fluorescence. In the assays with Ca(II) or Mn(II), the substrate

was diluted to 100 μ M. For the assays with Zn(II) (60 μ M), CP-Ser (30 μ M) and Zn(II) were combined in the assay buffer and the GluC substrate was added last. This modification was made because precipitation occurred when Zn(II) was introduced into solutions containing the substrate. The reactions were initiated by adding GluC to 67 nM. The reaction was monitored by fluorescence spectroscopy with all slits set to 0.8 mm, excitation at 340 nm. The progress of the reaction was determined by monitoring the fluorescence emission at 410 nm. The results from these assays are presented in Appendix 1.

2.2.8. Antimicrobial Activity Assays

The growth inhibitory activities of CP-Ser, I60K, I60E, and Δ SHKE against *Escherichia coli* ATCC 25922, *Staphylococcus aureus* ATCC 25923 and *Lactobacillus plantarum* WCFS1 (CP-Ser and Δ SHKE only) were assayed at 30 °C as described previously.^{19,24} The antimicrobial activity assay medium, hereafter AMA medium, was a 62:38 ratio of 20 mM Tris-HCl, pH 7.5, 100 mM NaCl, 5 mM BME, 3 mM Ca(II) and tryptic soy broth (TSB) with 0.25% (w/v) dextrose. For *L. plantarum*, MRS broth (CRITERION) without additional dextrose was used in place of TSB. To prevent evaporation of the medium, the plates were sealed with parafilm and a beaker of water was housed in the incubator shaker.

2.2.9. Antimicrobial Activity Assay with Trypsin

The growth inhibitory activities of CP-Ser, I60E and I60K pre-incubated with trypsin (Affymetrix) were assayed by modifying a literature protocol for standard antimicrobial activity assays.¹⁹ Protein aliquots were thawed at room temperature and buffer exchanged into AMA buffer (20 mM Tris-HCl, 100 mM NaCl, 3 mM Ca(II)) three times using spin filters (0.5 mL, 10-kDa MWCO, Amicon) that were sterilized by exposure to UV light for 15 min. For each protein, two aliquots (233 μ M, 45 μ L) were prepared. Trypsin

(≈ 2 mg) was dissolved in AMA buffer, the trypsin concentration was determined using the reported extinction coefficient ($\epsilon_{280} = 30\,000\text{ M}^{-1}\text{cm}^{-1}$, Table 2.1)⁴⁶ and the sample was diluted to $4.5\ \mu\text{M}$ using AMA buffer. For each set of $45\text{-}\mu\text{L}$ protein aliquots, a $5\text{-}\mu\text{L}$ aliquot of trypsin was added to one and a $5\text{-}\mu\text{L}$ aliquot of AMA buffer to the other. A trypsin-only solution was prepared that contained $0.45\ \mu\text{M}$ trypsin and no protein substrate. The solutions were incubated at $37\ ^\circ\text{C}$ for ≈ 20 h and subsequently used in the antibacterial activity assay.

E. coli ATCC 25922 was inoculated into 5 mL of TSB containing 0.25% (w/v) dextrose and grown overnight at $37\ ^\circ\text{C}$ in a rotating wheel (≈ 16 h). The culture was diluted 1:100 into 5 mL of fresh TSB with (0.25% w/v) dextrose and grown with shaking ($37\ ^\circ\text{C}$, ≈ 2 h) until the OD_{600} reached 0.6. The culture was diluted 1:500 into fresh AMA medium. The antibacterial activity assay was carried out in sterile polystyrene 96-well plates (Corning). Each well contained $10\ \mu\text{L}$ of the digested protein, undigested protein (no protease control), trypsin only, or buffer only and $90\ \mu\text{L}$ of the diluted bacterial culture. Control wells containing $10\ \mu\text{L}$ of trypsin and $90\ \mu\text{L}$ of sterile AMA medium were also included, and no bacterial growth was observed in these wells. The final concentration of each CP-Ser sample was $500\ \mu\text{g/mL}$ ($21\ \mu\text{M}$), and previous work has shown that CP-Ser inhibits growth of *E. coli* and *S. aureus* at this concentration.^{19,21} Each condition was set up in triplicate. Each plate was sealed with parafilm and incubated at $30\ ^\circ\text{C}$ with shaking at 150 rpm in a tabletop incubator-shaker containing a beaker filled with water. Bacterial growth was monitored by OD_{600} values, which were measured at two time points (0 to 20 h) by using a plate reader (BioTek). Three independent replicates were conducted on different days. Different *E. coli* freezer stocks were used for each replicate, and at least two independent medium preparations were employed, and two different preparations of each protein were used over the triplicate. The resulting averages and standard errors of the mean are reported ($n=9$).

2.2.10 *Mn(II) Competition Experiments with ZP1*

Competition between CP variants and Zinpyr-1 (ZP1) for Mn(II) using an established assay where Mn(II) was titrated into a solution of 1 μ M ZP1 and 4 μ M CP-Ser or variant.²⁰ Averages and the standard deviations are reported ($n=3$). Experiments to measure the number of equivalents of Ca(II) required for CP variants to outcompete ZP1 for Mn(II) were carried out as previously described, but the ZP1 and Mn(II) concentrations were 1 μ M and 3.5 μ M, respectively.²⁰

2.2.11. *Circular Dichroism Spectroscopy*

An Aviv Model 202 circular dichroism (CD) spectrometer thermostatted at 25 °C was employed for CD spectroscopy. A 1-mm path-length CD cell (Hellma) was employed for all CD measurements. All protein samples (10 μ M protein, 300 μ L, 1 mM Tris, 0.5 mM EDTA, pH 8.5, \pm 2 mM Ca(II)) were made at the same time before beginning data acquisition. Wavelength scans were carried out from 190-260 nm with 1-nm steps (5 s averaging time, three averaged scans).

2.3. Results and Discussion

2.3.1 *Design and Preparation of Tetramer-Deficient Variants of CP*

In order to investigate whether Ca(II)-induced tetramerization of human CP affords protease resistance, we sought to compare the stabilities of Ca(II)-bound heterodimers and Ca(II)-bound heterotetramers in protease degradation assays. These experiments require CP variants that remain heterodimeric following Ca(II) complexation. The crystal structure of Mn(II), Ca(II)-, and Na(I)-bound CP-Ser (PDB 4XJK²²) reveals that the tetramer interface between CP heterodimers is \approx 3700 \AA^2 and largely comprised of contacts between the S100A8 subunits. Moreover, a cluster of hydrophobic residues occurs at the heterotetramer interface (Figure 2.1). The S100A8 subunit of each

heterodimer contributes (A8)Ile60 and (A8)Ile73, and (A8)Ile76 (not shown), and the S100A9 subunits contribute (A9)Trp88. We hypothesized that this hydrophobic region is a “hot spot” for tetramerization,⁴⁸ and reasoned that point mutations of the hydrophobic residues may provide the requisite CP-Ser variants that retain the ability to coordinate Ca(II) but cannot undergo Ca(II)-induced tetramerization. We mutated (A8)Ile60 to Glu and Lys as a case study, and focus on these variants herein. We reasoned that introduction of charged residues at position 60 of S100A8 should disfavor tetramerization by decreasing the hydrophobic driving force and introducing electrostatic repulsion.

Moreover, the parity of charges introduced by the Glu and Lys mutations provides a control to minimize the likelihood that any biophysical or functional differences between CP and the variants are artifacts of a given amino acid substitution. Lastly, it was important to preserve the metal-binding properties of CP. Because (A8)Ile60 does not contribute to metal-ion coordination and is distant from both the EF-hand domains and the transition metal binding sites (His₃Asp, His_{4/6}), we reasoned that mutating this residue would not perturb the metal-ion coordination spheres. We abbreviate the CP-Ser variants bearing the (A8)Ile60Glu and (A8)Ile60Lys mutations I60E and I60K, respectively.

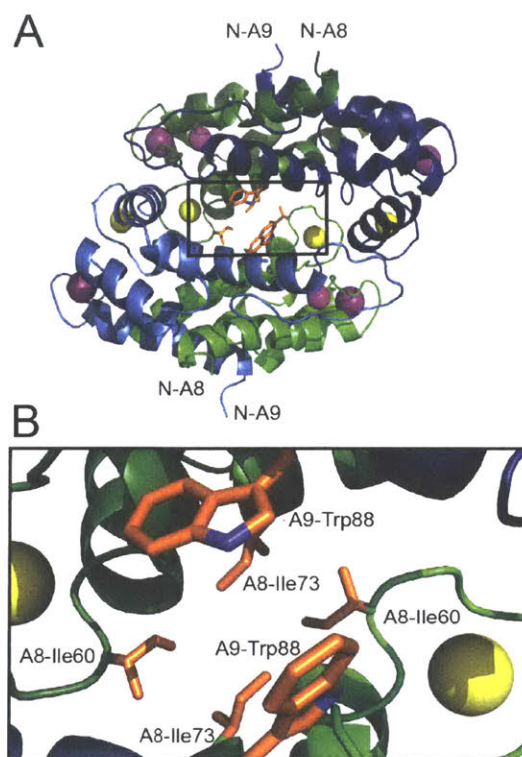


Figure 2.1. Crystal structure of the Ca(II)-, Na(I)-, and Mn(II)-bound human CP-Ser heterotetramer (PDB: 4XJK).²² (A) The heterotetramer with select hydrophobic residues at the tetramer interface shown as sticks. The outlined box corresponds to the region displayed in panel B. (B) An expanded view of the heterotetramer interface that illustrates the clustering of hydrophobic side chains. The green chains are the S100A8 subunits and the blue chains are the S100A9 subunits. One heterodimer is depicted in dark shading and the second heterodimer is depicted in light shading. The Ca(II) ions are shown as yellow spheres, the Na(I) ions are shown as purple spheres, and the Mn(II) ions are shown as magenta spheres.

We prepared pET41a-S100A8(C42S)(I60E) and pET41a-S100A8(C42S)(I60K) plasmids by site-directed mutagenesis, and we overexpressed and purified I60E and I60K as described previously for CP-Ser.¹⁹ The variants were obtained in yields of approximately 28 and 15 mg/L of culture, respectively. The proteins were isolated as the $\alpha\beta$ heterodimers in high purity, and the S100A8 and S100A9 subunits were present in equal amounts as judged by gel electrophoresis (Figure A2.1). The identities of the subunits were confirmed by mass spectrometry (Table 2.2), and circular dichroism spectroscopy verified that the mutations did not affect the overall α -helical secondary

structure of the CP scaffold (Figure A2.2). We employed two established competition assays to probe the metal-binding properties of I60E and I60K.²⁰ First, a competition titration employing the fluorescent metal-ion sensor Zinpyr-1 (ZP1, apparent $K_{d1,Mn} = 550$ nM)⁴⁹ confirmed that I60E and I60K coordinate Mn(II) with high affinity when excess Ca(II) is included in the buffer. Like CP-Ser, both variants outcompeted ZP1 for Mn(II) in the presence of excess Ca(II), which indicated that the apparent $K_{d,Mn}$ value of each variant is less than 550 nM (Figure A2.3). Moreover, titration of Ca(II) into a solution containing ZP1, Mn(II), and protein demonstrated that CP-Ser, I60E and I60K show comparable Ca(II)-dependent Mn(II)-binding properties. Each protein required ≈ 20 equivalents of Ca(II) to fully sequester Mn(II) from ZP1 (Figure A2.4). Taken together, the results from these titrations demonstrate that the Mn(II)-binding properties of I60E and I60K are calcium dependent, and that these variants behave like CP-Ser, at least in the context of ZP1 competition assays.

2.3.2. *(S100A8)I60E and (S100A8)I60K Mutations Disrupt Ca(II)-Induced Tetramerization*

To probe whether the I60E and I60K variants display perturbed oligomerization properties in the presence of Ca(II), we employed analytical size-exclusion chromatography (SEC), and determined the elution volumes and corresponding molecular weights of the proteins of in the absence and presence of excess Ca(II) (Figure 2.2). In this set of experiments, apo CP-Ser (30 μ M) exhibited a peak elution volume at 11.5 mL (≈ 35 kDa), and the peak shifted to 10.7 mL (≈ 48 kDa) when excess Ca(II) (600 μ M) was included in the running buffer (75 mM HEPES, 100 mM NaCl, pH 7.5). This behavior was in agreement with our prior analytical SEC studies of CP-Ser,¹⁹ and demonstrates the expected Ca(II)-dependent formation of the $\alpha_2\beta_2$ tetramer (Figure 2.2). Apo I60E and I60K exhibited the same peak elution volume as apo CP-Ser, indicating that the mutants are heterodimers in the absence of Ca(II) (Figure 2.2). In contrast to CP-

Ser, both I60E and I60K exhibited a slight peak shift to a later elution volume (11.8 mL, \approx 31 kDa) when Ca(II) (600 μ M) was included in the running buffer (Figure 2.2). This behavior suggests that (i) I60E and I60K bind Ca(II), which is in agreement with the competition titrations described above; (ii) Ca(II) complexation causes the hydrodynamic radii of I60E and I60K to decrease relative to the apo proteins; and (iii) Ca(II)-bound I60E and I60K do not form $\alpha_2\beta_2$ heterotetramers under these experimental conditions.

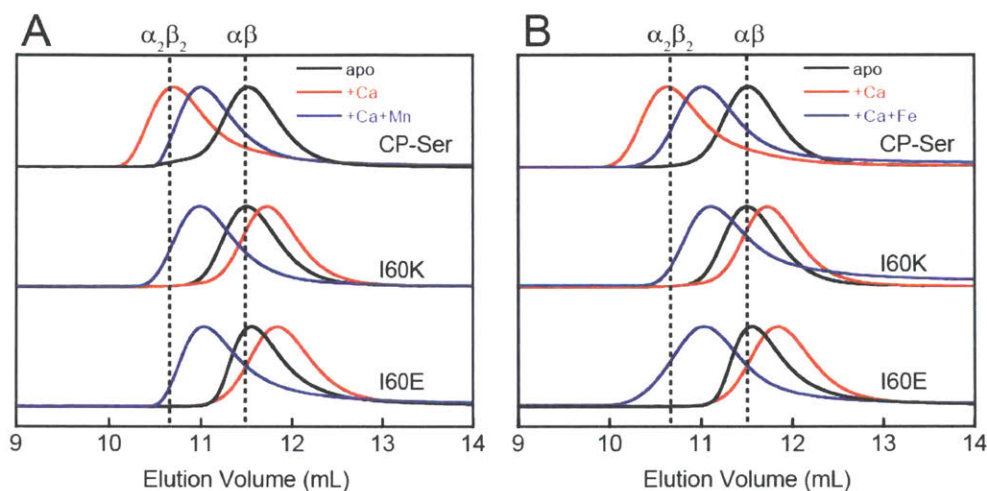


Figure 2.2. Analytical SEC traces of CP-Ser, I60E and I60K (30 μ M) in absence and presence of various metals (75 mM HEPES, 100 mM NaCl, pH 7.5, 4 $^{\circ}$ C). (A) Black traces, no metal added. Red traces, 600 μ M Ca(II) in running buffer and protein sample. Blue traces, 600 μ M Ca(II) in running buffer and sample, 33 μ M Mn(II) in the protein sample only. (B) Black traces, no metal added. Red traces, 600 μ M Ca(II) in running buffer and protein sample. Blue traces, 600 μ M Ca(II) in running buffer and sample, 33 μ M Fe(II) in the protein sample only. Each chromatogram was normalized to a maximum peak value of 1. The vertical dashed lines indicate the peak elution volumes of the $\alpha\beta$ (-Ca) and the $\alpha_2\beta_2$ (+Ca) forms of CP-Ser. Chromatograms for CP-Ser, I60E and I60K pre-incubated with Mn(II) only and Fe(II) only are provided in Figures A2.5 and A2.6.

To confirm that the I60E and I60K mutations disrupted Ca(II)-induced tetramerization, we employed analytical ultracentrifugation (AUC) and determined sedimentation coefficients for CP-Ser, I60E, and I60K in the absence and presence of 20 equivalents of Ca(II) (75 mM HEPES, 100 mM NaCl, pH 7.5). We obtained theoretical sedimentation coefficients ($s_{20,w}$) using HYDROPRO⁴⁵ and the available CP-Ser crystal

structures as models (PDB 1XK4,³⁶ 4GGF,²³ and 4XJK²²). HYDROPRO afforded predicted sedimentation coefficients of 2.1 S and 3.7 S for the heterodimer and heterotetramer, respectively. We also determined the maximum theoretical sedimentation coefficient for the heterodimer and heterotetramer to be 2.8 S and 4.5 S, respectively.⁵⁰

The sedimentation distributions of apo CP-Ser, I60E, and I60K determined using SEDFIT each displayed a single major species with an S value between 2.3 S and 2.4 S (Figure 2.3 and Table 2.4), which are in agreement with the predicted S value for the heterodimer. When 20 equivalents of Ca(II) were added to the sample, the sedimentation distribution for CP-Ser was dominated by a single species at 3.7 S, which corresponds to the predicted S value for the $\alpha_2\beta_2$ heterotetramer (Figure 2.3 and Table 2.4). In contrast, the major species for both I60E and I60K remained at \approx 2.3 S when the samples contained excess Ca(II). In agreement with the SEC experiments, the AUC data demonstrate that I60E and I60K remain heterodimeric with Ca(II). Analysis of the AUC data using DCDT+ afforded the same conclusions (Figure 2.4 and Table 2.5).

2.3.3. I60E and I60K Variants Form Heterotetramers in the Presence of Mn(II) or Fe(II)

CP coordinates Mn(II) with high affinity at a hexahistidine site comprised of (A8)His17, (A8)His27, (A9)His91, (A9)His95, (A9)His103, and (A9)His105.²¹⁻²³ Prior analytical SEC studies revealed that preincubation of CP-Ser ($\alpha\beta$, -Ca) with 10 equivalents of Mn(II) results in a new peak (11.0 mL, \approx 43 kDa) that elutes between the apo heterodimer and Ca(II)-bound heterotetramer (Figure A2.5).^{20,21} In contrast, preincubation of I60E and I60K with 10 equivalents of Mn(II) and no Ca(II) afforded peaks with the same peak elution volumes as the apo heterodimer (11.5 mL, \approx 35 kDa). Nevertheless, the peaks broadened under these conditions, which indicates that the samples contain heterotetramers as well as heterodimers (Figure A2.5). To determine the effect of Mn(II) and Ca(II) on the elution properties of I60K and I60E, the proteins (30 μ M) were pre-incubated with 20 equivalents of Ca(II) and 1.1 equivalents of Mn(II),

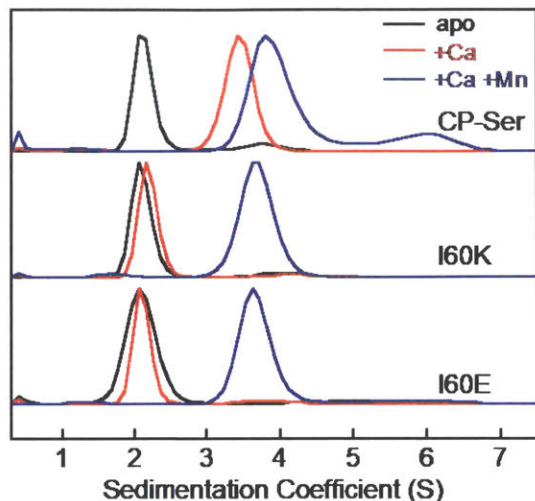


Figure 2.3. Sedimentation distributions of CP-Ser, I60E, and I60K (27.5 μM) obtained with the $c(s)$ model in SEDFIT. (75 mM HEPES, 100 mM NaCl, pH 7.5, 20 $^{\circ}\text{C}$). Black traces, no metal added. The CP-Ser sample included 550 μM EDTA. Red traces, 550 μM of Ca(II) in the sample. Blue traces, 550 μM Ca(II) and 27.5 μM Mn(II) in the sample. Each sedimentation distribution is normalized to the maximum $c(s)$.

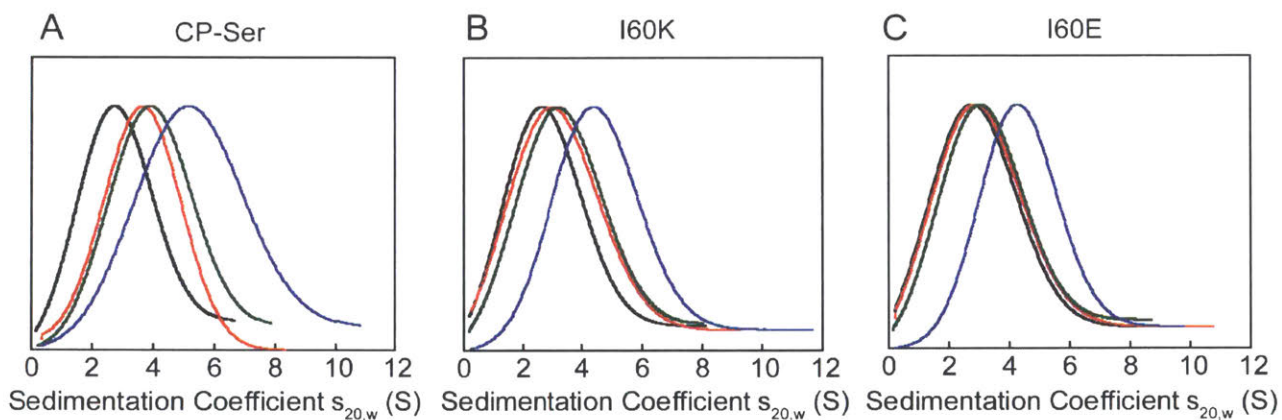


Figure 2.4. Sedimentation coefficient distributions of CP-Ser (A), I60K (B), and I60E (C) (27.5 μM) obtained using DCDT+. Buffer: 75 mM HEPES, 100 mM NaCl, ± 540 μM Ca(II), ± 27.5 μM Mn(II), pH 7.5 at 20 $^{\circ}\text{C}$. For apo CP-Ser, 1.35 mM EDTA was included and no metals were added. The data are normalized to a maximum peak height of 1.

Table 2.4. Calculated sedimentation coefficients using Sedfit^a

Protein	Concentration (μM)	$s_{20,w}$ (S)	MW (kDa)	Partial Specific Volume (mL/g)
CP-Ser ^b	27.5	2.4	22.7	0.7388
CP-Ser ^d	27.5	3.9	43.5	0.7388
CP-Ser ^e	27.5	2.4 (35%), 4.1 (65%)	20.6, 46.1	0.7388
CP-Ser ^f	27.5	4.5 (85%), 6.5 (15%)	40.8, 70.8	0.7388
I60K ^c	27.5	2.4	23.0	0.7388
I60K ^d	27.5	2.4	24.1	0.7388
I60K ^e	27.5	2.4 (73%), 4.1 (27%)	22.9, 51.3	0.7388
I60K ^f	27.5	4.1 S	43.7	0.7388
I60E ^c	27.5	2.3	22.8	0.7388
I60E ^d	27.5	2.3	24.9	0.7388
I60E ^e	27.5	2.2 (84%), 3.9 (16%)	23.8, 56.0	0.7388
I60E ^f	27.5	4.0	44.9	0.7388

^aAll experiments were conducted at 20 °C. The units of viscosity are in centipoise (cP) (1 Poise $\text{g cm}^{-1} \text{s}^{-1}$). Sedimentation coefficients are in Svedbergs (1 Svedberg = 100 fs = 1×10^{-13} s). The c(s) method was used for fitting the data. All scans that began at the baseline were used in fitting. ^bThe sample buffer was 75 mM HEPES, 100 mM NaCl, 1.35 mM EDTA, pH 7.5. $s_{20,w}$ values were adjusted with solvent density (ρ) of 1.00825 g/mL, solvent viscosity (η) of 1.0563 cP. ^cThe sample buffer was 75 mM HEPES, 100 mM NaCl, pH 7.5 $s_{20,w}$ values were adjusted with solvent density (ρ) of 1.0082 g/mL, solvent viscosity (η) of 1.0565 cP pH 7.5 at 20 °C. ^dThe sample buffer was 75 mM HEPES, 100 mM NaCl, 540 μM Ca(II) (20 equivalents), pH 7.5. The parameters for converting to $s_{20,w}$ from ^c were used. ^eThe sample buffer was 75 mM HEPES, 100 mM NaCl, 27.5 μM Mn(II), pH 7.5. The parameters from ^c for converting to $s_{20,w}$ were used. ^fThe sample buffer was 75 mM HEPES, 100 mM NaCl, 540 μM Ca(II), (20 equivalents), 27.5 μM Mn(II), pH 7.5. The parameters from ^c for converting to $s_{20,w}$ were used.

Table 2.5. Calculated sedimentation coefficients using DCDT+^a

Protein	Concentration (μM)	$s_{20,w}$ (S)	D (F)	MW (kDa)	Partial Specific Volume (mL/g)
CP-Ser ^b	27.5	2.4	12.0	18.8	0.7388
CP-Ser ^c	27.5	3.8	7.80	45.3	0.7388
CP-Ser ^d	27.5	3.6	10.7	31.2	0.7388
CP-Ser ^e	27.5	4.8	12.5	35.6	0.7388
I60K ^b	27.5	2.3	11.8	18.7	0.7388
I60K ^c	27.5	2.6	13.3	17.9	0.7388
I60K ^d	27.5	2.8	12.3	13.5	0.7388
I60K ^e	27.5	4.1	8.9	42.8	0.7388
I60E ^b	27.5	2.4	10.8	20.9	0.7388
I60E ^c	27.5	2.5	10.8	22.3	0.7388
I60E ^d	27.5	2.7	13.4	18.8	0.7388
I60E ^e	27.5	4.0	8.4	44.4	0.7388

^aAll experiments were conducted at 20 °C. The units of viscosity are in centipoise (cP) (1 Poise $\text{g cm}^{-1} \text{s}^{-1}$). Sedimentation coefficients are in Svedbergs (1 Svedberg = 100 fs = 1×10^{-13} s). Diffusion coefficients correspond to the best-fit molecular mass in Fick units (1 Fick = 1×10^{-7} cm^2/s). The dc/dt method was used for all data except the following: CP-Ser+Ca(II) where $g(s^*)$ was used. The typical scan range was 14-21 and the peak broadening limit was always greater than 60 kDa. For the manganese samples, only six scans were used. ^b The sample buffer was 75 mM HEPES, 100 mM NaCl, 1.35 mM EDTA, pH 7.5. $s_{20,w}$ values were adjusted with solvent density (ρ) of 1.00825 g/mL, solvent viscosity (η) of 1.0563 cP. ^c The sample buffer was 75 mM HEPES, 100 mM NaCl, pH 7.5 $s_{20,w}$ values were adjusted with solvent density (ρ) of 1.0082 g/mL, solvent viscosity (η) of 1.0565 cP pH 7.5 at 20 °C. ^d The sample buffer was 75 mM HEPES, 100 mM NaCl, 540 μM Ca(II) (20 equivalents), pH 7.5. The parameters for converting to $s_{20,w}$ from ^c were used. ^e The sample buffer was 75 mM HEPES, 100 mM NaCl, 27.5 μM Mn(II), pH 7.5. The parameters from ^c for converting to $s_{20,w}$ were used. ^f The sample buffer was 75 mM HEPES, 100 mM NaCl, 540 μM Ca(II) (20 equivalents), 27.5 μM Mn(II), pH 7.5. The parameters from ^c for converting to $s_{20,w}$ were used.

and excess Ca(II) (600 μ M) was included in the running buffer. Under these conditions, I60E and I60K afforded peaks with elution volumes of \approx 11 mL (Figures 2.2A and A2.5). Taken together, these data suggest I60E and I60K are a mixed population of the dimeric and tetrameric forms in the presence of Mn(II) alone, whereas the combination of Mn(II) and excess Ca(II) results in complete conversion to the heterotetramer.

We employed AUC to further investigate how Mn(II) coordination influences the quaternary structure of CP-Ser, I60E, and I60K in the absence of presence of Ca(II). The sedimentation distributions for samples containing CP-Ser and one equivalent of Mn(II) revealed two main species at 2.4 and 4.1 S (Figure A2.7). The species at 4.1 S comprises \approx 65% of the distribution area. In the absence of Ca(II), CP-Ser coordinates Mn(II) with relatively low affinity and the reported dissociation constant at the His₆ site is in the micromolar range ($K_{d1} \approx 5 \mu$ M by room-temperature electron paramagnetic resonance spectroscopy).^{20,22} Using this K_d value and the CP-Ser and Mn(II) concentrations employed for the AUC sample, we calculate that the sample contained \approx 34% apo and \approx 66% Mn(II)-bound CP-Ser. On the basis of this analysis, we assign the 2.4 S species to the apo CP-Ser heterodimer and the 4.1 S species to a Mn(II)-bound heterotetramer. This analysis informs our prior SEC results that revealed addition of Mn(II) to CP-Ser causes a shift in peak elution volume (*vide supra*), and we conclude that apo heterodimers and Mn(II)-bound heterotetramers are present in the sample. Moreover, When I60E and I60K were pre-incubated with one equivalent of Mn(II), the sedimentation distributions exhibited the same dimer (\approx 2.3 S) and tetramer species (\approx 4.0 S) (Figure A2.7); however, the dimer comprised \approx 80% of the total area, indicating that Mn(II)-induced tetramerization is disrupted in the I60E and I60K variants. This analysis is consistent with the SEC results, which showed a peak elution volume consistent with heterodimers and marked peak broadening indicative of heterotetramers.

When 20 equivalents of Ca(II) and one equivalent of Mn(II) were added to the buffer, CP-Ser, I60E, and I60K exhibited similar sedimentation distributions (Figure 2.3).

The major species appeared at ≈ 4.0 S for all three proteins, which we assign to the Ca(II)- and Mn(II)-bound heterotetramer. The CP-Ser distribution also contained a less abundant species at 6.5 S. The theoretical maximum sedimentation coefficient for the CP tetramer is ≈ 4.5 S, suggesting that a higher order oligomer forms under these conditions. This species warrants further investigation, and is reminiscent of prior SEC studies that revealed low-abundant peaks with lower elution volumes (higher molecular weight) than the $\alpha_2\beta_2$ heterotetramer.¹⁹ In total, the AUC results are in agreement with those obtained from SEC and indicate that (i) the quaternary structure of CP is modulated by both Ca(II) and Mn(II), (ii) heterotetramerization is not restricted to Ca(II) because the CP-Ser samples containing only Mn(II) also form heterotetramers, and (iii) the I60E and I60K mutations do not preclude formation of tetramers when Ca(II) and Mn(II) are present. Moreover, crystal structures of Ca(II)- and Mn(II)-bound CP-Ser reveal heterotetramers,^{22,23} and the current work confirms that heterotetramers also form in solution.

We also employed SEC to examine the effect of Fe(II) on the oligomerization properties of CP-Ser, I60E and I60K in the absence and presence of excess Ca(II). In agreement with our previous work, we observed a shift in peak elution volume following addition of Fe(II) to CP-Ser.²⁴ After preincubation with 10 equivalents of Fe(II), CP-Ser, I60E, and I60K (30 μ M) shifted to an earlier peak elution volume (11.1 mL, ≈ 43 kDa) (Figure A2.6). In contrast to the Mn(II)-only I60E and I60K samples (Figure A2.5), the chromatograms for the Fe(II)-only samples exhibited a complete shift to earlier elution volumes and no broadening, which indicated that addition of Fe(II) favored tetramerization more than Mn(II) alone. Moreover, preincubation of the proteins with 1.1 equivalents of Fe(II) and 20 equivalents of Ca(II) afforded the same peak elution volume of 11.1 mL (Figures 2.2B and A2.6). The higher affinity of CP for Fe(II) than Mn(II) at the His₆ site may explain why Fe(II) causes more tetramerization of I60E and I60K than Mn(II) in the absence of Ca(II).²⁴ We note that one prior study reported Zn(II)-induced formation of

heterotetramers by mass spectrometry, albeit the Zn(II)/CP stoichiometries obtained from this analysis are unlikely to be relevant because the number of bound Zn(II) ions reported exceeds the number of Zn(II)-binding sites per CP heterotetramer.³⁷ Taken together, these studies illuminate the multifaceted and metal-dependent oligomerization properties of CP. At present, the molecular basis for the metal-dependent oligomerization properties of CP-Ser and the I60 variants is unclear from standpoints of Ca(II) coordination at the EF-hand domains as well as transition metal binding at the His₆ site. It is possible that the I60 mutations abrogate Ca(II)-induced tetramerization, but allow tetramerization to occur via transition-metal binding. This notion is consistent with the observations that Fe(II), which binds to CP with higher affinity than Mn(II), causes complete tetramerization and that increasing the affinity of the proteins for Mn(II) by adding Ca(II) allows Mn(II) to cause quantitative tetramerization. Further characterization of these metal-dependent self-assembly pathways is an avenue for future work.

2.3.4. Tetramerization Protects Calprotectin against Host Proteases

To ascertain whether Ca(II)-induced tetramerization of CP-Ser confers resistance to proteolysis, we evaluated trypsin, chymotrypsin, and human neutrophil elastase (HNE) as host proteases in degradation assays. We selected trypsin, chymotrypsin, and HNE because we reasoned that co-localization of these proteases with CP is likely to occur *in vivo*. CP is expressed by the intestinal epithelium and serves as a biomarker for inflammation in the gut, where trypsin and chymotrypsin are abundant.⁵¹ Neutrophils are a major source of extracellular CP and also release HNE, the latter of which is stored in azurophilic granules.^{9,52,53} We employed Ca(II)-bound CP-Ser, I60E and I60K in these studies to compare the proteolytic stabilities of the Ca(II)-bound heterotetramer (CP-Ser) and heterodimers (I60E and I60K). Because proteases such as trypsin and chymotrypsin are activated/stabilized by Ca(II) ions, a degradation study of the apo CP-Ser heterodimer degradation would necessitate utilizing incompletely active proteases and direct

comparison with the Ca(II)-bound heterotetramer would not be possible. With the tetramer-deficient variants, it is possible to compare the stability of the Ca(II)-bound dimer and the Ca(II)-bound tetramer under the same experimental conditions that provide equally active proteases.

We established an analytical HPLC protocol that affords separation of the S100A8 (\approx 38 min) and S100A9 (39.8 min) subunits on a C4 column. We confirmed the identity of each peak by LCMS, and used HPLC to monitor the proteolytic stability of each subunit over time. The chromatograms from the trypsin digestions revealed that S100A8 and S100A9 subunits of Ca(II)-bound CP-Ser display resistance to trypsin, whereas both subunits were rapidly degraded for Ca(II)-bound I60E and I60K (Figures 2.5 and A2.8). Quantification of the S100A8 and S100A9 peak area revealed that \approx 80% of each CP-Ser subunit persisted after 4 h whereas both subunits were undetectable for I60K and I60E at this time point (Figure 2.5). Similar results were obtained with chymotrypsin (Figure A2.9) and HNE (Figures 2.6 and A2.10); both proteases degraded Ca(II)-bound I60K and I60E more readily than Ca(II)-bound CP-Ser. We also observed that HNE digested I60E more rapidly than I60K. The reason for the difference is unclear because HNE preferably cleaves after small hydrophobic residues, so the I60K and I60E mutations are not expected to affect the HNE cleavage pattern.^{54,55} Addition of both Mn(II) and Ca(II) to I60K and I60E, which causes heterotetramer formation (*vide supra*), resulted in enhanced stability to digestion by trypsin, chymotrypsin, and HNE. The corresponding chromatograms indicate negligible loss of full-length S100A8 and S100A9, and new species were not observed (Figures 2.5, 2.6, and A2.8-A2.10). Taken together, these assays demonstrate that tetramerization of the CP-Ser scaffold affords enhanced resistance to degradation by three host proteases.

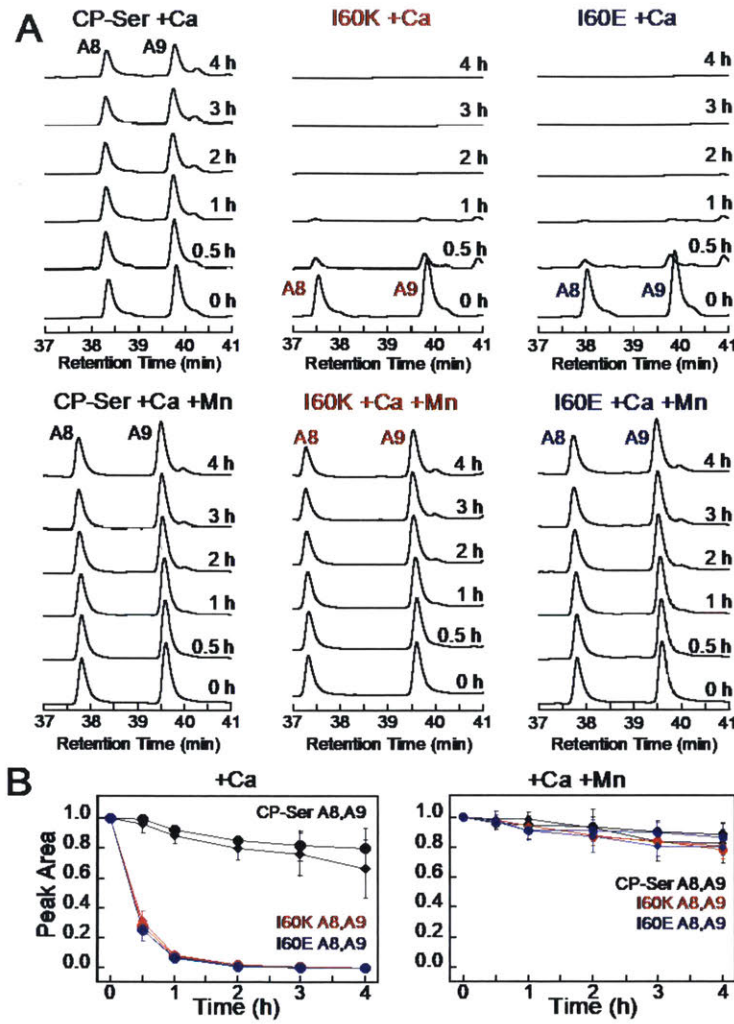


Figure 2.5. Susceptibility of Ca(II)-bound CP-Ser, I60E, and I60K (30 μ M) to degradation by trypsin (0.45 μ M). (A) Representative HPLC traces illustrating the full-length S100A8 and S100A9 subunits following incubation with trypsin for 0–4 h at 37 $^{\circ}$ C (75 mM HEPES, 100 mM NaCl, pH 7.5, \pm 1.5 mM Ca(II), \pm 30 μ M Mn(II), pH 7.5). (B) Reduction in the S100A8 and S100A9 integrated peak area as a function of time (mean \pm SDM, $n=3$). Full chromatograms are given in Figure A2.8.

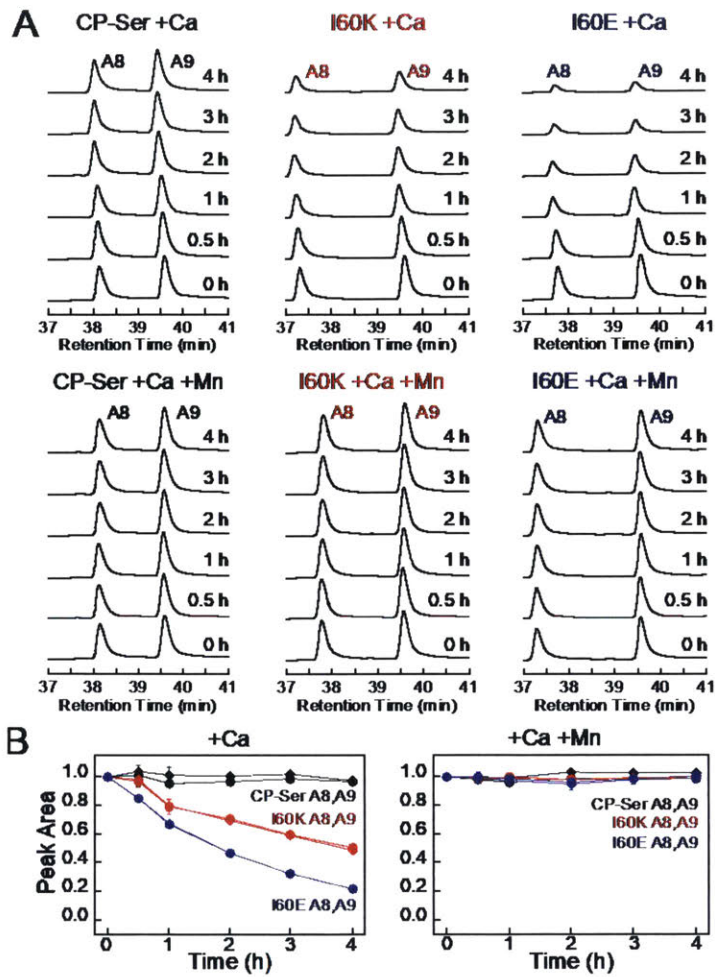


Figure 2.6. Susceptibility of Ca(II)-bound CP-Ser, I60E, and I60K (30 μ M) to degradation by HNE (0.3 μ M). (A) Representative HPLC traces illustrating the full-length S100A8 and S100A9 subunits following incubation with HNE for 0–4 h at 37 $^{\circ}$ C (75 mM HEPES, 100 mM NaCl, pH 7.5, \pm 1.5 mM Ca(II), \pm 30 μ M Mn(II), pH 7.5). (B) Reduction in the S100A8 and S100A9 integrated peak area as a function of time (mean \pm SDM, $n=3$). Full chromatograms are given in Figure A2.10.

2.3.5. Proteolysis by Trypsin Abolishes Antibacterial Activity

The current model states that CP inhibits microbial growth in a Ca(II)-dependent manner by sequestering essential transition metal ions in the extracellular space.^{13,56} This antibacterial mechanism requires that the Ca(II) and transition metal binding sites at the S100A8/S100A9 interface remain intact and that the coordinated transition metals remain bound and inaccessible to an invading microbe. In accord with this model, it is reasonable to expect that proteolytic destruction of the metal-binding sites and heterooligomeric assembly results in attenuated antimicrobial activity.

We performed standard *in vitro* antimicrobial activity assays with I60E and I60K, and observed that these variants inhibited the growth of *E. coli* ATCC 29522 in a concentration-dependent manner that is comparable to CP-Ser (Figure A2.11). This result indicates that the defective self-assembly properties of I60E and I60K do not compromise *in vitro* antibacterial activity, at least against this *E. coli* strain. Prior studies established that the His₆ site of CP contributes more to the *in vitro* antibacterial activity against *E. coli* than the His₃Asp site.^{19,21,23} Thus, the result from this antimicrobial activity assay is expected because I60K and I60E retain a functional His₆ site (Figure A2.3).

The S100A8 and S100A9 subunits have multiple cleavage sites for the host proteases evaluated in this work, and our proteolysis studies revealed that Ca(II)-bound I60E and I60K were degraded into many proteolytic fragments by these enzymes (Figures A2.8-A2.10). We therefore ascertained how pre-incubation with trypsin impacts the antibacterial activity of CP-Ser, I60E, and I60K against *E. coli* ATCC 25922. Samples of CP-Ser, I60E, and I60K with and without trypsin were prepared in an antimicrobial activity assay buffer supplemented with Ca(II), incubated at 37 °C for ≈20 h, and subsequently employed in antimicrobial activity assays. Under standard conditions using the assay medium employed in this work, CP-Ser exhibits full growth inhibition of *E. coli* 25922 at 250 μg/mL.¹⁹ For the antibacterial activity assays including protease, we employed a final protein concentration of 500 μg/mL. The untreated samples exhibited antimicrobial

activity, demonstrating that the CP-Ser, I60E, and I60K were stable and active after the overnight incubation (Figure 2.7). Trypsin-treated CP-Ser retained the same antimicrobial activity as untreated CP-Ser, whereas trypsin-treated I60E and I60K provided slight growth enhancement relative to the untreated and trypsin-only controls (Figure 2.7). HPLC analysis of the protein samples following the overnight incubation with trypsin revealed that $\approx 50\%$ of CP-Ser remained, whereas I60E and I60K were completely digested (Figure A2.12). The latter result indicates $\approx 250 \mu\text{g/mL}$ of CP-Ser is present when the antimicrobial activity assay was initiated.

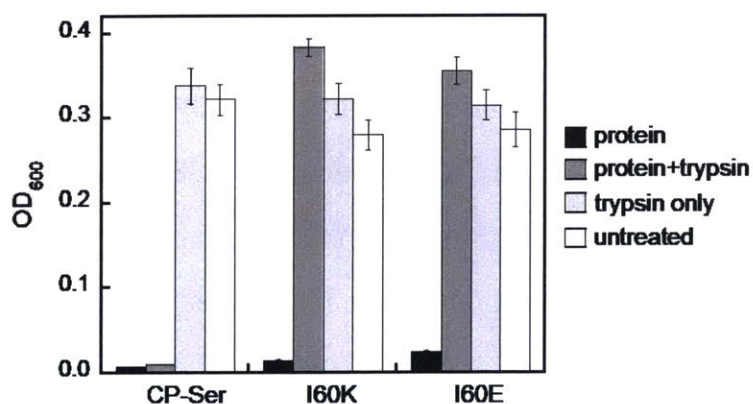


Figure 2.7. Antimicrobial activity assays performed with untreated and trypsin-treated CP-Ser, I60K and I60E against *E. coli* ATCC 25922. The OD₆₀₀ values were recorded at t=20 h (mean \pm SEM, n=3).

2.3.6. The Staphylococcal Protease GluC Cleaves the S100A8 Subunit in the Absence of Zn(II)

Many bacterial pathogens produce extracellular proteases that are capable of degrading proteins central to the immune response.⁵⁷⁻⁵⁹ To evaluate whether CP is a substrate for an extracellular serine protease produced by a human pathogen, we selected staphylococcal glutamyl endoproteinase (GluC) as an initial case study. This protease is readily available from commercial sources because of its specificity for cleaving after Asp. Moreover, GluC may be a virulence factor,⁶⁰⁻⁶² and CP is abundant at

sites of *S. aureus* infection,^{16,63} which suggests that it will encounter extracellular proteases released by this pathogen. In contrast to the host proteases that more readily degraded Ca(II)-bound heterodimers, GluC exhibited no preference for either Ca(II)-bound CP-Ser or the I60E and I60K variants; each substrate was cleaved in a similar manner (Figure 2.8). Moreover, the HPLC traces revealed that the presence of GluC results in negligible change to the S100A9 peak (39.8 min) and loss of the S100A8 peak (38.4 min) with concomitant formation of one new peak at 38.7min (Figure 2.8). LCMS analysis of this new species revealed that GluC cleaves S100A8 between Glu89–Ser90, resulting in a truncated S100A8 where the last four C-terminal residues (Ser90-His91-Lys92-Glu93) are removed (m/z calc. 10336.9 Da, obs.10337.3 Da).

The C-terminal region of S100A8 includes His83 and His87, residues that comprise the His₃Asp metal-binding site, and the GluC cleavage site is in close proximity to His87. Moreover, crystallographic studies of CP-Ser revealed that the S100A8 C-terminus is disordered in the absence of a bound metal at the His₃Asp site.²² The His₃Asp site coordinates Zn(II) with high affinity, and we questioned whether Zn(II) coordination at this site would afford GluC resistance (Figure 2.8). Because each CP heterodimer has two high-affinity Zn(II) sites,^{19,21} we performed GluC degradation assays with CP-Ser pre-incubated with two equivalents of Zn(II). Under these conditions, both S100A8 and S100A9 HPLC peaks exhibited negligible change and the A8 cleavage product was not observed (Figure 2.8). To confirm that Zn(II) coordination to the His₃Asp site provided protection against GluC, we took advantage of the different properties of the two transition-metal binding sites and performed an experiment where the protein substrate was pre-incubated with one equivalent of Mn(II). Because the Mn(II) affinities of the His₃Asp and His₆ sites vary substantially and Mn(II) preferentially populates the His₆ site, the His₃Asp site remains vacant when CP-Ser (+Ca) is incubated with one equivalent of Mn(II).^{20,22} In these +Mn(II) experiments, GluC cleaved S100A8 between Glu89 and Ser90 (Figure 2.8). Likewise, the addition of Mn(II) to the I60E and I60K variants afforded

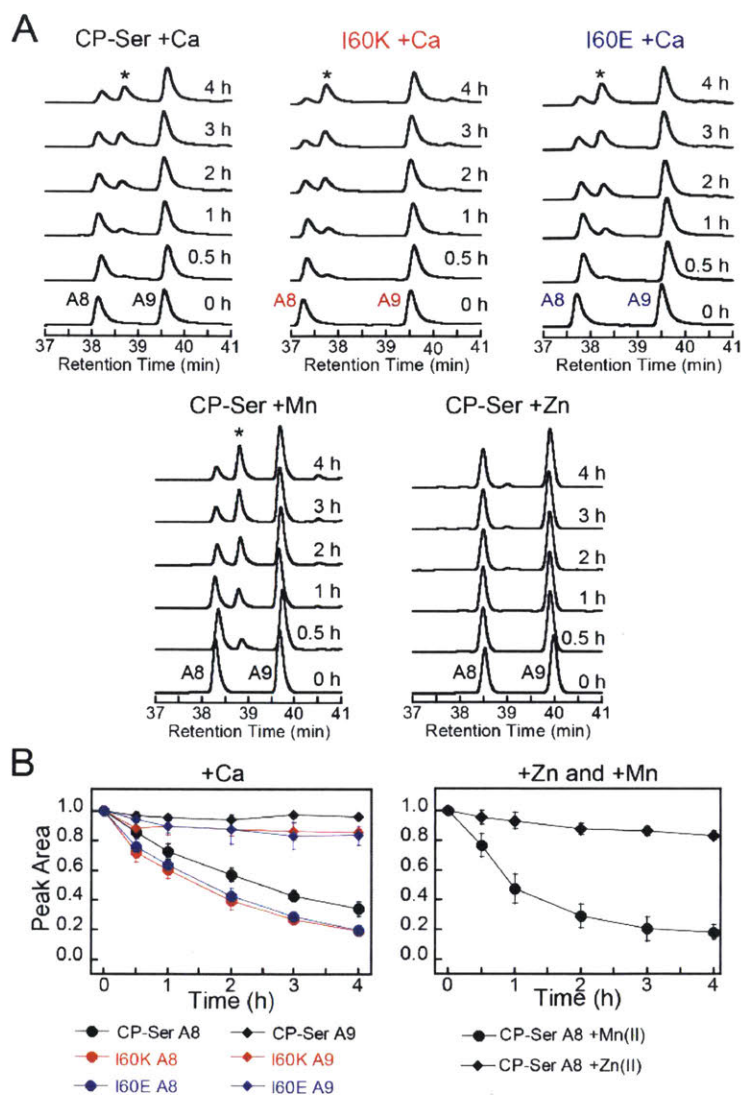


Figure 2.8. Susceptibility of Ca(II)-bound CP-Ser, I60E, and I60K (30 μ M) to degradation by staphylococcal GluC (0.3 μ M). (A) Representative HPLC traces illustrating the full-length S100A8 and S100A9 subunits following incubation with GluC for 0–4 h at 37 $^{\circ}$ C (75 mM HEPES, 100 mM NaCl, pH 7.5, \pm 1.5 mM Ca(II), \pm 30 μ M Mn(II), \pm 60 μ M Zn(II), pH 7.5). The asterisk denotes the Δ SHKE truncation product. (B) Reduction in the S100A8 and S100A9 integrated peak area as a function of time (mean \pm SDM, $n=3$). Full chromatograms are given in Figure A2.13.

afforded no protection of the GluC cut site (Figure 2.8).

2.3.7. The GluC Degradation Product Exhibits *in vitro* Antibacterial Activity

To evaluate the consequences of GluC truncation of the S100A8 subunit, we overexpressed the S100A8 truncation product identified from the GluC digests and the purified S100A8(C42S)(S90Stop)/S100A9 heterodimer, abbreviated Δ SHKE herein. This CP-Ser variant exhibits the expected α -helical fold and forms heterotetramers in the presence of Ca(II) (Figures A2.2 and A2.14). Antibacterial activity assays employing *E. coli* ATCC 25922, *S. aureus* ATCC 25923, and *L. plantarum* WCFS1 revealed that Δ SHKE exhibits the same *in vitro* growth inhibitory activity as CP-Ser against each strain (Figure 2.9). Thus, the last four residues of the S100A8 C-terminus are not essential for *in vitro* antibacterial activity of human CP against these three strains. We selected these strains on the basis of metabolic metal requirements and how the metal-binding sites of CP-Ser contribute to *in vitro* growth inhibition.^{19,21,24} Prior studies showed that the His₆ site, which sequesters Mn(II), Fe(II) and Zn(II), contributes more to growth inhibition of *E. coli* and *S. aureus* than the His₃Asp site under these assay conditions.^{19,21,23,24} The His₃Asp site sequesters Zn(II) but not Fe(II) or Mn(II), and this site is essential for antibacterial activity against *L. plantarum*.²⁴ This microbe has no metabolic iron requirement and is sensitive to Zn(II) restriction under the assay conditions; thus, growth studies with *L. plantarum* allow for interrogation of the His₃Asp site. The fact that the Δ SHKE variant showed full growth inhibitory activity against *L. plantarum*, indicated that loss of the four C-terminal residues of S100A8 does not impair the ability of the His₃Asp site to sequester Zn(II) from this organism. Moreover, these *in vitro* data suggest that GluC cleavage of S100A8 is not an effective staphylococcal resistance mechanism against human CP, although it is possible that synergism with other factors occurs in the complex milieu of an infection site. In light of these observations, we note that the C-terminus of human S100A8 differs from the C-termini of other mammalian orthologues.

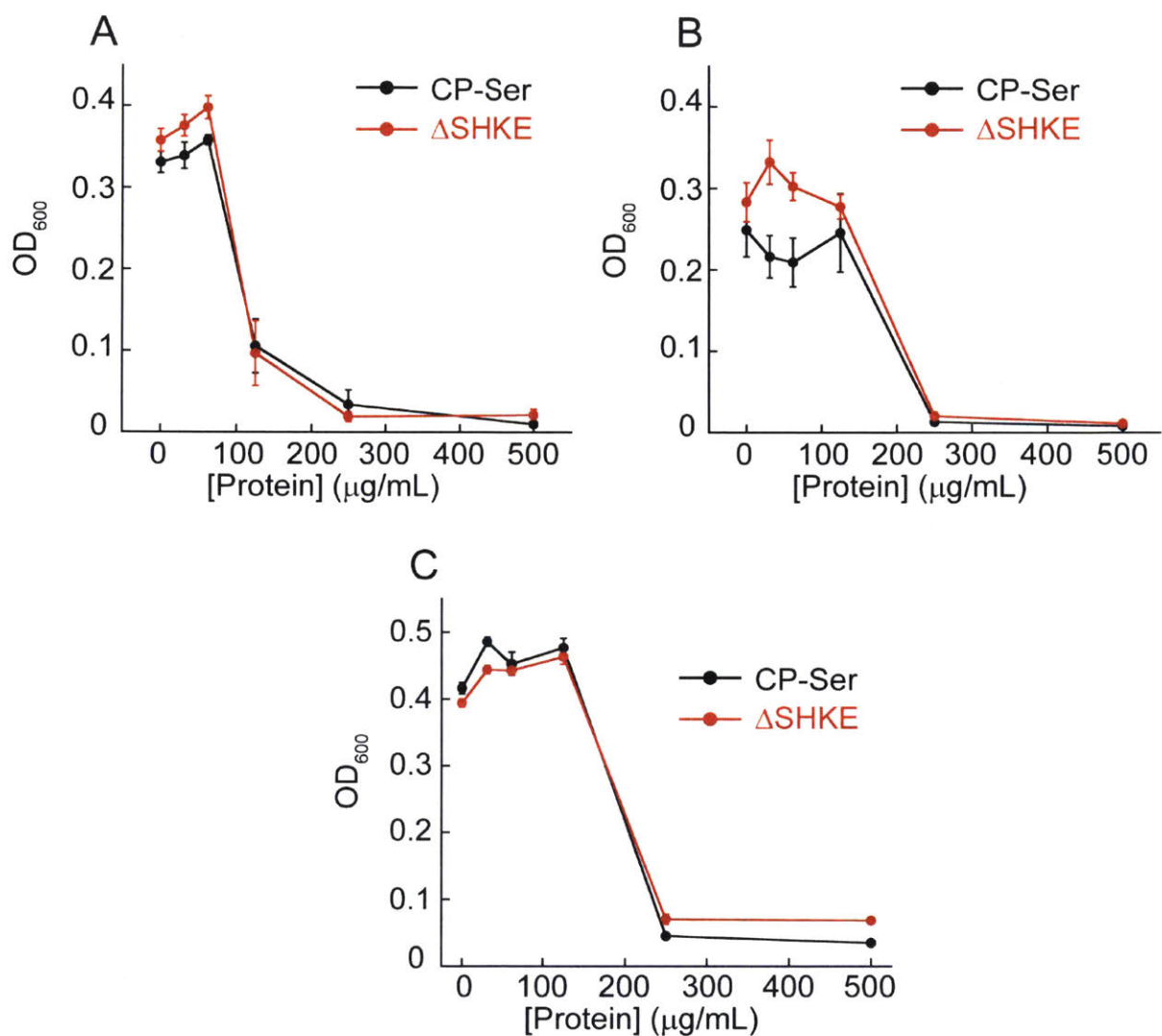


Figure 2.9. Antibacterial activity of CP-Ser and Δ SHKE against *E. coli* ATCC 25922 (A), *S. aureus* ATCC 25923 (B), *L. plantarum* WCFS1 (C) with 2 mM Ca(II) in the AMA medium. The OD_{600} values were recorded at $t = 20$ h. Averages \pm SEM for three independent replicates ($n=9$).

Human S100A8 is four residues longer than other sequenced mammalian S100A8 polypeptides, and these additional four residues occur in the C-terminal region. The C-terminal residues 87-93 of human S100A8 are HEESHKE, and the C-terminal residues 87-89 of other mammalian S100A8 are HKE. Whether this difference has functional significance for human CP is unclear.

2.3.8. *Biological Implications and Outlook*

This work provides the first comprehensive evaluation of how metal binding and changes in quaternary structure influence the proteolytic stability of human CP. Our results indicate that Ca(II)-induced heterotetramerization and Zn(II) chelation enable CP to resist degradation by select host and bacterial serine proteases. We reason that the metal-induced structural changes enable CP to persist in the protease-rich extracellular space and thereby function in metal withholding and the inflammatory response. It will be important to determine whether these observations pertain to the fate of CP in the presence of other proteases, particularly those employed by bacterial pathogens to thwart the innate immune response. Although the current data indicate that CP exhibits remarkable metal-dependent resistance to the proteases evaluated in this work, pathogens overcome the host response to infection. We therefore expect that certain pathogenic microbes deploy degradation machinery that can disarm CP. Another important avenue for future inquiry is to consider the current observations in the context of biological concentrations, regulation, and other factors that come into play in the variable and dynamic extracellular environments of infection and inflammatory sites. In broad terms, this work provides an additional and previously unappreciated facet to how Ca(II) ions influence CP function, and further exemplifies the fact that CP is a complex and multifaceted protein and that its functional properties will be governed by its speciation.

2.4. Acknowledgements

We gratefully acknowledge financial support from the NIH (1DP2OD007045), the Kinship Foundation (Searle Scholar Award to EMN), and the Stephen J. Lippard Fellowship Fund (summer graduate fellowship to JRS). We thank Dr. Megan Brunjes Brophy for a pilot AUC study of CP, suggesting the I60K variant, and preparing the *pET41a-S100A8(C42S)(I60K)* plasmid, and Dr. Andrew Wommack for guidance with AUC data analysis. The CD spectrometer and analytical ultracentrifuge are housed in the MIT Biophysical Instrumentation Facility for the Study of Complex Macromolecular Systems, which is supported by grant NSF 0070319.

2.5. References

1. McNamara, M. P.; Wiessner, J. H.; Collins-Lech, C.; Hahn, B. L.; Sohnle, P. G., Neutrophil Death as a Defense-Mechanism against *Candida-Albicans* Infections. *Lancet* **1988**, 2 (8621), 1163-1165.
2. Steinbakk, M.; Naess-Andresen, C. F.; Lingaas, E.; Dale, I.; Brandtzaeg, P.; Fagerhol, M. K., Antimicrobial actions of calcium binding leukocyte L1 protein, calprotectin. *Lancet* **1990**, 336, 763-765.
3. Golden, B. E.; Clohessy, P. A.; Russell, G.; Fagerhol, M. K., Calprotectin as a marker of inflammation in cystic fibrosis. *Arch. Dis. Child.* **1996**, 74 (2), 136-139.
4. Johne, B.; Fagerhol, M. K.; Lyberg, T.; Prydz, H.; Brandtzaeg, P.; Naess-Andresen, C. F.; Dale, I., Functional and clinical aspects of the myelomonocyte protein calprotectin. *J. Clin. Pathol: Mol. Pathol.* **1997**, 50 (3), 113-123.
5. Stříž, I.; Trebichavský, I., Calprotectin - a pleiotropic molecule in acute and chronic inflammation. *Physiological Research* **2004**, 53 (3), 245-253.
6. Goyette, J.; Geczy, C. L., Inflammation-associated S100 proteins: new mechanisms that regulate function. *Amino Acids* **2011**, 41 (4), 821-842.

7. Zackular, J. P.; Chazin, W. J.; Skaar, E. P., Nutritional Immunity: S100 Proteins at the Host-Pathogen Interface. *J. Biol. Chem.* **2015**, *290* (31), 18991-18998.
8. Urban, C. F.; Ermert, D.; Schmid, M.; Abu-Abed, U.; Goosmann, C.; Nacken, W.; Brinkmann, V.; Jungblut, P. R.; Zychlinsky, A., Neutrophil extracellular traps contain calprotectin, a cytosolic protein complex involved in host defense against *Candida albicans*. *PLOS Pathog.* **2009**, *5* (10), e1000639.
9. Nathan, C., Neutrophils and immunity: challenges and opportunities. *Nat. Rev. Immunol.* **2006**, *6* (3), 173-182.
10. Brinkmann, V.; Zychlinsky, A., Beneficial suicide: why neutrophils die to make NETs. *Nat. Rev. Microbiol.* **2007**, *5* (8), 577-582.
11. Loser, K.; Vogl, T.; Voskort, M.; Lueken, A.; Kupas, V.; Nacken, W.; Klenner, L.; Kuhn, A.; Foell, D.; Sorokin, L.; Luger, T. A.; Roth, J.; Beissert, S., The Toll-like receptor 4 ligands Mrp8 and Mrp14 are crucial in the development of autoreactive CD8(+) T cells. *Nat. Med.* **2010**, *16* (6), 713-717.
12. McCormick, A.; Heesemann, L.; Wagener, J.; Marcos, V.; Hartl, D.; Loeffler, J.; Heesemann, J.; Ebel, F., NETs formed by human neutrophils inhibit growth of the pathogenic mold *Aspergillus fumigatus*. *Microbes Infect.* **2010**, *12* (12-13), 928-936.
13. Hood, M. I.; Skaar, E. P., Nutritional immunity: transition metals at the pathogen-host interface. *Nat. Rev. Microbiol.* **2012**, *10* (8), 525-537.
14. Sohnle, P. G.; Collins-Lech, C.; Wiessner, J. H., The zinc-reversible antimicrobial activity of neutrophil lysates and abscess fluid supernatants. *J. Infect. Dis.* **1991**, *164* (1), 137-142.
15. Clohessy, P. A.; Golden, B. E., Calprotectin-Mediated Zinc Chelation as a Biostatic Mechanism in Host-Defense. *Scand. J. Immunol.* **1995**, *42* (5), 551-556.
16. Corbin, B. D.; Seeley, E. H.; Raab, A.; Feldmann, J.; Miller, M. R.; Torres, V. J.; Anderson, K. L.; Dattilo, B. M.; Dunman, P. M.; Gerads, R.; Caprioli, R. M.; Nacken, W.;

- Chazin, W. J.; Skaar, E. P., Metal chelation and inhibition of bacterial growth in tissue abscesses. *Science* **2008**, *319* (5865), 962-965.
17. Kehl-Fie, T. E.; Chitayat, S.; Hood, M. I.; Damo, S.; Restrepo, N.; Garcia, C.; Munro, K. A.; Chazin, W. J.; Skaar, E. P., Nutrient metal sequestration by calprotectin inhibits bacterial superoxide defense, enhancing neutrophil killing of *Staphylococcus aureus*. *Cell Host Microbe* **2011**, *10* (2), 158-164.
18. Liu, J. Z.; Jellbauer, S.; Poe, A. J.; Ton, V.; Pesciaroli, M.; Kehl-Fie, T. E.; Restrepo, N. A.; Hosking, M. P.; Edwards, R. A.; Battistoni, A.; Pasquali, P.; Lane, T. E.; Chazin, W. J.; Vogl, T.; Roth, J.; Skaar, E. P.; Raffatellu, M., Zinc sequestration by the neutrophil protein calprotectin enhances *Salmonella* growth in the inflamed gut. *Cell Host Microbe* **2012**, *11* (3), 227-239.
19. Brophy, M. B.; Hayden, J. A.; Nolan, E. M., Calcium ion gradients modulate the zinc affinity and antibacterial activity of human calprotectin. *J. Am. Chem. Soc.* **2012**, *134* (43), 18089-18100.
20. Hayden, J. A.; Brophy, M. B.; Cunden, L. S.; Nolan, E. M., High-affinity manganese coordination by human calprotectin is calcium-dependent and requires the histidine-rich site formed at the dimer interface. *J. Am. Chem. Soc.* **2013**, *135* (2), 775-787.
21. Brophy, M. B.; Nakashige, T. G.; Gaillard, A.; Nolan, E. M., Contributions of the S100A9 C-terminal tail to high-affinity Mn(II) chelation by the host-defense protein human calprotectin. *J. Am. Chem. Soc.* **2013**, *135* (47), 17804-17817.
22. Gagnon, D. M.; Brophy, M. B.; Bowman, S. E. J.; Stich, T. A.; Drennan, C. L.; Britt, R. D.; Nolan, E. M., Manganese binding properties of human calprotectin under conditions of high and low calcium: X-ray crystallographic and advanced electron paramagnetic resonance spectroscopic analysis. *J. Am. Chem. Soc.* **2015**, *137* (8), 3004-3016.
23. Damo, S. M.; Kehl-Fie, T. E.; Sugitani, N.; Holt, M. E.; Rathi, S.; Murphy, W. J.; Zhang, Y. F.; Betz, C.; Hench, L.; Fritz, G.; Skaar, E. P.; Chazin, W. J., Molecular basis

- for manganese sequestration by calprotectin and roles in the innate immune response to invading bacterial pathogens. *Proc. Natl. Acad. Sci. U. S. A.* **2013**, *110* (10), 3841-3846.
24. Nakashige, T. G.; Zhang, B.; Krebs, C.; Nolan, E. M., Human calprotectin is an iron-sequestering host-defense protein. *Nat. Chem. Biol.* **2015**, *11* (10), 765-771.
25. Vogl, T.; Tenbrock, K.; Ludwig, S.; Leukert, N.; Ehrhardt, C.; van Zoelen, M. A. D.; Nacken, W.; Foell, D.; van der Poll, T.; Sorg, C.; Roth, J., Mrp8 and Mrp14 are endogenous activators of Toll-like receptor 4, promoting lethal, endotoxin-induced shock. *Nat. Med.* **2007**, *13* (9), 1042-1049.
26. Selsted, M. E.; Ouellette, A. J., Mammalian defensins in the antimicrobial immune response. *Nat. Immunol.* **2005**, *6* (6), 551-557.
27. Zhao, L.; Lu, W., Defensins in innate immunity. *Curr. Opin. Hematol.* **2014**, *21* (1), 37-42.
28. Maemoto, A.; Qu, X.; Rosengren, K. J.; Tanabe, H.; Henschen-Edman, A.; Craik, D. J.; Ouellette, A. J., Functional analysis of the alpha-defensin disulfide array in mouse cryptdin-4. *J. Biol. Chem.* **2004**, *279* (42), 44188-44196.
29. Wanniarachchi, Y. A.; Kaczmarek, P.; Wan, A.; Nolan, E. M., Human defensin 5 disulfide array mutants: disulfide bond deletion attenuates antibacterial activity against *Staphylococcus aureus*. *Biochemistry* **2011**, *50* (37), 8005-8017.
30. Brock, J. H.; Arzabe, F.; Lampreave, F.; Pineiro, A., The effect of trypsin on bovine transferrin and lactoferrin. *Biochim. Biophys. Acta* **1976**, *446* (1), 214-225.
31. Brines, R. D.; Brock, J. H., The effect of trypsin and chymotrypsin on the in vitro antimicrobial and iron-binding properties of lactoferrin in human milk and bovine colostrum. Unusual resistance of human apolactoferrin to proteolytic digestion. *Biochim. Biophys. Acta* **1983**, *759* (3), 229-235.
32. Hunter, M. J.; Chazin, W. J., High level expression and dimer characterization of the S100 EF-hand proteins, migration inhibitory factor-related proteins 8 and 14. *J. Biol. Chem.* **1998**, *273* (20), 12427-12435.

33. Propper, C.; Huang, X. H.; Roth, J.; Sorg, C.; Nacken, W. G., Analysis of the MRP8-MRP14 protein-protein interaction by the two-hybrid system suggests a prominent role of the C-terminal domain of S100 proteins in dimer formation. *J. Biol. Chem.* **1999**, *274* (1), 183-188.
34. Vogl, T.; Roth, J.; Sorg, C.; Hillenkamp, F.; Strupat, K., Calcium-induced noncovalently linked tetramers of MRP8 and MRP14 detected by ultraviolet matrix-assisted laser desorption/ionization mass spectrometry. *J. Am. Soc. Mass Spectrom.* **1999**, *10* (11), 1124-1130.
35. Strupat, K.; Rogniaux, H.; Van Dorsselaer, A.; Roth, J.; Vogl, T., Calcium-induced noncovalently linked tetramers of MRP8 and MRP14 are confirmed by electrospray ionization-mass analysis. *J. Am. Soc. Mass Spectrom.* **2000**, *11* (9), 780-788.
36. Korndorfer, I. P.; Brueckner, F.; Skerra, A., The crystal structure of the human (S100A8/S100A9)₂ heterotetramer, calprotectin, illustrates how conformational changes of interacting alpha-helices can determine specific association of two EF-hand proteins. *J. Mol. Biol.* **2007**, *370* (5), 887-898.
37. Vogl, T.; Leukert, N.; Barczyk, K.; Strupat, K.; Roth, J., Biophysical characterization of S100A8 and S100A9 in the absence and presence of bivalent cations. *Biochim. Biophys. Acta* **2006**, *1763* (11), 1298-1306.
38. Williams, R. J. P., Calcium binding proteins in normal and transformed cells, Perugia, May 1996. *Cell Calcium* **1996**, *20* (1), 87-93.
39. Nacken, W.; Kerkhoff, C., The hetero-oligomeric complex of the S100A8/S100A9 protein is extremely protease resistant. *FEBS Lett.* **2007**, *581* (26), 5127-5130.
40. Riva, M.; He, Z.; Källberg, E.; Ivars, F.; Leanderson, T., Human S100A9 protein is stabilized by inflammatory stimuli via the formation of proteolytically-resistant homodimers. *PLOS ONE* **2013**, *8* (4), e61832.

41. Dumoulin, E. N.; Van Biervliet, S.; Langlois, M. R.; Delanghe, J. R., Proteolysis is a confounding factor in the interpretation of faecal calprotectin. *Clin. Chem. Lab Med.* **2015**, *53* (1), 65-71.
42. Brophy, M. B.; Hayden, J. A.; Nolan, E. M., Calcium ion gradients modulate the zinc affinity and antibacterial activity of human calprotectin. *J. Am. Chem. Soc.* **2012**, *134* (43), 18089-18100.
43. Laue, M.; Shah, B. D.; Ridgeway, T. M.; Pelletier, S. L., SEDNTERP primary referene. *Analytical Ultracentrifugation in Biochemistry and Polymer Science* **1992**, (Harding, S.; Rose, A., Eds.) pp 90-125, Royal Society of Chemistry.
44. Wommack, A. J.; Robson, S. A.; Wanniarachchi, Y. A.; Wan, A.; Turner, C. J.; Wagner, G.; Nolan, E. M., NMR solution structure and condition-dependent oligomerization of the antimicrobial peptide human defensin 5. *Biochemistry* **2012**, *51* (48), 9624-9637.
45. Ortega, A.; Amorós, D.; García de la Torre, J., Prediction of hydrodynamic and other solution properties of rigid proteins from atomic- and residue-level models. *Biophys. J.* **2011**, *101* (4), 892-8.
46. Shaw, E.; Mares-Guia, M.; Cohen, W., Evidence for an active-center histidine in trypsin through use of a specific reagent, 1-chloro-3-tosylamido-7-amino-2-heptanone, the chloromethyl ketone derived from N^α-tosyl-L-lysine. *Biochemistry* **1965**, *4* (10), 2219-2224.
47. Santoro, M. M.; Bolen, D. W., Unfolding free energy changes determined by the linear extrapolation method. 1. Unfolding of phenylmethanesulfonyl alpha-chymotrypsin using different denaturants. *Biochemistry* **1988**, *27* (21), 8063-8068.
48. Bogan, A. A.; Thorn, K. S., Anatomy of hot spots in protein interfaces. *J. Mol. Biol.* **1998**, *280* (1), 1-9.
49. You, Y.; Tomat, E.; Hwang, K.; Atanasijevic, T.; Nam, W.; Jasanoff, A. P.; Lippard, S. J., Manganese displacement from Zinpyr-1 allows zinc detection by fluorescence

microscopy and magnetic resonance imaging. *Chem. Commun.* **2010**, 46 (23), 4139-4141.

50. Lebowitz, J.; Lewis, M. S.; Schuck, P., Modern analytical ultracentrifugation in protein science: A tutorial review. *Protein Sci.* **2002**, 11, 2067-2079.

51. Keller, P. J.; Cohen, E.; Neurath, H., The proteins of bovine pancreatic juice. *J. Biol. Chem.* **1958**, 233 (2), 344-349.

52. Stapels, D. A.; Geisbrecht, B. V.; Rooijackers, S. H., Neutrophil serine proteases in antibacterial defense. *Curr. Opin. Microbiol.* **2015**, 23, 42-48.

53. Sinha, S.; Watorek, W.; Karr, S.; Giles, J.; Bode, W.; Travis, J., Primary structure of human neutrophil elastase. *Proc. Natl. Acad. Sci. U. S. A.* **1987**, 84 (8), 2228-2232.

54. O'Donoghue, A. J.; Jin, Y.; Knudsen, G. M.; Perera, N. C.; Jenne, D. E.; Murphy, J. E.; Craik, C. S.; Hermiston, T. W., Global substrate profiling of proteases in human neutrophil extracellular traps reveals consensus motif predominantly contributed by elastase. *PLOS ONE* **2013**, 8 (9), e75141.

55. Korkmaz, B.; Gauthier, F., Elastase-2/Leukocyte Elastase. *Handbook of Proteolytic Enzymes, Vols 1 and 2, 3rd Edition* **2013**, 2653-2661.

56. Brophy, M. B.; Nolan, E. M., Manganese and microbial pathogenesis: sequestration by the mammalian immune system and utilization by microorganisms. *ACS Chem. Biol.* **2015**, 10 (3), 641-651.

57. Date, S. V.; Modrusan, Z.; Lawrence, M.; Morisaki, J. H.; Toy, K.; Shah, I. M.; Kim, J.; Park, S.; Xu, M.; Basuino, L.; Chan, L.; Zeitschel, D.; Chambers, H. F.; Tan, M. W.; Brown, E. J.; Diep, B. A.; Hazenbos, W. L., Global gene expression of methicillin-resistant *Staphylococcus aureus* USA300 during human and mouse infection. *J. Infect. Dis.* **2014**, 209 (10), 1542-1550.

58. Kilian, M.; Mestecky, J.; Schrohenloher, R. E., Pathogenic species of the genus *Haemophilus* and *Streptococcus pneumoniae* produce immunoglobulin A1 protease. *Infect. Immun.* **1979**, 26 (1), 143-149.

59. Potempa, M.; Potempa, J., Protease-dependent mechanisms of complement evasion by bacterial pathogens. *Biol. Chem.* **2012**, 393 (9), 873-888.
60. Drapeau, G. R.; Boily, Y.; Houmard, J., Purification and properties of an extracellular protease of *Staphylococcus aureus*. *J. Biol. Chem.* **1972**, 247 (20), 6720-6726.
61. Prokešová, L.; Potužníková, B.; Potempa, J.; Zikán, J.; Radl, J.; Hachová, L.; Baran, K.; Porwit-Bohr, Z.; John, C., Cleavage of human immunoglobulins by serine proteinase from *Staphylococcus aureus*. *Immunol. Lett.* **1992**, 31 (3), 259-2565.
62. Jusko, M.; Potempa, J.; Kantyka, T.; Bielecka, E.; Miller, H. K.; Kalinska, M.; Dubin, G.; Garred, P.; Shaw, L. N.; Blom, A. M., Staphylococcal proteases aid in evasion of the human complement system. *J. Innate Immun.* **2014**, 6 (1), 31-46.
63. Kehl-Fie, T. E.; Zhang, Y.; Moore, J. L.; Farrand, A. J.; Hood, M. I.; Rathi, S.; Chazin, W. J.; Caprioli, R. M.; Skaar, E. P., MntABC and MntH contribute to systemic *Staphylococcus aureus* infection by competing with calprotectin for nutrient manganese. *Infect. Immun.* **2013**, 81 (9), 3395-3405.

Chapter 3: NMR Spectroscopy Reveals the Effect of Ca(II) on the Dynamics of the Calprotectin Dimer

3.1 Contributions

Dr. R. Silvers performed the NMR experiments and processed the NMR data. Design of the NMR experiments, analysis of the NMR data, preparation of the figures, and writing were accomplished with close collaboration between Mr. J. Stephan and Dr. R. Silvers. Dr. R. Griffin provided NMR expertise.

3.2. Introduction

Human calprotectin (CP) is a host-defense protein that is a heterooligomer of S100A8 (α subunit, 10.8 kDa) and S100A9 (β subunit, 13.2 kDa).¹ The subunits are members of the S100 family, which are characterized by their two Ca(II)-binding EF-hand domains and small size.² CP forms a heterodimer ($\alpha\beta$ oligomer), which has interface two transition-metal-binding sites at the dimer interface.³ CP exerts antimicrobial activity by binding Mn(II),⁴⁻⁶ Fe(II),⁷ Ni(II),⁸ and Zn(II).^{1,9} with high affinity thereby starving microbes of these essential nutrients. In the presence of Ca(II) ions, CP forms a dimer of dimers termed the tetramer ($\alpha_2\beta_2$).^{3,10} As a tetramer, CP displays increased transition-metal affinities, higher thermal stability, enhanced antimicrobial activity, and increased protease stability.^{9,11} Due to the low Ca(II) concentration (hundreds of nanomolar) in the cytosol of resting cells,¹² where CP is stored in neutrophils and epithelial cells, the working model is that CP is stored in the relatively low-affinity heterodimer form. During release into the extracellular space, CP is exposed to high Ca(II) concentrations (2 mM),¹² which is thought to result in Ca(II) binding and formation of the CP heterotetramer, which affords antimicrobial activity as well as longevity in the extracellular space. It has also been found that Ca(II) causes cytosolic CP to polymerize tubulin more effectively,¹³ to protect epithelial cells from bacterial invasion,¹⁴ and to bind unsaturated fatty acids with higher affinity.¹⁵

Though the functional consequences of Ca(II) chelation by CP have been the subject of many studies, the biophysical underpinnings for the remarkable Ca(II)-induced changes remain elusive. Currently, crystallographic structural information is available for only the tetramer,^{3,8,16,17} and no solution structure of the dimer or tetramer has been reported. As a consequence, molecular-level details describing the transformation from the apo dimer to the Ca(II)-bound tetramer are lacking. In lieu of such information, the molecular basis of tetramerization as well as the observed increased metal affinities are not known. One possibility is that Ca(II) binding and tetramerization cause significant changes in the protein fold, which result in the assembly of the transition-metal-binding and tetramerization sites; however, this scenario is unlikely considering the lack of change in the circular dichroism spectrum after addition of Ca(II)⁹ and the homology between structures of CP, the S100A8 homodimer, and the S100A9 homodimer.^{3,18-20} Studies of other S100 proteins have shown that Ca(II) causes helices III and IV to move apart to create a site for binding target proteins;²¹ however, neither transition metal binding nor tetramerization occur between helices III and IV. As an alternative possibility, we hypothesized that modulating the dynamics of CP via Ca(II) coordination governs transition metal binding and tetramerization. This hypothesis is supported by recent work on the allosteric Zn(II)-responsive transcription factor CzrA.²² It had been shown that the apo and Zn(II)-bound forms of CzrA displayed nearly identical structures in solid and solution states; therefore, the mechanism by which Zn(II) decreased the affinity of CzrA for DNA was unknown.^{23,24} Through NMR spectroscopy experiments where the methyl groups of amino acid side chains (Ala β , Ile δ 1, Leu δ 1/ δ 2, Met ϵ , Val γ 1/ γ 2) of CzrA were selectively ¹H, ¹³C labeled in a ²H, ¹²C background, it was experimentally demonstrated that Zn(II) decreased the affinity of CzrA for DNA by redistributing conformational entropy among methyl side chains in CzrA, which prevented the gain entropy that the methyl side chains experienced upon DNA binding.²² Along similar lines, a computational study of lapine S100A11, a homolog of human S100A8 and S100A9, suggested that Ca(II)-

mediated affinity for annexin arose from stiffening hydrophobic residues. Reducing the entropy of those residues halted a cascade of structural rearrangements that began with breakage of a labile salt bridge, and terminated with closure of the annexin binding site.²⁵ These studies and others provide compelling evidence that allosteric properties can arise from behavior that can only be observed in solution.²⁶⁻²⁹

In order to gain insight into the transformation from the apo CP dimer to the Ca(II)-bound CP tetramer, we chose to employ NMR spectroscopy to study the dynamic properties of a tetramer-deficient variant of CP termed I60K. The variant has (A8)C42S and (A9)C3S mutations to prevent disulfide formation and the (A8)I60K mutation to prevent Ca(II)-induced tetramerization.¹¹ Using the I60K variant, we were able to compare the structural and dynamical properties of the apo heterodimer and the Ca(II)-bound heterodimer, allowing us to obtain detailed information on CP species that have not been studied from a structural perspective. We assigned the I60K subunits most successfully using conditions with excess Ca(II). We found that I60K had dihedral angles consistent with crystal structures of the heterotetramer, except in certain small regions. The regions with disagreement displayed changes in dynamics upon Ca(II) binding, and provide evidence that Ca(II) stabilizes folding in regions that bind transition metals as well as promotes the movement of helices III and IV that had been observed for other S100 proteins. The insights gained from these studies demonstrate that Ca(II) causes changes in dynamics throughout both subunits, suggesting that rigidity imparted by Ca(II) chelation drives the emergent properties of the CP tetramer as opposed to a more traditional allosteric mechanism of conformational selection.

3.2. Experimental

3.2.1 *General Materials and Methods*

All solvents, reagents, and chemicals were obtained from commercial suppliers and used as received. All buffers and metal solutions were prepared using Milli-Q water (18.2 M Ω •cm, 0.22- μ m filter, Millipore). All buffers for NMR experiments were prepared with Ultrol grade HEPES (free acid, Calbiochem), TraceSELECT NaCl (Fluka), and aqueous TraceSELECT NaOH (Sigma) was used for pH adjustments. The highest available purity of calcium chloride (99.99%) was purchased from Alfa Aesar. Stock solutions of CaCl₂ (1 M, 50 mL) were prepared by using Milli-Q water and acid-washed volumetric glassware. All buffers and metal solutions were stored in polypropylene bottles and tubes. Protein concentration was determined by optical absorbance at 280 nm using a BioTek Synergy HT plate reader outfitted with a Take3 Micro-Volume plate. The extinction coefficient calculated by ExPASy server ProtParam tool (<http://web.expasy.org/protparam>) for the CP-Ser heterodimer ($\epsilon_{280} = 18450 \text{ M}^{-1}\text{cm}^{-1}$) was employed for determining protein concentration. All CP-Ser variants used in this work have the same extinction coefficient. All reported concentrations refer to the concentration of the heterodimer.

3.2.2 *Site-Directed Mutagenesis*

A modified Quick-Change site-directed mutagenesis protocol was employed to generate plasmids encoding S100A9(C3S)(P107A) and S100A9(C3S)(P114A). The template was pET41a-S100A9(C3S). This plasmid has the S100A9(C3S) gene inserted into the NdeI and XhoI sites of pET41a.⁹ The primers are listed in Table 3.1. PCR amplification was carried out using PfuTurbo DNA polymerase. The PCR protocol was 95 °C for 30 sec, 95 °C for 30 sec, 63.0 °C (P107A mutation) or 57.7 °C (P114A mutation), 68 °C for 17 min, (25 cycles), and 4 °C hold. After PCR amplification, the template DNA

was digested at 37 °C for 3 h using DpnI (New England Biolabs) by adding 1.5 µL of the enzyme to 50 µL of a PCR reaction, and adding an additional 1.5 µL of the enzyme after 1.5 h of incubation. The digestion products were transformed into chemically competent *E. coli* TOP10 cells that were subsequently plated on Luria Broth (LB) agar plates containing 50 µg/mL kanamycin (Kan) and incubated at 37 °C overnight. The following day, overnight cultures (5 mL LB, 50 µg/mL Kan) were grown from single colonies. The plasmids were isolated using a miniprep kit (Qiagen). The presence of the mutations and integrity of the coding sequences were verified by DNA sequencing (Quintara Biosciences). Plasmids encoding other S100A8 and S100A9 variants (Table 3.2) have been reported previously, and all expression plasmids are based on pET41a, unless otherwise specified.^{6,9,11}

Table 3.1. Primers used for mutagenesis.

Primer	Sequence ^a
P107A-1	5'-GGCCACCATCACAAA <u>GCG</u> GGTCTGGGCGAAGG -3'
P107A-2	5'-CCTTCGCCCAGACC <u>GCG</u> TTTGTGATGGTGGCC-3'
P114A-1	5'-CTGGGCGAAGGTACT <u>GCG</u> TAACTCGAGCACCCAC-3'
P114A-2	5'-GTGGTGCTCGAGTTA <u>GCG</u> AGTACCTTCGCCCAG-3'

^aThe codons containing mutations are underlined and colored red.

3.2.3 Protein Expression and Purification – General Protocol

The S100A8 and S100A9 subunits were expressed, and the CP heterodimers were reconstituted and purified, based on reported protocols with several modifications as detailed below.^{9,17} All isotopically-enriched compounds and 99.8% deuterium oxide (D₂O) used for protein expression were purchased from Cambridge Isotope Labs. For uniformly labeled [¹⁵N]- and [¹³C,¹⁵N]-labeled proteins, sterile 2-L or 4-L baffled flasks were charged with the following minimal medium prepared in Milli-Q water and sterile-

filtered: 6 g/L Na₂HPO₄, 3 g/L KH₂PO₄, 0.5 g/L NaCl, 2g/L D-glucose, 1 g/L NH₄Cl, 2 mM MgSO₄, and 100 μM CaCl₂. For ¹⁵N labeling, the natural abundance NH₄Cl was replaced with 99% ¹⁵NH₄Cl. For ¹³C labeling, the natural abundance D-glucose was replaced with 99% ¹³C-D-glucose and the resulting pellets were combined prior to lysis.⁹ For all isotopically-labeled protein purifications, both subunits were overexpressed in the minimal medium to ensure that comparable quantities were produced. For the preparation of perdeuterated proteins, the same minimal medium was prepared in 99.8% D₂O and perdeuterated ¹³C-D-glucose was used. Protein with randomly distributed deuteration (≈55% deuteration based on MS analysis) was prepared by growing cells in a medium containing a 3:1 ratio of D₂O:H₂O.

Table 3.2. Protein nomenclature and examples of isotopic labeling nomenclature.^a

Protein Name	Subunits	Ref.
CP-Ser	S100A8(C42S) / S100A9(C3S)	5
I60K	S100A8(C42S)(I60K) / S100A9(C3S)	11
I60K(H103A)	S100A8(C42S)(I60K) / S100A9(C3S)(H103A)	This work
I60K(H105A)	S100A8(C42S)(I60K) / S100A9(C3S)(H105A)	This work
I60K(P107A)	S100A8(C42S)(I60K) / S100A9(C3S)(P107A)	This work
I60K(P114A)	S100A8(C42S)(I60K) / S100A9(C3S)(P114A)	This work
[¹⁵ N]-A8-I60K	I60K with the A8 subunit uniformly ¹⁵ N labeled	This work
[¹⁵ N(Phe)]-A8-I60K	I60K with uniform ¹⁵ N labeling of Phe in A8	This work
[¹ H/ ² H, ¹³ C, ¹⁵ N]-A8-I60K	I60K with uniform ¹³ C, ¹⁵ N and random fractional deuteration labeling of the A8 subunit	This work

^a All protein variants are based on CP-Ser.

Overnight cultures of *E. coli* BL21(DE3) transformed with the appropriate expression plasmid were grown in 50 mL of LB medium containing 50 μg/mL Kan as

previously described (16 h, 37 °C, 150 rpm).⁹ Then, the overnight cultures were transferred to separate 50-mL conical tubes, and pelleted by centrifugation (3 600 rpm x 20 min, 4 °C). The supernatants were decanted, and to wash the cells, the pellets were resuspended in 25 mL of the minimal medium before repeating the centrifugation, decanting, and resuspension. After the second round of washing, the bacteria were resuspended in 25 mL of minimal medium, and then 12.5 mL of the resuspended cells were diluted into 2 L of minimal medium or 25 mL of the resuspended cells were diluted into 4 L of minimal medium. To each culture, Kan (final concentration 50 µg/mL), and a 400-µL aliquot of a vitamin mix (400 mg choline chloride, 500 mg folic acid, 1.1 g sodium pantothenoate, 500 mg nicotinamide, 500 mg of myo-inositol, 500 mg pyridoxal•HCl, 500 mg thiamine•HCl, and 50 mg riboflavin suspended in 15 mL of Milli-Q water) were added as well as a spatula tip's worth of iron(III) chloride hexahydrate, biotin, and thiamine•HCl. The cultures were then incubated at 37 °C with shaking at 150 rpm. When the cultures reached $OD_{600} \approx 0.6$, protein overexpression was induced by the addition of IPTG (final concentration 0.5 mM). When the cultures were grown in medium prepared in H₂O, the cultures reached $OD_{600} \approx 0.6$ after 3.5-4 h, whereas 8.5-9.5 h was required to reach $OD_{600} \approx 0.6$ for cultures grown in minimal medium prepared in D₂O. The cultures were grown for an additional 4 h and then harvested by centrifugation (3 000 rpm x 20 min, 5 °C). The cell pellets were transferred to 50-mL conical flasks, frozen with liquid nitrogen, and stored at -80 °C. The wet cell pellet yield ranged from 1-3 g cells/L of culture.

Proteins were purified as previously described.⁹ The protein yields ranged from 5-14 mg / L of culture. Purity and isotope incorporation of the proteins were evaluated by SDS-PAGE (Figures A2.15-A2.18) and mass spectrometry (Tables 3.3 and 3.4).

Table 3.3. Mass spectrometry of proteins with nonspecific labeling.

Protein	Mass (Da)
A8(C42S)(I60K)	Obs: 10 834.5 Theo: 10 834.5
[¹⁵ N]-A8(C42S)	Obs: 10 944.3 Theo: 10 945.4
[¹⁵ N]-A8(C42S)(I60K)	Obs: 10 961.1 Theo: 10 961.5
[¹³ C, ¹⁵ N]-A8(C42S)(I60K)	Obs: 11 442.1 Theo: 11 449.9
[² H, ¹³ C, ¹⁵ N]-A8(C42S)(I60K)	Obs: 12 042.4 Theo: 12 212.6
[¹ H/ ² H, ¹³ C, ¹⁵ N]-A8(C42S)(I60K)	Obs: 11 785.7 (≈56% ² H incorporation)
A9(C3S) ^a	Obs: 13 094.7 Theo: 13 094.7
[¹⁵ N]-A9(C3S) ^a	Obs: 13 254.7 Theo: 13 255.7
[¹⁵ N]-A9(C3S)(H103A) ^a	Obs: 13 186.6 Theo: 13 187.5
[¹⁵ N]-A9(C3S)(H105A) ^a	Obs: 13 186.5 Theo: 13 187.5
[¹⁵ N]-A9(C3S)(P107A) ^a	Obs: 13 229.2 Theo: 13 229.5
[¹³ C, ¹⁵ N]-A9(C3S) ^a	Obs: 13 815.9 Theo: 13 825.3
[² H, ¹³ C, ¹⁵ N]-A9(C3S) ^a	Obs: 14 503.8 Theo: 14 728.8
[¹ H/ ² H, ¹³ C, ¹⁵ N]-A9(C3S) ^a	Obs: 14 205.7 (≈55% ² H incorporation)

^a In all preparations, the dominant purified species of the S100A9 subunit lacked the N-terminal methionine. The masses reported here are the observed and theoretical values for S100A9(C3S) lacking Met1.

Table 3.4. Mass spectrometry of proteins with selective ¹⁵N labeling.

Protein	Mass (Da)
[¹⁵ N(Phe)]-A8(C42S)(I60K)	Obs: 10 837.6 Theo: 10 838.5
[¹⁵ N(Leu)]-A8(C42S)(I60K)	Obs: 10 843.8 Theo: 10 843.5
[¹⁵ N(Ile)]-A8(C42S)(I60K)	Obs: 10 840.0 Theo: 10 839.5
[¹⁵ N(Val)]-A8(C42S)(I60K)	Obs: 10 839.5 Theo: 10 840.5
[¹⁵ N(Phe)]-A9(C3S) ^a	Obs: 13 099.6 Theo: 13 099.7
[¹⁵ N(Leu)]-A9(C3S) ^a	Obs: 13 105.7 Theo: 13 105.7
[¹⁵ N(Ile)]-A9(C3S) ^a	Obs: 13 100.6 Theo: 13 100.7
[¹⁵ N(Val)]-A9(C3S) ^a	Obs: 13 097.6 Theo: 13 097.7

^a In all preparations, the dominant purified species of the S100A9 subunit lacked the N-terminal methionine. The masses reported here are the observed and theoretical values for S100A9(C3S) lacking Met1.

3.2.4. Protein Overexpression and Purification – Selective ¹⁵N Labeling of Phe, Leu, Ile or Val

To prepare proteins with selective ¹⁵N labeling of Phe, Leu, Ile, or Val, the pET15b, pET41a-S100A8(C42S)(I60K), and pET41a-S100A9(C3S) plasmids were digested with XbaI and XhoI, and the S100A8(C42S)(I60K) and S100A9(C3S) genes were subcloned into the XbaI and XhoI sites of pET15b. The resulting plasmids were confirmed by DNA sequencing and transformed into chemically competent *E. coli* CT19,^{30,31} which are derived from *E. coli* BL21(DE3) and are auxotrophic for Phe, Leu, Ile, and Val. It was necessary to use ampicillin (Amp) as a selection marker because CT19 cells have a biosynthetic gene knocked out with a Kan resistance cassette. For antibiotic selection, a working concentration of 100 µg/mL Amp was used. Overnight cultures were prepared as described above except that the medium was supplemented with Amp. The overnight cultures were washed and diluted into the minimal media as described above. A different

minimal medium, which contained all of the proteinogenic amino acids, was used for selective labeling. The recipe for this medium is provided in Table 3.5. Two batches of 5x-concentrated media were prepared. In one preparation, Phe, Leu, Ile, and Val were omitted. Trp was omitted from both media preparations. After autoclaving the 5x media, it was diluted to 1x using sterile-filtered Milli-Q water, and then 1% (w/v) glucose, 100 μ M CaCl₂, and 2 mM MgSO₄ were added. To the medium lacking the Phe, Leu, Ile, and Val, three of the four amino acids were added that contained natural abundance isotopes. For the fourth amino acid, a ¹⁵N-labeled isotopologue was added in place of the natural abundance amino acid. Immediately after inoculating the washed bacteria into the minimal media, a spatula tip's worth of iron(III) chloride hexahydrate, biotin, and thiamine•HCl were added as well as 100 mg/L NAD and 100 mg/L Trp. Overexpression was induced as described above, and the proteins were purified as described previously.⁹ The medium used for selective labeling did not have a systematic effect on the growth rate or protein yield compared to the medium used for uniform labeling.

3.3.5. Mass Spectrometry

An Agilent 1260 series LC system equipped with an Agilent 6230 TOF system housing an Agilent Jetstream ESI source or an Agilent 1290 LC system equipped with an Agilent 6510 Q-TOF ESI source was employed to perform high-resolution mass spectrometry. An Agilent Poroshell 300SB-C18 (5- μ m pore) and denaturing protocol were used for all LC-MS analyses. Solvent A was 0.1% formic acid/H₂O. Solvent B was 0.1% formic acid/MeCN. The S100A8 and S100A9 subunits were eluted using either a 5–85% B over 10 min or 10–90% B over 15 min gradient. The resulting mass spectra were deconvoluted using the maximum entropy algorithm in MassHunter BioConfirm (Agilent).

Table 3.5. Components for selective labeling medium

Component	Mass (g/L)	Component	Mass (g/L)
Alanine	2.5	Proline	0.5
Arginine	2.0	Serine	10.5
Asparagine	2.3	Threonine	1.15
Aspartate	2.0	Tyrosine	0.85
Cysteine	0.36	Valine	1.15
Glutamate	3.73	Adenosine	2.5
Glutamine	2.0	Guanosine	3.25
Glycine	2.75	Thymine	1.0
Histidine	0.5	Uracil	2.5
Isoleucine	1.15	NH ₄ Cl	2.5
Leucine	1.15	NaCl	2.5
Lysine	2.6	KH ₂ PO ₄	15
Methionine	1.25	Na ₂ HPO ₄ •7H ₂ O	64
Phenylalanine	0.65		

For the media used for selective ¹⁵N labeling, Phe, Ile, Leu, and Val were omitted. The pH was adjusted to 7.4 using NaOH before autoclaving, and then diluted to 1x using sterile-filtered Milli-Q water. Sterile-filtered glucose, CaCl₂, and MgSO₄, were added to 1% (w/v), 100 μM, and 2 mM, respectively, to the 1x medium. For the media to be used for selective ¹⁵N labeling, three of the four omitted amino acids were added at natural abundance from sterile-filtered 100-mM solutions. The ¹⁵N-labeled amino acid was added following inoculation of the resulting medium as described below.

Immediately after inoculating the medium with bacteria from an overnight culture (LB with 100 μg/mL Amp) that were pre-washed in this minimal medium, the following components were added: 100 mg/L tryptophan, 100 mg/L nicotinamide adenine dinucleotide, ¹⁵N amino acid of interest (one-fifth of the amount listed in Table 3.5), and a spatula tip's worth of FeCl₃ hexahydrate, thiamine•HCl and biotin. Lastly, Amp was added to 100 μg/mL in the overexpression cultures.

3.3.6. Analytical Size-Exclusion Chromatography

An Äkta purifier (GE Lifesciences) housed in a 4 °C cold room outfitted with a 100- μ L sample loop was used to perform all analytical size exclusion chromatography experiments. A Superdex 75 10/300 GL column (GE Lifesciences equilibrated in running buffer) was calibrated with a low-molecular-weight calibration mixture (GE Lifesciences) as described previously.⁹ The proteins were thawed at room temperature, and then concentrated and buffer exchanged into the running buffer (75 mM HEPES, 100 mM NaCl, pH 7.5) with three rounds of buffer exchanging using 0.5-mL 10K MWCO Amicon spin filters. For experiments performed in the presence of Ca(II), we added Ca(II) to 10 mM in the samples and running buffer.

3.3.7. NMR Sample Preparation

Using 10 K MWCO 0.5-mL Amicon spin filters, the proteins were buffer exchanged from the final dialysis buffer used during purification (20 mM HEPES, 100 mM NaCl, pH 8.0) to 11 mM HEPES, 11 mM NaCl, pH 7.0 through three rounds of centrifugal concentration (13 000 rpm, 5 min, 4 °C) before or after flash freezing and storage at -80 °C. Next, the proteins were diluted to 555 μ M using the NMR buffer, and then D₂O was added to 10% (v/v). Higher protein concentrations were used for select experiments. When recording the ¹⁵N relaxation experiments with [¹⁵N]-A8-I60K on the 900 MHz spectrometer, a protein concentration of 880 μ M was employed. For the experiments with [¹H/²H, ¹³C, ¹⁵N]-A9-I60K and [¹³C, ¹⁵N]-A9-I60K using the 800 MHz spectrometer, protein concentrations of 1 mM and 820 μ M were used, respectively. Lastly, for spectra with [¹H/²H, ¹³C, ¹⁵N]-A8-I60K recorded on the 800 MHz spectrometer, the protein concentration was 1.3 mM.

Before preparing the samples, the NMR tubes were washed three times with water, three times with 20% HNO₃, three times with water, and then dried. The +Ca(II) conditions contained 20 mM Ca(II) that had been added from a 1 M stock solution. Typically, spectra

of the apo protein were acquired before adding Ca(II). After leaving an apo sample overnight in a NMR tube, a white precipitate formed. Comparing 1D ^1H -spectra before and after formation of the precipitate indicated that the protein concentration did not significantly change after the precipitation. Buffer exchanging the protein before or after storage had a negligible effect on the amount of precipitate that formed (as evaluated by eye). Additionally, the rate of precipitation could be dramatically slowed by performing the experiments with the protein solution contained in a PTFE tube liner (Norell) that was housed in standard NMR tube. The solubility of the protein was improved when excess Ca(II) was present in the sample. Under such conditions, negligible precipitation was observed following overnight incubation in a NMR tube.

3.3.8. *General NMR Spectroscopy Methods*

NMR data recorded at 600 MHz or 900 MHz was acquired and processed using Topspin 3.2 (Bruker BioSpin). NMR data recorded at 591 MHz was acquired using RNMR (courtesy of Dr. David Ruben at the MIT Francis Bitter Magnet Laboratory) and processed using NMRPipe.³² All NMR data was analyzed using SPARKY.³³ Detailed acquisition and processing parameters can be found in Tables A3.1-A3.8. Chemical shifts were used to determine the dihedral angles in I60K variants in the absence or presence of Ca(II). For such analysis, ^1H , ^{15}N , $^{13}\text{C}^\alpha$, $^{13}\text{C}^\beta$ and, where available, $^{13}\text{C}'$ were analyzed using TALOS-N.³⁴

3.3.9. *Backbone Resonance Assignment*

Amide backbone resonance of I60K variants were assigned through 3D HNCACB experiments on $\approx 500 \mu\text{M}$ uniformly ^2H , ^{13}C , ^{15}N labelled sample. Amino acid specific labelling was used to guide assignment using ^{15}N isotopically labelled isoleucine, leucine, phenylalanine, and valine samples. To confirm the assignment of the H103-H104-H105 portion of the C-terminal extension, we used two I60K variants carrying either a H103A

or H105A mutation.⁶ [¹H,¹⁵N]-TROSY³⁵⁻³⁶ spectra of [²H,¹³C,¹⁵N]-A8-I60K and [²H,¹³C,¹⁵N]-A9-I60K, both in the absence and presence of Ca(II), were acquired at 298 K on a 900 MHz spectrometer (Bruker Avance II). 3D [¹H,¹³C,¹⁵N]-HNCO³⁷ spectra of [²H,¹³C,¹⁵N]-A9-I60K in the absence and presence of Ca(II) were acquired at 298 K on a 900 MHz spectrometer (Bruker Avance II). 3D [¹H,¹³C,¹⁵N]-HNCACB³⁸⁻³⁹ spectra of [²H,¹³C,¹⁵N]-A8-I60K in the presence of Ca(II), as well as [²H,¹³C,¹⁵N]-A9-I60K in the absence and presence of Ca(II) were acquired at 298 K on a 900 MHz spectrometer (Bruker Avance II). [¹H,¹⁵N]-HSQC⁴⁰ spectra of [¹⁵N-Ile]-A9-I60K, [¹⁵N-Val]-A9-I60K, [¹⁵N-Phe]-A9-I60K, and [¹⁵N-Leu]-A9-I60K, all in absence and presence of Ca(II), as well as [¹⁵N]-A9-I60K(H103A) and [¹⁵N]-A9-I60K(H105A) in absence and presence of Ca(II) were acquired at 298 K on a 591 MHz spectrometer operating under RNMR (courtesy of Dr. David Ruben) equipped with a Nalorac 5 mm indirect triple resonance [¹H,¹³C,¹⁵N] probe with z-gradient. [¹H,¹⁵N]-HSQC⁴⁰ spectra of [¹⁵N-Ile]-A8-I60K, [¹⁵N-Leu]-A8-I60K, [¹⁵N-Val]-A8-I60K, and [¹⁵N-Phe]-A8-I60K, all in the absence or presence of Ca(II) (except [¹⁵N-Leu]-A8-I60K), were acquired at 298 K on a 600 MHz spectrometer (Bruker Avance I). The chemical shifts of the assigned resonances are listed in Tables A3.9-A3.12.

3.3.10. NMR Spectroscopy of I60K Variants

[¹H,¹⁵N]-HSQC⁴⁰ spectra of [¹⁵N]-A9-I60K, as well as [¹⁵N]-A9-I60K(P107A) and [¹⁵N]-A9-I60K(P114A) in the absence or presence of Ca(II) were acquired at 298 K on a 600 MHz spectrometer (Bruker Avance I).

3.2.11. Estimation of Molecular Weight from Magnetic Relaxation Rates

The molecular weight of the I60K variant in the presence and absence of Ca(II) was determined by T_2/T_1 ratio as previously described: http://www.nmr2.buffalo.edu/nescg.wiki/NMR_determined_Rotational_correlation_time.

3.2.12. Chemical Shift Perturbations

Chemical shifts of the backbone amide resonances were compared by calculating the chemical shift perturbations with the following equation:

$$CSP = \sqrt{(0.1\delta_{15N}^A - 0.1\delta_{15N}^B)^2 + (\delta_{1H}^A - \delta_{1H}^B)^2}$$

where $\delta_{1H/15N}$ describes the chemical shift in ppm (either 1H or ^{15}N , respectively). A and B designates the two states that are compared.

3.3.13. Relaxation and Model-Free Analysis

T_1 , T_2 and hetNOE data on A8-I60K in absence of Ca(II) as well as A9-I60K in absence and presence of Ca(II) was recorded on 500 μ M uniformly ^{15}N labelled samples on a 900 MHz spectrometer (Bruker Avance II). The relaxation delays chosen for A8-I60K in the presence of Ca(II) and A9-I60K in the absence and presence of Ca(II) were 0.02, 0.1, 0.1, 0.3 0.5, 0.8, 1.0, 1.0, 2.0, 2.5 s for T_1 , and 17.0, 17.0, 33.9, 50.9, 67.8, 67.8, 102.0, 136.0, 136.0, 170. ms for T_2 . Duplication of relaxation delays is used for error estimation. T_1 and T_2 rates were analysed using SPARKY.³³ Model-free analysis was conducted using TENSOR2.⁴¹

3.4. Results and Discussion

3.4.1. Prior Structures of CP

Several crystal structures of the metal-bound CP-Ser heterotetramer have been reported (Figure 3.1).^{3,8,16,17} These structures have confirmed that CP adopts a fold common to the S100 family. Each subunit is composed of two helix-loop-helix motifs termed EF-hand domains.⁴² The helices of the EF-hands are numbered I–IV ordered from the N- to C-termini (Figure 3.1C). The loop in each EF-hand forms a Ca(II)-binding site.

The C-terminal EF-hands of S100 proteins resemble those of calmodulin, and are often referred to as “canonical” EF-hands. The N-terminal EF-hands of S100 proteins are structurally similar to canonical EF-hands; however, they have unique qualities, and are often termed pseudo EF-hands or “non-canonical” EF-hands. Pseudo EF-hand loops are usually two amino acids longer than canonical EF-hand loops, contain fewer negatively charged residues, and have lower coordination numbers. Thus, it is accepted that these EF-hands bind Ca(II) with relatively low affinity.⁴² There is a small region referred to as a linker between the N-terminal and C-terminal EF-hands that contains a short helix, and this region will be referred to as the linker-helix (Figure 3.1C).²¹

CP also displays several features that are uncommon among members of the S100 family. First, at the interface of the heterodimer there are two transition metal binding sites composed of residues from both subunits of the heterodimer. CP is unique in that it has two non-identical transition-metal binding sites. Site 1 is a His₃Asp motif that binds Zn(II) with high affinity,⁹ and site 2 is a His₆ site that binds Mn(II),^{6,16,43} Fe(II),⁷ Ni(II),⁸ and Zn(II)^{9,44} with high affinity. Furthermore, S100A9 is the longest human S100 protein due to a C-terminal extension defined by residues G102-P114, colloquially termed “the S100A9 tail.” This region is important for the metal-sequestering function because H103 and H105 contribute to transition metal coordination at the His₆ site.^{6,16} Another feature of CP that is uncommon among S100 proteins is that it forms higher-order oligomers. In the presence of excess Ca(II) and/or a transition metal bound at site 2, two CP heterodimers self-associate to form a dimer of dimers termed the heterotetramer (Figure 3.1B).^{3,10}

In this study, we used a variant of CP that has the (A8)I60K mutation, which has been shown to prevent Ca(II)-induced tetramerization.¹¹ In order to distinguish the I60K system CP-Ser system, we will henceforth use the following naming convention. When discussing any subunits that are part of the heterodimer or heterotetramer in the I60K system, we will use A8-I60K and A9-I60K, even though only S100A8 is the carrier of the

I60K mutation. Analogously, we will use A8-CP-Ser and A9-CP-Ser for the parent S100A8 and S100A9 subunits, respectively. Lastly, (A9)M1 is cleaved during overexpression; therefore, the N-terminal residue of the recombinant protein is (A9)T2.

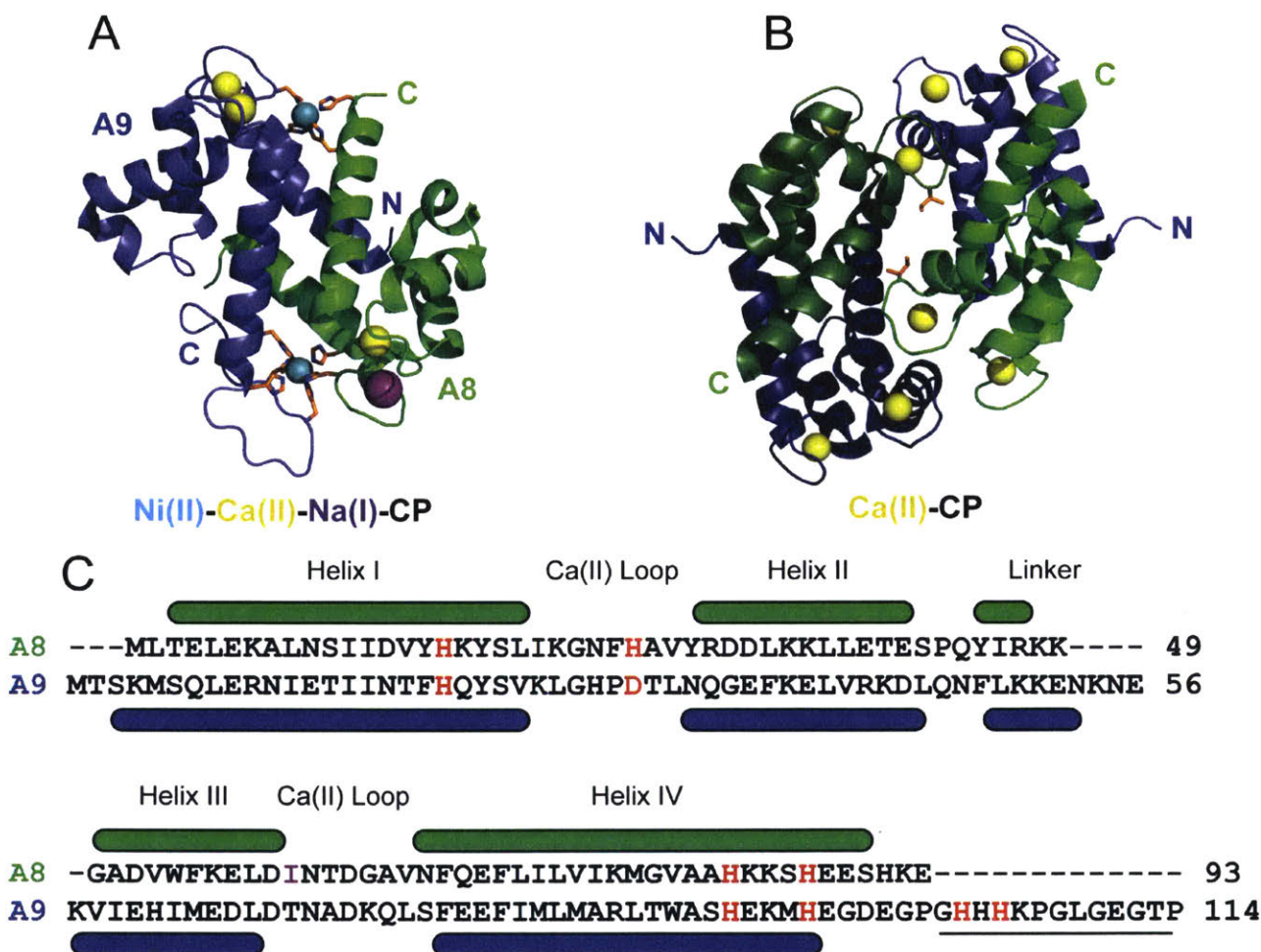


Figure 3.1. Structure of CP-Ser and amino acid sequences of S100A8 and S100A9. S100A8 is shown in green and S100A9 is shown in blue. (A) Structure of the CP heterodimer (PDB 5W1F) with Ni(II), Ca(II), and Na(I) bound. (B) Structure of the CP heterotetramer with Ca(II) bound (PDB 1XK4). One dimer is shown in light colors and the other is shown in dark colors. Residue I60 in A8 is shown in sticks. (C) Alignment of the S100A8 and S100A9 sequences with secondary structural elements mapped onto the sequences. Transition-metal-binding residues are shown in red. (A8)I60 is shown in purple. The S100A9 C-terminal extension is underlined.

3.4.2. Assignment of the I60K Subunits in the Presence and Absence of Ca(II)

Before beginning comprehensive NMR studies, it was necessary to characterize the oligomeric properties of I60K at high concentrations because I60K had been incompletely studied at 500 μ M previously.¹¹ We performed SEC with 500 μ M I60K in the absence of Ca(II) and 500 μ M CP-Ser in the presence and absence of 10 mM Ca(II), and compared these data to our previously reported chromatogram of 500 μ M I60K+Ca(II) (Figure A2.19). The SEC chromatograms of 500 μ M I60K were consistent with previously reported SEC experiments that were performed with 30 μ M I60K.¹¹ In both sets of experiments, we observed that the protein eluted at the characteristic dimer volume in the absence of Ca(II), and shifted to a later elution volume, indicating that the protein had become more compact. CP, in contrast, shifted to a later elution volume characteristic of the heterotetramer. Additionally, we calculated the molecular weight of I60K using the ratio of T_1/T_2 obtained from relaxation experiments (Figure A3.1), and found that it was approximately 24 kDa in the presence and absence of Ca(II), further supporting the notion that the protein remained a dimer under the NMR sample conditions.

Studying I60K by NMR spectroscopy requires isotopically labeled proteins. Accordingly, we prepared protein samples with a single subunit isotopically enriched, which simplified spectral analysis because only one subunit was visible in multidimensional experiments. A variety of ^2H -, ^{13}C -, and ^{15}N -labeled samples were employed for this study. Furthermore, to resolve ambiguities in the resonance assignments of A8-I60K and A9-I60K, amino-acid-specific labeling was utilized. By employing the auxotrophic *E. coli* CT19 strain,³⁰ we were able to selectively introduce [^{15}N]-Phe, [^{15}N]-Ile, [^{15}N]-Leu, and [^{15}N]-Val into A8-I60K and A9-I60K. The selectively labeled proteins were used in [^1H - ^{15}N]-HSQC experiments (Figures A3.2-A3.5). Because we encountered difficulties in assigning H103, H104, and H105 of A9-I60K, we prepared [^{15}N]-A9-I60K(H103A) and [^{15}N]-A9-I60K(H105A), and used these variants in [^1H - ^{15}N]-HSQC experiments (Figures A3.6 and A3.7). For each variant, we found that a single

peak disappeared and another peak displayed a minor perturbation. By combining this information with the data from an HNCACB experiment using [^2H , ^{13}C , ^{15}N]-A9-I60K, we were able to assign H103, H104, and H105.

When working to assign the resonances, we used proteins with a single subunit of I60K with [^2H -, ^{13}C -, ^{15}N] labeling and recorded 3D HNCACB spectra. We encountered difficulties observing cross peaks in 3D assignment experiments that depended strongly on the subunit and the presence of Ca(II). This problem was more pronounced in the samples without Ca(II) for both A8-I60K and A9-I60K, and the most dramatic example of this behavior was S100A8 in the absence of Ca(II). Hence, A9-I60K was more amenable to assignment than A8-I60K. In the absence of Ca(II), we were able to assign 99 of the 108 expected backbone amides as well as the W88N^{e1} resonance (Figures 3.2A and 3.3A). The N-terminal amine as well as prolines are not observed in [^1H - ^{15}N]-TROSY spectra. The unassigned residues were S3-M5, K54, H95-D98, and K106 are most likely absent due to exchange broadening. It is interesting to note that that residue H95 is one of the transition-metal binding residues that is part of site 2, and the succeeding residues form the initial part of the C-terminal extension of A9-I60K. Our inability to assign this important region of the protein in the absence of Ca(II) suggests that it is undergoing intermediate conformational exchange.

In the presence of Ca(II), we assigned 102 of the 108 expected backbone amides, and the single W88N^{e1} resonance in A9-I60K (Figures 3.2B and 3.3B). Most of the missing assignments in the +Ca(II) spectra of A9-I60K were different than those in the -Ca(II) spectra. The only unassigned residues in the [^1H - ^{15}N]-TROSY spectra of A9-I60K in the presence of Ca(II) were S3, S6, G27, H28, T87, and K106. The residues in the A9-I60K C-terminal extension did not exhibit a Ca(II)-induced shift. In the first crystal structure of CP-Ser, the C-terminal extension of the A9 subunit was not visible due to disorder;³ however, in later structures that were solved with the protein bound to a transition metal, much of the C-terminal extension could be modeled because it contributes two

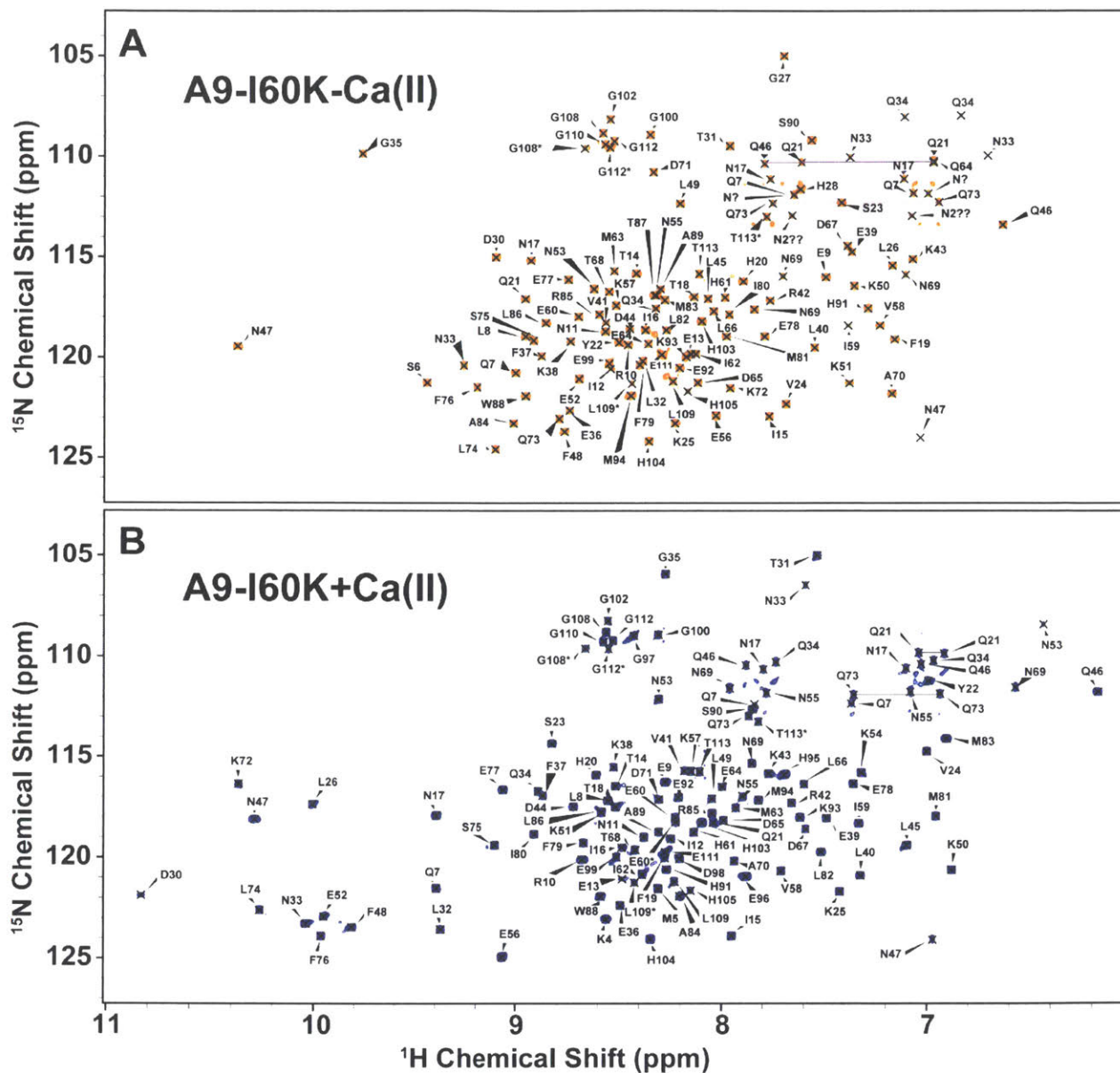
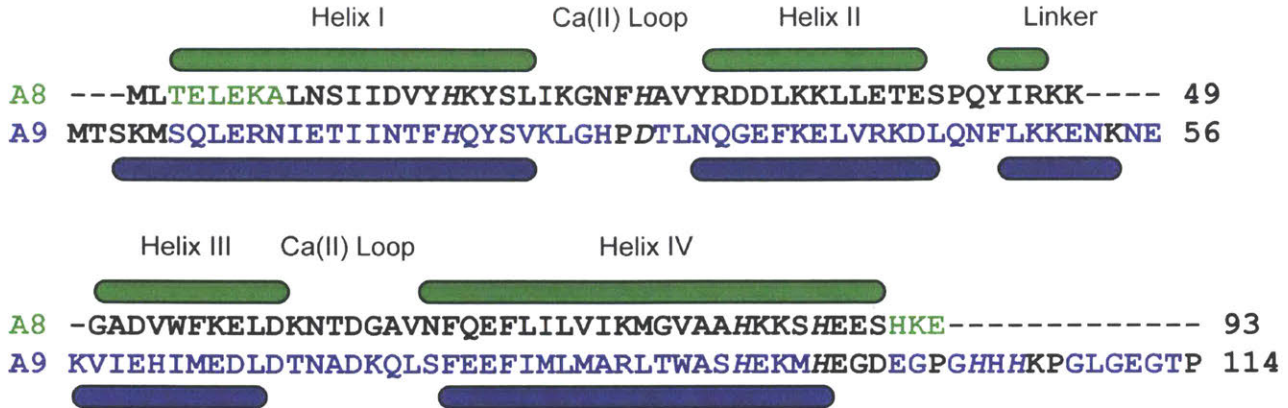


Figure 3.2. TROSY spectra of (A) ^{15}N -A8-I60K-Ca(II) and (B) ^{15}N -A8-I60K+Ca(II). Conditions: 10 mM HEPES, 10 mM NaCl, pH 7.0, 500 μM I60K, and ± 20 mM Ca(II).

A



B

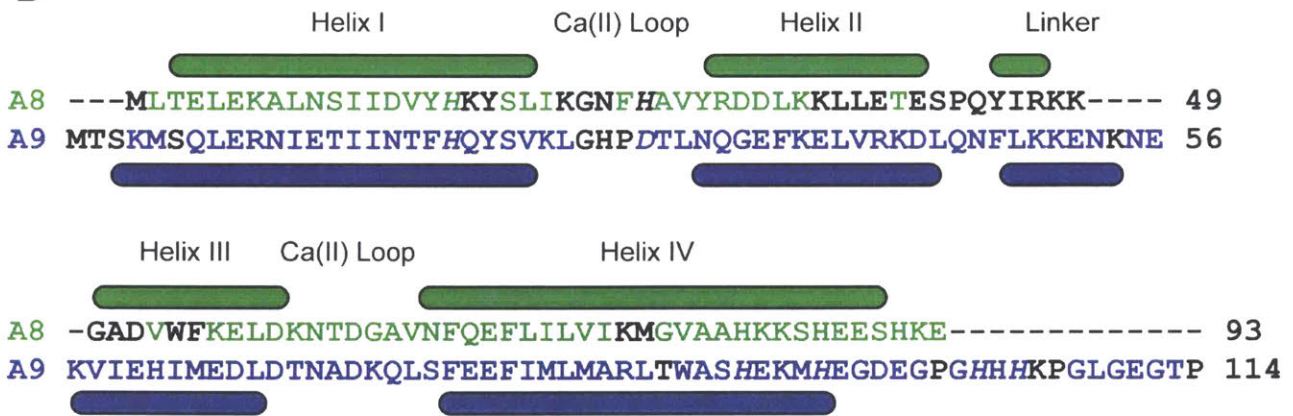


Figure 3.3. Depiction of assigned residues in the (A) absence of Ca(II) and (B) presence of Ca(II). Black residues were unassigned. Green residues indicate that that an A8-I60K residue was assigned. Blue residues indicate that an A9-I60K residue was assigned. Italicized residues are transition-metal binding residues.

residues (H103 and H105) to site 2, which caused the C-terminal extension to become more ordered.^{8,16,17} The lack of chemical shift dispersion of the glycine residues in the C-terminal extension suggests that this region of the protein is disordered in the absence and presence of Ca(II), and can be considered an intrinsically unstructured peptide in the absence of transition metals. No Ca(II)-induced chemical shift changes were observed upon addition of Ca(II), which signified that the behavior of the A9-I60K tail does not change with Ca(II).

Also of note, we observed two sets of resonances that were consistent with (A9)P107 (CA and CB only), (A9)G108, (A9)L109, (A9)G112, and (A9)T113 in both S100A9 spectra (Figure 3.1A,B). We considered that the high Pro content of the S100A9 tail could result in the presence of slowly converting cis and trans Pro amide bonds, giving rise to two sets of resonances. To evaluate this possibility, we prepared [¹⁵N]-A9-I60K variants where either (A9)P107 or (A9)P114 was mutated to Ala to lock an amide bond in a trans conformation, which would cause one of the sets of resonances to disappear. The mutations resulted in perturbations in the chemical shifts of the neighboring residues; however, the twin sets of resonances were present in the [¹H-¹⁵N]-HSQC spectra of both variant proteins (Figures A3.8 and A3.9), which led us to conclude that isomerization of a single Pro amide bond was not responsible for the observed peak doubling. We are currently unable to ascribe a cause for this phenomenon.

Though the [¹H-¹⁵N]-TROSY spectra of A8-I60K in the absence of Ca(II) were initially promising (Figure 3.4A), we were not able to obtain a significant number of cross peaks in standard 3D triple resonance experiments using [²H, ¹³C, ¹⁵N]-A8-I60K. By reducing the dimensionality of the 3D triple resonance experiments to 2D, we were able to obtain spectra of sufficient signal-to-noise to yield the assignment of 6 N-terminal (T3-A8) and last 4 C-terminal (S90-E93) residues of A8-I60K (Figures 3.3A and 3.4A). These difficulties are associated with unfavorable transverse (T_2) relaxation properties of ¹³C nuclei that can arise from conformational exchange in the intermediate time regime and/or

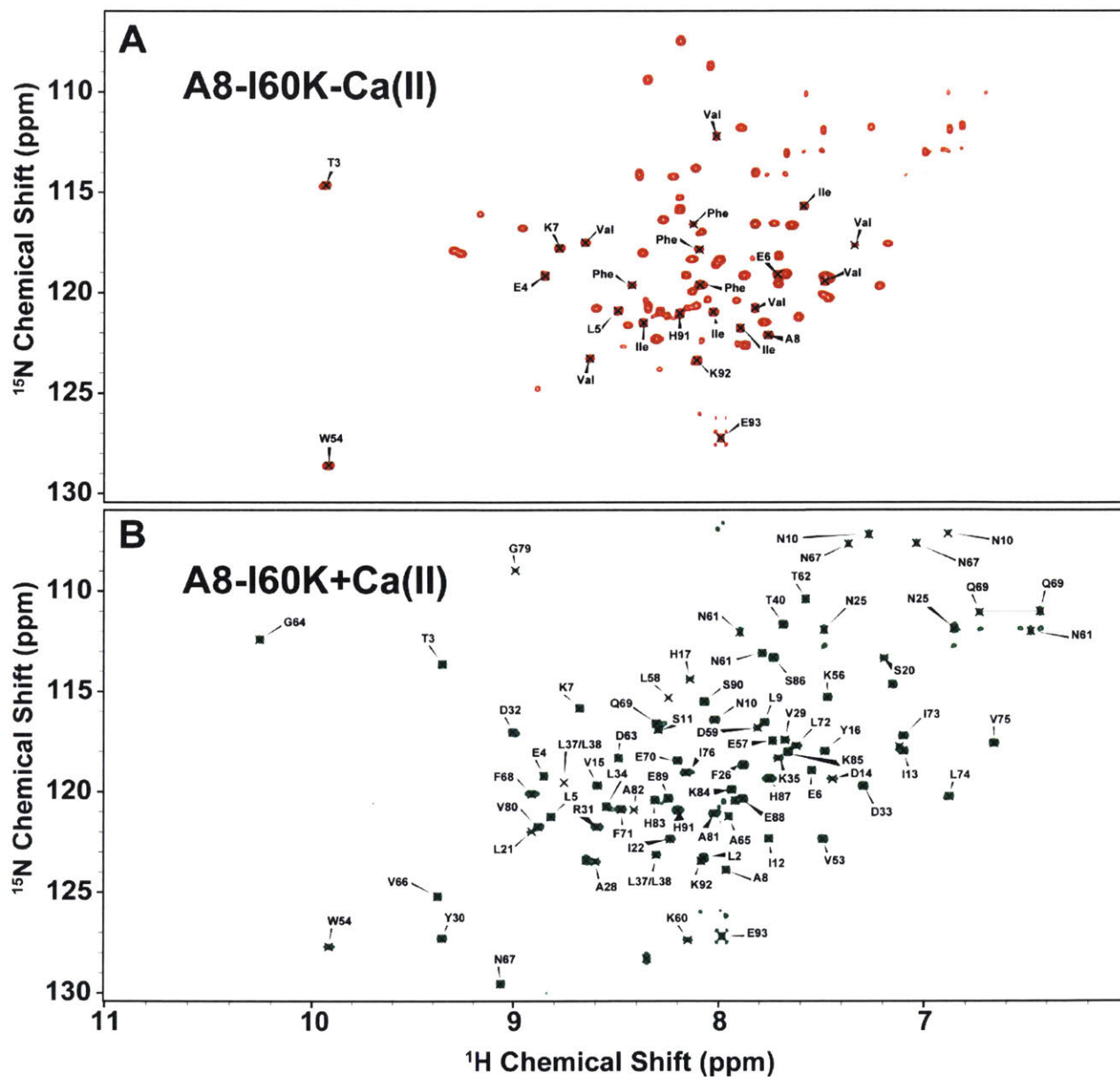


Figure 3.4. TROSY spectra of (A) [^{15}N]-A9-I60K-Ca(II) and (B) [^{15}N]-A9-I60K+Ca(II) Conditions: 10 mM HEPES, 10 mM NaCl, pH 7.0, 500 μM I60K, and ± 20 mM Ca(II).

large molecules. Although the molecular weight of the complex (24 kDa) is approaching the limit for problematic T_2 rates,⁴⁵ we reason that the major factor for fast transverse relaxation is conformational exchange in A8-I60K. This notion is supported by the observation that the A8-I60K subunit contains a single Trp residue (W54), and we found that HSQC spectra at 600 MHz displayed two peaks in the spectral region of the W54N^{ε1} nucleus (Figure A3.2). In contrast, only a single peak in the W54N^{ε1} region was observed in the 900 MHz spectrum (Figure 3.4A). This behavior is a hallmark conformational exchange, and further supports the notion that a large portion of the A8-I60K subunit exhibits a significant exchange contribution in the absence of Ca(II).

Our ability to assign the backbone amides of A8-I60K improved dramatically in the presence of Ca(II). We assigned 66 backbone amides of the 91 possible (excluding M1 and P43) and a single W54N^{ε1} resonance (Figures 3.3B and 3.4B). There were two peaks that we could not unambiguously assign to either L37 or L38. In the presence of Ca(II), only one W54N^{ε1} resonance was observed at both 600 MHz and 900 MHz. Considering that a single resonance from the W54 side chain was observed and our success in assigning a significant portion of the protein, we reasoned that Ca(II) dramatically alters the dynamics of the A8-I60K subunit. It is noteworthy that of the 25 unassigned residues, 15 were in a contiguous region from E41-F55 (Figure 3.3B), and within that region V53 was only assignable by process of elimination that was facilitated by selective ¹⁵N labeling. This region extends from the end of helix II through the linker region and ends halfway through helix III (Figure 3.3B), and it appears that this region continues to undergo intermediate exchange even in the presence of Ca(II).

3.4.3. *Chemical Shift Perturbation Analysis Reveals Regions that Respond to the (A8)I60K Mutation and Ca(II)*

We recorded [¹H-¹⁵N]-HSQC spectra of [¹⁵N]-A8-CP-Ser and [¹⁵N]-A9-CP-Ser in absence and presence of Ca(II), and overlaid them onto the corresponding spectra of A8-

I60K and A9-I60K, respectively, to determine which regions of the protein were most affected by introduction of the (A8)I60K mutation (Figures 3.5 and 3.6). Many of the resonances in the [^1H - ^{15}N]-HSQC spectra of A8-I60K were shifted and 14 resonances in the [^1H - ^{15}N]-HSQC of spectra of A9-I60K shifted due to the (A8)I60K mutation, which is consistent with the notion that the (A8)I60K mutation results in changes in dynamics that are felt in several regions of both subunits. Nevertheless, there were notable exceptions. The A8-CP-Ser and A9-CP-Ser N-termini were able to be assigned due to their similarity to the apo [^1H - ^{15}N]-HSQC spectra of A8-I60K and A9-I60K, respectively. Along similar lines, the N-termini of I60K and CP-Ser both displayed small chemical shift perturbations (CSPs) due to Ca(II) (Figure 3.7). These results suggest that N-termini of the CP subunits are largely unaffected by Ca(II) and tetramerization. On the basis of these observations, the large distance between the N-termini from the tetramer interface (Figure 3.7), and the proximity of the S100A8 and S100A9 N-termini in previous crystal structures (Figure 3.7), we postulate that the N-termini of the protein contribute to heterodimerization.

With the assignments of I60K in hand, it was possible to assess which regions of the protein were most dramatically affected by Ca(II). Because of the limited number assignments of A8-I60K in the absence of Ca(II), this analysis could only be applied to a few N- and C-terminal residues. We calculated chemical shift perturbations (CSPs) between -Ca(II) and +Ca(II) TROSY spectra for the assigned backbone resonances (Figure 3.7). We found that the N- and C-termini of A8-I60K exhibited minimal Ca(II)-induced changes in chemical shifts (Figure 3.3A). We note that the N-terminus of S100A8 is positioned far away from the tetramer interface and is in close proximity to the S100A9 N-terminus (Figure 3.7).

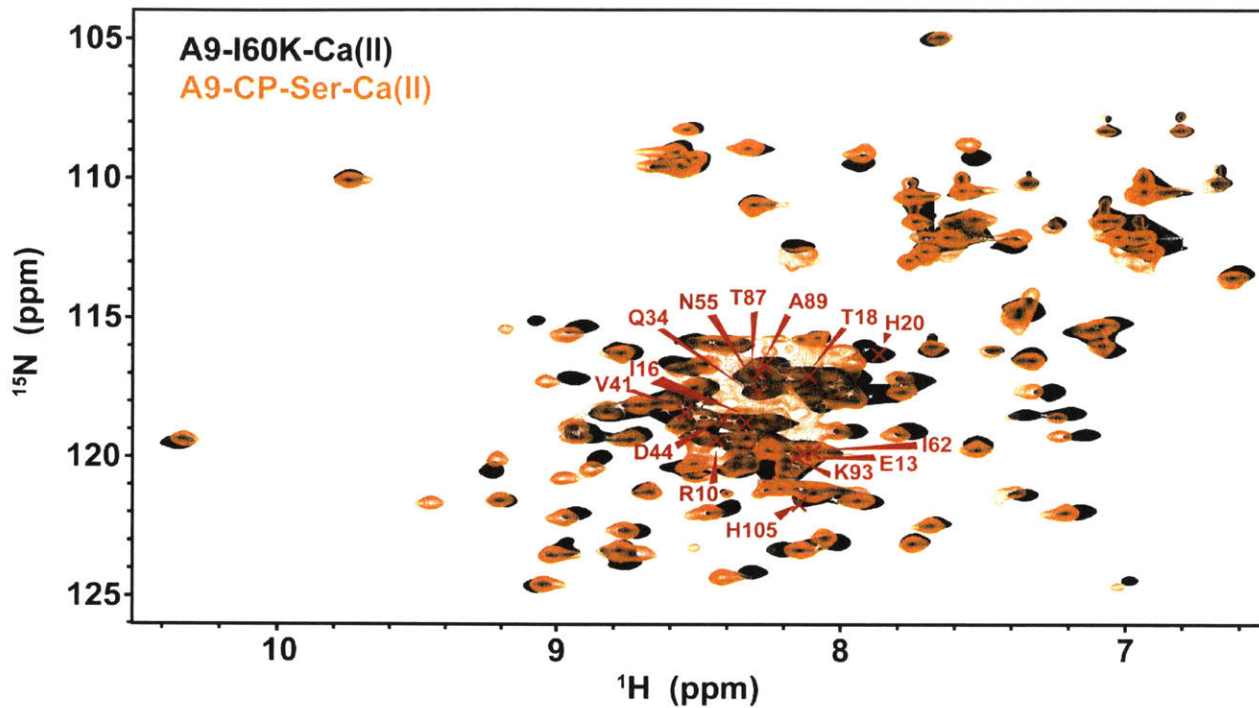


Figure 3.5. Overlay of A9-I60K (black) and A9-CP-Ser (orange) [^1H - ^{15}N]-HSQC spectra in the absence of Ca(II). The peaks marked in red are those where an assigned peak in the A9-I60K spectrum did not have an obvious cognate peak in the A9-CP-Ser spectrum.

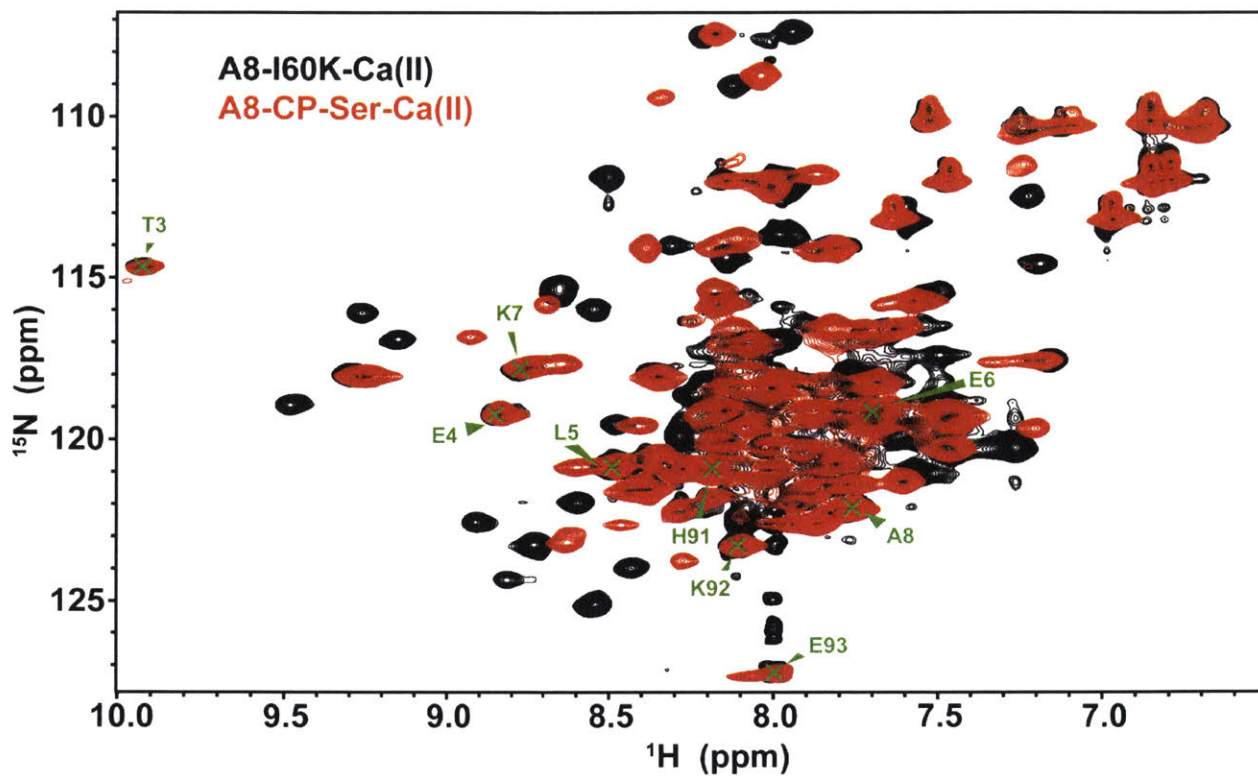


Figure 3.6. Overlay of A8-I60K (black) and A8-CP-Ser (red) [^1H - ^{15}N]-HSQC spectra in the absence of Ca(II). The peaks marked in green are those where an assigned peak in the A8-I60K had a matching peak in the A8-CP-Ser spectrum. All of the assigned A80-I60K peaks had a match.

A comprehensive analysis of the Ca(II)-induced CSPs on amides of A9-I60K was possible because of nearly complete assignments of the subunit in the presence and absence of Ca(II). Ca(II)-induced changes in A9-I60K can be classified as (a) changes due to effects directly related to the binding of the Ca(II) ion and (b) changes due to effects off-site of the Ca(II) binding site, so-called long-range effects. We found that the greatest Ca(II)-induced changes of chemical shift were in the EF-hand loops, specifically residues S23-N33 and D71-D74 (Figures 3.1C and 3.7). We reasoned that these changes were due to two factors: (i) structural rearrangement of the loop and (ii) presence of the positively charged Ca(II) ion. Residues distant from the Ca(II)-binding sites also experienced large CSPs; thus, Ca(II) binding leads to various long-range effects in A9-I60K. Residues F48-N53, which constitute the linker region, displayed exceptionally high CSPs as well as S90-M94, which is at the C-terminus of helix IV and in close proximity to residues taking part in transition-metal binding site 2 (H91 and H95) (Figures 3.1C and 3.7). We note that H95 could not be assigned in the absence of Ca(II) due to conformational exchange. The region around M81-M83, which forms the N-terminal region of helix IV, exhibits greater changes than much of the protein, though less than the linker and the C-terminal region of helix IV (Figures 3.1C and 3.7). Interestingly, M81 is involved in tetramerization (see Chapter 4). These results demonstrate that Ca(II) binding causes changes to the chemical environment in the EF-hand loops, the linker region, the C-terminal portion of helix IV, and the N-terminal portion of helix IV.

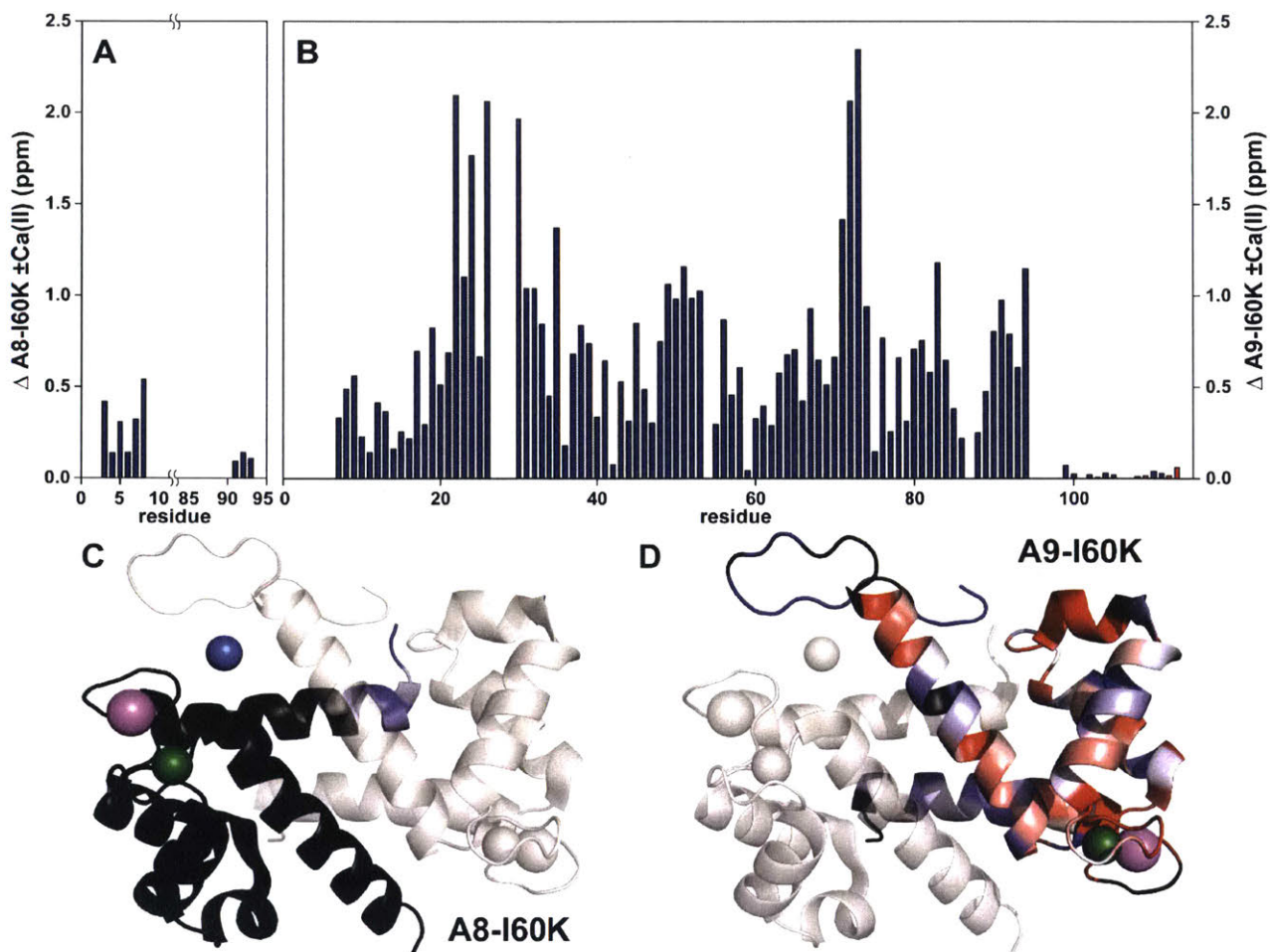


Figure 3.7. Plots of Ca(II)-induced CSPs for I60K. (A) CSPs for A8-I60K. (B) CSPs for A9-I60K. (C) A8-I60K CSPs plotted onto the S100A8 subunit of the 4XJK structure. (D) A9-I60K CSPs plotted onto the S100A9 subunit of the 4XJK structure. The color coding for the structures are as follows: black is an unassigned residue, blue is a small CSP, white is a moderate CSP, and red is a large CSP.

3.4.4. TALOS-N Highlights Regions that Rearrange with Ca(II)

Chemical shifts can be used to predict protein backbone torsion angles using TALOS-N,⁴⁶ an artificial neural network program used to empirically predict protein backbone Φ/Ψ torsion angles as well as secondary structure elements using a combination of six chemical shift assignments ($^1\text{H}_\text{N}$, H^α , C^α , C^β , C' , N). We subjected the chemical shifts of A8-I60K and A9-I60K in the absence and presence of Ca(II) to TALOS-N analysis (Figures 3.8-3.11). We compared the predicted Φ and Ψ to those of the

heterotetramer in the 4XJK crystal structure (Figures 3.8-3.11).¹⁷ In general, there was strong agreement between the TALOS-N predictions and the crystallographic data for A8-I60K and A9-I60K in the presence of Ca(II). These results signify that in the presence of Ca(II), the subunits of I60K resemble the X-ray structures of the heterotetramer. In the absence of Ca(II), the TALOS-N predictions for A9-I60K agree well with the experimental structures, and we posit that the secondary structure of A8-I60K remains largely the same after addition of Ca(II) as well. These data favor a model where Ca(II) coordination to the protein causes changes in dynamics and helix orientations as opposed to largescale reconfiguration of secondary structure, and confirms that much of the secondary structure is conserved between the heterodimer and heterotetramer.

There are several regions that show telling similarities and differences with the Mn(II)-Ca(II)-CP-Ser structure (PDB 4XJK). One major area of discrepancy is in the C-terminal extension of A9-I60K in the presence and absence of Ca(II) (Figures 3.10 and 3.11). TALOS-N predicts that the C-terminal extension of A9-I60K does not have a well-defined secondary structure, which agrees with the experimental data; however, the values of the dihedral angles do not agree. These differences most likely arise from differences in the crystallization and NMR spectroscopy conditions. In the crystal structure, the C-terminal extension of A9-CP-Ser adopted a fold that allows H103 and H105 to participate in Mn(II) coordination at site 2, whereas there are no such restrictions under the transition-metal free conditions of our NMR experiments. TALOS-N does predict dihedral angles consistent with a β -sheet for (A9)H103-H105. These residues are flanked by unstructured polypeptide, which suggests that (A9)H103-H105 has intrinsic structure. We posit that the intrinsic structure arises from the presence of three consecutive His residues, which would favor an extended β -strand conformation to prevent steric clashing between the bulky side chains and repulsion due to charge repulsion. Having H103-H105 intrinsically adopt an extended β -strand may also help preorganize H103 and H105 to coordinate transition metals. We note that we did not

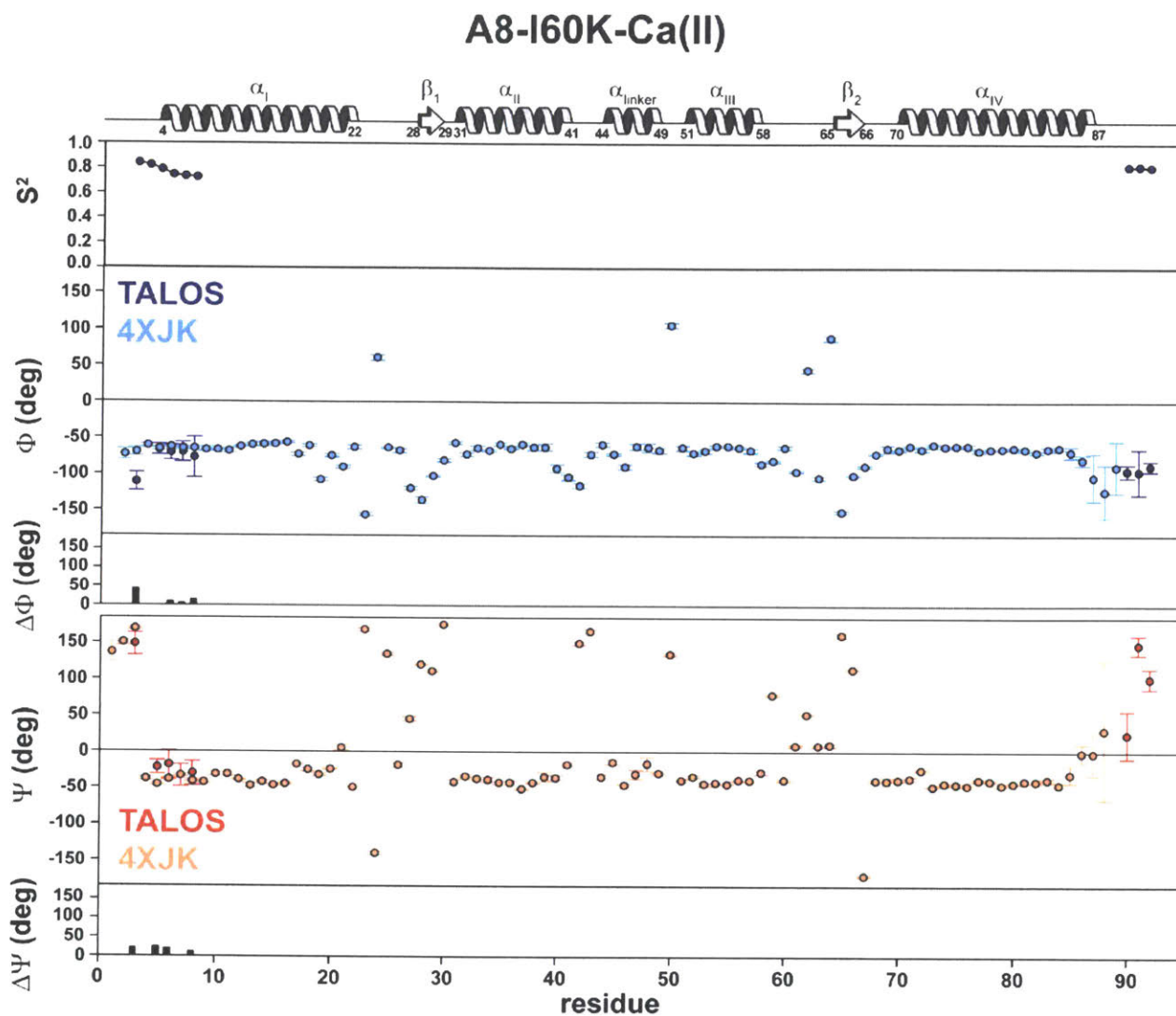


Figure 3.8. TALOS-N analysis of A8-I60K in the absence of Ca(II). A cartoon of the secondary structure is included. The predicted S^2 (order parameter) for assigned residues, predicted and observed (4XJK) Φ angles, differences between the predicted and observed Φ , predicted and observed (4XJK) Ψ angles, and differences between the predicted and observed Ψ are shown. The error bars represent the standard deviation from the average calculated from all of the molecules in the unit cell.

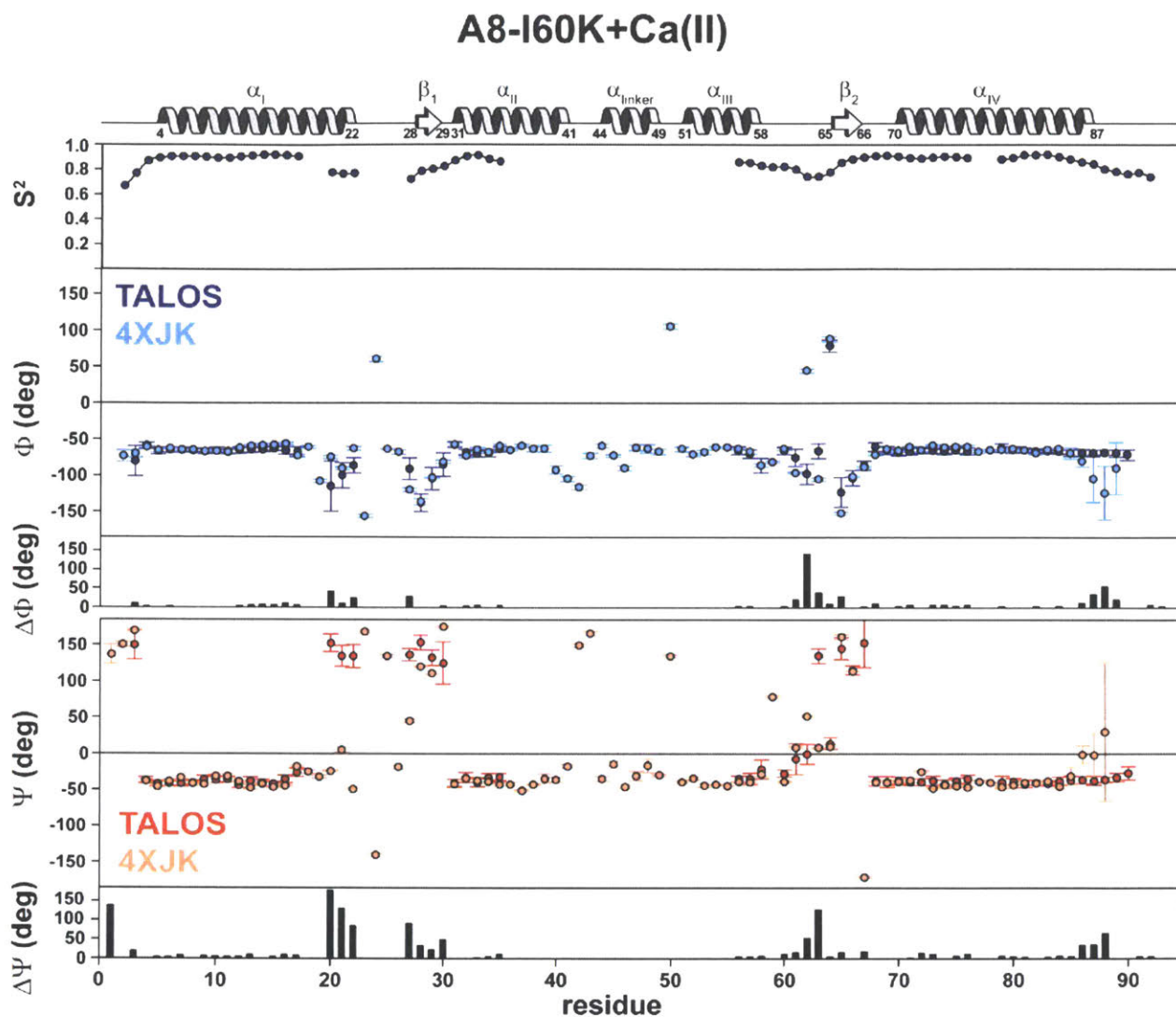


Figure 3.9. TALOS-N analysis of A8-I60K in the presence of Ca(II). A cartoon of the secondary structure is included. The predicted S^2 (order parameter) for assigned residues, predicted and observed (4XJK) Φ angles, differences between the predicted and observed Φ , predicted and observed (4XJK) Ψ angles, and differences between the predicted and observed Ψ are shown. The error bars represent the standard deviation from the average calculated from all of the molecules in the unit cell.

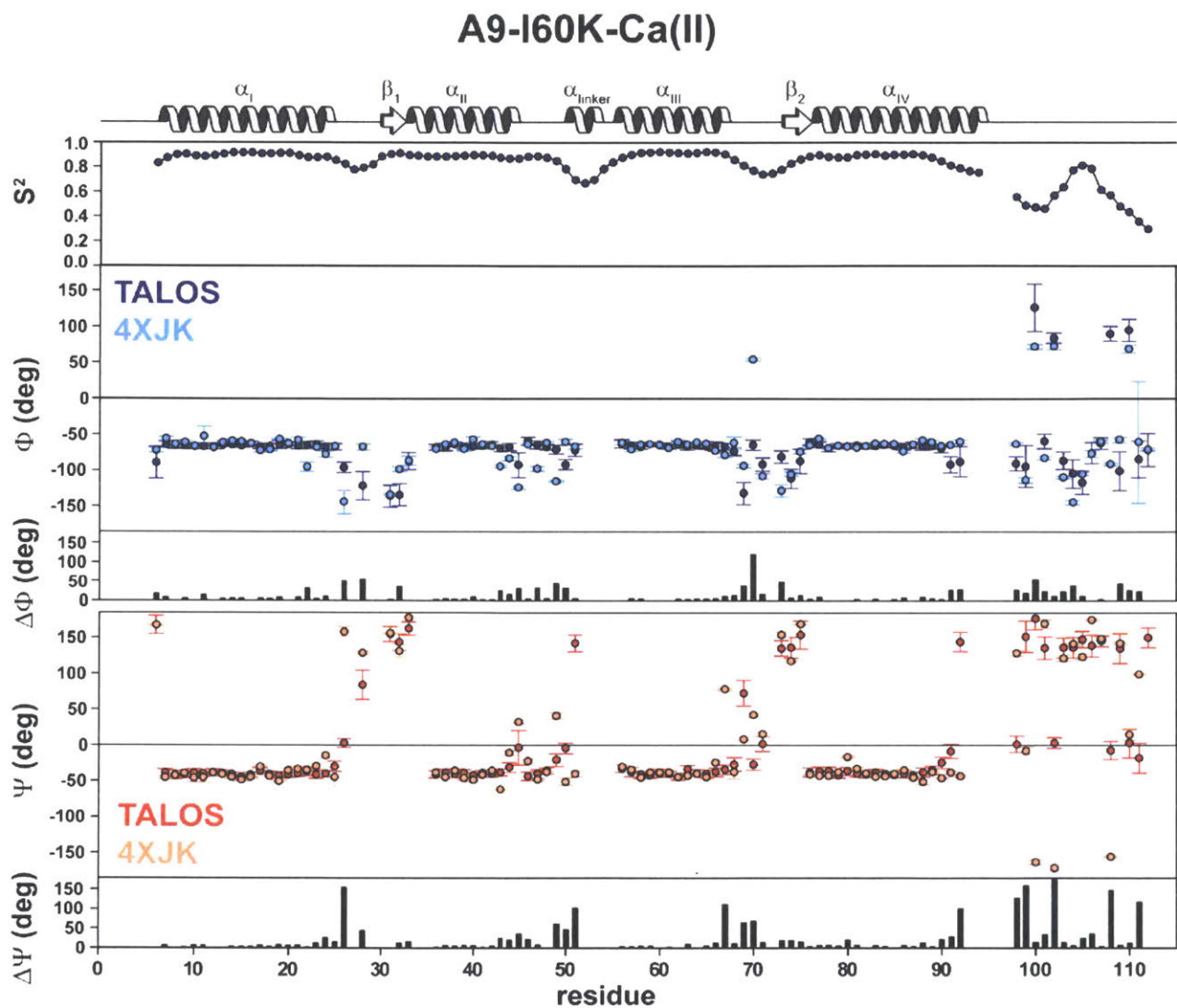


Figure 3.10. TALOS-N analysis of A9-I60K in the absence of Ca(II). A cartoon of the secondary structure is included. The predicted S^2 (order parameter) for assigned residues, predicted and observed (4XJK) Φ angles, differences between the predicted and observed Φ , predicted and observed (4XJK) Ψ angles, and differences between the predicted and observed Ψ are shown. The error bars represent the standard deviation from the average calculated from all of the molecules in the unit cell.

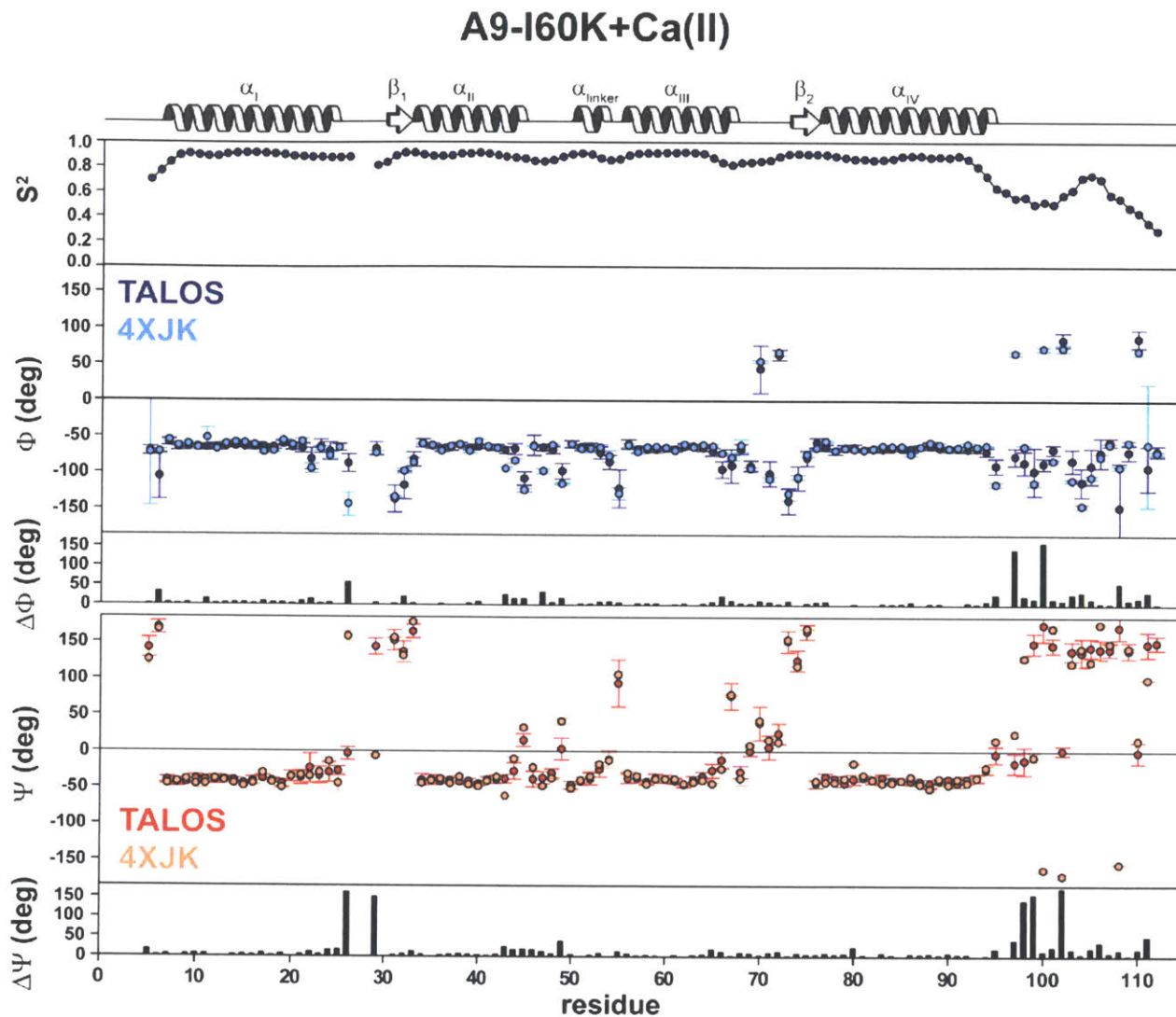


Figure 3.11. TALOS-N analysis of A9-I60K in the presence of Ca(II). A cartoon of the secondary structure is included. The predicted S^2 (order parameter) for assigned residues, predicted and observed (4XJK) Φ angles, differences between the predicted and observed Φ , predicted and observed (4XJK) Ψ angles, and differences between the predicted and observed Ψ are shown. The error bars represent the standard deviation from the average calculated from all of the molecules in the unit cell.

detect any differences in Mn(II) coordination after introducing an H104A mutation,⁶ which would relieve some of the pressure to adopt a β -strand structure.

The regions that exhibited the largest Ca(II)-induced CSPs also exhibited differences between the experimental and predicted secondary structures. Sections of the Ca(II) binding loops of both subunits were predicted to have dihedral angles that differed from the 4XJK structure in the presence and absence of Ca(II) (Figures 3.8-3.11). In the absence of Ca(II), the differences may have occurred because the loops adopt a different orientation when they are Ca(II)-free. This notion is supported by a recent crystal structure of Ni(II)-CP-Ser where the pseudo EF-hand was found in a significantly different conformation that was significantly different than the Ca(II)-containing structures.⁴⁷ In the presence of Ca(II), the differences could reflect properties of the loops that are not captured in the crystal structure and/or the positive charge of the Ca(II) ion altering the chemical shifts of the backbone atoms in a way that cannot be tracked by the neural-network-trained TALOS-N. The linker region also displayed Ca(II)-induced CSPs; however, only the TALOS-N predictions for A9-I60K in the absence of Ca(II) show significant deviations. In the absence of Ca(II), TALOS-N predicts that the linker helix is smaller and helices II and III are longer compared to the +Ca(II) conditions (Figure 3.10). The predicted Ca(II)-induced changes in the linker region suggest that Ca(II) causes the linker region to undergo significant changes going from primarily unstructured to forming a short helix. Another region with significant deviations is the C-terminus of helix IV in A9-I60K in the absence of Ca(II) (Figure 3.10). Without Ca(II), helix IV is predicted to be shorter and more dynamic. The unassigned region is likely experiencing intermediate exchange. In the presence of Ca(II), the C-terminus of A9-I60K helix IV is fully assigned and formed, and the dihedral angles are predicted to closely agree with the 4XJK structure (Figure 3.11). The predicted Ca(II)-induced changes in the C-terminus of helix IV indicate that this region, which comprises one-third of the site 2 undergoes a significant transition in in dynamics and structure due to Ca(II) coordination. In contrast to the other regions

that exhibited Ca(II)-induced CSPs, the predicted secondary structure for the N-terminal section of (A9)-I60K helix IV agrees well with the 4XJK in the presence and absence of Ca(II) (Figures 3.10 and 3.11). Given that the N-terminal section of (A9)-I60K displayed Ca(II)-induced CSPs without predicted changes in secondary structure, we concluded that this region of the protein experiences changes in the chemical environment after Ca(II) binding without changing its secondary structure. In sum, our results point towards a model where the linker and the C-terminus of helix IV acquire more helical character while the N-terminus of helix IV experiences changes in its surroundings.

3.4.5. *Relaxation Analysis Uncovers Ca(II)-Induced Dynamics Changes*

We measured T_1 , T_2 , and hetNOE for the amides of A8-I60K in the presence of Ca(II) and A9-I60K in the presence and absence of Ca(II) at 900 MHz and performed a model-free analyses. We encountered difficulties with the model-free analyses because we struggled to find a rigid a reference frame. An additional limitation is that we performed the model-free fitting with data collected at a single field strength. For these reasons, the exchange rate measurements should be considered in a qualitative manner to be used for identifying regions of chemical exchange. We found that the N-termini of the I60K subunits were suitable for a reference frame, which suggests that they are the least dynamic regions of the proteins. The dynamical properties of the C-terminal extension of A9-I60K were also invariant with Ca(II). In the presence and absence of Ca(II), both sets of resonance corresponding to the A9-I60K C-terminal extension were highly flexible (Figures 3.12 and 3.13).

In contrast, the A9-I60K linker, the N-terminal region of helix IV of A9-I60K, and the C-terminal section of A9-I60K all exhibited changes in dynamics due to Ca(II) coordination. In the absence of Ca(II), the A9-I60K linker was found to be in exchange; however, in the presence of Ca(II), the exchange in this region was decreased (Figure 3.12). Ca(II) dampening exchange in the linker is consistent with our observation that

Ca(II) caused the linker to stably form a helix. Along similar lines, the exchange in the C-terminal region helix IV in A9-I60K was dampened with Ca(II). Again, TALOS-N predicts that this region gains α -helical structure in the presence of Ca(II). The effect of Ca(II) inhibiting exchange in at the C-terminus of helix IV of A9-I60K is further supported by the observation that H95 is only exchange broadened in the absence of Ca(II). The existence of exchange in these two regions that is prevented with Ca(II) suggests that these regions convert between unfolded and α -helical structures in the absence of Ca(II); however, Ca(II) causes these regions to preferentially adopt an α -helical structure. Introducing rigidity into the C-terminus of helix IV in S100A9 is particularly important because two histidines in this region constitute part of the transition-metal-binding site 2, and we reason that the previously observed increase in transition-metal affinity in the presence of Ca(II) is due, at least in part, to Ca(II) allosterically introducing order into this region. The N-terminal section of helix IV in A9-I60K differed from the other regions that experienced dynamical changes due to Ca(II) coordination. Addition of Ca(II) caused these residues to undergo chemical exchange (Figure 3.13). This region also exhibited Ca(II)-induced CSPs; however, TALOS-N did not predict any Ca(II)-induced changes in secondary structure. Taken together, these observations suggest that Ca(II) causes the position and/or environment around this region of the protein to change. We hypothesize that this region of the protein is alternating between orientations that are tetramerization incompetent and tetramerization competent. This hypothesis is reasonable because M81 participates in the tetramer interface (see Chapter 4), and Ca(II) may favor surface exposure of M81 as part of the allosteric changes that precede tetramer formation, and preventing tetramerization with the (A8)I60K mutation inhibits the N-terminal section of A9-I60K from stably adopting the tetramerization competent orientation.

Though a significant portion of the A8-I60K subunit remains unassigned in the presence of Ca(II), the knowledge that these regions are experiencing intermediate exchange reports on the behavior of the protein. The dynamical properties of A9-I60K

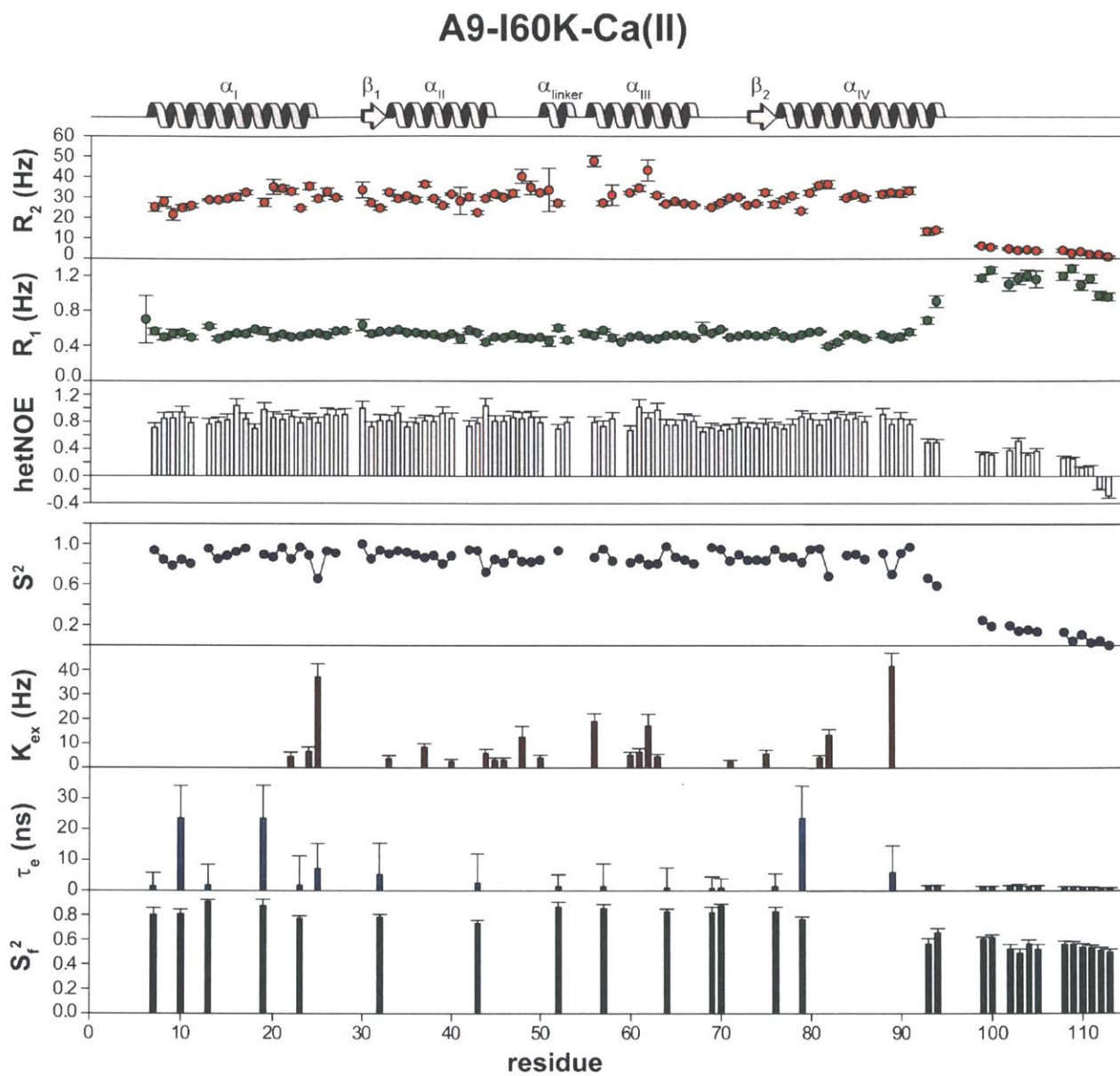


Figure 3.12. Relaxation and model-free analysis of A9-I60K in the absence of Ca(II).

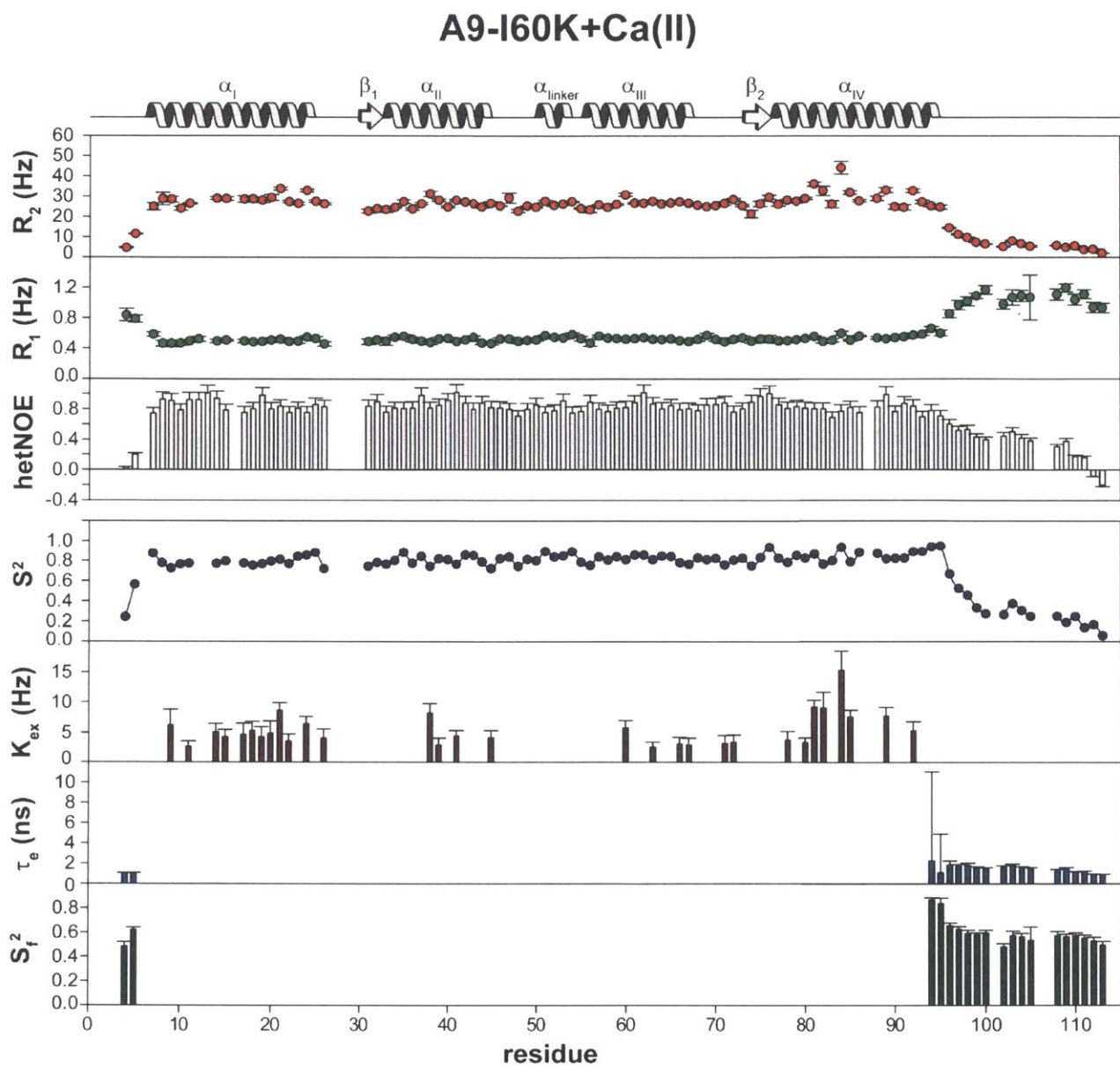


Figure 3.13. Relaxation and model-free analysis of A9-I60K in the presence of Ca(II).

appear to be exaggerated in A8-I60K. Problems due to exchange broadening with the A8-I60K subunit improved in the presence of Ca(II). For the A8-I60K subunit, the protein was essentially unassignable without Ca(II). In the presence of Ca(II), the linker region remained unassignable due to exchange broadening (Figure 3.2B). Additionally, almost the entirety of helix III in A8-I60K was unassignable due to exchange broadening (Figure 3.2B), suggesting that the linker and helix III are allosterically linked. Without more information, we are unable to unambiguously define how Ca(II) influences A8-I60K; however, the current evidence indicates that the changes are similar to the A9-I60K subunit though protein is inherently more dynamic.

3.4.6. *Conclusions and Outlook*

Our results extend and build upon prior work on S100 proteins that gave rise to a model where Ca(II) causes helix III to separate from helix IV to open a site for binding a partner protein.²¹ Recent computational studies on S100A11 elaborated upon this model.²⁵ The simulations indicated that helix III would stochastically alternate between the closed and open orientations (Figure 3.14). It was hypothesized that a labile salt bridge between helices II and III weakly stabilized the open orientation. The models suggested that Ca(II) binding to the C-terminal EF-hand stabilizes a “hydrophobic shoulder” that forms between helix III and residues near the EF-hand, which prevents helices III from pivoting and packing against helix IV when the labile salt bridge spontaneously breaks.

By combining the findings from prior work and our data, it is possible to gain new insights into the effects of Ca(II) on CP. We hypothesize that the (A8)I60K mutation disrupts tetramerization by inhibiting formation of the hydrophobic shoulder. Although the homologous residue in lapine S100A11, L66, was not identified as one of the contributors to the hydrophobic shoulder, it is in close proximity, and introducing a positive charge in place of an aliphatic residue may weaken the putative hydrophobic shoulder. This notion

is supported by the observation that the linker and helix III of A8-I60K are exchange broadened in the presence of Ca(II), likely because the putative hydrophobic shoulder cannot properly form. Additionally, the CP subunits have H-bond donors and acceptors at positions homologous to those in lapine S100A11, although S100A9 has a Gln at position 34 rather than Arg or Lys. In addition to these factors, we posit that increasing the helical content of the linker region acts as a spring to disfavor helix III from returning to the closed conformation, which stands in contrast to previous hypotheses that the linker contributed to dimerization and/or recognition of a target protein. We note that S100A8 has a Pro at position 43 in the linker region (Figure 3.1C), and future work can address how structural constraints due to Pro dictate propensity for helix formation in the S100A8 linker and by extension impact the dynamic properties of the protein as a whole.

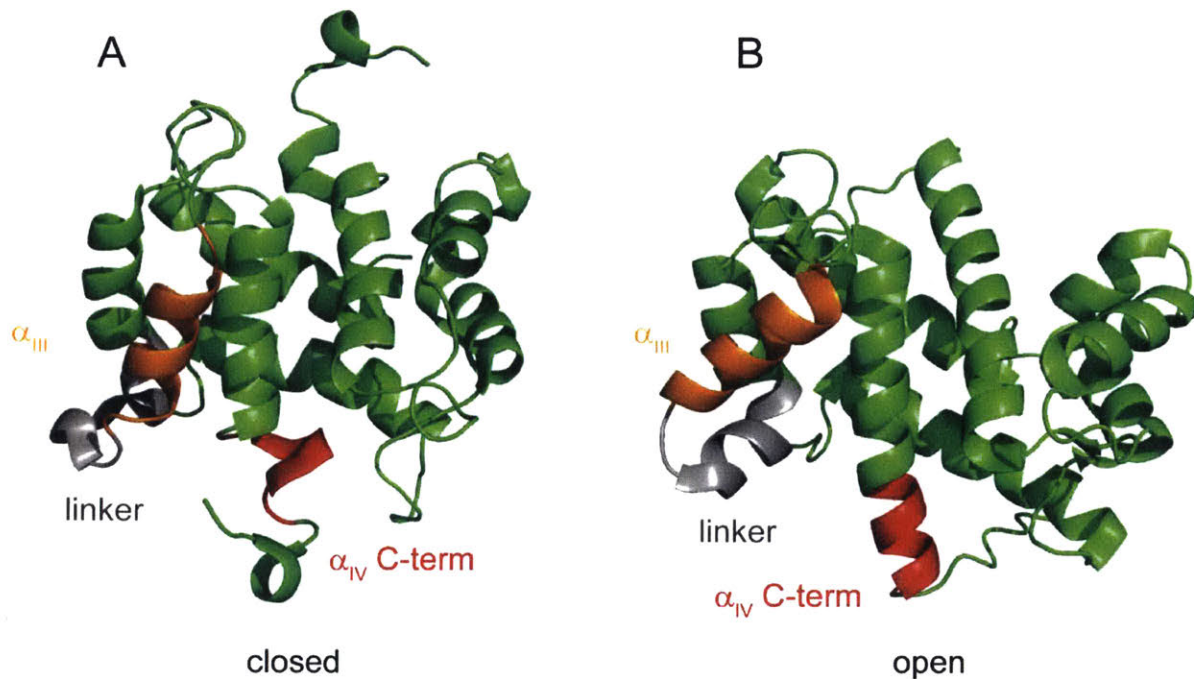


Figure 3.14. Comparisons of (A) apo S100A11 (PDB: 1NSH) and (B) Ca(II)-S100A11 (PDB: 2LUC). The linker region is shown in gray, helix III is shown in orange, and the residues in the C-terminus of helix IV is shown in red. Only the residues that aligned with those in the C-terminal region of helix IV in S100A9 that exhibited major Ca(II) changes are highlighted in red.

While informative, these prior models of the Ca(II) effects on S100 proteins have limited utility in explaining how Ca(II) results in tetramerization and increased transition metal affinity. It is possible that the pivot of helix III to the open orientation causes (A8)I60 to be positioned in such a way that enables contacts between heterodimers based on the rearrangements that occur in S100A11; however, tetramerization does not occur at the same interface as the annexin–S100A11 interaction⁴⁸ (Figure 3.15). Based on our NMR data, we propose that the open conformation allows M81 to stably adopt an orientation/become solvent accessible such that the residue may make contacts between heterodimers. Our data also inform how Ca(II) modulates transition metal affinity. Our data are consistent with a model where the His₆ is site in exchange and partially unfolded in the absence of Ca(II), and that Ca(II) allosterically favors the state with helix IV fully formed, which is competent for metal binding. This model is consistent with

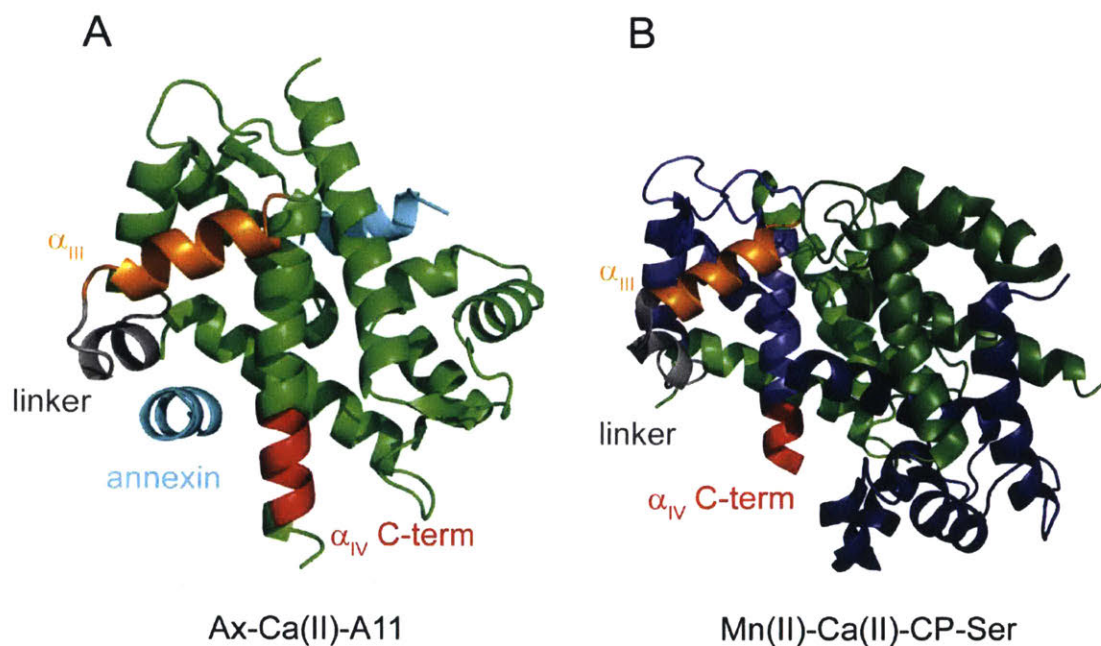


Figure 3.15. Comparison of S100A11 with Ca(II) and an annexin (Ax) peptide bound (PDB: 1QLS) versus Mn(II)-Ca(II)-CP-Ser (PDB: 4XJK) with both heterodimers shown. (A) S100A11 bound to Ca(II) and annexin. (B) CP-Ser with Ca(II) and Mn(II) bound, which adopts a similar open conformation to S100A11. S100A8 is shown in green and S100A9 is shown in blue. One heterodimer is shown in light colors and the other in dark colors. The metal ions and A9 C-terminal extension were omitted for clarity. Annexin binding and tetramerization occur on opposite sides of helix IV.

observations from apo and holo S100A11 where the C-terminus of helix IV is unfolded and sequestered (Figure 3.14). Perhaps because S100A11 and several other S100 proteins do not coordinate transition metals, these Ca(II)-induced changes were overlooked.² It appears that CP, and perhaps other transition-metal-binding S100 proteins as well, co-opted the Ca(II)-induced changes common to S100 proteins, and placed residues for transition-metal chelation in a region where the dynamic and structural properties are highly affected by Ca(II). Furthermore, a transition metal bound at site 2 may communicate a similar allosteric message to Ca(II) by reducing the dynamic behavior in the C-terminal region of helix IV, which cascades through the rest of the protein. This notion can be evaluated by more comparisons of S100 structures in the absence and presence of their ligand(s). The similarity of the Ca(II)-CP-Ser and Ni(II)-CP-Ser crystal structures supports agrees with our proposal that Ca(II) and Ni(II) cause similar allosteric changes (Figure 3.16). The hypothesis of control by Ca(II) through changing the dynamical properties in S100 proteins now has substantial experimental evidence, and future work can leverage sophisticated NMR spectroscopy methods to assign S100A8 and obtain quantitative exchange rate information to create more complete biophysical model of CP function.

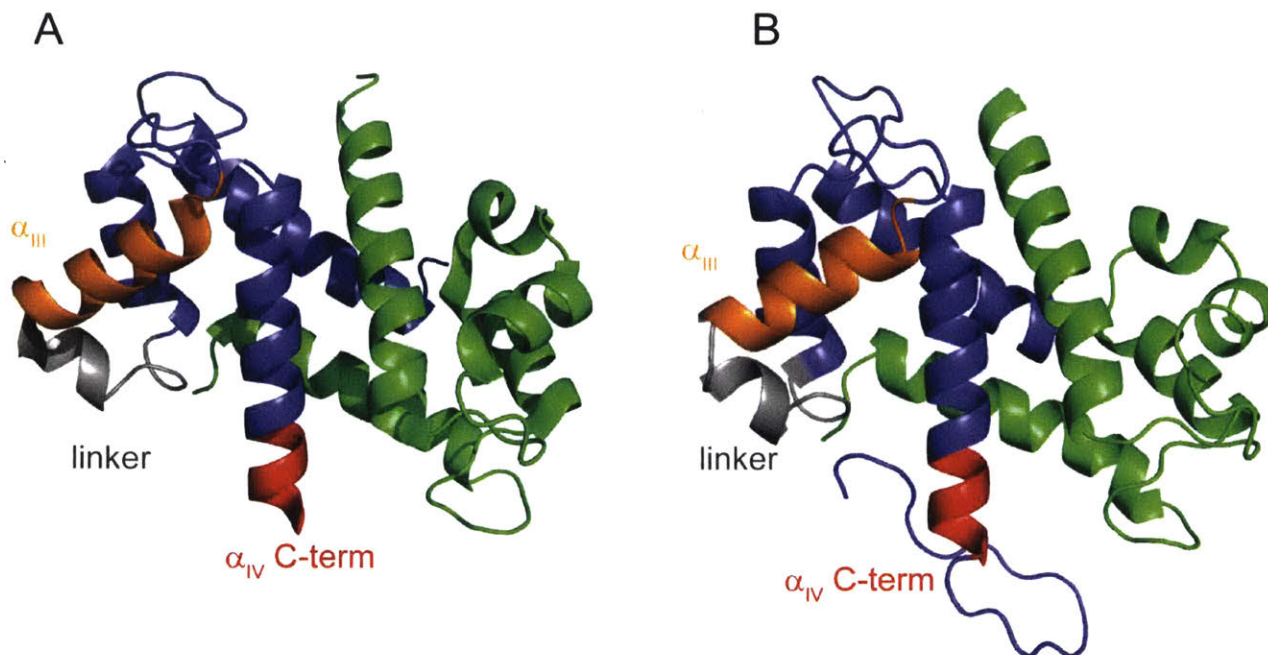


Figure 3.16. Comparison of CP heterodimers (A) Ca(II)-CP-Ser (PDB: 1XK4, Electron density was not observed for the A9-CP-Ser C-terminal extension in this structure.) and (B) Ni(II)-CP-Ser (structure not yet submitted). S100A8 is shown in green and S100A9 is shown in blue. In one of the S100A9 subunits the linker is shown in gray, helix III is shown in orange, and the residues that displayed large changes due to Ca(II) in the helix IV C-terminus are shown in red. The presence of a transition metal at site 2 is sufficient for helix III to separate from helix IV. Comparison to Figure 3.14 demonstrates that these the linker regions and orientation of helices III and IV in these CP-Ser structures more strongly resemble Ca(II)-S100A11 (Figure 3.14B) than apo S100A11 (Figure 3.14A).

3.5. Acknowledgements

We thank the NIH (R01GM118695, AG058504, EB001960), for financial support. We are grateful to Dr. K. Saxena for the kind gift of *E. coli* CT19 cells. We thank Dr. D. Ruben for technical assistance.

3.6. References

1. Steinbakk, M.; Naess-Andresen, C. F.; Lingaas, E.; Dale, I.; Brandtzaeg, P.; Fagerhol, M. K., Antimicrobial actions of calcium-binding leukocyte L1 protein, calprotectin. *Lancet* **1990**, *336* (8718), 763-765.
2. Donato, R., S100: a multigenic family of calcium-modulated proteins of the EF-hand type with intracellular and extracellular functional roles. *Int. J. Biochem. Cell Biol.* **2001**, *33* (7), 637-668.
3. Korndörfer, I. P.; Brueckner, F.; Skerra, A., The Crystal structure of the human (S100A8/S100A9)₂ heterotetramer, calprotectin, illustrates how conformational changes of interacting α -Helices can determine specific association of two EF-hand proteins. *J. Mol. Bio.* **2007**, *370* (5), 887-898.
4. Corbin, B. D.; Seeley, E. H.; Raab, A.; Feldmann, J.; Miller, M. R.; Torres, V. J.; Anderson, K. L.; Dattilo, B. M.; Dunman, P. M.; Gerads, R.; Caprioli, R. M.; Nacken, W.; Chazin, W. J.; Skaar, E. P., Metal chelation and inhibition of bacterial growth in tissue abscesses. *Science* **2008**, *319* (5865), 962-965.
5. Damo, S. M.; Kehl-Fie, T. E.; Sugitani, N.; Holt, M. E.; Rathi, S.; Murphy, W. J.; Zhang, Y. F.; Betz, C.; Hench, L.; Fritz, G.; Skaar, E. P.; Chazin, W. J., Molecular basis for manganese sequestration by calprotectin and roles in the innate immune response to invading bacterial pathogens. *Proc. Natl. Acad. Sci. U. S. A.* **2013**, *110* (10), 3841-3846.
6. Brophy, M. B.; Nakashige, T. G.; Gaillard, A.; Nolan, E. M., Contributions of the S100A9 C-terminal tail to high-affinity Mn(II) chelation by the host-defense protein human calprotectin. *J. Am. Chem. Soc.* **2013**, *135* (47), 17804-17817.
7. Nakashige, T. G.; Zhang, B.; Krebs, C.; Nolan, E. M., Human calprotectin is an iron-sequestering host-defense protein. *Nat. Chem. Biol.* **2015**, *11* (10), 765-771.

8. Nakashige, T. G.; Zygiel, E. M.; Drennan, C. L.; Nolan, E. M., Nickel sequestration by the host-defense protein human calprotectin. *J. Am. Chem. Soc.* **2017**, *139* (26), 8828-8836.
9. Brophy, M. B.; Hayden, J. A.; Nolan, E. M., Calcium ion gradients modulate the zinc affinity and antibacterial activity of human calprotectin. *J. Am. Chem. Soc.* **2012**, *134* (43), 18089-18100.
10. Vogl, T.; Roth, J.; Sorg, C.; Hillenkamp, F.; Strupat, K., Calcium-induced noncovalently linked tetramers of MRP8 and MRP14 detected by ultraviolet matrix-assisted laser desorption/ionization mass spectrometry. *J. Am. Soc. Mass Spectrom.* **1999**, *10* (11), 1124-1130.
11. Stephan, J. R.; Nolan, E. M., Calcium-induced tetramerization and zinc chelation shield human calprotectin from degradation by host and bacterial extracellular proteases. *Chem. Sci.* **2016**, *7* (3), 1962-1975.
12. Brini, M.; Ottolini, D.; Cali, T.; Carafoli, E., Calcium in health and disease. *Met. Ions Life Sci.* **2013**, *13*, 81-137.
13. Leukert, N.; Vogl, T.; Strupat, K.; Reichelt, R.; Sorg, C.; Roth, J., Calcium-dependent Tetramer Formation of S100A8 and S100A9 is Essential for Biological Activity. *J. Mol. Bio.* **2006**, *359* (4), 961-972.
14. Champaiboon, C.; Sappington, K. J.; Guenther, B. D.; Ross, K. F.; Herzberg, M. C., Calprotectin S100A9 calcium-binding loops I and II are essential for keratinocyte resistance to bacterial invasion. *J. Biol. Chem.* **2009**, *284* (11), 7078-7090.
15. Siegenthaler, G.; Roulin, K.; Chatellard-Gruaz, D.; Hotz, R.; Saurat, J. H.; Hellman, U.; Hagens, G., A Heterocomplex Formed by the Calcium-binding Proteins MRP8 (S100A8) and MRP14 (S100A9) Binds Unsaturated Fatty Acids with High Affinity. *J. Biol. Chem.* **1997**, *272* (14), 9371-9377.
16. Damo, S. M.; Kehl-Fie, T. E.; Sugitani, N.; Holt, M. E.; Rathi, S.; Murphy, W. J.; Zhang, Y.; Betz, C.; Hench, L.; Fritz, G.; Skaar, E. P.; Chazin, W. J., Molecular basis for

manganese sequestration by calprotectin and roles in the innate immune response to invading bacterial pathogens. *Proc. Natl. Acad. Sci. U. S. A.* **2013**, *110* (10), 3841-3846.

17. Gagnon, D. M.; Brophy, M. B.; Bowman, S. E. J.; Stich, T. A.; Drennan, C. L.; Britt, R. D.; Nolan, E. M., Manganese binding properties of human calprotectin under conditions of high and low calcium: X-ray crystallographic and advanced electron paramagnetic resonance spectroscopic analysis. *J. Am. Chem. Soc.* **2015**, *137* (8), 3004-3016.

18. Ishikawa, K.; Nakagawa, A.; Tanaka, I.; Suzuki, M.; Nishihira, J., The structure of human MRP8, a member of the S100 calcium-binding protein family, by MAD phasing at 1.9 Å resolution. *Acta Cryst.* **2000**, *56* (5), 559-566.

19. Itou, H.; Yao, M.; Fujita, I.; Watanabe, N.; Suzuki, M.; Nishihira, J.; Tanaka, I., The crystal structure of human MRP14 (S100A9), a Ca²⁺-dependent regulator protein in inflammatory process¹¹ Edited by R. Huber. *J. Mol. Bio.* **2002**, *316* (2), 265-276.

20. Chang, C.-C.; Khan, I.; Tsai, K.-L.; Li, H.; Yang, L.-W.; Chou, R.-H.; Yu, C., Blocking the interaction between S100A9 and RAGE V domain using CHAPS molecule: A novel route to drug development against cell proliferation. *Biochim. Biophys. Acta* **2016**, *1864* (11), 1558-1569.

21. Smith, S. P.; Shaw, G. S., A change-in-hand mechanism for S100 signalling. *Biochem. Cell Biol.* **1998**, *76* (2-3), 324-333.

22. Capdevila, D. A.; Braymer, J. J.; Edmonds, K. A.; Wu, H.; Giedroc, D. P., Entropy redistribution controls allostery in a metalloregulatory protein. *Proc. Natl. Acad. Sci. U. S. A.* **2017**, 4424-4429.

23. Chakravorty, D. K.; Wang, B.; Lee, C. W.; Guerra, A. J.; Giedroc, D. P.; Merz, K. M., Solution NMR refinement of a metal ion bound protein using metal ion inclusive restrained molecular dynamics methods. *J. Biomol. Nmr* **2013**, *56*, 125-137.

24. Eicken, C.; Pennella, M. A.; Chen, X.; Koshlap, K. M.; VanZile, M. L.; Sacchettini, J. C.; Giedroc, D. P., A Metal-Ligand-mediated Intersubunit Allosteric Switch in Related SmtB/ArsR Zinc Sensor Proteins. *J. Mol. Bio.* **2003**, *333* (4), 683-695.

25. Xiao, Y.; Shaw, G. S.; Konermann, L., Calcium-Mediated Control of S100 Proteins: Allosteric Communication via an Agitator/Signal Blocking Mechanism. *J. Am. Chem. Soc.* **2017**, *139* (33), 11460-11470.
26. Tzeng, S.-R.; Kalodimos, C. G., Allosteric inhibition through suppression of transient conformational states. *Nat. Chem. Biol.* **2013**, *9* (7), 462.
27. Tzeng, S.-R.; Kalodimos, C. G., Protein activity regulation by conformational entropy. *Nature* **2012**, *488* (7410), 236.
28. Petit, C. M.; Zhang, J.; Sapienza, P. J.; Fuentes, E. J.; Lee, A. L., Hidden dynamic allostery in a PDZ domain. *Proc. Natl. Acad. Sci. U. S. A.* **2009**, *106* (43), 18249-18254.
29. Cooper, A.; Dryden, D. T., Allostery without conformational change. A plausible model. *Eur. Biophys. J.* **1984**, *11* (2), 103-109.
30. Waugh, D. S., Genetic tools for selective labeling of proteins with alpha-15N-amino acids. *J. Biomol. NMR* **1996**, *8* (2), 184-192.
31. Fiaux, J.; Bertelsen, E. B.; Horwich, A. L.; Wüthrich, K., Uniform and Residue-specific 15N-labeling of Proteins on a Highly Deuterated Background. *J. Biomol. NMR* **2004**, *29* (3), 289-297.
32. Delaglio, F.; Grzesiek, S.; Vuister, G. W.; Zhu, G.; Pfeifer, J.; Bax, A., NMRPipe: a multidimensional spectral processing system based on UNIX pipes. *J. Biomol. NMR* **1995**, *6* (3), 277-93.
33. Goddard, T. D.; Kneller, D. G., SPARKY Version 3.115, Univ. California, San Francisco. **2008**.
34. Shen, Y.; Bax, A., Protein structural information derived from NMR chemical shift with the neural network program TALOS-N. *Methods Mol. Biol.* **2015**, *1260*, 17-32.
35. Czisch, M.; Boelens, R., Sensitivity enhancement in the TROSY experiment. *J. Magn. Reson.* **1998**, *134* (1), 158-60.
36. Pervushin, K. V.; Wider, G.; Wuthrich, K., Single Transition-to-single Transition Polarization Transfer (ST2-PT) in [15N,1H]-TROSY. *J. Biomol. NMR* **1998**, *12* (2), 345-8.

37. Salzmann, M.; Pervushin, K.; Wider, G.; Senn, H.; Wuthrich, K., TROSY in triple-resonance experiments: new perspectives for sequential NMR assignment of large proteins. *Proc. Natl. Acad. Sci. U. S. A.* **1998**, *95* (23), 13585-90.
38. Eletsky, A.; Kienhofer, A.; Pervushin, K., TROSY NMR with partially deuterated proteins. *J. Biomol. NMR* **2001**, *20* (2), 177-80.
39. Salzmann, M.; Wider, G.; Pervushin, K.; Wuthrich, K., Improved sensitivity and coherence selection for $[^{15}\text{N},^1\text{H}]$ -TROSY elements in triple resonance experiments. *J. Biomol. NMR* **1999**, *15* (2), 181-4.
40. Schleucher, J.; Schwendinger, M.; Sattler, M.; Schmidt, P.; Schedletsky, O.; Glaser, S. J.; Sorensen, O. W.; Griesinger, C., A general enhancement scheme in heteronuclear multidimensional NMR employing pulsed field gradients. *J. Biomol. NMR* **1994**, *4* (2), 301-6.
41. Dosset, P.; Hus, J. C.; Blackledge, M.; Marion, D., Efficient analysis of macromolecular rotational diffusion from heteronuclear relaxation data. *J. Biomol. NMR* **2000**, *16* (1), 23-8.
42. Gifford, J. L.; Walsh, M. P.; Vogel, H. J., Structures and metal-ion-binding properties of the Ca^{2+} -binding helix-loop-helix EF-hand motifs. *Biochem. J.* **2007**, *405* (2), 199-221.
43. Hayden, J. A.; Brophy, M. B.; Cunden, L. S.; Nolan, E. M., High-affinity manganese coordination by human calprotectin is calcium-dependent and requires the histidine-rich site formed at the dimer interface. *J. Am. Chem. Soc.* **2013**, *135* (2), 775-787.
44. Nakashige, T. G.; Stephan, J. R.; Cunden, L. S.; Brophy, M. B.; Wommack, A. J.; Keegan, B. C.; Shearer, J. M.; Nolan, E. M., The hexahistidine motif of host-defense protein human calprotectin contributes to zinc withholding and its functional versatility. *J. Am. Chem. Soc.* **2016**, *138* (37), 12243-12251.
45. Venters, R. A.; Thompson, R.; Cavanagh, J., Current approaches for the study of large proteins by NMR. *J. Mol. Struct.* **2002**, *602-603*, 275-292.

46. Shen, Y.; Bax, A., Protein backbone and sidechain torsion angles predicted from NMR chemical shifts using artificial neural networks. *J. Biomol. NMR* **2013**, *56* (3), 227-241.
47. Nakashige, T. G.; Bowman, S. E. J.; Zygiel, E. M.; Drennan, C. L.; Nolan, E. M., Biophysical examination of the calcium-modulated nickel-binding properties of human calprotectin reveals conformational change in the EF-hand domains and His₃Asp site. *Submitted 2018*.
48. Réty, S.; Osterloh, D.; Arié, J.-P.; Tabaries, S.; Seeman, J.; Russo-Marie, F.; Gerke, V.; Lewit-Bentley, A., Structural basis of the Ca²⁺-dependent association between S100C (S100A11) and its target, the N-terminal part of annexin I. *Structure* **2000**, *8* (2), 175-184.

Chapter 4: Oxidative Post-Translational Modification Accelerates Proteolysis of Calprotectin

4.1. Contributions

Dr. F. Yu performed exploratory experiments with CP-Ser and hydrogen peroxide. Ms. R. Costello carried out many replicates of protease digestion experiments and provided technical assistance. Dr. B. Bleier at Massachusetts Eye and Ear Infirmary extracted nasal mucus from human patients.

4.2. Introduction

Reactive oxygen species (ROS) are important players in the host/pathogen interaction. Neutrophils, white blood cells that are first responders during the innate immune response, generate and release ROS at infection sites in an attempt to kill invading microbial pathogens. These reactive small molecules also have the capacity to post-translationally oxidize host biomolecules.¹ Motivated by the need to further understand the molecular complexity of infection sites, this work examines the biophysical and functional consequences of post-translational oxidation of an abundant neutrophil protein named calprotectin (CP, S100A8/S100A9 oligomer). These studies provide a new conceptual framework for considering the speciation and lifetime of CP at sites of infection and inflammation, and the role of methionine sulfoxide and disulfide bonds in directing the fate of CP during the innate immune response.

CP is an abundant metal-sequestering protein that contributes to the innate immune response.²⁻⁴ The protein is produced by several types of epithelial cells and white blood cells.⁵ It is particularly abundant in neutrophils where it constitutes $\approx 40\%$ of cytosolic protein.⁶ In the current working model, CP is released by neutrophils into the extracellular space at concentrations that can exceed $40 \mu\text{M}$ (1 mg/mL).⁷ In this milieu, CP limits microbial growth by competing with invading microbes for bioavailable transition metal ions that are essential nutrients.^{2,4,8-11} Over the past decade, biophysical and functional

studies have illuminated the molecular basis for this metal-sequestration model as described below.^{8-10,12,13} Recent investigations have also probed how microbial pathogens such as *Staphylococcus aureus*,¹⁴ *Salmonella enterica* serovar Typhimurium,¹⁵ *Acinetobacter baumannii*,¹⁶ and *Neisseria* spp.^{17,18} adapt to metal limitation caused by CP. In contrast, to the best of our knowledge, no reports have addressed what happens next for CP, either metal-free or metal-bound, in the context of this model.

In addition to its antimicrobial properties, CP contributes to the inflammatory response. Data suggesting that CP is an activator of toll-like receptor 4 (TLR4) have been reported.¹⁹⁻²¹ Moreover, murine model studies indicated that CP-mediated proinflammatory signaling can lead to negative outcomes for the host, including promotion of lethal endotoxin-induced shock and generation of autoreactive T cells.^{19,20} Taken together, these studies highlight that CP is multi-functional and can be either beneficial or harmful to the host. In considering this duality, we reasoned that negative outcomes associated with CP-mediated signaling may result from dysregulated proinflammatory signaling related to a failure to clear CP, and this line of reasoning highlighted the shortcomings of the working model in describing what happens to CP after release.

Previously, we approached this question by examining the molecular basis for metal sequestration by CP. In the apo form, CP exists as a 24-kDa heterodimer of S100A8 (93 amino acids, 10.8 kDa, α subunit) and S100A9 (114 amino acids, 13.2 kDa, β subunit).^{2,22,23} The CP heterodimer contains six different sites for coordinating cations. Each subunit contains two Ca(II)-binding EF-hand domains, and two sites for transition metal ions form at the S100A8/S100A9 interface.^{9,22,24} Site 1 is a His₃Asp site that binds Zn(II) with high affinity,⁹ and site 2 is a His₆ site that binds Mn(II),²⁵ Fe(II),¹¹ Ni(II),²⁶ and Zn(II)^{9,12} with high affinity. Ca(II) binding to CP has important structural and functional consequences. In the presence of excess Ca(II) ions, two CP heterodimers self-associate to form an $\alpha_2\beta_2$ heterotetramer.^{22,24,27} Conditions of high Ca(II) that promote

heterotetramer formation also result in enhanced transition metal affinities, protease stability, and antimicrobial activity.^{9,11,13,25} Because Ca(II) ion concentrations are ≈ 100 nM in the cytoplasm of resting cells and extracellular Ca(II) ion concentrations are ≈ 2 mM,²⁸ these observations have led to a working model where the heterodimer is the major cytosolic species and the Ca(II)-bound heterotetramer is the major extracellular species.⁹ This Ca(II) effect allows CP to sequester metals and persist in the harsh extracellular space that contains host and bacterial proteases.

Over the course of our studies that addressed the biological coordination chemistry of CP, several reports identified the methionine sulfoxide (MetO) post-translational modification on CP during *ex vivo* analyses of human or mouse specimens by mass spectrometry.²⁹⁻³¹ A variety of oxidants, including hydrogen peroxide (H₂O₂), superoxide (O₂⁻), hypochlorous acid (HOCl) are generated by the neutrophil oxidative burst.³²⁻³⁴ These oxidants can oxidize the methionine sidechain to MetO.¹ To us, these observations were intriguing and suggested an as-yet unappreciated complexity to the speciation of CP at biological sites. The Met/MetO redox couple is often considered to serve as an antioxidant because the MetO post-translational modification can be reversed by the action of methionine sulfoxide reductases MsrA and MsrB, which are found in many cell types, including neutrophils.³⁵⁻³⁸ On the other hand, accumulation of MetO post-translational modifications is associated with protein dysfunction.³⁹ There are only limited studies on the consequences arising from MetO modification of CP,^{29,40} and we reasoned that understanding these consequences would shed light on the biological fate of CP.

In this work, we identify oxidized CP species in human specimens, and we test our new hypothesis that oxidative post-translational modifications affect the function and fate of CP in the biological milieu. Our biochemical and functional results support a model where methionine oxidation and disulfide bond formation attenuate the proteolytic stability of Ca(II)-bound CP. In the absence of a divalent transition metal ion bound at the His₆ site, oxidation of (A9)M81 disfavors Ca(II)-induced tetramerization, which leads to

accelerated proteolysis by a variety of proteases. Remarkably, disulfide bonds within and between CP heterodimers also caused accelerated proteolysis, an effect is particularly apparent when the disulfide bond includes (A8)C42. In total, these results support a new extension to the working model where extracellular CP can be oxidized by neutrophil-derived ROS and subsequently degraded by proteases. We further hypothesize that accelerated degradation caused oxidative modification serves to dampen the proinflammatory signal of CP. Because transition-metal binding rescues tetramerization and protease resistance, it appears that the host strategically avoids degrading transition-metal-bound CP to prevent release of nutrients to microbes.

4.3. Experimental

4.3.1. General Materials and Methods

All solvents, reagents, and chemicals were obtained from commercial suppliers and used as received. All buffers and metal solutions were prepared using Mili-Q water (18.2 M Ω ·cm, 0.22- μ m filter, Millipore). All mobile phases for chromatography experiments were prepared with Ultrol grade HEPES (free acid, Calbiochem) and TraceSELECT NaCl (Fluka), and aqueous TraceSELECT NaOH (Sigma) was used for pH adjustments. Buffers for all other experiments, except where specified otherwise, were prepared using microbiology grade HEPES, NaCl, and NaOH (Sigma) that was treated with Chelex 100 resin (Biorad 10 g/L) for 1 h in a polypropylene beaker. The Chelex resin was removed by filtration with a 0.22- μ m bottle-top filter. All buffers were stored in polypropylene bottles. The highest available purity of calcium chloride (99.99%) and manganese chloride (99.99%) were purchased from Alfa Aesar, and anhydrous zinc chloride (99.999%) and (NH₄)₂Fe(SO₄)₂·6H₂O (99.997%) were purchased from Sigma. Stock solutions of Ca(II) (1 M, 100 mL), Mn(II) (1 M, 50 mL), Fe(II) (100 mM, 10 mL), and Zn(II) (100 mM, 100 mL) were prepared by using Mili-Q water and acid-washed volumetric

glassware, and the solutions were stored in polypropylene tubes. The Fe(II) solution was prepared under a nitrogen atmosphere in an anaerobic glove box (Vacuum Atmospheres Co.). All iron-containing samples were prepared and manipulated in the glove box. Protein concentrations were determined by optical absorbance at 280 nm using a BioTek Synergy HT plate reader outfitted with a Take3 Micro-Volume plate. The extinction coefficients for the employed proteins are listed in Tables 4.1 and 4.2.

Table 4.1. Molecular weights and extinction coefficients for the S100A8 and S100A9 subunits of proteins examined in this study.

Protein	Molecular Weight (Da)	ϵ_{280} ($M^{-1} cm^{-1}$) ^a
A8(C42S)	10 818.5 ^b	11 460
A8(C42S)+O	10 834.5 ^b	11 460
A8	10 834.5 ^b	11 460
A8+O	10 850.5 ^b	11 460
A8+2O	10 866.5 ^b	11 460
¹⁵ N-A8(C42S)	10 944.1 ^c	11 460
¹⁵ N-A9(C3S)	13 253.8 ^{c, d}	6 990
A9(C3S)	13 094.7 ^{b, d}	6 990
A9(C3S)+3O	13 142.7 ^{b, d}	6 990
A9(C3S)+4O	13 158.7 ^{b, d}	6 990
A9(C3S)(M63A)	13 034.6 ^{b, d}	6 990
A9(C3S)(M81A)	13 034.6 ^{b, d}	6 990
A9(C3S)(M83A)	13 034.6 ^{b, d}	6 990
A9	13 110.8 ^{b, d}	6 990
A9+2O	13 142.8 ^{b, d}	6 990
A9+3O	13 158.8 ^{b, d}	6 990
A9+4O	13 174.8 ^{b, d}	6 990

^a Extinction coefficients (280 nm) were calculated by using the ProtParam tool. ^b Molecular weights were calculated by using the ProtParam tool available on the ExPASy server (<http://web.expasy.org/protparam>). ^c The theoretical mass was calculated using 99% ¹⁵N and 1% ¹⁴N. ^d In all preparations, LCMS revealed that the dominant purified species lacked the N-terminal methionine. The molecular weight shown is the theoretical value for S100A9(C3S) lacking the N-terminal Met residue.

Table 4.2. Molecular weights and extinction coefficients for commercial proteins.

Protein	Molecular Weight (Da) ^a	ϵ_{280} (M ⁻¹ cm ⁻¹)	ϵ_{405} (M ⁻¹ cm ⁻¹)
Trypsin	23 300	30 000 ⁴¹	-
Chymotrypsin	25 000	50 000 ⁴²	-
Proteinase K	28 900	36 580 ^b	-
HNE	28 500	-	-
Catalase	250 000	-	324 000 ⁴³

^a Molecular weights were calculated by using the ProtParam tool available on the ExPASy server (<http://web.expasy.org/protparam>). ^b Extinction coefficients (280 nm) were calculated by using the ProtParam tool.

4.3.2. General Instrumentation

For analytical high-performance liquid chromatography (HPLC), an Agilent 1200 series instrument equipped with a thermostatted column compartment set to 20 °C, and a multi-wavelength detector set at 220 and 280 nm (500 nm reference wavelength with 100 nm bandwidth), was used. A Proto C4 column (5- μ m pore, 4.6 x 250 mm, Higgins Analytical Inc.) set at a flow rate of 1 mL/min was employed for all analytical HPLC experiments. HPLC-grade acetonitrile (MeCN) and trifluoroacetic acid (TFA) were routinely purchased from EMD and Alfa Aesar, respectively. For all HPLC runs, mobile phase A was 0.1% TFA/H₂O and mobile phase B was 0.1% TFA/MeCN.

For routine high-resolution mass spectrometric characterization of purified protein and the products of oxidation by H₂O₂, an Agilent 1260 series LC system equipped with an Agilent 6230 TOF system housing an Agilent Jetstream ESI source was employed. A Poroshell 300SB-C18 column (5- μ m pore, 2.1 x 75 mm, Agilent) and denaturing protocol were utilized for all LC-MS analyses. Mobile phase A was 0.1% formic acid/H₂O. Mobile phase B was 0.1% formic acid/MeCN. The S100A8 and S100A9 subunits were eluted by using a gradient 5-85% over 10 min. The resulting mass spectra were deconvoluted using the maximum entropy algorithm in MassHunter BioConfirm (Agilent).

For mass spectrometry analyses of human mucus and pus samples, an Agilent 1290 Infinity HPLC system equipped with an Agilent 6520 Accurate-Mass ESI-Q-TOF system was employed. A Zorbax 300SB-C3 column (5 μ m-pore, 2.1 x 150 mm, Agilent)

was utilized for the separation. Mobile phase A was 0.1% formic acid/H₂O. Mobile phase B was 0.1% formic acid/MeCN. Details for the gradients employed are provided in subsection 4.3.9.

For fluorescence spectroscopy, emission spectra were collected on a Photon Technologies International QuantaMaster 40 fluorimeter outfitted with a continuous xenon source for excitation autocalibrated QuadraScopic monochrometers, a multimode PMT detector, and a circulating water bath maintained at 25 °C. This instrument was controlled by the FelixGX software package. FelixGX was used to integrate the emission spectra.

For circular dichroism (CD) spectroscopy, A JASCO Model J-1500 CD spectrometer thermostatted at 25 °C was used. A 1-mm path-length CD cell (Hellma) was employed for all CD measurements. All protein samples (10 μM protein, 300 μL, 1 mM Tris, ±2 mM CaCl₂, pH 8.5) were made at the same time prior to data acquisition. Wavelength scans were recorded from 190 nm to 260 nm in 0.5 nm steps at a rate of 50 nm/min. The averages from three scans for each condition are presented.

4.3.3. Site-Directed Mutagenesis

A modified Quick-Change site-directed mutagenesis protocol was employed to generate plasmids encoding S100A9(C3S)(M63A), S100A9(C3S)(M81A), and S100A9(C3S)(M83A). The template gene, S100A9(C3S), was housed in a pET41a vector, and had been ligated into the plasmid using *NdeI* and *XhoI* restriction sites, which resulted in the proteins being expressed without an affinity tag.⁹ The mutagenesis primers are listed in Table 4.3. PCR amplification was carried out using PfuTurbo DNA polymerase (Agilent). The annealing temperature for M63A was 57 °C, and the annealing temperature for M81A and M83A was 62 °C. The PCR protocol was 95 °C for 30 sec, 95 °C for 30 sec, 57 °C (M63A mutation) or 62 °C (M81A or M83A mutations), 68 °C for 17 min, (25 cycles), and 4 °C hold. After PCR amplification, the template DNA was digested at 37 °C for 3 h by DpnI (New England Biolabs) by adding 0.75 μL of the enzyme to 25

μ L of a PCR reaction, and adding an additional 0.75- μ L aliquot of the enzyme after 1.5 h. The digestion products were transformed into chemically competent *E. coli* TOP10, which were plated on LB plates with 50 μ g/mL kanamycin and incubated at 37 °C overnight. The following day, overnight cultures (5 mL LB+50 μ g/mL kanamycin) were grown from single colonies, and the plasmids were isolated using a miniprep kit (Qiagen). The presence of each mutation and fidelity of the coding sequences were verified by DNA sequencing (Quintara Biosciences).

Table 4.3. Primers employed for site-directed mutagenesis.

Primer	Sequence ^a
M63A-1	5'-GTGATTGAACACATT <u>GCG</u> GAGGATCTGGACACC-3'
M63A-2	5'-GGTGTCCAGATCCTC <u>CGC</u> AATGTGTTCAATCAC-3'
M81A-1	5'-CTTTGAAGAGTTCATC <u>GCG</u> CTGATGGCCCGTCTG-3'
M81A-2	5'-CAGACGGGCCATCAG <u>CGC</u> GATGAACTCTTCAAAG-3'
M83A-1	5'-GAGTTCATCATGCTG <u>GCG</u> GCCCGTCTGACGTGG-3'
M83A-2	5'-CCACGTCAGACGGGC <u>CGC</u> CAGCATGATGAACTC-3'

^a The codons containing mutations are underlined and colored red. The template *S100A9(C3S)* gene had been ligated into the pET41a vector using *NdeI* and *XhoI* restriction sites.⁹

4.3.4. Preparation and Purification of CP and Variants

CP and CP-Ser were prepared and handled as previously described.⁹ This purification protocol affords the apo CP/CP-Ser heterodimer. The same purification protocol was employed to prepare the new CP-Ser variants reported in this study, CP-Ser(A9-M63A), CP-Ser(A9-M81A), and CP-Ser(A9-M83A). These variants were obtained in yields of 40-50 mg/L culture, and each protein was evaluated by ESI-MS, SDS-PAGE, and CD spectroscopy (Table 4.4, Figures A2.20, and A2.21). ¹⁵N-CP-Ser was prepared according to a published protocol.⁴⁴

4.3.5. Preparation and Purification of Oxidized CP-Ser Variants

The reactions to generate CP with oxidized Met residues produced mixtures of species. The mixture where the dominant species were S100A8 with one additional oxygen atom and S100A9 with three additional oxygen atoms is referred to as CP-Ser O₄. The more heavily oxidized mixture where the dominant species were S100A8 with one additional oxygen atom and S100A9 with four additional oxygen atoms is referred to as CP-Ser O₅. CP-Ser O₄ and CP-Ser O₅ were prepared by modifying the standard CP-Ser purification protocol.⁹ The S100A8(C42S) and S100A(C3S) subunits were overexpressed and a denaturing protocol was employed to obtain a mixture (≈120 mL) of the soluble and unfolded subunits as reported previously. This mixture was dialyzed once against 75 mM HEPES, 100 mM NaCl, pH 8.0 (4 L, 4 °C, 12 h). Then, the protein solution was transferred to 50-mL Falcon tubes covered with aluminum foil. To prepare CP-Ser O₄, H₂O₂ (Sigma, 50% w/w in H₂O, 17.6 M) was added to the protein solution to give a final concentration of 50 mM, and the reaction was incubated for 2.5 h or 5 h at 37 °C on a nutating platform. To prepare CP-Ser O₅, the protein was incubated with either 50 mM H₂O₂ for 6 h or 75 mM H₂O₂ for 6.5 h at 37 °C on a nutating platform. At the reaction end point, the solution was centrifuged at 3 600 rpm, 4 °C for 30 min. The supernatant was transferred to dialysis tubing, and three additional 12-h rounds of dialysis against 4 L of refolding buffer (20 mM HEPES, pH 8.0) were performed at 4 °C. The resulting protein sample was purified by anion exchange chromatography and size exclusion chromatography as described for CP-Ser.⁹ The yields for the CP-Ser O₄ and CP-Ser O₅ ranged from 30-40 mg per liter of culture. Protein purity was assessed by SDS-PAGE (Figure A2.20). The extent of oxidation of CP-Ser was ascertained using mass spectrometry (Table 4.4 and Figure A2.22).

Table 4.4. Mass spectrometric analysis of CP and variants.

Protein	S100A8 Observed Mass (g/mol)	S100A9 Observed Mass ^a (g/mol)
CP	10 834.1	13 110.4
MetO-dsl-CP	10 850.5, 10 866.6	13 159.0, 13 174.0
CP-Ser	10 818.6	13 094.7
CP-Ser O ₄	10 834.4	13 142.7
CP-Ser O ₅	10 834.5	13 159.0
CP-Ser(A9-M63A)	10 818.9	13 034.6
CP-Ser(A9-M81A)	10 818.6	13 034.6
CP-Ser(A9-M83A)	10 818.8	13 034.6

^a In all preparations, the dominant purified species of the S100A9 subunit lacked the N-terminal methionine. The masses reported here are the observed values for S100A9(C3S) lacking the N-terminal Met residue.

4.3.6. Oxidation of CP

CP, which contains two Cys residues, was buffer exchanged from the storage buffer (that contained 10 mM β -mercaptoethanol (BME)) into the assay buffer (75 mM HEPES, 100 mM NaCl, pH 7.5) with three rounds of centrifugal concentration using a 0.5-mL 10-kDa MWCO Amicon filter. The protein was then diluted to 30 μ M in the assay buffer, and Ca(II) was added to give a final concentration of 1.5 mM. After 15 min of incubation at room temperature, H₂O₂ was added to give a final concentration of 100 μ M, and the reaction was then incubated at 37 °C. Because we sought to study disulfide-linked protein, it was essential to remove the H₂O₂ without reducing the disulfide bonds. To quench the reaction, we employed catalase to rapidly consume the H₂O₂ by diluting catalase (Sigma) to a final concentration of 10 nM from a freshly prepared 100 nM stock solution.

We also sought to study the properties of disulfide linked CP that contained methionine sulfoxide modifications. First the disulfide-bonds were formed by treating 30 μ M CP with 100 μ M H₂O₂ for 23 h at 37 °C in 75 mM HEPES, 100 mM NaCl, pH 7.5, as described in the preceding paragraph. To oxidize methionine side chains, the protein was

then treated with 100 mM H₂O₂ for 7 h before quenching by diluting catalase 10-fold into the reaction to a final concentration of 10 nM.

4.3.7. *Collection of Human Nasal Mucus*

Mucus sampling was approved by the Massachusetts Eye and Ear Infirmary Institutional Review Board as previously described.⁴⁵ All samples were taken from patients undergoing sinonasal surgery. These patients had not been exposed to antibiotics or steroids for at least four weeks prior to surgery and sample collection. Mucus samples were taken from the internal valve or middle meatus by placing a compressed polyvinyl alcohol sponge (PVA, Medtronic, Minneapolis, MN) within the nasal cavity, taking care not to abrade the mucosa or contaminate the sponge with blood. The mucus was removed from the sponges by placing them into 0.65-mL polypropylene tubes that had the bottom removed with a razor. This tube was placed in a 1.7-mL polypropylene tube, and was centrifuged at 13 000 rpm for 30 min, 4 °C. The mucus from each patient was pooled, and then flash frozen with liquid nitrogen before storage at -80 °C.

4.3.8. *Collection of Human Pus*

Pus sampling was approved by the Massachusetts Institute of Technology Institutional Review Board. Both samples were taken from pimples of one graduate student. One pimple was located on the left shoulder and the other on the face. After washing his hands, the student used sterile isopropyl alcohol wipes to clean the area before breaking the pimple with his hands. The contents were transferred to a 1.7-mL polypropylene tube. A 2- μ L aliquot of 10.4 μ M ¹⁵N-CP-Ser was immediately added to the pus sample, followed by 50 μ L of Milli-Q water, and the resulting mixture was and mixed by pipetting. The samples were immediately processed for mass spectrometry.

4.3.9. Preparation of Human Mucus and Pus for LC-MS

Mucus samples 1 and 2 were thawed on ice, and 5 μL of thawed mucus was combined with 10 μL of an aqueous solution containing 100 mM $(\text{NH}_4)\text{HCO}_3$ and 20 mM TCEP. The resulting samples were incubated for 45 min at room temperature. Each sample was then centrifuged for 10 min at 13 000 rpm, 4 $^\circ\text{C}$. The supernatant was removed and transferred to a vial for LC-MS analysis. Total protein in the sample was determined by a standard Bradford (Bio-Rad) assay using bovine serum albumin as a standard. An Agilent 6520 mass spectrometer connected to an Agilent 1200 LC system was employed as described above. The injection volume was chosen such that approximately 9 μg of total protein was injected. The sample components were eluted using a gradient that linearly increased from 1%-61% B over 9 min at a flow rate of 0.8 mL/min.

All other mucus samples and the pus samples were prepared and analyzed differently. The mucus samples were thawed on ice and the two pus samples were prepared immediately after collection. We found that an acetone precipitation protocol improved our ability to observe protein signals in proteomics experiments presumably because small molecules that suppressed ionization were removed. The mucus and pus samples were precipitated by combining 10 μL of mucus or pus with 40 μL of acetone that had been chilled to -20 $^\circ\text{C}$. After mixing, the precipitation samples were stored at -20 $^\circ\text{C}$ overnight. The next day, the samples were centrifuged for 10 min, 13 000 rpm, at 4 $^\circ\text{C}$. The supernatant was aspirated, and the pellet was resuspended in a 4:1 mixture acetone:water at -20 $^\circ\text{C}$. The centrifugation step was repeated, and the supernatant was aspirated. The pelleted protein was dried on a lyophilizer for 1 h, and then redissolved in 75 μL of 4:1 6 M guanidine HCl and 20 mM TCEP: 75 mM HEPES, 100 mM NaCl with the pH adjusted to 7.2. After 2 h, equal volumes of the dissolved protein and 1:1 $\text{H}_2\text{O}:\text{MeCN}+0.1\%$ TFA were combined. The protein sample was centrifuged for 10 min, 13 000 rpm, at 4 $^\circ\text{C}$. For LC-MS analysis, 10 μL of the sample was injected, and separated

with the same instrumentation described above. A different gradient was used for these samples. The gradient began at 20% B and linearly increased to 45% B over 25 min at a flow rate of 0.8 mL/min.

4.3.10. Antimicrobial Activity Assays

The growth inhibitory activities of CP-Ser, CP-Ser O₄, and CP-Ser O₅ against *Escherichia coli* ATCC 25922 and *Staphylococcus aureus* ATCC 25923 were assayed at 30 °C as described previously.⁹ The antimicrobial activity assay medium, hereafter AMA medium, was a 62:38 ratio of 20 mM Tris-HCl, pH 7.5, 100 mM NaCl, 5 mM BME, 3 mM CaCl₂ and tryptic soy broth (TSB) with 0.25% (w/v) dextrose. To prevent evaporation of the medium, the plates were sealed with parafilm and a beaker of water was housed in the incubator shaker.

4.3.11. Metal Competition Experiments with ZP1

The ability of CP-Ser O₄ and CP-Ser O₅ to outcompete Zinpyr-1 (ZP1)⁴⁶ for Mn(II), Fe(II), Ni(II), and Zn(II) was assayed by using a modified competition protocol.²⁵ Quartz cuvettes (Starna) were charged with 2 mL of 75 mM HEPES, 100 mM NaCl, pH 7.5. ZP1 was stored at -20 °C in DMSO, and a fresh aliquot was thawed daily. ZP1 was added to 1 μM in each cuvette, mixed by pipetting, and stored in the dark for 1 h. The proteins were thawed at room temperature, and diluted to 4 μM, and then Ca(II) was added to 200 μM. After 15 min, emission spectra were collected. Using a 500 μM solution of metal, the metal of interest was added to 3 μM, and after 1 h emission spectra were collected. Next, using a 120 μM solution of metal, the metal concentration was increased to 3.6 μM, and after 10 min emission spectra were collected. For the Zn(II) titrations, additional data points were collected. Using a 500 μM solution, the Zn(II) concentration was adjusted to 6 μM, and after 1 h emission spectra were collected. Using a 500 μM solution, the Zn(II) concentration was adjusted to 7.2 μM, and emission spectra were recorded after 10 min.

For the experiments with Fe(II), the cuvettes were sealed with screw caps before removing them from the glove box, and all additions of Fe(II) were performed in the glove box. Excitation was provided at 490 nm, and the spectra were recorded over 500-650 nm. The ratio between the total integrated emission after metal addition to the total integrated emission before metal addition was plotted. Averages and the standard deviations are reported ($n=3$).

4.3.12. Analytical Size-Exclusion Chromatography

An Äkta purifier (GE Lifesciences) housed in a 4 °C cold room outfitted with a 100- μ L or 500- μ L sample loop was used for analytical size-exclusion chromatography (SEC). A Superdex 75 10/300 GL column (GE Lifesciences) equilibrated in mobile phase was calibrated with a low-molecular-weight calibration mixture (GE Lifesciences) as described previously.⁹ The largest protein in the calibration solution had an elution volume of 10.0 mL (77.5 kDa, 500- μ L loop), and an analyte eluting in the void volume (8.3 mL, 500- μ L loop) would have an apparent molecular weight of 150 kDa. A typical sample volume was 300 μ L.

For experiments that monitored the dissociation of the CP-Ser heterotetramer following H₂O₂ treatment, CP-Ser was thawed at room temperature, and diluted to 30 μ M into 75 mM HEPES, 100 mM NaCl, 1.5 mM CaCl₂, pH 7.5. For experiments that monitored the dissociation of the Mn(II)-bound CP-Ser heterotetramer following H₂O₂ treatment, Mn(II), the samples also contained 30 μ M Mn(II). A typical reaction volume was \approx 2 mL. After 15 min of incubation at room temperature, 300 μ L of the sample was combined with 33 μ L of 5 M aqueous BME to afford the 0 h sample. Another 300- μ L aliquot of the protein solution was transferred to a microfuge tube to yield the untreated sample. To initiate the reaction, a final concentration of 100 mM H₂O₂ was added to \approx 2 mL of CP-Ser solution, at which point the reaction and untreated sample were moved to 37 °C. At varying time points, a 300- μ L aliquot was removed from the reaction and quenched by addition of 33

μL of freshly prepared 5 M BME. The untreated sample was prepared for analysis in the same manner as the reaction aliquots after 23 h of incubation. The quenched samples were centrifuged at 13 000 rpm, 4 °C for 10 min. The supernatant was loaded onto the 100- μL loop. The loop was emptied with 0.5 mL of mobile phase (75 mM HEPES, 100 mM NaCl, 1.5 mM CaCl_2 , pH 7.5), and the protein was eluted over one column volume at a flow rate of 0.5 mL/min. For SEC experiments with the Met \rightarrow Ala CP-Ser variants, the above procedure was employed except that the final H_2O_2 concentration was 500 mM and the reactions were quenched by combining a 300- μL aliquot of the reaction with 45 μL of 5 M BME.

For experiments that monitored the oligomeric state of disulfide-linked CP, the SEC analysis was performed using similar methods to those above. To reduce the disulfides before elution, a 77- μL aliquot of 75 mM HEPES, 100 mM NaCl, 20 mM TCEP, pH 7.5 was added to a 700- μL aliquot of protein solution and the mixture was incubated at ambient temperature for 1 h. To remove Ca(II) from the protein, a 77- μL aliquot of 75 mM HEPES, 100 mM NaCl, 20 mM EDTA was added to a 700- μL aliquot of protein solution, and the mixture was incubated for 1 h at 4 °C. Before injection onto the SEC column, the solutions were centrifuged at 13 000 rpm, 4 °C, 10 min. The 500- μL loop was loaded with 600 μL of sample, and emptied with 500 μL of elution buffer. For the untreated and TCEP-treated protein, the mobile phase was 75 mM HEPES, 100 mM NaCl, 1.5 mM Ca(II), pH 7.5. For the EDTA-treated protein, the same mobile phase was used except the Ca(II) was omitted. The eluent was collected into 1-mL fractions using an automated fraction collector.

4.3.13. *Anion-Exchange Chromatography*

An Äkta purifier (GE Lifesciences) housed in a 4 °C cold room outfitted with a 500- μL sample loop was used for anion exchange chromatography. A MonoQ 10/100 column was employed. Mobile phase A was 20 mM HEPES, pH 8.0. Mobile phase B was 20 mM

HEPES, 1 M NaCl, pH 8.0. The gradient was 0–60% B over 15 column volumes (120 mL) at a flow rate of 1 mL/min. Samples of CP-Ser and S100A9(C3S) homodimer were thawed at room temperature, diluted to 100 μ M into mobile phase A, and centrifuged for 10 min at 13 000 rpm at 4 °C. The final volume of each sample was 300 μ L. The samples were injected onto the loop using a 1-mL syringe, and the loop was emptied with 0.5 mL of mobile phase A.

4.3.14. Analytical Ultracentrifugation (Sedimentation Velocity)

A Beckman XL-I Analytical Ultracentrifuge outfitted with an An-60 Ti rotor was employed for all sedimentation velocity experiments. The rotor housed conventional double-sector charcoal filled Epon centerpieces within the sample cells and contained quartz windows. The absorbance wavelength for optical detection was 280 nm. The samples were centrifuged at 42 000 rpm and 20 °C until sedimentation was complete. SEDNTERP⁴⁷ was employed to calculate the buffer viscosity (η), buffer density (ρ), and protein specific volume (\bar{v}). Additional details are provided with Tables 4.6 and 4.7.

For sample preparation, 1 L of 75 mM HEPES, 100 mM NaCl, pH 7.5 dialysis buffer containing 10 g of Chelex resin (Biorad) was prepared and chilled at 4 °C. Each protein was thawed at room temperature and then diluted to 30 μ M using 75 mM HEPES, 100 mM NaCl, pH 7.5. Each protein sample was transferred to 3.5 k MWCO dialysis tubing (Spectrum Labs) and dialyzed overnight at 4 °C in the dialysis buffer with gentle stirring. The following day, the protein and dialysis buffer aliquots were transferred to 1.7-mL polypropylene tubes and centrifuged at 13 000 rpm, 10 min, 4 °C to sediment any contaminating Chelex resin. Solutions of 1 mM EDTA (diluted from 100 mM in H₂O) and 100 mM Ca(II) were prepared using the centrifuged dialysis buffer. Matched protein and reference samples were prepared by adding 30 μ M EDTA or 600 μ M Ca(II) to the protein and buffer-only samples. The protein samples and reference samples were incubated at ambient temperature while the window assemblies were constructed (\approx 1.5 h). The

window assemblies were each loaded with 410 μL of the reference buffer or 400 μL of a protein sample. The oxidized proteins were analyzed under both conditions using samples of protein from independent preparations in separate experiments.

4.3.15. *Protease Digestion of Oxidized CP-Ser*

Trypsin (Affymetrix), proteinase K (Affymetrix), and chymotrypsin (Amresco) were obtained as lyophilized powders, stored at 4 $^{\circ}\text{C}$, and dissolved in water to afford solutions of $\approx 50\text{--}100$ μM immediately before use. Extinction coefficients for trypsin, proteinase K, and chymotrypsin are reported in Table 4.2. Human neutrophil elastase (Enzo Life Sciences) was obtained as a lyophilized powder, and the entire portion of protease was dissolved in 75 mM HEPES, 100 mM NaCl, pH 7.5 to afford a solution with a concentration of ≈ 1 mg/mL. HNE was divided into single-use aliquots, frozen with liquid nitrogen, and stored at -80 $^{\circ}\text{C}$. Protease digestion assays with CP-Ser O₄ and CP-Ser O₅ were performed on a 500- μL scale at pH 7.5 (75 mM HEPES, 100 mM NaCl). Aliquots of CP-Ser, CP-Ser O₄, and CP-Ser O₅ were thawed at room temperature and diluted (30 μM , 750 μL) using the assay buffer. Ca(II) (1.5 mM) was added to all samples and Mn(II) (30 μM) was added to select samples. To initiate each digestion assay, an aliquot (between 5- and 10- μL as appropriate) of protease was added to the 500- μL protein solution to afford protease concentrations of 0.45 μM (trypsin), 0.5 μM (HNE), or 1 μM (chymotrypsin, proteinase K). The resulting solution was immediately mixed with a pipette and incubated at 37 $^{\circ}\text{C}$. Aliquots (45 μL) of the reaction were quenched with 5 μL of aqueous 6% (v/v) TFA and 150 μL of 6 M guanidinium chloride at $t = 0, 0.5, 1, 2,$ and 3 h (trypsin and proteinase k), $t = 0, 4, 8,$ and 24 h (HNE), or $t = 0, 1, 3, 5,$ and 8 h (chymotrypsin). The quenched solutions were centrifuged (13 000 rpm, 10 min, 4 $^{\circ}\text{C}$), and the resulting samples were analyzed by analytical HPLC using a gradient of 10–60% B over 50 min.

4.3.16. *Protease Digestion of Oxidized CP*

dsl-CP and MetO-dsl-CP were prepared as described in subsection 4.3.6, and stored overnight at 4 °C. The next day, these samples were used in trypsin digestion assays. To monitor the degradation of dsl-CP and MetO-dsl-CP, the reactions were quenched at different time points, and the reaction progress was evaluated using reversed-phase HPLC. At each time point, one 45- μ L aliquot of the digest was quenched in the absence of a reducing agent (150 μ L of 6 M guanidine hydrochloride and 5 μ L of 6% TFA), and a second 45- μ L aliquot was quenched in the presence of a reducing agent (40 mM HEPES, 6 M guanidine hydrochloride, 20 mM TCEP, pH 7.5). After rapid mixing with the micropipette, each sample quenched under reducing conditions was heated at 95 °C for 10 min to allow reduction of the disulfide bonds without trypsin activity. After heating, 5 μ L of 6% TFA was added, the quenched samples were centrifuged at 13 000 rpm, 4 °C for 10 min, and 100 μ L aliquots were analyzed by analytical HPLC, and using a gradient of 10–60% B over 50 min.

4.3.17. *SDS-PAGE and Western Blots*

Samples were prepared for SDS-PAGE by combining 5x Laemmli buffer (312 mM Tris-HCl, 10% SDS, 0.05% bromophenol blue (w/v), BME (v/v), pH 6.8) and protein samples in a 1:4 (v/v) ratio. For analysis of CP disulfide speciation after oxidation, the BME was omitted from the Laemmli buffer. The samples were heated at 95 °C for 5 min, and then 10 μ L was loaded onto the gel. For all experiments, gels of 1-mm width were used. The stacking gel was made from 125 mM Tris-HCl, 0.1% SDS, 5% acrylamide (19:1 acrylamide:bis acrylamide), 0.05% ammonium persulfate, 0.1% tetramethylethylenediamine, pH 6.8. The resolving gel was made from 250 mM Tris-HCl, 1% SDS, 15% acrylamide (19:1 acrylamide:bis acrylamide), 0.05% ammonium persulfate, 0.05% tetramethylethylenediamine, pH 8.8. The products of the disulfide-bond-formation reactions of CP and the fractions from SEC of disulfide-linked CP were

run at 200 V for 90 min. The gels were stained with using Coomassie Brilliant Blue G-250.

For western blots, the protein was transferred to a nitrocellulose membrane using a Trans-Blot Turbo (Bio-Rad). The transfers were performed at 25 V for 10 min. The membrane was blocked for 30 min using 5% milk in Tris-buffered saline (TBS, 2 mM Tris, 138 mM NaCl, pH 7.5). The blot was probed at 4 °C overnight with goat-anti S100A9 (Santa Cruz Biotech, sc-8114, 250-fold diluted) in TBS+5% bovine serum albumin. The next day, the blot was washed three times for 5 min using TBS+0.1% Tween 20, and then rinsed with water. The blot was then stained for 1 h at ambient temperature with 1:10 000-fold diluted donkey anti-goat 800CW (Li-COR) in TBS+5% milk. After rinsing the blot with water, the blot was imaged using an Odyssey scanner (Li-COR). The same probing, washing, and imaging protocol was repeated to detect S100A8. A murine monoclonal antibody (Santa Cruz Biotech, sc-48352) was used to probe for S100A8 and a goat anti-mouse 680CW (Li-COR) antibody was used to visualize S100A8.

4.4. Results

4.4.1. Oxidized CP Subunits are Observed in Human Mucus and Pus

Subunits of CP containing MetO have been observed in murine kidney abscesses, human cystic fibrosis bronchoalveolar fluid, and human kidney stones.²⁹⁻³¹ Because methionine side chains can be easily oxidized, it is often unclear whether the oxidation occurred *in vivo*, following sample collection, or during analysis. Nevertheless, we were intrigued by these findings, and therefore sought to ascertain whether methionine oxidation of CP occurs *in vivo* and whether this post-translational modification has physiological relevance. We focused on the collection and *ex vivo* analyses of two types of readily available human samples, nasal mucus and pimple pus, where we expected to find CP. We selected LC-MS as an analytical method to identify unmodified and modified

CP subunits. Moreover, in prior biophysical studies of CP, we overexpressed and purified ^{15}N -labeled CP-Ser, a S100A8(C42S)/S100A9(C3S) variant where each subunit is globally labeled with the ^{15}N isotope.⁴⁴ We reasoned that we could use ^{15}N -labeled CP-Ser as an internal standard by spiking samples with this protein immediately after collection from the human subject and thereby monitor for whether methionine oxidation of CP occurs before or after sample collection.

We collected and analyzed 26 nasal mucus samples from patients prior to surgery, and detected both CP subunits in 15 of these samples by LC-MS (Table 4.5). These analyses revealed full-length S100A8 and two truncated forms of S100A9 bearing N-terminal acetylation. Full-length S100A9 was not observed. One truncated S100A9 species lacked the initiator methionine residue and the other lacked the first five amino acids of S100A9, indicating that translation was initiated at Met5 rather than Met1 (Figure 4.1C). These truncated, N-acetylated forms of S100A9 have been previously observed in human kidney stones.³¹ LC-MS also revealed that four of the CP-containing mucus samples exhibited deconvoluted masses consistent with oxidized CP subunits. Although the extent of CP oxidation varied depending on the sample, some common species were observed (Figures 4.1A,B 4.2A,B, and Table 4.5). In two of the four of the samples, a population of S100A8 that bore a single additional oxygen atom (+16 Da) was found. All three samples contained S100A9 with at least one additional oxygen atom (+16 Da). In three of the four samples, S100A9 with five additional oxygen atoms (+80 Da) was observed. One sample exhibited a series of +16 Da species ending with a molecule that appeared to have eight additional oxygen atoms (+128 Da) (Figure 4.1B). In order to monitor for oxidation that might occur after sample collection, we added ^{15}N -CP-Ser to a mucus sample immediately after collection (Figure 4.1D,E). This sample contained oxidized CP subunits, and we observed neither oxidized ^{15}N -S100A8(C42S) nor oxidized ^{15}N -S100A9(C3S) in the sample.

During the course of the mucus studies, we found that many samples were viscous and that oxidized CP subunits were only detected in ca. 60% of the samples. Thus, we extended the analyses to human pus samples isolated from pimples, which we found to be easier to handle than mucus. LC-MS revealed the presence of the CP subunits in two pus samples (Figure 4.3). Similar to the mucus samples, we observed full-length S100A8 and truncated, N-acetylated forms of S100A9. Both pus samples also contained oxidized S100A8 and S100A9 species. The oxidized S100A8 species contained one additional oxygen atom (+16 Da) and up to five additional oxygen atoms were observed for the oxidized S100A9 species. We spiked both of these pus samples with ¹⁵N-CP-Ser, and

Table 4.5 Summary of mucus samples analyzed.^a

Sample	A8	A8+O	A9	A9+O	A9+2O	A9+3O	A9+4O	A9+5O
Mucus 1	X	-	X	X	X	-	-	-
Mucus 2	X	X	X	X	X	X	X	X
Mucus 3	-	-	-	-	-	-	-	-
Mucus 4	-	-	-	-	-	-	-	-
Mucus 5	-	-	-	-	-	-	-	-
Mucus 6	X	-	-	X	-	-	-	-
Mucus 7	X	-	-	X	-	-	-	-
Mucus 8	-	-	-	-	-	-	-	-
Mucus 9	-	-	-	-	-	-	-	-
Mucus 10	X	-	X	X	-	-	-	X
Mucus 11	X	-	X	-	-	-	-	-
Mucus 12	-	-	-	-	-	-	-	-
Mucus 13	X	-	X	-	-	-	-	-
Mucus 14	X	-	X	-	-	-	-	-
Mucus 15	-	-	X	-	-	-	-	-
Mucus 16	-	-	-	-	-	-	-	-
Mucus 17	X	-	X	-	-	-	-	-
Mucus 18	-	-	-	-	-	-	-	-
Mucus 19	-	-	-	-	-	-	-	-
Mucus 20	-	-	-	-	-	-	-	-
Mucus 21	X	-	X	X	-	-	-	-
Mucus 22	X	X	X	X	-	-	-	X
Mucus 23	X	X	X	-	-	-	-	-
Mucus 24	X	X	X	X	-	-	-	-
Mucus 25	X	-	X	-	-	-	-	-
Mucus 26	X	-	X	-	-	-	-	-

^a Species that were observed are marked with an "X."

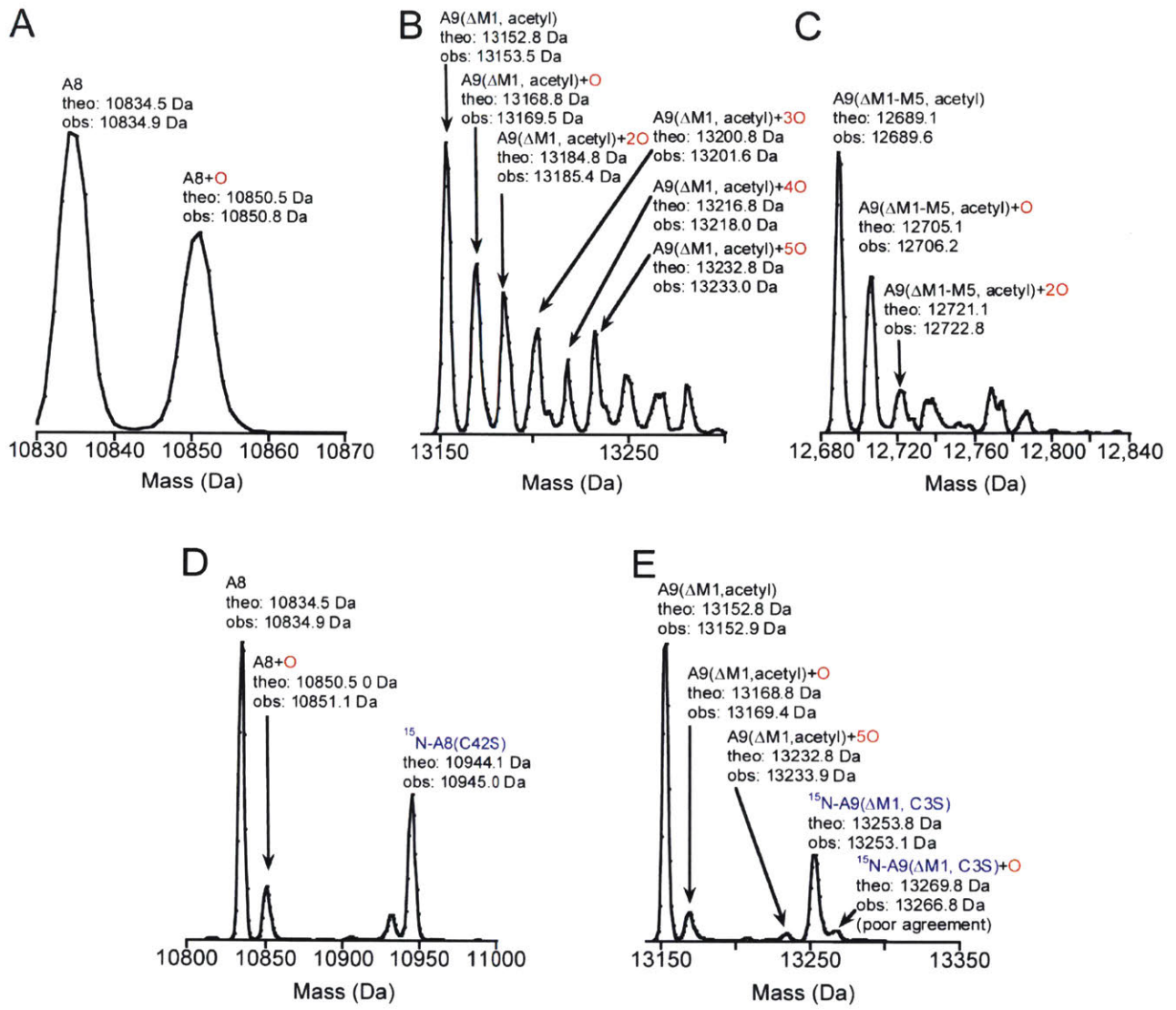


Figure 4.1. Deconvoluted mass spectra of human nasal mucus. The S100A8 panels are normalized to the wild-type S100A8 peak and S100A9 panels are normalized to the most abundant S100A9 peak. Data from (A) mucus sample 2 expanded around S100A8, (B) mucus sample 2 expanded around S100A9, (C) mucus sample 2 expanded around S100A9(Δ M1-5), (D) mucus sample 22 expanded around S100A8 that shows ¹⁵N-A8(C42S), (E) mucus sample 22 expanded around S100A9 that shows ¹⁵N-A9(Δ M1, C3S).

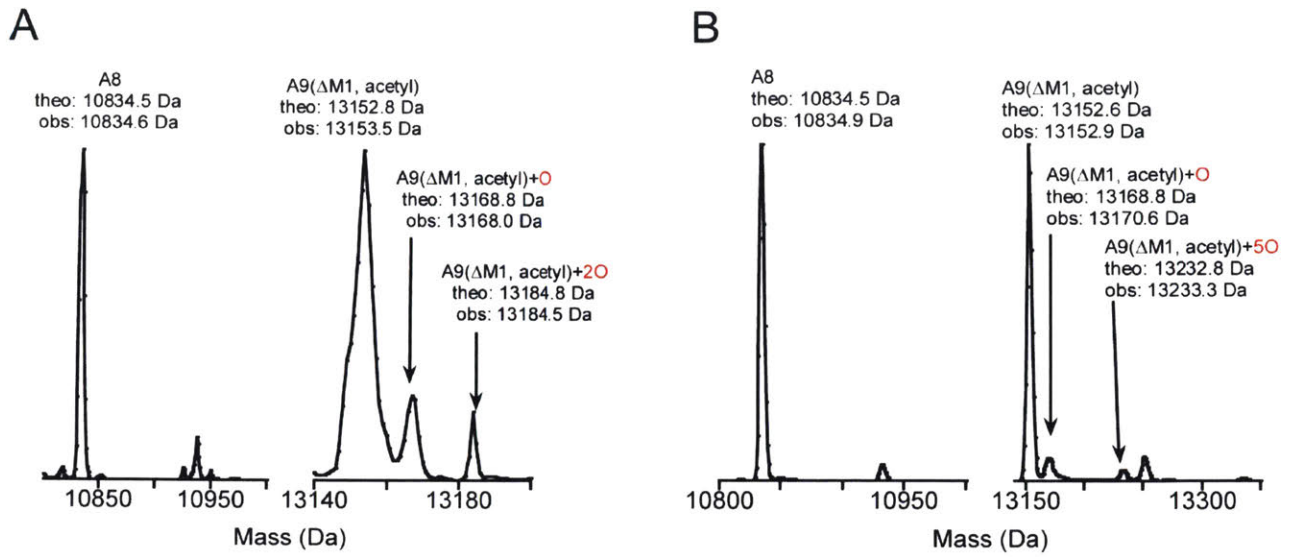


Figure 4.2 Mass spectrometry of additional human nasal mucus samples. Deconvoluted mass spectra expanded around S100A8 and S100A9. (A) Mucus sample 1, (B) mucus sample 10.

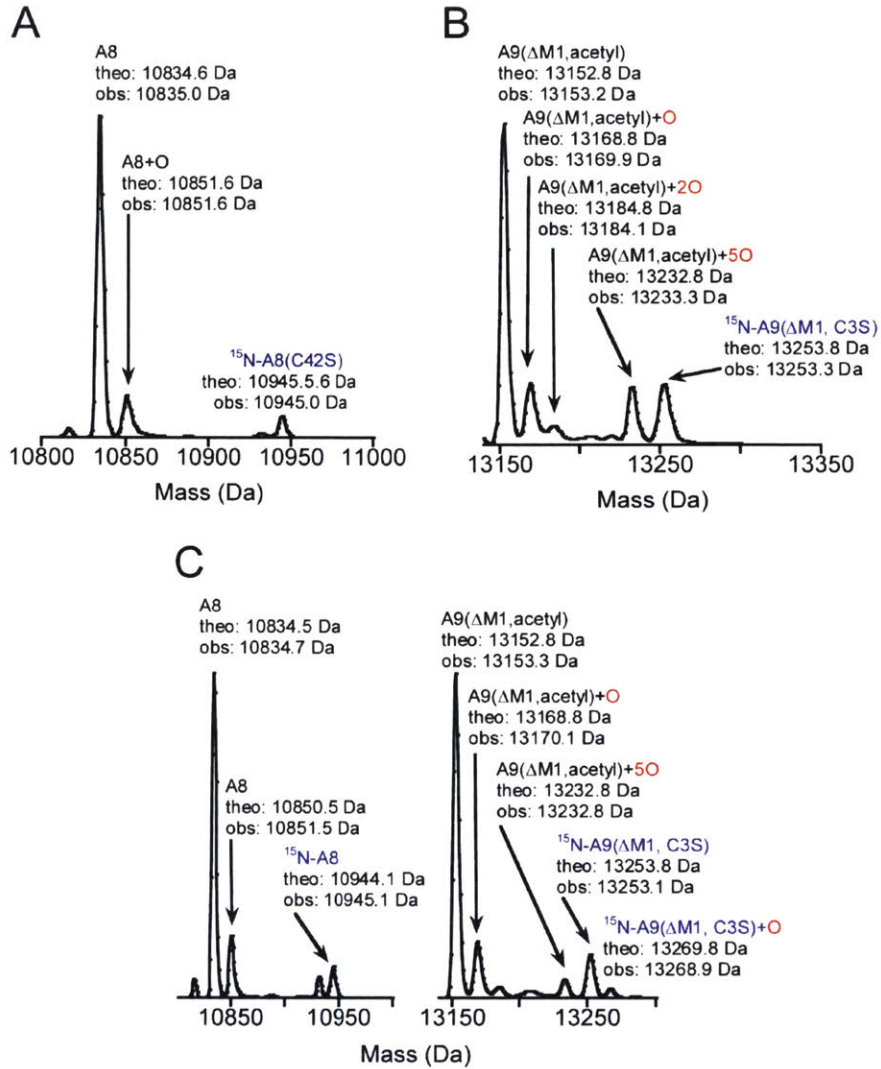


Figure 4.3. Deconvoluted mass spectra of human pus with ¹⁵N-CP-Ser added immediately after collection. S100A8 and S100A9. (A) Data from pus sample 2 expanded around S100A8, (B) data from pus sample 2 expanded around S100A9, (C) data from pus sample 1 expanded around S100A8 and S100A9.

observed no oxidized ^{15}N -S100A8(C42S) species in either sample, and a small fraction of ^{15}N -S100A9 bearing a single additional oxygen atom (+16 Da) was detected in in one of the two samples (Figure 4.3).

These *ex vivo* studies of nasal mucus and pimple pus provide further support for the existence of oxidized CP subunits in different human fluids. Importantly, the lack of oxidation of the ^{15}N -CP-Ser internal standard indicates that the oxidative post-translational modifications of the CP subunits occurred *in vivo* and not during sample collection, storage, or analysis. Full-length S100A8 has two Met residues, and full-length S100A9 has six Met residues. We interpret these data to indicate that one Met of S100A8 and up to five Met of S100A9 can be oxidized to methionine sulfoxide. These results are in agreement with prior work that observed oxidized CP subunits in *ex vivo* and *in vivo* tissues.²⁹⁻³¹ Taken together, these observations strengthen the notion that methionine sulfoxide is a physiologically relevant post-translational modification of CP.

4.4.2. Methionine Oxidation of CP-Ser Causes Heterotetramer Dissociation

To investigate the consequences of methionine oxidation on the biophysical properties of CP, we first treated the Ca(II)-bound CP-Ser heterotetramer with H_2O_2 , an oxidant that oxidizes Cys and Met residues with high specificity,⁴⁸ and monitored the reaction by analytical size-exclusion chromatography (SEC) and LC-MS (Figure 4.4A,B). SEC revealed that the CP-Ser heterotetramer peak (10.9 mL, 45.9 kDa) decreased in intensity and a new peak corresponding to the CP-Ser heterodimer (11.5 mL, 34.9 kDa) appeared (Figure 4.4A). In these chromatograms, tetramer dissociation was readily apparent at the 7-h time point, and the dimer became the major species at the 23-h time point. LC-MS of the corresponding samples demonstrated that, as heterotetramers dissociated into heterodimers, the number of oxygen atoms on the CP subunits increased (Figure 4.4B). S100A8 had gained a single additional oxygen atom (+16 Da) within 1 h of incubation, and no further oxidative modification was observed until the 23-h time point

where S100A8 with two additional oxygen atoms (+32 Da) became the major species. In contrast, the extent of oxidation of S100A9 increased at each time point. Because the dissociation of the Ca(II)-bound heterotetramer appeared to coincide with the extent of methionine oxidation on S100A9, we reasoned that the trigger for heterotetramer dissociation was oxidation of one or more Met residues on S100A9.

In prior work, we demonstrated that coordination of Mn(II) or Fe(II) at the His₆ site of CP-Ser in the absence of Ca(II) causes two heterodimers to self-associate into a heterotetramer, and caused tetramerization of CP-Ser variants harboring (A8)I60K or (A8)I60E point mutations that could not tetramerize with Ca(II) alone.¹³ Thus, we questioned whether a Ca(II)- and transitional-metal-bound heterotetramer dissociates into heterodimers upon methionine oxidation. We oxidized CP-Ser with H₂O₂ in the presence of excess Ca(II) and one equivalent of Mn(II), which selectively binds to the His₆ site, and monitored the reaction by SEC and LC-MS (Figure 4.4C,D). In contrast to the oxidation in the presence of only Ca(II), a peak with a maximum elution volume consistent with the heterotetramer (11.0 mL, 43.8 kDa) was only observed, indicating that the Ca(II)- and Mn(II)-bound protein remained a heterotetramer over the 23-h time course. Analysis of samples by LC-MS revealed that both subunits were oxidized in the presence of Ca(II) and Mn(II) at a rate that appeared comparable to that observed for the Ca(II)-only sample. These data indicate that coordination of both Ca(II) and Mn(II) stabilizes the heterotetramer, and that that Mn(II) chelation at the His₆ site does not protect Met residues from oxidation by H₂O₂.

4.4.3. (A9)MetO81 Serves as the Determinant for Heterotetramer Dissociation

In order to better understand the molecular basis of H₂O₂-induced dissociation of the Ca(II)-bound CP-Ser heterotetramer, we investigated the contributions of individual S100A9 Met residues to this process. We overexpressed and purified three new CP-Ser variants that each contain a single Met→Ala mutation at position 63, 81, or 83 of

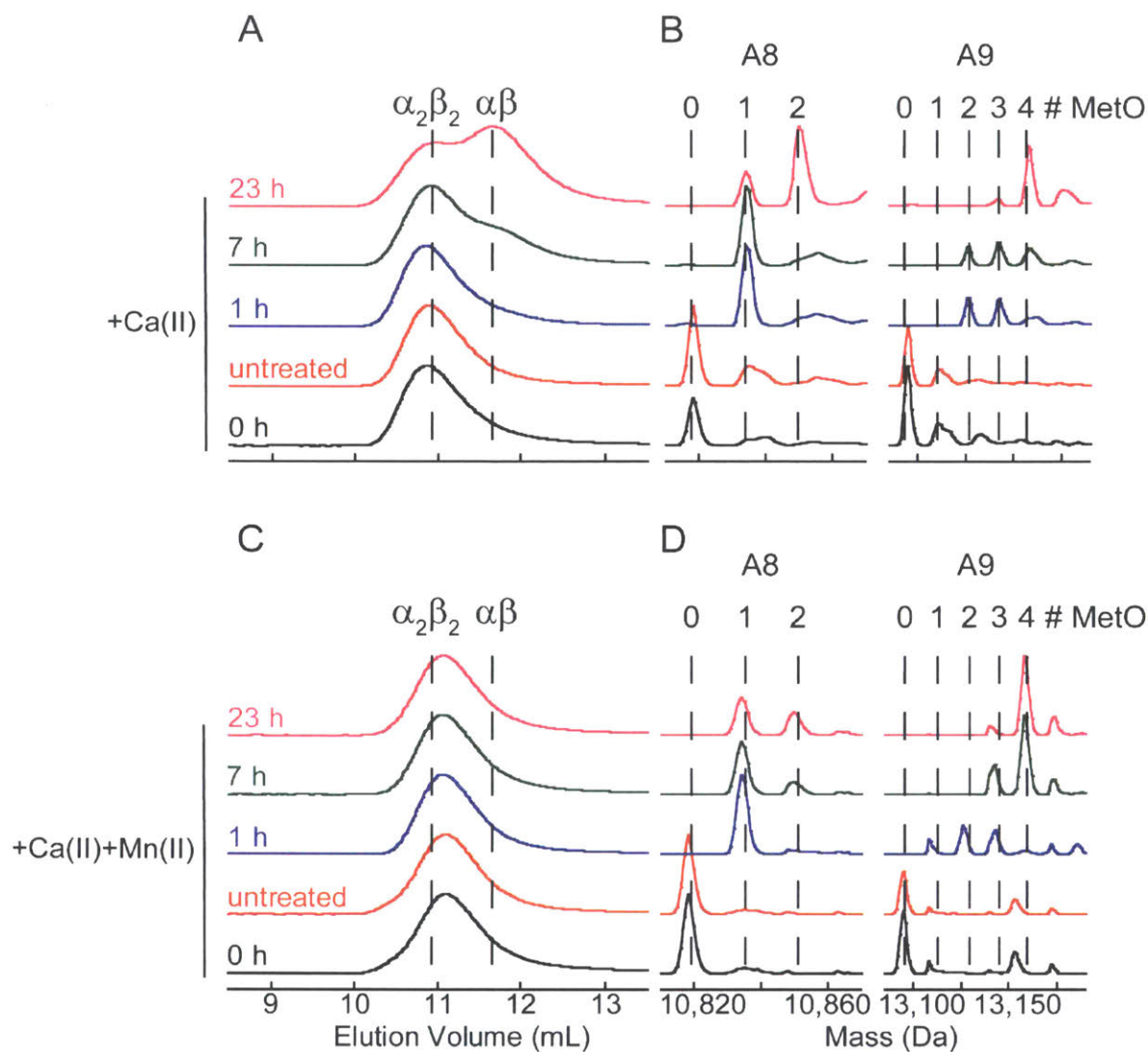


Figure 4.4. SEC chromatograms and corresponding deconvoluted mass spectra of CP-Ser treated with 100 mM H_2O_2 +Ca(II) and Ca(II)+Mn(II) after various reaction times. Note that the Mn(II)-Ca(II)-CP-Ser tetramer elutes slightly later than the +Ca(II)-CP-Ser tetramer. (A) +Ca SEC. (B) +Ca MS. (C) +Ca(II)+Mn(II) SEC. (D) +Ca(II)+Mn(II) MS. In the chromatograms, the dashed lines represent the elution volumes of the tetramer and dimer. In the mass spectra, the dashed lines represent the expected masses of the CP-Ser subunits with additional oxygen atoms. The chromatograms and mass spectra were normalized to a maximum value of 1.

S100A9(C3S) (Table 4.4). (A9)M63 is close to the C-terminal EF-hand, (A9)M81 appears to participate in the dimer-dimer interface, and (A9)M83 is close to the dimer-dimer interface (Figure A2.23). These variants were obtained as pure heterodimers (Figure A2.20). Circular dichroism (CD) spectroscopy in the absence and presence of Ca(II) demonstrated that the α -helicity of the proteins was not perturbed by the mutations (Figure A2.21). SEC performed in the presence of Ca(II) indicated that all three Ca(II)-bound CP-Ser variants eluted as tetramers (Figure 4.5), indicating that the Met→Ala mutations in S100A(C3S) did not perturb Ca(II)-induced tetramerization, at least as ascertained by this technique. Moreover, SEC revealed that treatment of the Met→Ala variants with H₂O₂ in the presence of Ca(II) caused the CP-Ser(A9-M63A) and CP-Ser(A9-M83A) variants to dissociate into dimers, whereas the CP-Ser(A9-M81A) variant remained a tetramer (Figure 4.5). LC-MS of the Met→Ala variants after H₂O₂ treatment displayed oxidation comparable to CP-Ser (Table 4.1). These results show that H₂O₂-induced dissociation of the Ca(II)-bound heterotetramer is dependent on oxidation of (A9)M81.

4.4.4. *Preparation of Oxidized CP-Ser*

In order to further study CP-Ser bearing MetO modifications, we developed and optimized a protocol to obtain milligram quantities of oxidized CP-Ser. We followed our reported procedures⁹ for overexpressing the S100A8(C42S) and S100A9(C3) polypeptides and reconstituting the CP-Ser heterodimer except that, following the first round of dialysis in refolding buffer (75 mM HEPES, 100 mM NaCl, pH 7.5), we treated the protein with H₂O₂ at 37 °C. We found that treating the dialyzed protein with 50 mM H₂O₂ for 2.5 or 5 h afforded a mixture of species where the dominant species was oxidized CP-Ser comprised of S100A8 with one additional oxygen atom and S100A9 with three additional oxygen atoms. We named this protein mixture CP-Ser O₄ to denote most prevalent number of additional oxygen atoms per heterodimer (Table 4.4 and

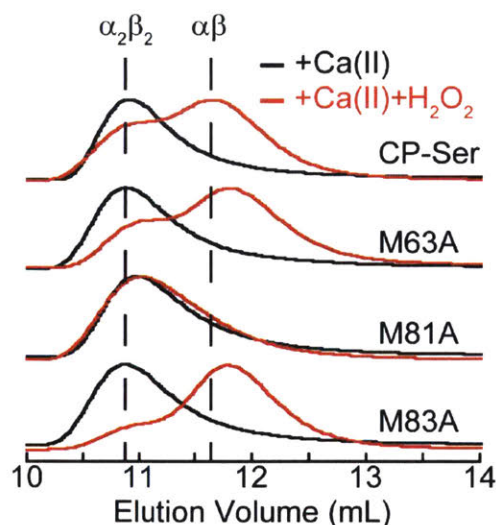


Figure 4.5. SEC chromatograms of CP-Ser and Met to Ala variants in the presence of Ca(II) before (black traces) and after (red traces) treatment with 500 mM H₂O₂ for 7 h. Each chromatogram was normalized to a maximum absorbance of 1. Conditions: 75 mM HEPES, 100 mM NaCl, 1.5 mM Ca(II), pH 7.5, 30 μM protein, 500 mM H₂O₂.

Figure A2.8). When we treated the protein with 50 mM H₂O₂ for 6 h or with 75 mM H₂O₂ for 6.5 h, we obtained mixtures where the dominant species was oxidized CP-Ser was comprised of S100A8+O with one additional oxygen atom and S100A9 with four additional oxygen atoms (Table 4.4 and Figure A2.8). We named this protein mixture CP-Ser O₅. Following treatment with H₂O₂, the protein was centrifuged to remove a precipitate that formed during oxidation, dialyzed against refolding buffer, and then the heterodimers were purified by anion exchange and gel filtration chromatography as previously reported for CP-Ser (Figure A2.20).⁹ The yields for CP-Ser O₄ and CP-Ser O₅ ranged from 30-40 mg / L of overexpression culture. Analysis of the oxidized CP-Ser proteins by CD spectroscopy in the absence and presence of excess Ca(II) ions revealed that the α-helicity of the CP scaffold was unaffected by methionine oxidation (Figure A2.21).

4.4.5. CP-Ser O₄ and CP-Ser O₅ Exhibit Defective Ca(II)-Induced Tetramerization

To further examine the consequences of methionine oxidation on the biophysical properties of CP, we investigated the oligomeric states of CP-Ser O₄ and CP-Ser O₅ by SEC and anion exchange chromatography (AXC). We first examined CP-Ser O₄ and CP-Ser O₅ by using analytical SEC to determine if the purified oxidized proteins recapitulated the tetramerization-deficient behavior that occurred after treating CP-Ser with H₂O₂ (Figure 4.5). In the absence of added metal ions, CP-Ser O₄ and CP-Ser O₅ each had an elution volume of \approx 11.6 mL (33.4 kDa), consistent with the apo heterodimer (Figure 4.6). In the presence of excess Ca(II) ions, the CP-Ser O₄ and CP-Ser O₅ peaks maintained a maximum peak height consistent with the heterodimer elution volume. However, the peaks broadened, suggesting that both between dimeric and tetrameric species exist under these high-Ca(II) conditions (Figure 4.6). When Mn(II) or both Ca(II) and Mn(II) were present, CP-Ser O₄ and CP-Ser O₅ tetramerized (Figure 4.6). Thus, the SEC experiments with CP-Ser O₄ and CP-Ser O₅ demonstrated that the proteins displayed oligomeric properties consistent with H₂O₂-treated CP-Ser, and would be useful for further studying the effects of Met oxidation on CP-Ser.

AXC allows separation of CP-Ser heterodimers from S100A9(C3S) homodimers, and we employed this technique to ascertain whether Met oxidation caused conversion of the S100A8/S100A9 heterodimer to the S100A8 and S100A9 homodimers (Figure A2.24). We attempted to include the S100A8(C42S) homodimer in this analysis; however, its peak profile and retention time was highly variable between runs. The chromatograms for CP-Ser, CP-Ser O₄, and CP-Ser O₅ each revealed a single peak with an elution volume of 29.3 mL consistent with the S100A8(C42S)/S100A9(C3S) heterodimer. No peak corresponding to the S100A9(C3S) homodimer (37.2 mL) was observed in the CP-Ser, CP-Ser O₄, and CP-Ser O₅ samples. Thus, we concluded that methionine oxidation does not cause CP heterooligomers to convert into S100A8 and S100A9 homodimers.

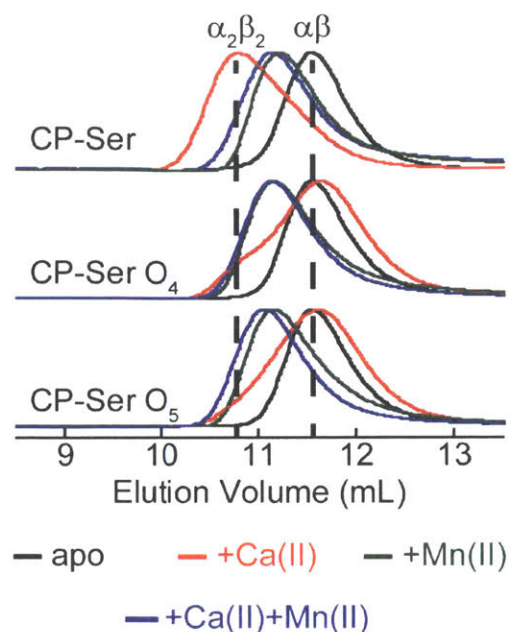


Figure 4.6. SEC of CP-Ser, CP-Ser O₄, and CP-Ser O₅ under -Ca(II), +Ca(II), and +Ca(II)+Mn(II) conditions. Each chromatogram was normalized to a maximum absorbance of 1. The dashed lines represent the elution volumes of the tetramer and dimer. Conditions: 75 mM HEPES, 100 mM NaCl, 30 μM CP, ±1.5 mM Ca(II), ±30 μM Mn(II).

4.4.6. CP-Ser O₄ and CP-Ser O₅ Interconvert between Heterodimers and Heterotetramers

To further elucidate the oligomerization behavior of CP-Ser O₄ and CP-Ser O₅ in the presence of excess Ca(II) ions, we employed velocity analytical ultracentrifugation (AUC), which is a powerful technique for studying protein oligomerization capable of differentiating between interacting and non-interacting systems.^{49,50} Along these lines, two scenarios that would give rise to the observed SEC peak shapes for CP-Ser O₄ and CP-Ser O₅ can be considered: (i) the oxidized proteins containing a population of tetramers and a population of dimers that do not interconvert or (ii) the oxidized proteins are in a dynamic equilibrium between heterodimer and heterotetramer. For a system of two species that interconvert on a slow timescale or do not interconvert, analysis of AUC data by Sedfit will afford a sedimentation profile where the two species have S values

identical to those of the species in isolation and the S values will be invariant with protein concentration, but the relative amount of each species will change with protein concentration.^{49,50} In contrast, systems that interconvert on the timescale of sedimentation will have peak profiles that change as a function of protein concentration, and the S value(s) observed will be in between those of the two species in isolation when analyzed by Sedfit.^{49,50}

We repeated an earlier AUC analysis of CP-Ser in the absence and presence of excess Ca(II) ions (Figure 4.7 and Table 4.6), and obtained peak profiles and S values in good agreement with our prior data for the apo heterodimer ($s_{20,w} = 2.2$ S) and the Ca(II)-bound heterotetramer ($s_{20,w} = 3.7$ S).¹³ We also examined two independent preparations of CP-Ser O₄ and CP-Ser O₅. In the absence of Ca(II) ions, the sedimentation profiles of CP-Ser O₄ and CP-Ser O₅ were indistinguishable from that of CP-Ser (Figure 4.7), which was consistent with the AXC and SEC studies and indicated that Met oxidation of CP-Ser did not perturb the oligomerization of the apo protein. In the presence of Ca(II) ions, the sedimentation profiles of CP-Ser O₄ and CP-Ser O₅ were more complex than the CP-Ser profile, and displayed the hallmarks of dynamically interconverting systems (Figure 4.7). In particular, the peaks in the sedimentation profiles broadened, in some cases to the point where the heterodimer and heterotetramer peaks could not be resolved. Accordingly, the calculated S values for the observed peaks were in between those of the heterodimer and heterotetramer. In the profiles shown here (Figure 4.7), CP-Ser O₄ (+Ca(II)) displayed two broad peaks with S values between the dimer and tetramer ($s_{20,w} = 2.5$ S and 3.5 S), and CP-Ser O₅ exhibited a single broad peak ($s_{20,w} = 3.3$ S). When we repeated the experiment with independent preparations of the oxidized proteins, the profiles differed from those obtained in the first experiment (Figure 4.7B and Table 4.6); however, the results were consistent with the oxidized proteins undergoing dynamic interconversion between heterodimers and heterotetramers. The observed differences may have arisen from multiple factors that include variable patterns of oxidation between

preparations and protein concentrations. We also analyzed the AUC data using DCDT+,^{51,52} which yielded results consistent with the Sedfit analyses (Figure 4.8 and Table 4.7). For the data of oxidized CP-Ser in the presence of Ca(II), DCDT+ models with a single species provided the best fits. The single peaks had S values between the heterodimer and heterotetramer, in agreement with the fits from Sedfit. Taken together, we concluded that Met oxidation of CP-Ser does not fully prevent tetramerization. Rather, the heterodimer-heterodimer equilibrium is strongly shifted to the heterodimer in the presence of excess Ca(II) ions.

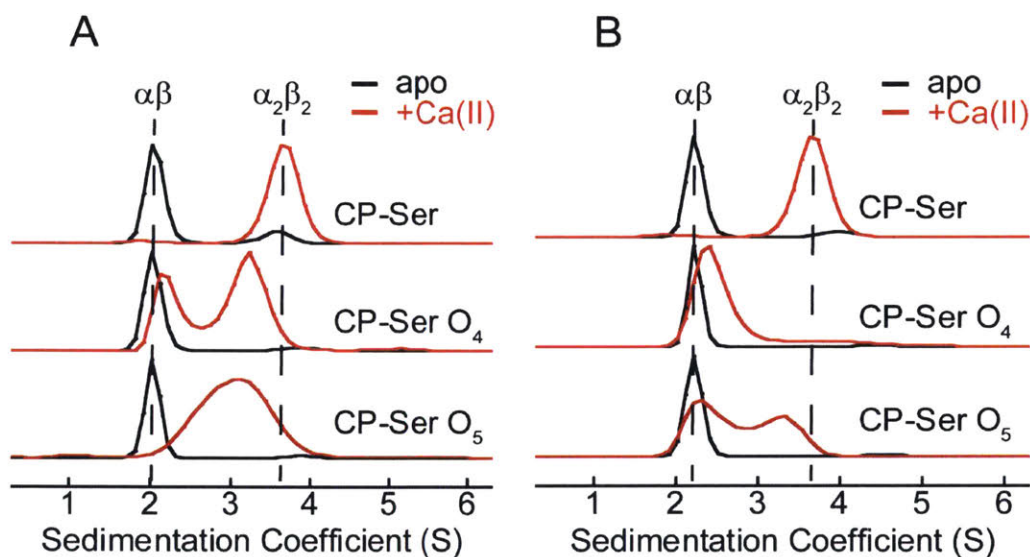


Figure 4.7. Sedimentation velocity distributions of CP-Ser, CP-Ser O₄, and CP-Ser O₅ ±Ca(II) analyzed by SEDFIT using the *c(s)* model. The peaks were normalized to a maximum value of 1. The dashed lines represent the S value of the dimer and tetramer. Conditions: 75 mM HEPES, 100 mM NaCl, pH 7.5, 30 μM CP, ±30 μM EDTA, 600 μM CaCl₂, 20 °C. In the apo experiments (black traces) EDTA was added, and in the +Ca(II) experiments CaCl₂ was added. Sedimentation coefficients and fitting details can be found in Table 4.6.

Table 4.6. Calculated sedimentation coefficients and molecular weights using Sedfit.^a

Protein	Concentration (μM)	$s_{20,w}$ (S)	MW (kDa)	Partial Specific Volume (mL/g)
CP-Ser	30	2.2, 3.9	22.8, 52.0	0.7388
CP-Ser+Ca(II)	30	4.0	41.4	0.7388
CP-Ser O ₄ ^b	30	2.2	23.8	0.7388
CP-Ser O ₄ ^c	30	2.4	22.6	0.7388
CP-Ser O ₄ +Ca(II) ^b	30	2.5, 3.5	22.4, 37.5	0.7388
CP-Ser O ₄ +Ca(II) ^c	30	2.7, 4.5	23.2, 49.8	0.7388
CP-Ser O ₅ ^d	30	2.2	23.3	0.7388
CP-Ser O ₅ ^e	30	2.4	23.1	0.7388
CP-Ser O ₅ +Ca(II) ^d	30	3.3	40.7	0.7388
CP-Ser O ₅ +Ca(II) ^e	30	2.4, 3.5	22.9, 35.9	0.7388

^aAll experiments were conducted at 20 °C. The units of viscosity are in centipoise (cP) (1 Poise = $\text{g cm}^{-1} \text{s}^{-1}$). For experiments without Ca(II), the buffer was 75 mM HEPES, 100 mM NaCl, 30 μM EDTA, pH 7.5. For experiments in the presence of Ca(II), the buffer was 75 mM HEPES, 100 mM NaCl, 600 μM CaCl₂, pH 7.5. For both conditions, $s_{20,w}$ values were adjusted with solvent density (ρ) of 1.0082 g/mL, solvent viscosity (η) of 1.0565 cP and pH 7.5 at 20 °C. The $c(s)$ method was used for fitting the data. All scans that began at the baseline were used in fitting. The units of viscosity are in centipoise (cP) (1 Poise $\text{g cm}^{-1} \text{s}^{-1}$). Sedimentation coefficients are in Svedbergs (1 Svedberg = 100 fs = 1×10^{-13} s). ^c Data obtained using the second preparation of protein. ^b Data obtained using protein oxidized with 50 mM H₂O₂ for 2.5 h. ^c Data obtained using protein oxidized with 50 mM H₂O₂ for 5 h. ^d Data obtained using protein oxidized with 50 mM H₂O₂ for 6 h. ^e Data obtained with protein oxidized for 75 mM H₂O₂ for 6.5 h.

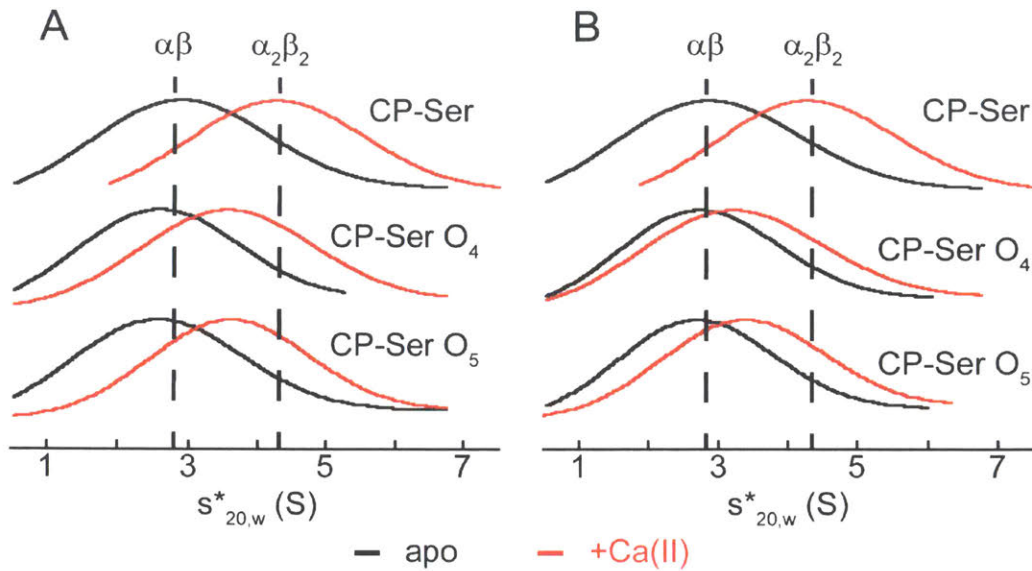


Figure 4.8. DCDT+ analysis of sedimentation velocity experiments with CP-Ser, CP-Ser O₄, CP-Ser O₅. (A) Sedimentation profiles with data from the first preparations of CP-Ser O₄ and CP-Ser O₅. (B) Sedimentation profiles with data from the second preparations of CP-Ser O₄ and CP-Ser O₅. Conditions: 75 mM HEPES, 100 mM NaCl, 30 μ M protein, ± 30 μ M EDTA, ± 1.5 mM Ca(II), 20 °C. Sedimentation coefficients and fitting details can be found in Table 4.7.

Table 4.7. Calculated sedimentation coefficients and molecular weights using DCDT+.^a

Protein	Concentration (μM)	$s_{20,w}$ (S)	D (F)	MW (kDa)	Partial Specific Volume (mL/g)
CP-Ser	30	2.6	12.5	18.9	0.7388
CP-Ser+Ca(II)	30	4.0	9.1	41.2	0.7388
CP-Ser O ₄ ^b	30	2.3	10.6	20.4	0.7388
CP-Ser O ₄ ^c	30	2.5	10.9	21.0	0.7388
CP-Ser O ₄ +Ca(II) ^b	30	3.3	11.0	28	0.7388
CP-Ser O ₄ +Ca(II) ^c	30	2.9	13.8	19.6	0.7388
CP-Ser O ₅ ^d	30	2.3	10.0	21.3	0.7388
CP-Ser O ₅ ^e	30	2.4	10.3	22.1	0.7388
CP-Ser O ₅ +Ca(II) ^d	30	3.4	9.0	35.0	0.7388
CP-Ser O ₅ +Ca(II) ^e	30	3.1	12.1	23.9	0.7388

^aAll experiments were conducted at 20 °C. The units of viscosity are in centipoise (cP) (1 Poise = $\text{g cm}^{-1} \text{s}^{-1}$). Sedimentation coefficients are in Svedbergs (1 Svedberg = 100 fs = 1×10^{-13} s). Diffusion coefficients correspond to the best-fit molecular mass in Fick units (1 Fick = $1 \times 10^{-7} \text{cm}^2/\text{s}$). The dc/dt method was used to fit all data. Between 10 and 12 scans were used for fitting. The first and last scans used ranged from the 19th to the 47th. The peak broadening limit was always greater than 80 kDa. For experiments without Ca(II), the buffer was 75 mM HEPES, 100 mM NaCl, 30 μM EDTA, pH 7.5. For experiments in the presence of Ca(II), the buffer was 75 mM HEPES, 100 mM NaCl, 600 μM CaCl₂, pH 7.5. For both conditions $s_{20,w}$ values were adjusted with solvent density (ρ) of 1.0082 g/mL, solvent viscosity (η) of 1.0565 cP and pH 7.5 at 20 °C. ^bData obtained using protein oxidized with 50 mM H₂O₂ for 2.5 h. ^cData obtained using protein oxidized with 50 mM H₂O₂ for 5 h. ^dData obtained using protein oxidized with 50 mM H₂O₂ for 6 h. ^eData obtained with protein oxidized for 75 mM H₂O₂ for 6.5 h.

4.4.7. CP-Ser Retains Antimicrobial Activity after Methionine Oxidation

To evaluate the effect of methionine oxidation on the antimicrobial activity (AMA) of CP, we performed AMA assays against *Escherichia coli* 25922 and *Staphylococcus aureus* 25923 using CP-Ser, CP-Ser O₄ and CP-Ser O₅ (Figure 4.9). The assays were performed in Tris:TSB medium supplemented with 2 mM Ca(II) to mimic the extracellular Ca(II) concentration. Under these growth conditions, CP-Ser and the oxidized species displayed concentration-dependent growth inhibition of both bacterial species. A comparison of CP-Ser to CP-Ser O₄ and CP-Ser O₅ indicates that methionine oxidation caused some attenuation of antibacterial activity. For *E. coli*, this trend is most evident at 250 µg/mL of protein where CP-Ser completely inhibited growth and CP-Ser O₄ and CP-Ser O₅ inhibited growth to a lesser degree. For *S. aureus*, CP-Ser O₄ and O₅ were less active than CP-Ser at 250 and 500 µg/mL. Nevertheless, *ex vivo* analyses of human fluids has indicated that CP concentrations can reach >1 mg/mL at infection sites,⁷ and both CP-Ser O₄ and O₅ fully inhibit bacterial growth at these concentrations. We note that our finding that methionine oxidation does not abolish the activity of CP refutes conclusions from prior work where oxidation of (A8)M1 was reported to abolish the antimicrobial activity of CP.²⁹ This study used hypochlorous acid as the oxidant, which likely oxidized other sites of the protein as well.

4.4.8. Oxidized CP-Ser Binds Transition Metals with High Affinity

To provide an initial evaluation of the metal-withholding capabilities of oxidized CP-Ser, we compared the abilities of CP-Ser, CP-Ser O₄, and CP-Ser O₅ to compete with the Ca(II)-insensitive fluorescent metal-ion sensor Zinpyr-1 (ZP1)⁴⁶ for Mn(II), Fe(II), Ni(II), and Zn(II) (Figure 4.10). Under conditions of excess Ca(II) ions, CP-Ser, CP-Ser O₄ and CP-Ser O₅ outcompeted ZP1 for these four transition metal ions. Although these results do not rule out the possibility that methionine oxidation perturbs the binding affinities of CP for transition metal ions, these results demonstrate that, in the presence of Ca(II), CP-

Ser O₄ and CP-Ser O₅ coordinate transition metals with sufficiently high affinity to outcompete ZP1. The ability of CP-Ser O₄ and CP-Ser O₅ to chelate transition metals with high affinity is consistent with the observed growth inhibitory activity (Figure 4.9).

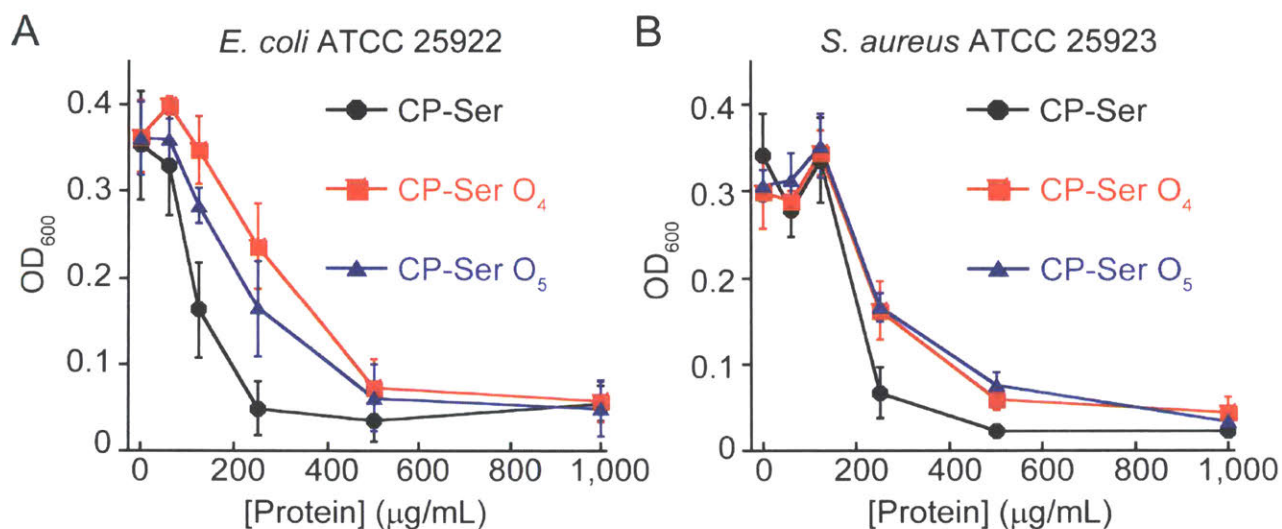


Figure 4.9. AMA assays with CP-Ser, CP-Ser O₄ and CP-Ser O₅ against (A) *E. coli* and (B) *S. aureus*. OD₆₀₀ was recorded after 20 h (mean ± SEM, *n*=3).

4.4.9 Oxidized CP-Ser is Protease Sensitive

In prior work, we observed that a Ca(II)-bound tetramer-deficient variant of CP was more easily degraded by host proteases than Ca(II)-bound CP-Ser.¹³ We therefore questioned whether methionine oxidation enhances the protease susceptibility of CP-Ser and performed protease digestion assays with CP-Ser, CP-Ser O₄, and CP-Ser O₅ using trypsin, human neutrophil elastase (HNE), chymotrypsin, and proteinase K. These assays were performed in the presence of excess Ca(II) or in the presence of both excess Ca(II) and one equivalent of Mn(II) (Figures 4.11, 4.12, and A2.25-A2.27). The reactions were analyzed by HPLC using a gradient that separated S100A8 (37.9 min), S100A9 (39.4 min, S100A8+O (37.3 min), S100A9+3O (37.8 min), and S100A9+4O (36.1 min). With

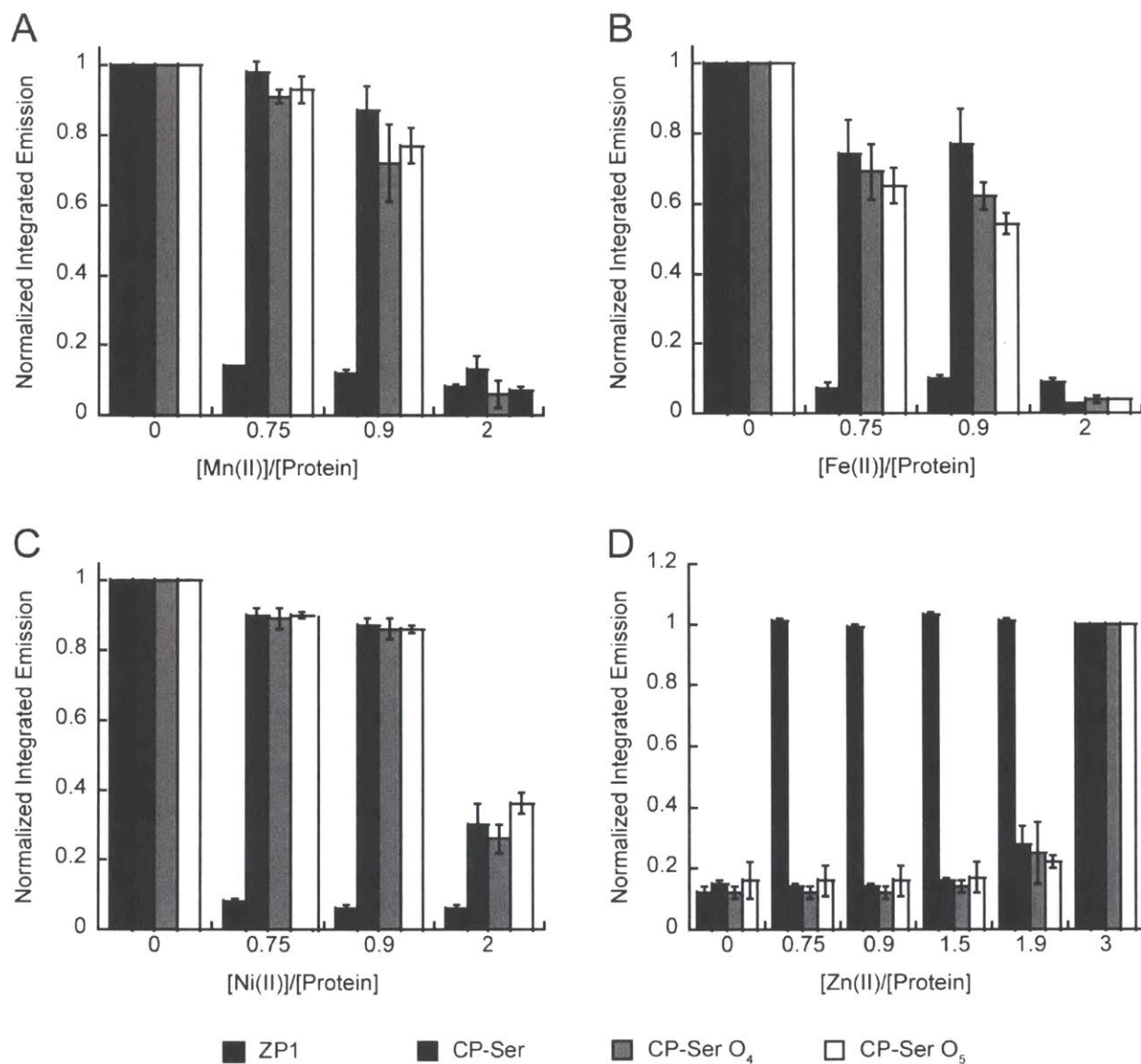


Figure 4.10. Competition between ZP1 and CP-Ser, CP-Ser O₄, and CP-Ser O₅ for (A) Mn(II), (B) Fe(II), (C) Ni(II), (D) and Zn(II) in the presence of Ca(II). Excitation was provided at 490 nm, and the emission spectra were integrated from 500 to 650 nm and normalized with respect to apo ZP1 emission for the Mn(II), Fe(II), and Ni(II) experiments (mean \pm SDM, $n=3$). For the Zn(II) experiment, peak area was integrated with respect to emission after adding 12 μ M Zn(II) (mean \pm SDM, $n=3$). Conditions: 75 mM HEPES, 100 mM NaCl, pH 7.5, 4 μ M CP, 200 μ M Ca(II), 1 μ M ZP1, 25 $^{\circ}$ C.

this gradient, doubling of the oxidized S100A9 peaks occurred. Although the precise origin of the peak doubling is unknown, the phenomenon may arise from a mixture of MetO diastereomers and/or MetO regioisomers.

In agreement with prior work,¹³ inhibiting Ca(II)-induced tetramerization resulted in accelerated proteolysis of CP-Ser (Figures 4.11A, 4.12, and A2.25-A2.27). In the presence of trypsin and excess Ca(II), we did not observe cleavage of CP-Ser, whereas CP-Ser O₄ and CP-Ser O₅ were nearly quantitatively degraded after 3 h (Figure 4.11A). In the presence of chymotrypsin and Ca(II) ions, CP-Ser exhibited slow cleavage of the S100A9 tail while CP-Ser O₄ and CP-Ser O₅ were cleaved to peptides (Figure A2.25). In prior work, we did not compare the protease stability of the CP heterodimer and -tetramer against proteinase K; however, we demonstrated that proteinase K cleaves after (A8)E89 and (A9)H104 in the presence of excess Ca(II).¹² In this work, S100A8+O displayed a peak shift consistent with cleavage after E89 within 30 min of proteinase K (Figure A2.27). At later times in the reaction, the CP-Ser O₄ and CP-Ser O₅ subunits were proteolyzed to peptides, whereas the truncated CP-Ser subunits persisted (Figure A2.27). Although all of the proteases displayed greater activity against CP-Ser O₄ and CP-Ser O₅ than CP-Ser in the presence of Ca(II), HNE degraded the oxidized proteins much more slowly than the other proteases (Figure 4.12). Additionally, HNE was the only protease for which we observed a marked difference in the degradation rate between S100A9+3O and S100A9+4O (Figures 4.12, A2.27, and A2.28). We reasoned that a greater proportion of S100A9+4O will have the (A9)MetO81 modification, leading to more of the protein in the dimer state and a concomitant increase in degradation. When we performed the same experiments with 1 equivalent of Mn(II), we observed no degradation of CP-Ser, CP-Ser O₄, or CP-Ser O₅ (Figures 4.11B and A2.25-A2.27). Under conditions with Mn(II), unmodified and oxidized CP-Ser tetramerize; therefore, we attribute the recovery of protease stability to Mn(II)-induced tetramerization.

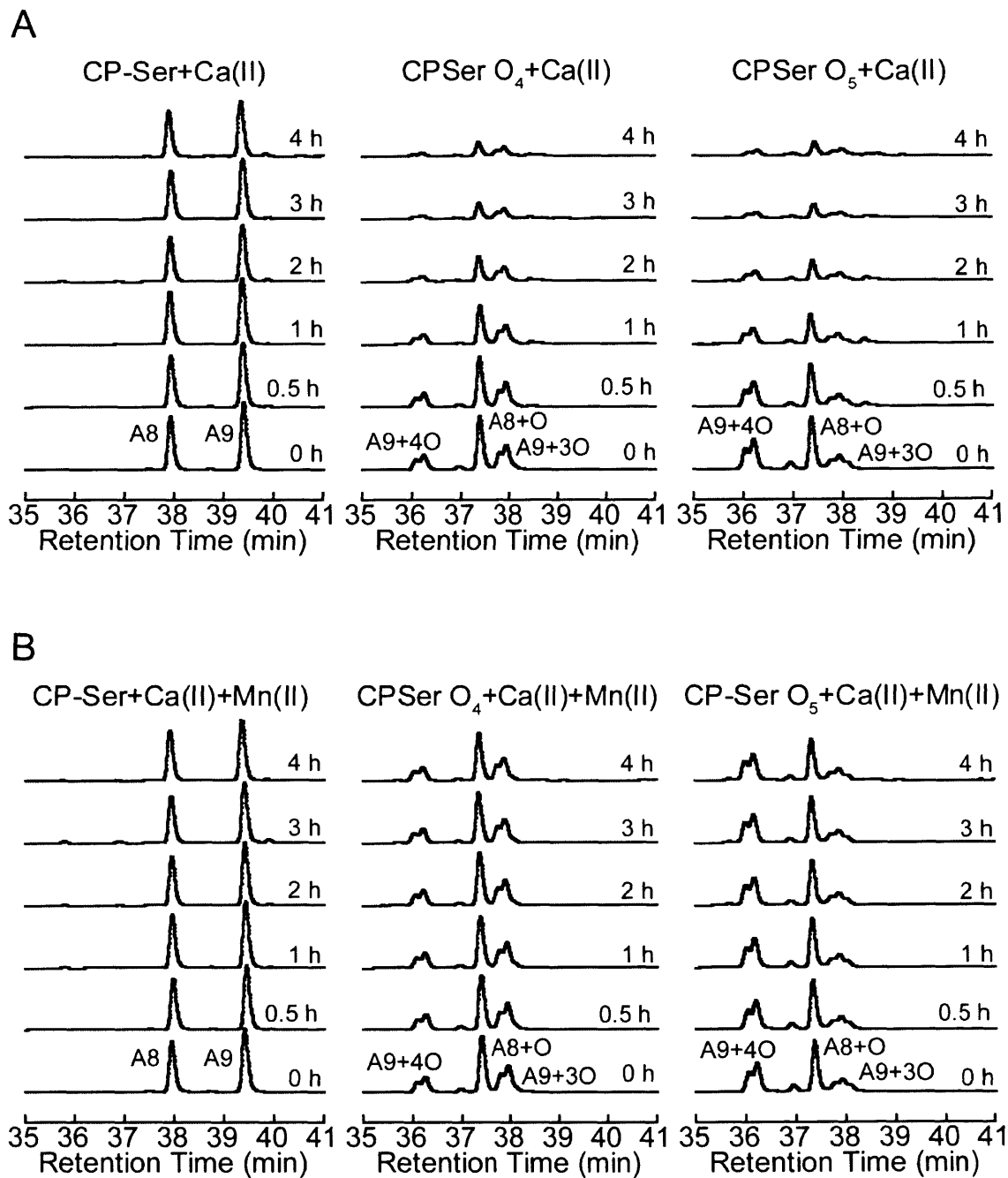


Figure 4.11. Representative HPLC traces from trypsin digestions of CP-Ser, CP-Ser O₄, and CP-Ser O₅ under (A) +Ca(II) and (B) +Ca(II)+Mn(II). Conditions: 75 mM HEPES, 100 mM NaCl, 1.5 mM CaCl₂, ±30 μM MnCl₂, pH 7.5, 30 μM CP, 0.45 μM trypsin at 37 °C.

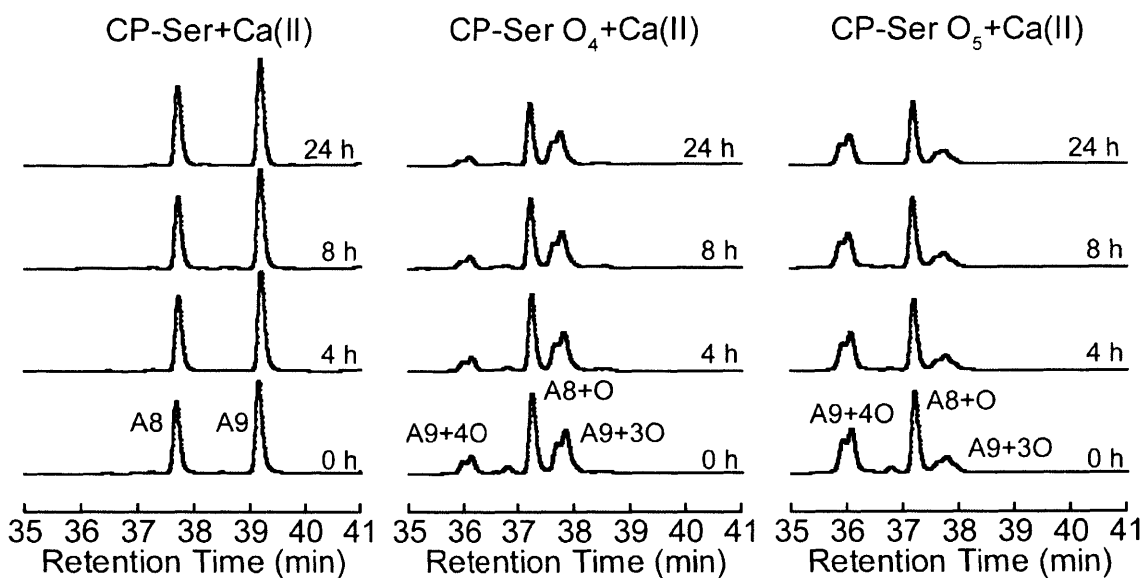


Figure 4.12. Representative HPLC chromatograms from HNE digestions of CP-Ser, CP-Ser O₄, and CP-Ser O₅ in the presence of Ca(II). Conditions: 75 mM HEPES, 100 mM NaCl, 1.5 mM CaCl₂, pH 7.5, 30 μM CP, 1 μM HNE at 37 °C.

4.4.10 Oxidation of CP Yields Disulfide-Linked Oligomers

CP contains two Cys residues, which are located at position 42 of S100A8 and position 3 of S100A9. Similar to methionine, Cys residues are susceptible to oxidation by H₂O₂.⁴⁸ Thus, our studies with CP-Ser did not take the possibility of H₂O₂-mediated oxidation of (A8)C42 or (A9)C3 into account. With understanding of the consequences of methionine oxidation in CP-Ser in hand, we shifted our focus to studying the more complex native protein.

We began by examining whether treating CP with a relatively low concentration of H₂O₂ (100 μM) resulted in disulfide-bond formation in the absence or presence of excess Ca(II) ions by non-reducing SDS-PAGE and western blot (Figure 4.13). Under our conditions, we observed minimal formation of disulfide bonds when CP was incubated without H₂O₂ (Figure 4.13). In the absence of Ca(II), we observed bands consistent with disulfide-linked S100A8–S100A9 and S100A9–S100A9 species at the 1-h time point (Figure 4.13). Over time, the band attributed to the S100A9–S100A9 species became

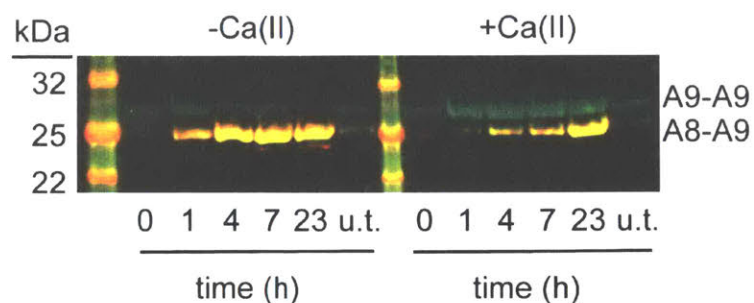


Figure 4.13. A non-reducing western blot of 30 μM CP treated with 100 μM H_2O_2 or untreated (u.t.) in the presence and absence of 1.5 mM $\text{Ca}(\text{II})$. S100A8 was stained red (mouse anti-S100A8, 680 CW dye), S100A9 was stained green (goat anti-S100A9, 800CW dye), and the overlap appeared stained yellow. The ladder proteins were visualized by a covalently linked dye that fluoresced during scanning. Reaction buffer: 75 mM HEPES, 100 mM NaCl, pH 7.5.

less prominent and the band assigned to a disulfide-linked S100A8–S100A9 species became the major product. We also note that a weak band assigned to a disulfide-linked S100A8–S100A8 species appeared at 7 h and 23 h (Figure 4.13). In the presence of excess $\text{Ca}(\text{II})$, the disulfide reactivity changed (Figure 4.13). At the 1-h time point, the S100A9–S100A9 species was dominant and negligible S100A8–S100A9 species was detected. Over time, the S100A9–S100A9 species became less abundant, while the amount of the S100A8–S100A9 species increased over the 23-h time course. Moreover, in the presence of $\text{Ca}(\text{II})$, no band attributed to a disulfide-linked S100A8–S100A8 species was detected. We reason that the different disulfide reactivity likely results from $\text{Ca}(\text{II})$ -induced structural changes that impact the accessibility of (A8)C42, which is located in the linker region between the N- and C-terminal EF-hands. In contrast, (A9)C3 is fully solvent exposed. Moreover, the conversion of S100A9–S100A9 species to the S100A8–S100A9 species at later time points indicates that disulfide bonds involving (A8)C42 are more stable. We also performed reactions with a CP variant containing a (A9)C3S mutation to mimic the truncated CP species observed in the human samples lacking (A9)C3. Non-reducing SDS-PAGE revealed no evidence for disulfide bond formation

following treatment of the CP(C3S) variant with 100 μM H_2O_2 (Figure 4.14). Because oxidation of CP *in vivo* is presumed to occur in the extracellular space, we further characterized CP after treatment with 100 μM H_2O_2 for 23 h in the presence of Ca(II), and we name this protein dsl-CP.

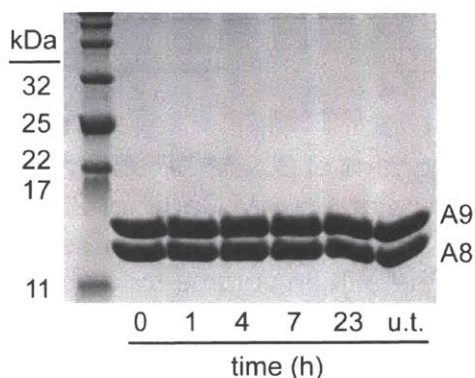


Figure 4.14. SDS-PAGE gel (Tris-HCl glycine, 15% acrylamide) of CP(C3S) after before and after treatment with 100 μM H_2O_2 . Reaction conditions: 75 mM HEPES, 100 mM NaCl, 30 μM CP, 1.5 mM Ca(II), 100 μM H_2O_2 , pH 7.5, 37 °C. The ladder was P7712S from New England Biolabs.

To further decipher the speciation of CP after exposure to 100 μM H_2O_2 for 23 h in the presence of excess Ca(II), we treated dsl-CP with TCEP to reduce the disulfide bonds prior to mass spectrometry. The reaction product displayed the expected masses for unmodified S100A8 and S100A9, and no peaks that corresponded to species containing additional oxygen atoms were found (Figure A2.29). This analysis indicated that 100 μM H_2O_2 is insufficient to oxidize the methionine residues of CP under our reaction conditions. For the SEC analyses, we treated aliquots of the sample from the 23-h time point in three different ways such that the effects of Ca(II) ions and disulfide bond formation on protein oligomerization could be assessed (Figure 4.15A). The first protein aliquot was untreated and eluted with a mobile phase that contained 1.5 mM Ca(II). The second protein aliquot

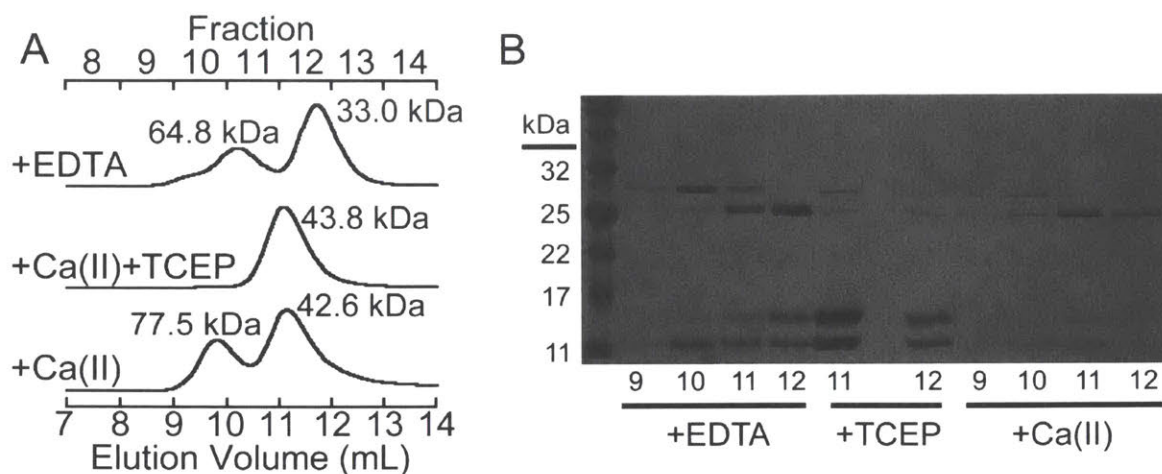


Figure 4.15. (A) SEC chromatograms of 30 μM CP after a disulfide-bond forming reaction with 100 μM H_2O_2 in the presence of 1.5 mM $\text{Ca}(\text{II})$ for 23 h at 37 $^\circ\text{C}$. Prior to elution, the protein was treated with 2 mM EDTA, 2 mM TCEP, or left untreated. A 500 μL injection loop was employed; therefore, the elution volume for a given molecular weight is different than prior SEC experiments. (B) Nonreducing SDS-PAGE of the fractions collected from the SEC runs. We note that the protein reduced with TCEP contained a detectable disulfide-linked protein, indicating that the reduction was not quantitative. The S100A8–S100A9, and S100A9–S100A9 disulfide linked species had apparent molecular weights of 25 kDa and 30 kDa, respectively.

was treated with 2 mM EDTA to remove bound $\text{Ca}(\text{II})$ ions from the protein and eluted with a mobile phase that did not contain added $\text{Ca}(\text{II})$. The third protein aliquot was treated with 2 mM TCEP to reduce the disulfide bonds, and this sample eluted with a mobile phase that contained excess $\text{Ca}(\text{II})$ ions. When dsl-CP was eluted in the presence of excess $\text{Ca}(\text{II})$ ions, two peaks with elution volumes of 10.2 mL (77.5 kDa) and 11.1 mL (42.6 kDa) were observed. In the presence of EDTA and no $\text{Ca}(\text{II})$ ions added to the mobile phase, dsl-CP eluted as two major species with elution volumes of 9.8 mL (64.8 kDa) and 11.7 mL (33.0 kDa). Reduction of dsl-CP with TCEP in the presence of $\text{Ca}(\text{II})$ caused the protein to elute as a single peak indicative of a heterotetramer (11.1 mL, 43.8 kDa), demonstrating that the effects of disulfide bond formation could be reversed via reduction. We note that the larger oligomers observed in this experiment are within the linear range of the column; therefore, the calculated molecular weights should be

reasonable estimates, indicating that the disulfide-forming reaction conditions did not produce aggregates.

SDS-PAGE analysis of the fractions obtained from SEC revealed that, regardless of the sample treatment, all fractions contained S100A8 and S100A9 subunits (Figure 4.15B), suggesting that CP retained native-like noncovalent heterooligomers after the formation of disulfide bonds. Moreover, all of the fractions contained the disulfide-linked S100A8–S100A9 species, and the fractions corresponding to the relatively low-molecular-weight peaks (11.1 mL, 42.6 kDa, +Ca(II); 11.7 mL, 33.0 kDa, +EDTA) exclusively contained the disulfide-linked S100A8–S100A9 species. The 11.7 mL (33.0 kDa) peak in the +EDTA sample was close to the apparent molecular weight of the CP heterodimer (34.9 kDa), and in the presence of Ca(II) in the mobile phase this species appeared to shift to an apparent molecular weight comparable to the CP heterotetramer (45.9 kDa). We reason that, in the absence of Ca(II), this protein was dimeric CP and contained an intramolecular disulfide bond, which would explain why the S100A8–S100A9 disulfide linkage is more prevalent in the lower molecular weight fractions. Examination of CP-Ser crystal structures revealed that the N-terminus of S100A9 is in close proximity to (A8)C42, indicating that formation of an (A9)C3–(A8)C42 “intradimer” disulfide bond is reasonable. The molecular identity of the 64.8-kDa peak in the sample that was treated with EDTA is unclear; however, a trimer of $\alpha\beta$ heterodimers or a larger oligomer are possible species. The 64.8 kDa species shifted to 77.5 kDa when Ca(II) ions were present in the mobile phase, indicating that this species binds Ca(II) ions, causing formation of a higher-order oligomer. In conclusion, we established that (i) all species in the dsl-CP displayed Ca(II)-induced oligomerization (ii) the major species in the dsl-CP mixture was the CP heterotetramer that contained at least one (A9)C3–(A8)C42 intradimer disulfide bond, and (iii) the minor product was a molecules of CP that were disulfide linked.

Next, we sought to prepare and study dsl-CP species that contained oxidized methionine residues. We developed a two-step procedure to obtain these proteins. First, dsl-CP was prepared in the presence of excess Ca(II) ions using the disulfide-bond formation reaction described above (100 μ M H₂O₂, 23 h, 37 °C). In the second step, dsl-CP was treated with 100 mM H₂O₂ at 37 °C for up to 23 h. Mass spectrometry of the reaction mixture at the 7-h time point demonstrated that S100A8+O, S100A9+3O and S100A9+4O were the predominant species (Figure A2.28). SDS-PAGE of reaction aliquots taken at varying time points during the 23-h reaction period revealed a gradual loss of the disulfide-linked S100A9–S100A9 species and increase in the disulfide-linked S100A8–S100A8 species (Figure A2.30). We also observed a small increase in the apparent molecular weight of all the bands after Met oxidation, which is a known phenomenon.⁵³ This analysis indicated the disulfide bonds were not cleaved to cysteic acid under the reaction conditions. We concluded that treating dsl-CP for 7 h with 100 mM H₂O₂ afforded the sufficient Met oxidation to resemble CP-Ser O₄ and CP-Ser O₅ while minimally perturbing the disulfide bonds, and we named this reaction product MetO-dsl-CP.

4.4.11. *dsl-CP is Protease Sensitive*

We assayed the susceptibility of dsl-CP, obtained from H₂O₂ oxidation in the presence of Ca(II) ions, to degradation by trypsin. We quenched reaction aliquots in the absence and presence of TCEP at varying time points and analyzed the mixtures by HPLC (Figure 4.16). At the 0 h time point, the chromatogram of the TCEP-treated sample exhibited two major peaks corresponding to S100A8 and S100A9, and the peak intensities decreased over time, indicating trypsin-catalyzed degradation of each subunit (Figure 4.16B). The chromatogram of the sample that was not treated with a reductant was more complex and exhibited three major peaks along with a minor peak (Figure

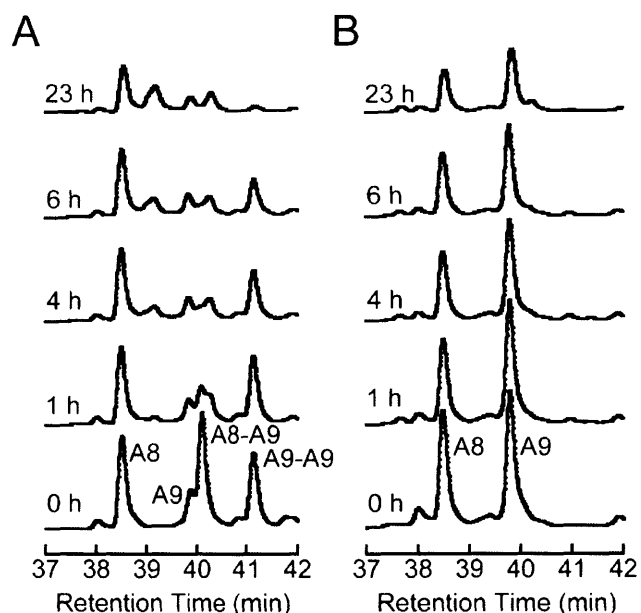


Figure 4.16. Representative HPLC chromatograms of dsl-CP digested by trypsin. Time points were quenched in the (A) absence and (B) presence of TCEP. Conditions: 75 mM HEPES, 100 mM NaCl, 1.5 mM CaCl₂, 30 μM CP, 0.45 μM trypsin, 37 °C.

4.16A). One of the major peaks (38.5 min) was assigned to the S100A8 monomer, and the identities of the other two major peaks were determined by mass spectrometry (Figure 4.16A, Table 4.4). The 40.0 min peak was identified as the disulfide-linked S100A8–S100A9 dimer and the 41.1 min peak was identified as the disulfide-linked S100A9–S100A9 dimer. The minor peak (39.9 min) was assigned to the S100A9 monomer. Analysis of the samples obtained at later time points revealed several points about the trypsin susceptibility of these species: (i) that CP containing an intradimer disulfide bond was almost completely degraded by trypsin after only 1 h, (ii) the S100A9–S100A9 dimer was almost completely degraded after 23 h, and (iii) the CP subunits that had not formed disulfide bonds were digested to a lesser extent than the disulfide-linked protein (Figure 4.16A). From these results, we concluded that disulfide bond formation between CP subunits sensitizes CP to proteolysis by trypsin, and that disulfides that involve (A8)C42 are particularly destabilizing. We find this observation to be particularly intriguing given

that disulfide bond formation typically stabilizes proteins and provides additional protection against proteolysis.

4.4.12. *dsl-CP and MetO-dsl-CP are Degraded by Trypsin at Comparable Rates*

With the knowledge methionine oxidation sensitized CP to proteolysis by weakening noncovalent oligomerization, we sought to compare the stability of *dsl-CP* and *MetO-dsl-CP*. We performed trypsin degradation assays, and at each time point, quenched samples in the absence and presence of TCEP. Without TCEP reduction, the HPLC trace of *MetO-dsl-CP* exhibited a broad peak, and we were unable to resolve individual species (Figure 4.17A). In contrast, treatment of the protein with TCEP during the quench gave rise to a chromatogram reminiscent of CP-Ser O₄ and CP-Ser O₅ (Figure 4.17B). We assigned the peaks at 36.5 min, 37.2 min, and 37.7 min to S100A9+4O, S100A9+3O, and S100A8+O by LC-MS, respectively. The fraction containing S100A9+3O also contained a detectable amount of S100A8+2O.

We anticipated that *MetO-dsl-CP* would be degraded more quickly than *dsl-CP* given our observations with CP-Ser O₄ and CP-Ser O₅. Trypsin hydrolyzed *MetO-dsl-CP*, as expected (Figure 4.17). However, comparison of the degradation of *dsl-CP* and *MetO-dsl-CP* revealed that methionine oxidation did not result in a significant increase in digestion (Figure 4.17C). We also noted that rapid degradation of *dsl-CP* and *MetO-dsl-CP* occurred during the first hour of digestion, and then markedly slowed.

4.5. Discussion

This work demonstrates that post-translational oxidation of CP has structural and functional consequences. In particular, methionine oxidation and disulfide-bond formation alters the stability of CP to proteases. This work also highlights the complex speciation of CP in the biological milieu. Prior studies have considered speciation of CP primarily from

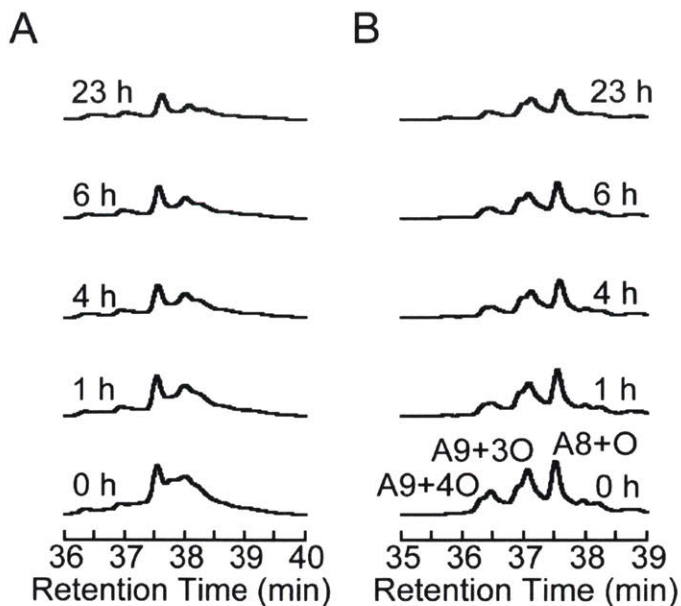


Figure 4.17. Representative HPLC chromatograms of MetO-dsl-CP digested by trypsin. Time points were quenched in the (A) absence and (B) presence of TCEP. (C) A plot of the total area in the –TCEP dsl-CP and MetO-dsl-CP chromatograms for the retention windows shown as a function of digestion time. The areas were normalized to the area of the 0 h chromatograms (mean \pm SDM, $n=3$). Conditions: 75 mM HEPES, 100 mM NaCl, 1.5 mM CaCl₂, 30 μ M CP, 0.45 μ M trypsin, 37 $^{\circ}$ C.

the standpoint of the metalation,^{9,11,25,26,54} where each heterodimer unit contains six different sites for coordinating Ca(II) ions (four EF-hand domains) and two sites for transition metals (His₃Asp and Hi₆ sites). When one considers the potential diversity of CP arising from combinations of metalation and post-translational modifications, it becomes clear that the CP present at an infection site is likely highly heterogeneous.

In agreement with prior studies that reported methionine-oxidized CP subunits in samples from mice and humans,²⁹⁻³¹ we detected oxidized CP subunits in samples of human nasal mucus and human pus. Moreover, by using ¹⁵N-labeled CP-Ser as an internal standard to report on adventitious methionine oxidation, we obtained compelling support for the formation and relevance of methionine-oxidized CP *in vivo*. CP is an abundant neutrophil protein that is released into the extracellular space, and methionine oxidation of CP likely results from the neutrophil oxidative burst. This process occurs after neutrophil activation, and leads to production of ROS including O₂⁻, H₂O₂ and HOCl.³² Indeed, neutrophil activation increases methionine oxidation of neutrophil proteins and surrounding tissues,^{34,55} and α₂-proteinase is inactivated by methionine oxidation caused by neutrophil-derived ROS *in vivo*.^{33,56} Under certain circumstances, microbes may also cause oxidation of CP as an immune-evasion strategy. *Helicobacter pylori* can induce ROS generation in epithelial cells and macrophages,^{57,58} which could modify CP and result in its premature degradation.

In this study, we employed H₂O₂ to oxidize CP and CP-Ser because it is more selective for Met and Cys oxidation than other oxidants.⁴⁸ We recognize that the time and H₂O₂ concentrations required to oxidize CP in our experiments raise questions of kinetic competence *in vivo*. Indeed, an estimate of H₂O₂ in a neutrophil phagosome is between 1 to 4 μM, far below the concentrations we employed to obtain oxidized CP(-Ser) species.⁵⁹ It is important to note that the primary oxidant during the neutrophil oxidative burst is HOCl produced by myeloperoxidase. Although H₂O₂ is thermodynamically a strong oxidant, it is kinetically slow with a rate constant of 6x10⁻³ M⁻¹s⁻¹ for oxidizing Met

to MetO.¹ In contrast, the rate constant for HOCl reacting with Met to form MetO is $3.8 \times 10^7 \text{ M}^{-1}\text{s}^{-1}$.¹ Due to the extremely fast reactivity of HOCl with Met, we reason that this oxidant is responsible for producing the majority of the oxidized methionine residues observed in CP. With the results reported here as a foundation for future work, investigations of the consequences of HOCl and chloramines for the structure and function of CP-Ser and CP are warranted.

Large-scale purification of the CP-Ser O₄ and CP-Ser O₅ species facilitated studies to further understand the effects of Met oxidation on CP. Protease susceptibility assays performed in the presence of excess Ca(II) ions revealed that both CP-Ser O₄ and CP-Ser O₅ were more rapidly degraded by trypsin, chymotrypsin, and proteinase K, which we attribute to the consequences of (A9)M81 oxidation on the dimer-tetramer equilibrium. Crystal structures of the CP heterotetramer show that the side chain of (A9)M81 points directly into the dimer-dimer interface (Figure A2.23). Thus, we expect that conversion of Met to MetO decreases the driving force for tetramerization due to the hydrophilic nature of MetO, which is considerably more hydrophilic than Met. Indeed, MetO was calculated to be approximately as hydrophilic as lysine.⁶⁰ Protease resistance was rescued by addition of one equivalent of Mn(II) to CP-Ser O₄ and CP-Ser O₅, which coordinated to the His₆ site and caused the proteins to tetramerize. Thus, the increased protease resistance conferred by Mn(II) binding results from the metal ion converting CP-Ser O₄ and CP-Ser O₅ to the tetrameric state. This assessment is based on our previously reported observations with tetramer-deficient variants of CP-Ser, which showed that binding of a metal ion to the His₆ site results in tetramerization and overcomes the consequences of single mutations at the tetramer interface that prevent Ca(II)-induced oligomerization.¹³ The protease susceptibility assays also revealed that, in the presence of excess Ca(II) ions, CP-Ser O₄ and CP-Ser O₅ were poor substrates for HNE. It is possible that the low activity of HNE against CP-Ser O₄ and CP-Ser O₅, as well as CP-Ser, reflects a selected trait of CP. HNE and CP are both released by neutrophils, and we

can imagine that that resisting degradation by HNE allows CP to perform its function without being immediately degraded.

Native CP presents a more complex scenario because each full-length subunit contains a single cysteine residue that is susceptible to oxidation. By investigating the consequences of oxidative post-translational modifications to the native protein, we demonstrated that disulfide-bond formation between CP molecules also increased the rate of protease degradation. This effect was especially pronounced for the species containing the S100A8–S100A9 disulfide linkage, but the S100A9–S100A9 disulfide-linked protein was also degraded faster than the unmodified protein. We propose that disulfide bonds involving S100A8 are destabilizing because (A8)C42 is located in the “hinge” region between the N- and C- terminal EF-hands. Considering the reduction potential of the extracellular space and the ROS generated during the neutrophil response, it is reasonable to imagine that CP can form disulfide bonds with other CP molecules as well as other cysteine-containing biomolecules. Along these lines, human S100A7 was found to form high-molecular weight disulfide-linked oligomers in wounds.⁶¹ Amino acid sequence alignment of S100A8 polypeptides from 36 available genomes shows that (A8)C42 is highly conserved (Figure 4.18). This residue is surface exposed in human CP, which is unusual for Cys residues,⁶² it is likely surface exposed in orthologues from other mammals. Thus, it is possible that disulfide bond formation with S100A8 enhances the protease susceptibility of CP in many organisms.

Although we were initially surprised that Met oxidation of dsl-CP did not impart an appreciable increase in the degradation rate, we expect that this modification can influence the lifetime of CP at biological sites. *Ex vivo* analyses of various biological samples,²⁹⁻³¹ including results of the current work, indicate that there is a significant population of S100A9 that lacks the first 5 amino acids and thus the Cys residue at position 3. This truncated S100A9 species cannot form disulfides that afford enhanced

protease susceptibility, and we expect that methionine oxidation may accelerate clearance of CP containing this truncated S100A9 subunit.

Taken together, the investigations of CP and CP-Ser presented in this work afford an extension to the working model of CP. Previously, CP was thought to reside in the extracellular space as the Ca(II)-bound tetramer, with some fraction also coordinated to one or more transition metals ions. We propose a more dynamic picture where methionine oxidation and disulfide bonds modulate the lifetime of CP in this milieu by enhancing the susceptibility of Ca(II)-bound CP to proteolytic degradation. CP is multi-functional, and after its release, the host must attempt to balance its nutrient withholding role against its contributions to proinflammatory signaling. We hypothesize that Met oxidation helps the host achieve balance. Because the concentration of CP at an infection site is expected to exceed the concentration of bioavailable transition metal ions, we expect that the majority of CP exists in the Ca(II)-bound state and is thus susceptible to proteolytic degradation after post-translational oxidation. We reason that recovery of protease stability after binding a metal at the His₆ site is advantageous for the host because it allows it prevents premature release of transition metals. This scenario would allow the host to preferentially degrade excess or “unnecessary” CP while preserving CP that is actively withholding transition metal ions. Removing CP is likely important for preventing it from participating in inflammatory shock and the development of autoreactive CD8⁺ T cells.^{19,20}

Beyond the context CP in the host/microbe interaction and inflammation, this work agrees with previous work on the MetO post-translational modification. Various structural consequences of methionine oxidation have been described. For instance, the presence of MetO can disrupt interactions between protein domains,^{63,64} hinder formation of noncovalent heterocomplexes,^{56,65} and destabilize protein folds.⁶⁶ In addition, the connection between MetO and accelerated proteolysis has precedence. Met oxidation of calmodulin targeted it to the proteasome in an ubiquitin-independent fashion,⁶⁷ and our work demonstrated that Met oxidation of CP accelerated non-targeted proteolysis. Lastly,

the Met/MetO redox couple in the context of ROS have been considered to serve an antioxidant role.^{36,37} The hypothesis is that surface Met residues are oxidized to MetO, which can be reduced to methionine by Msr proteins, thereby protecting critical residues from ROS. Although we agree that Met can play an important sacrificial antioxidant function, our data and those of others also support a regulatory role for Met oxidation.^{63,68} Considering the observation that ROS enable neutrophil proteases to be active in the extracellular space by oxidizing Met to MetO,^{55,56} the necessity for ROS to form neutrophil extracellular traps,⁶⁹ and our finding that MetO modification sensitizes CP to proteolysis argues in favor of ROS and MetO also serving as signals during the immune response.

In closing, the results presented in this work support a model where methionine oxidation and disulfide bond formation promote proteolytic degradation of CP, providing new molecular-level insights into the fate of CP after release into the extracellular space. We propose that the host uses oxidative modification of CP to accelerate its proteolysis. We envision that, by sensitizing CP to proteolysis, the host can dispose of CP in a timely manner to prevent negative outcomes from CP-mediated proinflammatory signaling.

```

D2HJR9 Giant panda -----MLTELESAMNSLIDVYHKYSLEKGNHYHALYRDDLLKLLLETECPRYMKKK----DADTWFKELDVNSDGAINFEEFLILVIKVGVAAHEDIHKE---- 89
AOA2K5C7U2 Ma's night monkey -----MLTDLEKALNSLIDVYHKYSLIKGNYHAIYRDDLLKLLLETECPQYIRKK----SAEAWFKELDVNSDNAINFQEFLILVIKVGVAQAHKESHKE---- 89
P28782 Cow -----MLTDLECAINSLIDVYHKYSLKKGNYHAVYRDDLKQLLETECPKFMKKK----DADTWFKELDINQDGGINFEEFLVLVIKVGLEAHEEIHKE---- 89
E1AHZ7 Water buffalo -----MLTDLESAINSLIDVYHKYSLNQGNYHAVYRDDLLKLLLETECPKFMKKK----DADTWFKELDINQDGGINLEEFVLVLVIKVGVAHHEEIHKE---- 89
F7IHU7 White-tufted-ear marmoset -----MLTDLEKALNSLIDVYHKYSLIKGNYHAIYRDDLLKLLLETECPQYTKKK----SAEAWFKELDINSDNAINFQEFLILVIKVGVAQAHKESHKE---- 89
COLQL0 Dog -----MLTELESAINSLIEVYHKYSLVKGNYHALYRDDLLKLLLETECPQYMKKK----DADTWFKELDVNSDGAINFEEFLILVIKVGVAASHKDIHKE---- 89
AOA2K5R5R0 Cebus imitator -----MLTDLENALNSLIEVYHKYSLIKGNYHSIYRDDLLKLLLETECPAYINKK----SAEAWFKELDINSDNAINFQEFLILVVKVGVAAHKESHKE---- 89
AOA0D9S5P4 Green monkey -----MLTELEKALNSIIDVYHKYSLIKGNYHAIYKDDLLKLLLEAECPQYIRKK----GADAWFKELDINTDGAINFQEFLILVIKMGVAAHKESSHKEGHKE 93
AOA2K5JWV7 Peters' Angolan sabaeus -----MLTDLEKALNSIIDVYHKYSLIKGNYHAIYKDDLLKLLLETECPQYIRKK----GADAWFKELDINTDGAINFQEFLILVIKMGVAAHKESSHKEGHE- 92
AOA1S3F1S6 Ord's kangaroo rat -----MPSDLECALDGVIDVYHRYSLTQGNYSLSYKDDLLKLLAAEVNLLKKNK----DADTWFKVLDVNLGDGAINFQEFLIFVVIKMGVLAHEESHKN---- 89
F6YI13 Horse -----MLTDLENAINSLIDVYHNYSLKGNYHAIYRDDLLKLLLETECPQYLKKK----NADAWFKELDINEDGAVNFQEFLILVVKVGLLAHEDIHKE---- 89
AOA1S2Z01 Hedgehog -----MLTNLEKAINNIIIDIFHKYSLKTGNYSLSYRNDLKSLESECSMYLKEK----NADTWFKELDINSQAINFEEFLILVIKVAIAHAKASHKE---- 89
M3VWD6 Cat -----MLTELETAINCLIDVYHKYSLEKGNHYHALYRDDLLKLLLETECPRYMKKK----DADTWFKELDVNSDGAINFEEFLILVIKVGVAATHEDIHRE---- 89
P05109 Human -----MLTELEKALNSIIDVYHKYSLIKGNFHAVYRDDLLKLLLETECPQYIRKK----GADVWFKELDINTDGAINFQEFLILVIKMGVAAHKESSHKE 93
I3MT07 Striped gopher -----MPTDLEKALDSLVCVHFHKYSLKKGNYHALYRDDLLKMLTTECPHYTKNK----DADTWFKELDVNADNAVNFEEYLVVIKVGVAEAKHLSHKE---- 89
G3TZS9 African elephant -----MLTDLEKALNSLIEVYHKYSLKGNNAHALYRDDFKQLLETEGRRYLRIK----DANAWFKELDVNSDNAINFEEFLILVVKMGVIAHEDIHKE---- 89
F6QJD8 Rhesus macaque -----MLTDLEKALNSIIDVYHKYSLIKGNYHAIYKDDLLKLLLETECPYIRKK----GADAWFKELDINTDGAINFQEFLILVIKMGVAAHKESSHKEHDKE 93
AOA2K6A0D5 Drill -----MLTDLEKALNSIIDVYHKYSLIKGNYHAIYKDDLLKLLLETECPQYIRKK----GADAWFKELDINTDGAINFQEFLILVIKMGVAAHKESSHKEHDRE 93
AOA1U7R3M2 Golden hamster -----MLSELEKALENIVNVYHQYSGTKGNHHALYRDDLLKLLTTECPFIQKK----NAETLFEKELDVNQDNAVNFEEFLVLMIKVGLAAHEDSHKGC--- 90
P27005 Mouse -----MPSELEKALNSLIDVYHNYSNIQGNHHALYKNDFKMVTTECPQFVQNI----NIENLFEKELDINSDNAINFEEFLAMVIKVGVAASHKESHKE---- 89
M3YAE9 Ferret -----MLTELESAMNSLIDVYHKYSLEKGNHYHALYRDDLLKLLLETECPRFLLKKK----DADTWFKELDINSDGAINFEEFLILVIKVGVAASHEDIHRE---- 89
G1NYX9 Little brown bat -----MLTEMENTLNNFIEIYHKYSLIQGSDHLYGNDFKLLEDECPHFLQNK----NAATWFKELDINRDNAINFQEFLILVIKVGVAHHEEIHKE---- 89
AOA2I3HUD2 Gibbon -----MLTELEKALNSIIDVYHKYSLIKGNYHAVYRDDLLKLLLETECPQYIRKK----GADAWFKELDINTDGAINFQEFLILVVKMGVAAHKKSHESHKE 93
G1SXG6 Rabbit -----MPTDLENSLNSIISVYHKYSLKGNHYHALYRDDLLKLLLETECPQYTKKK----DADTWFKELDINSDGAINFQEFLILVIKVGVAHEDIHKA---- 89
H0WH36 Garnett's greater bushbaby -----MPTDLECALNSVIDVYHKYSLRKGNYHAIYRDDLLKSLLETECPQYMKKK----DANTLFEKELDINSDGAINFQEFLVLMIKVGVAAHEDSHRE---- 89
W5NQK9 Sheep RWGKSLDNMLTDLESAINSLIDVYHNYSLKGNHYHAVYRDDLLKRLLETECPKFLKKK----DADTWFKELDINQDGGINFEEFLVLVIKVGGLAAHEDIHKE---- 97
H2Q028 Chimpanzee -----MLTELEKALNSIIDVYHKYSLIKGNFHAVYRDDLLKLLLETECPQYIRKK----GADVWFKELDINTDGAINFQEFLILVIKMGVAAHKKSHESHKE 93
AOA2I3MWT7 Olive baboon -----MLTDLEKALNSIIDVYHKYSLIKGNYHAIYKDDLLKLLLETECPQYIRKK----GADAWFKELDINTDGAINFQEFLILVIKMGVAAHKESSHKEHDKE 93
H2N5P6 Sumatran orangutan -----MLTELEKALNSIIEVYHKYSLIKGNYHAVYRDDLLKLLLETECPYIRKK----GADAWFKELDINTDGAINFQEFLILVIKMGVAAHKKSHEEGHKE 93
AOA2K6EG83 Coquerel's sifaka -----MLTDLENALDSFIDVYHKYSLRQGNHAIYIDDLKQLLETECPQYMKKK----DANTWFKELDINSDGAINFQEFLMFVVIKGLVAAHEDIHKV---- 89
P50115 Rat -----MATELEKALSNVIEVYHNYSGIKGNHHALYRDDFRKMTTECPQFVQNK----NTESLFEKELDVNSDNAINFEEFLVLVIRVGVAHAKESHKE---- 89
AOA2K6QU61 Snub-nosed monkey -----MLTDLEKALNSIIDVYHKYSLIKGNYHAVYKDDLLKLLLETECPQYIRKK----GADAWFKELDINTDGAINFQEFLILVIKMGVAAHKESSHKEGHKE 93
AOA2K6SS78 Bolivian squirrel monkey -----MPTDLEKALNSLIDVYHKYSLIKGNYHAIYRDDLLKLLLETECPYINKK----SAEAWFKELDINSDNAINFQEFLILVIKVGVAHKESSHKE---- 89
G3W262 Tasmanian devil -----MVTKLEGAVNCLVTVFHKYSLASGHYHTLSKDKFRKLLLETEIPEVLKPKPKPTVEKILKEVDSNKGMINFEEFLFLATRLLLVDAHATHE---- 92
C3S7K5 Pig -----MLTDLESAINSLIEVYHKYSLEKGNHYHAIYADDLLKRLLETECPRYMKKK----DAETWFKELDINKDGAINFEEFLILVIKVGVAHEDIHKE---- 89
AOA1U7TQ23 Philippine tarsier -----MPTDLEKALNSVIDIYHKYSLIKGNYHAIYKDDLLKLLLETECPQYTKKK----DAESWFKELDVNTDGAINFQEFLIFVVKIGVAAHAKESHKE---- 89

```

Figure 4.18. Alignment of all protein sequences corresponding to genes annotated as S100A8 from the Uniprot database. Only one organism from a given genus is shown. If there were two sequences for a single organism, then the shorter sequence was used. The excluded and included S100A8 genes from the same organism had the same amino acid at position 42. This alignment demonstrates that Cys42 (shown in red) is highly conserved. Ord's kangaroo rat, the African elephant, and the Tasmanian devil encode Val, Gly, and Ile at position 42, respectively.

4.6. Acknowledgements

We thank the NIH (R01GM118695) and the MIT Department of Chemistry for financial support. The MIT Biophysical Instrumentation Facility for the Study of Complex Macromolecular Systems is supported by NSF grant 0070319. We thank Prof. B. L. Pentelute for generously providing access to mass spectrometry instrumentation, Dr. A. Vinogradov for his assistance with mass spectrometry, and Ms. A. Nocera and Dr. B. Bleier for technical assistance with the human nasal mucus samples.

4.7. References

1. Davies, M. J., The oxidative environment and protein damage. *Biochim. Biophys. Acta* **2005**, *1703* (2), 93-109.
2. Steinbakk, M.; Naessandresen, C. F.; Lingaas, E.; Dale, I.; Brandtzaeg, P.; Fagerhol, M. K., Antimicrobial actions of calcium-binding leukocyte L1 protein, calprotectin. *Lancet* **1990**, *336* (8718), 763-765.
3. Hood, M. I.; Skaar, E. P., Nutritional immunity: transition metals at the pathogen-host interface. *Nat. Rev. Microbiol.* **2012**, *10* (8).
4. Corbin, B. D.; Seeley, E. H.; Raab, A.; Feldmann, J.; Miller, M. R.; Torres, V. J.; Anderson, K. L.; Dattilo, B. M.; Dunman, P. M.; Gerads, R.; Caprioli, R. M.; Nacken, W.; Chazin, W. J.; Skaar, E. P., Metal chelation and inhibition of bacterial growth in tissue abscesses. *Science* **2008**, *319* (5865), 962-965.
5. John, B.; Fagerhol, M. K.; Lyberg, T.; Prydz, H.; Brandtzaeg, P.; Naess-Andresen, C. F.; Dale, I., Functional and clinical aspects of the myelomonocyte protein calprotectin. *J. Clin. Pathol. Mol. Pathol.* **1997**, *50* (3), 113-123.

6. Edgeworth, J.; Gorman, M.; Bennett, R.; Freemont, P.; Hogg, N., Identification of p8,14 as a highly abundant heterodimeric calcium binding protein complex of myeloid cells. *J. Biol. Chem.* **1991**, *266* (12), 7706-7713.
7. Fagerhol, M. K.; Dale, I.; Andersson, T., Release and Quantitation of a Leucocyte Derived Protein (L1). *Scand. J. Haematol.* **1980**, *24* (5), 393-398.
8. Damo, S. M.; Kehl-Fie, T. E.; Sugitani, N.; Holt, M. E.; Rathi, S.; Murphy, W. J.; Zhang, Y.; Betz, C.; Hench, L.; Fritz, G.; Skaar, E. P.; Chazin, W. J., Molecular basis for manganese sequestration by calprotectin and roles in the innate immune response to invading bacterial pathogens. *Proc. Natl. Acad. Sci. U. S. A.* **2013**, *110* (10), 3841-3846.
9. Brophy, M. B.; Hayden, J. A.; Nolan, E. M., Calcium ion gradients modulate the zinc affinity and antibacterial activity of human calprotectin. *J. Am. Chem. Soc.* **2012**, *134* (43), 18089-18100.
10. Brophy, M. B.; Nakashige, T. G.; Gaillard, A.; Nolan, E. M., Contributions of the S100A9 C-terminal tail to high-affinity Mn(II) chelation by the host-defense protein human calprotectin. *J. Am. Chem. Soc.* **2013**, *135* (47), 17804-17817.
11. Nakashige, T. G.; Zhang, B.; Krebs, C.; Nolan, E. M., Human calprotectin is an iron-sequestering host-defense protein. *Nat. Chem. Biol.* **2015**, *11* (10), 765-771.
12. Nakashige, T. G.; Stephan, J. R.; Cunden, L. S.; Brophy, M. B.; Wommack, A. J.; Keegan, B. C.; Shearer, J. M.; Nolan, E. M., The hexahistidine motif of host-defense protein human calprotectin contributes to zinc withholding and its functional versatility. *J. Am. Chem. Soc.* **2016**, *138* (37), 12243-12251.
13. Stephan, J. R.; Nolan, E. M., Calcium-induced tetramerization and zinc chelation shield human calprotectin from degradation by host and bacterial extracellular proteases. *Chem. Sci.* **2016**, *7* (3), 1962-1975.
14. Garcia, Y. M.; Barwinska-Sendra, A.; Tarrant, E.; Skaar, E. P.; Waldron, K. J.; Kehl-Fie, T. E., A superoxide dismutase capable of functioning with iron or manganese

promotes the resistance of *Staphylococcus aureus* to calprotectin and nutritional immunity. *PLOS Pathog.* **2017**, *13* (1), e1006125.

15. Liu, Janet Z.; Jellbauer, S.; Poe, A. J.; Ton, V.; Pesciaroli, M.; Kehl-Fie, T. E.; Restrepo, Nicole A.; Hosking, M. P.; Edwards, Robert A.; Battistoni, A.; Pasquali, P.; Lane, Thomas E.; Chazin, Walter J.; Vogl, T.; Roth, J.; Skaar, Eric P.; Raffatellu, M., Zinc sequestration by the neutrophil protein calprotectin enhances *Salmonella* growth in the inflamed gut. *Cell Host & Microbe* **2012**, *11* (3), 227-239.

16. Nairn, B. L.; Lonergan, Z. R.; Wang, J.; Braymer, J. J.; Zhang, Y.; Calcutt, M. W.; Lisher, J. P.; Gilston, B. A.; Chazin, W. J.; de Crécy-Lagard, V.; Giedroc, D. P.; Skaar, E. P., The Response of *Acinetobacter baumannii* to Zinc Starvation. *Cell Host & Microbe* **2016**, *19* (6), 826-836.

17. Stork, M.; Grijpstra, J.; Bos, M. P.; Mañas Torres, C.; Devos, N.; Poolman, J. T.; Chazin, W. J.; Tommassen, J., Zinc piracy as a mechanism of *Neisseria meningitidis* for evasion of nutritional immunity. *PLoS Pathog.* **2013**, *9* (10), e1003733.

18. Jean, S.; Juneau, R. A.; Criss, A. K.; Cornelissen, C. N., *Neisseria gonorrhoeae* evades calprotectin-mediated nutritional immunity and survives neutrophil extracellular traps by production of TdfH. *Infect. Immun.* **2016**, *84* (10), 2982-2994.

19. Vogl, T.; Tenbrock, K.; Ludwig, S.; Leukert, N.; Ehrhardt, C.; van Zoelen, M. A. D.; Nacken, W.; Foell, D.; van der Poll, T.; Sorg, C.; Roth, J., Mrp8 and Mrp14 are endogenous activators of Toll-like receptor 4, promoting lethal, endotoxin-induced shock. *Nat. Med.* **2007**, *13* (9), 1042-1049.

20. Loser, K.; Vogl, T.; Voskort, M.; Lueken, A.; Kupas, V.; Nacken, W.; Klenner, L.; Kuhn, A.; Foell, D.; Sorokin, L.; Luger, T. A.; Roth, J.; Beissert, S., The Toll-like receptor 4 ligands Mrp8 and Mrp14 are crucial in the development of autoreactive CD8+ T cells. *Nat. Med.* **2010**, *16* (6), 713-717.

21. Austermann, J.; Friesenhagen, J.; Fassl, S. K.; Ortkras, T.; Burgmann, J.; Barczyk-Kahlert, K.; Faist, E.; Zedler, S.; Pirr, S.; Rohde, C.; Müller-Tidow, C.;

von Köckritz-Blickwede, M.; von Kaisenberg, C. S.; Flohé, S. B.; Ulas, T.; Schultze, J. L.; Roth, J.; Vogl, T.; Viemann, D., Alarmins MRP8 and MRP14 Induce Stress Tolerance in Phagocytes under Sterile Inflammatory Conditions. *Cell Reports* **2014**, *9* (6), 2112-2123.

22. Korndörfer, I. P.; Brueckner, F.; Skerra, A., The Crystal structure of the human (S100A8/S100A9)₂ heterotetramer, calprotectin, illustrates how conformational changes of interacting α -Helices can determine specific association of two EF-hand proteins. *J. Mol. Bio.* **2007**, *370* (5), 887-898.

23. Hunter, M. J.; Chazin, W. J., High Level Expression and Dimer Characterization of the S100 EF-hand Proteins, Migration Inhibitory Factor-related Proteins 8 and 14. *J. Biol. Chem.* **1998**, *273* (20), 12427-12435.

24. Vogl, T.; Roth, J.; Sorg, C.; Hillenkamp, F.; Strupat, K., Calcium-induced noncovalently linked tetramers of MRP8 and MRP14 detected by ultraviolet matrix-assisted laser desorption/ionization mass spectrometry. *J. Am. Soc. Mass Spectrom.* **1999**, *10* (11), 1124-1130.

25. Hayden, J. A.; Brophy, M. B.; Cunden, L. S.; Nolan, E. M., High-affinity manganese coordination by human calprotectin is calcium-dependent and requires the histidine-rich site formed at the dimer interface. *J. Am. Chem. Soc.* **2013**, *135* (2), 775-787.

26. Nakashige, T. G.; Zygiel, E. M.; Drennan, C. L.; Nolan, E. M., Nickel sequestration by the host-defense protein human calprotectin. *J. Am. Chem. Soc.* **2017**, *139* (26), 8828-8836.

27. Vogl, T.; Leukert, N.; Barczyk, K.; Strupat, K.; Roth, J., Biophysical characterization of S100A8 and S100A9 in the absence and presence of bivalent cations. *Biochim. Biophys. Acta* **2006**, *1763* (11), 1298-1306.

28. Brini, M.; Ottolini, D.; Cali, T.; Carafoli, E., Calcium in health and disease. *Met. Ions Life Sci.* **2013**, *13*, 81-137.

29. Magon, N. J.; Turner, R.; Gearry, R. B.; Hampton, M. B.; Sly, P. D.; Kettle, A. J., Oxidation of calprotectin by hypochlorous acid prevents chelation of essential metal ions and allows bacterial growth: Relevance to infections in cystic fibrosis. *Free Radic. Biol. Med.* **2015**, *86*, 133-144.
30. Spraggins, J. M.; Rizzo, D. G.; Moore, J. L.; Rose, K. L.; Hammer, N. D.; Skaar, E. P.; Caprioli, R. M., MALDI FTICR IMS of intact proteins: Using mass accuracy to link protein images with proteomics data. *J. Am. Soc. Mass Spectrom.* **2015**, *26* (6), 974-985.
31. Martelli, C.; Marzano, V.; Iavarone, F.; Huang, L.; Vincenzoni, F.; Desiderio, C.; Messina, I.; Beltrami, P.; Zattoni, F.; Ferraro, P. M.; Buchholz, N.; Locci, G.; Faa, G.; Castagnola, M.; Gambaro, G., Characterization of the protein components of matrix stones sheds light on the S100-A8 and A9 relevance in the inflammatory pathogenesis of these rare renal calculi. *J. Urol.* **2016**, *196* (3), 911-918.
32. Nathan, C., Neutrophils and immunity: challenges and opportunities. *Nat. Rev. Immunol.* **2006**, *6* (3), 173-182.
33. Weiss, S. J., Tissue Destruction by Neutrophils. *NEJM* **1989**, *320* (6), 365-376.
34. Maier, K.; Leuschel, L.; Costabel, U., Increased Levels of Oxidized Methionine Residues in Bronchoalveolar Lavage Fluid Proteins from Patients with Idiopathic Pulmonary Fibrosis. *Am. Rev. Respir. Dis.* **1991**, *143* (2), 271-274.
35. Levine, R. L.; Mosoni, L.; Berlett, B. S.; Stadtman, E. R., Methionine residues as endogenous antioxidants in proteins. *Proc. Natl. Acad. Sci. U.S.A.* **1996**, *93* (26), 15036-15040.
36. Moskovitz, J.; Berlett, B. S.; Poston, J. M.; Stadtman, E. R., The yeast peptide-methionine sulfoxide reductase functions as an antioxidant in vivo. *Proc. Natl. Acad. Sci. U. S. A.* **1997**, *94* (18), 9585-9589.

37. Levine, R. L.; Berlett, B. S.; Moskovitz, J.; Mosoni, L.; Stadtman, E. R., Methionine residues may protect proteins from critical oxidative damage. *Mech. Ageing Dev.* **1999**, *107* (3), 323-332.
38. Achilli, C.; Ciana, A.; Rossi, A.; Balduini, C.; Minetti, G., Neutrophil granulocytes uniquely express, among human blood cells, high levels of Methionine-sulfoxide-reductase enzymes. *J. Leukoc. Biol.* **2007**, *83* (1), 181-189.
39. Stadtman, E. R.; Van Remmen, H.; Richardson, A.; Wehr, N. B.; Levine, R. L., Methionine oxidation and aging. *Biochim. Biophys. Acta* **2005**, *1703* (2), 135-140.
40. Lim, S. Y.; Raftery, M. J.; Goyette, J.; Hsu, K.; Geczy, C. L., Oxidative modifications of S100 proteins: functional regulation by redox. *J. Leukoc. Biol.* **2009**, *86* (3), 577-587.
41. Shaw, E.; Mares-Guia, M.; Cohen, W., Evidence for an active-center histidine in trypsin through use of a specific reagent, 1-chloro-3-tosylamido-7-amino-2-heptanone, the chloromethyl ketone derived from N^α-tosyl-L-lysine. *Biochemistry* **1965**, *4* (10), 2219-2224.
42. Santoro, M. M.; Bolen, D. W., Unfolding free energy changes determined by the linear extrapolation method. 1. Unfolding of phenylmethanesulfonyl .alpha.-chymotrypsin using different denaturants. *Biochemistry* **1988**, *27* (21), 8063-8068.
43. Samejima, T.; Yang, J. T., Reconstitution of Acid-denatured Catalase. *J. Biol. Chem.* **1963**, *238* (10), 3256-3261.
44. Gagnon, D. M.; Brophy, M. B.; Bowman, S. E. J.; Stich, T. A.; Drennan, C. L.; Britt, R. D.; Nolan, E. M., Manganese binding properties of human calprotectin under conditions of high and low calcium: X-ray crystallographic and advanced electron paramagnetic resonance spectroscopic analysis. *J. Am. Chem. Soc.* **2015**, *137* (8), 3004-3016.

45. Nocera, A. L.; Miyake, M. M.; Seifert, P.; Han, X.; Bleier, B. S., Exosomes mediate interepithelial transfer of functional P-glycoprotein in chronic rhinosinusitis with nasal polyps. *Laryngoscope* **2017**, *127* (9), E295-E300.
46. Walkup, G. K.; Burdette, S. C.; Lippard, S. J.; Tsien, R. Y., A new cell-permeable fluorescent probe for Zn²⁺. *J. Am. Chem. Soc.* **2000**, *122* (23), 5644-5645.
47. Ortega, A.; Amorós, D.; García de la Torre, J., Prediction of hydrodynamic and other solution properties of rigid proteins from atomic- and residue-level models. *Biophys. J.* **2011**, *101* (4), 892-898.
48. Winterbourn, C. C., Chapter One - The Biological Chemistry of Hydrogen Peroxide. In *Methods in Enzymol.*, Cadenas, E.; Packer, L., Eds. Academic Press: 2013; Vol. 528, pp 3-25.
49. Brown, P. H.; Balbo, A.; Schuck, P., Characterizing Protein-Protein Interactions by Sedimentation Velocity Analytical Ultracentrifugation. In *Current Protocols in Immunology*, John Wiley & Sons, Inc.: 2001.
50. Lebowitz, J.; Lewis, M. S.; Schuck, P., Modern analytical ultracentrifugation in protein science: A tutorial review. *Protein Sci.* **2002**, *11* (9), 2067-2079.
51. Stafford, W. F., Boundary analysis in sedimentation transport experiments: a procedure for obtaining sedimentation coefficient distributions using the time derivative of the concentration profile. *Anal. Biochem.* **1992**, *203* (2), 295-301.
52. Philo, J. S., Improved methods for fitting sedimentation coefficient distributions derived by time-derivative techniques. *Anal. Biochem.* **2006**, *354* (2), 238-246.
53. Le, D. T.; Liang, X.; Fomenko, D. E.; Raza, A. S.; Chong, C.-K.; Carlson, B. A.; Hatfield, D. L.; Gladyshev, V. N., Analysis of Methionine/Selenomethionine Oxidation and Methionine Sulfoxide Reductase Function Using Methionine-Rich Proteins and Antibodies against Their Oxidized Forms. *Biochemistry* **2008**, *47* (25), 6685-6694.
54. Hadley, R. C.; Gagnon, D. M.; Brophy, M. B.; Gu, Y.; Nakashige, T. G.; Britt, R. D.; Nolan, E. M., Biochemical and Spectroscopic Observation of Mn(II) Sequestration

from Bacterial Mn(II) Transport Machinery by Calprotectin. *J. Am. Chem. Soc.* **2018**, *140* (1), 110-113.

55. Fliss, H.; Weissbach, H.; Brot, N., Oxidation of methionine residues in proteins of activated human neutrophils. *Proc. Natl. Acad. Sci. U. S. A.* **1983**, *80* (23), 7160-7164.

56. Taggart, C.; Cervantes-Laurean, D.; Kim, G.; McElvaney, N. G.; Wehr, N.; Moss, J.; Levine, R. L., Oxidation of either methionine351 or methionine358 in α 1-antitrypsin causes loss of anti-neutrophil elastase activity. *J. Biol. Chem.* **2000**.

57. Obst, B.; Wagner, S.; Sewing, K. F.; Beil, W., Helicobacter pylori causes DNA damage in gastric epithelial cells. *Carcinogenesis* **2000**, *21* (6), 1111-1115.

58. Chaturvedi, R.; Cheng, Y.; Asim, M.; Bussi re, F. I.; Xu, H.; Gobert, A. P.; Hacker, A.; Casero, R. A.; Wilson, K. T., Induction of Polyamine Oxidase 1 by Helicobacter pylori Causes Macrophage Apoptosis by Hydrogen Peroxide Release and Mitochondrial Membrane Depolarization. *J. Biol. Chem.* **2004**, *279* (38), 40161-40173.

59. Imlay, J. A., Oxidative Stress. *EcoSal Plus* **2009**, *3* (2).

60. Black, S. D.; Mould, D. R., Development of hydrophobicity parameters to analyze proteins which bear post- or cotranslational modifications. *Anal. Biochem.* **1991**, *193* (1), 72-82.

61. Lee, K. C.; Eckert, R. L., S100A7 (Psoriasin) – Mechanism of Antibacterial Action in Wounds. *J. Invest. Dermat.* **2007**, *127* (4), 945-957.

62. Janin, J.; Miller, S.; Chothia, C., Surface, subunit interfaces and interior of oligomeric proteins. *J. Mol. Bio.* **1988**, *204* (1), 155-164.

63. Ciorba, M. A.; Heinemann, S. H.; Weissbach, H.; Brot, N.; Hoshi, T., Modulation of potassium channel function by methionine oxidation and reduction. *Proc. Natl. Acad. Sci. U. S. A.* **1997**, *94* (18), 9932-9937.

64. Snijder, J.; Rose, R. J.; Raijmakers, R.; Heck, A. J. R., Site-specific methionine oxidation in calmodulin affects structural integrity and interaction with Ca^{2+} /calmodulin-dependent protein kinase II. *J. Struct. Biol.* **2011**, *174* (1), 187-195.

65. Bertolotti-Ciarlet, A.; Wang, W.; Lownes, R.; Pristatsky, P.; Fang, Y.; McKelvey, T.; Li, Y.; Li, Y.; Drummond, J.; Prueksaritanont, T.; Vlasak, J., Impact of methionine oxidation on the binding of human IgG1 to FcRn and Fcγ receptors. *Mol. Immunol.* **2009**, *46* (8), 1878-1882.
66. Gao, J.; Yin, D. H.; Yao, Y.; Sun, H.; Qin, Z.; Schöneich, C.; Williams, T. D.; Squier, T. C., Loss of Conformational Stability in Calmodulin upon Methionine Oxidation. *Biophys. J.* **1998**, *74* (3), 1115-1134.
67. Balog, E. M.; Lockamy, E. L.; Thomas, D. D.; Ferrington, D. A., Site-Specific Methionine Oxidation Initiates Calmodulin Degradation by the 20S Proteasome. *Biochemistry* **2009**, *48* (13), 3005-3016.
68. Erickson, J. R.; Joiner, M.-I. A.; Guan, X.; Kutschke, W.; Yang, J.; Oddis, C. V.; Bartlett, R. K.; Lowe, J. S.; O'Donnell, S. E.; Aykin-Burns, N.; Zimmerman, M. C.; Zimmerman, K.; Ham, A.-J. L.; Weiss, R. M.; Spitz, D. R.; Shea, M. A.; Colbran, R. J.; Mohler, P. J.; Anderson, M. E., A Dynamic Pathway for Calcium-Independent Activation of CaMKII by Methionine Oxidation. *Cell* **2008**, *133* (3), 462-474.
69. Brinkmann, V.; Zychlinsky, A., Beneficial suicide: Why neutrophils die to make NETs. *Nat. Rev. Micro.* **2007**, *5* (8), 577-582.

Appendix 1: Protease Activity Assays

This Appendix is adapted from *Chem. Sci.* **2016**, 7 (3), 1962-1975.

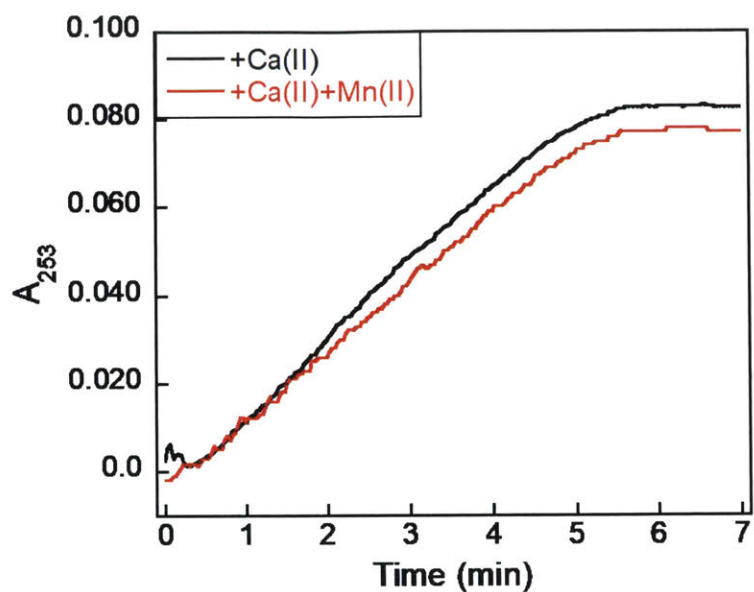


Figure A1.1. Effect of Mn(II) on trypsin activity. Trypsin (8.4 nM) activity was monitored by N_{α} -benzoyl-L-arginine ethyl ester (80 μ M) cleavage in 75 mM HEPES, 100 mM NaCl, pH 7.5, 1.5 mM Ca(II), ± 30 μ M MnCl₂ at 25 °C. Averages of three trials are shown.

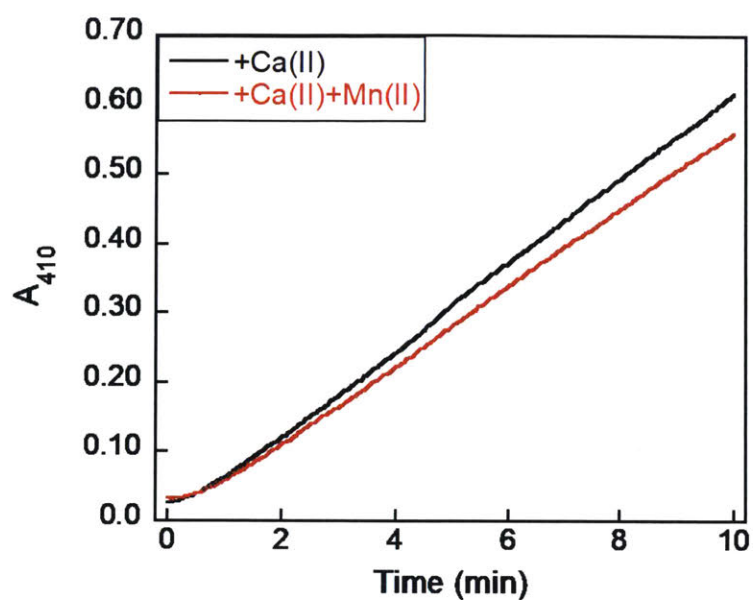


Figure. A3.2. Effect of Mn(II) on chymotrypsin activity. Activity of chymotrypsin (2 nM) was monitored by cleavage of *N*-succinyl-Ala-Ala-Pro-Phe *p*-nitroanilide (0.4 mM) in 75 mM HEPES, 100 mM NaCl, pH 7.5, 1% DMF, 1.5 mM CaCl₂, ±30 μM MnCl₂, at 25 °C. Averages of three experiments are shown.

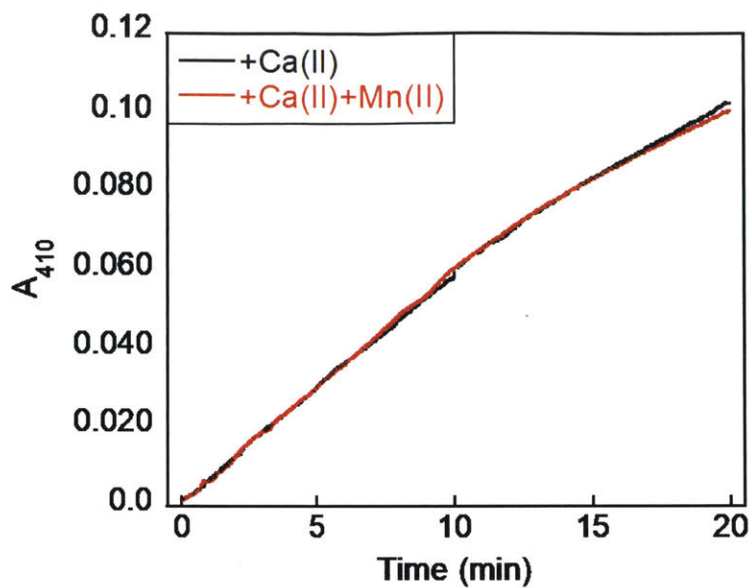


Figure A1.3. Effect of Mn(II) on human neutrophil elastase (10 nM) activity. Activity of human neutrophil elastase was monitored by cleavage of *N*-succinyl-Ala-Ala-Val-Ala *p*-nitroanilide (0.5 mM) in 75 mM HEPES, 100 mM NaCl, pH 7.5, 5% DMSO, 1.5 mM CaCl₂, ±30 μM MnCl₂ at 25 °C. Averages of three experiments are shown.

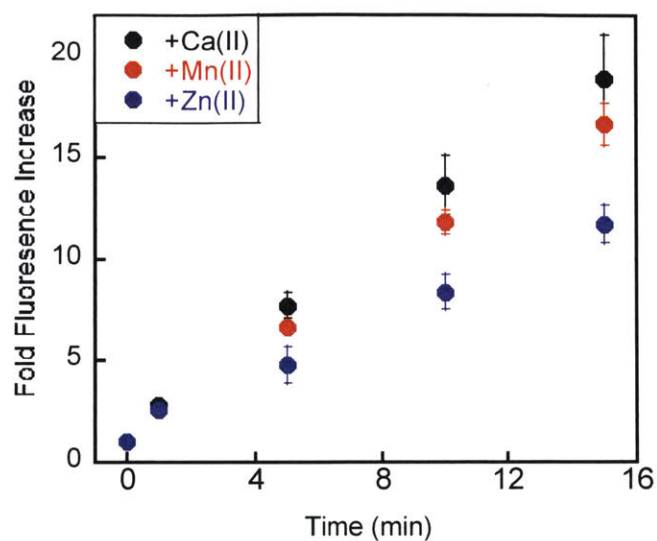


Figure A1.4. Effect of Mn(II) and Zn(II) on GluC (67 nM) activity. Activity of GluC as monitored by cleavage of carboxybenzyl-Leu-Leu-Glu β -naphthylamide (100 μ M +Ca(II) and +Mn(II) or 60 μ M +Zn(II)) in 75 mM HEPES, 100 mM NaCl, 10% DMSO, pH 7.5 with 1.5 mM CaCl₂, 30 μ M MnCl₂, 60 μ M ZnCl₂ (average \pm SDM, $n=3$). The zinc conditions also contained 30 mM CP-Ser because precipitation occurred when Zn(II) was added to solutions of substrate.

Appendix 2: Additional Characterization of CP Variants and Oxidized Species

A portion of this material is adapted from *Chem. Sci.* **2016**, 7 (3), 1962-1975.

A2.1. Additional Characterization for Chapter 2

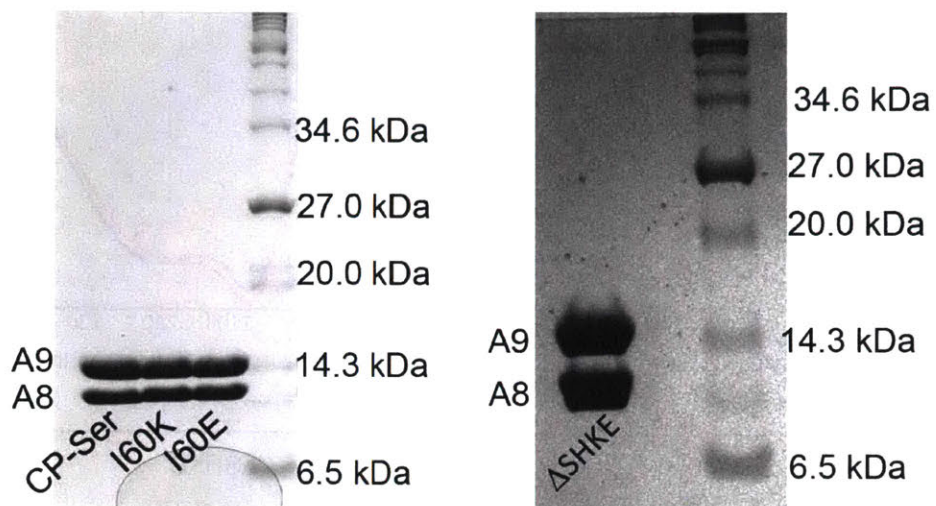


Figure A2.1. SDS-PAGE (15% acrylamide Tris-HCl, glycine gels) visualized with Coomassie Blue of purified CP-Ser, I60K, I60E, and Δ SHKE variants. The ladder is P7702S from New England Biolabs.

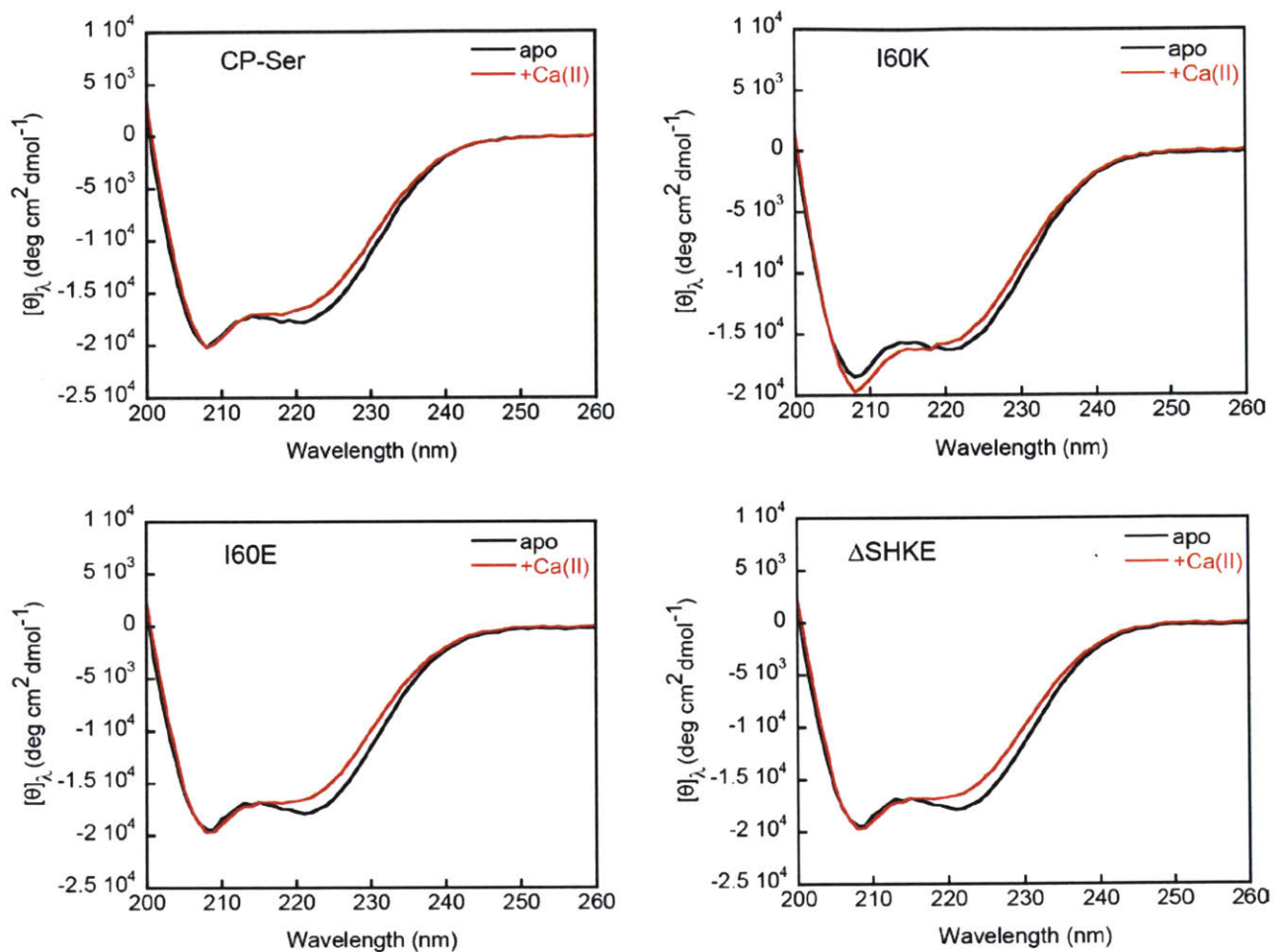


Figure A2.2. Circular dichroism spectra of CP-Ser and variants (10 μM) in 1 mM Tris-HCl, 0.5 EDTA, ± 2 mM CaCl_2 , pH 8.5 at 25 $^{\circ}\text{C}$.

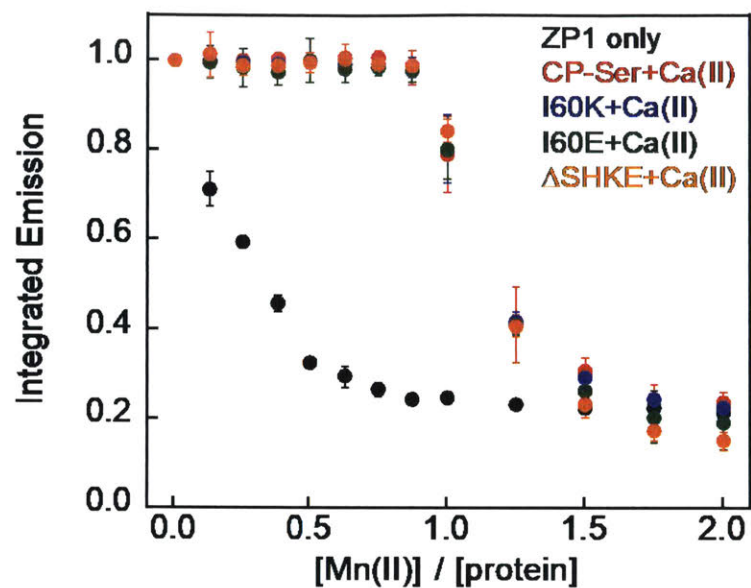


Figure A2.3. Competition between ZP1 (1 μ M) and CP (4 μ M) for Mn(II) in the presence of 200 μ M Ca(II) at pH 7.5 (mM HEPES, 100 mM NaCl) and 25 $^{\circ}$ C (mean \pm SDM, $n=3$). Excitation was provided at 490 nm, and the emission spectra were integrated from 500 to 650 nm and normalized with respect to apo ZP1 emission.

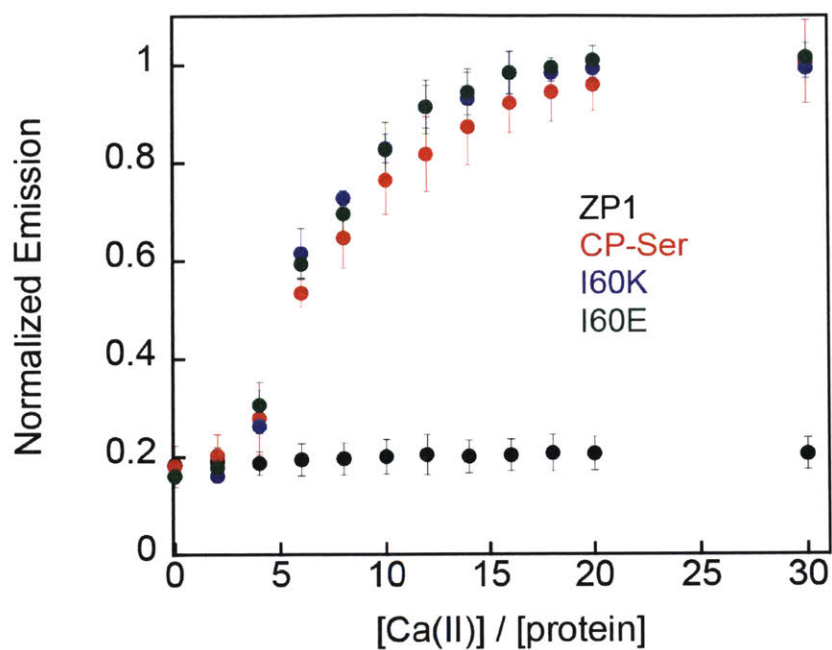


Figure A2.4. Competition between ZP1 (1 μM) and CP (4 μM) for 3.5 μM Mn(II) in the presence of increasing concentrations of Ca(II) at pH 7.5 (mM HEPES, 100 mM NaCl) and 25 $^{\circ}\text{C}$ (mean \pm SDM, $n=3$). Excitation was provided at 490 nm, and the emission spectra were integrated from 500 to 650 nm and normalized with respect to apo ZP1 emission.

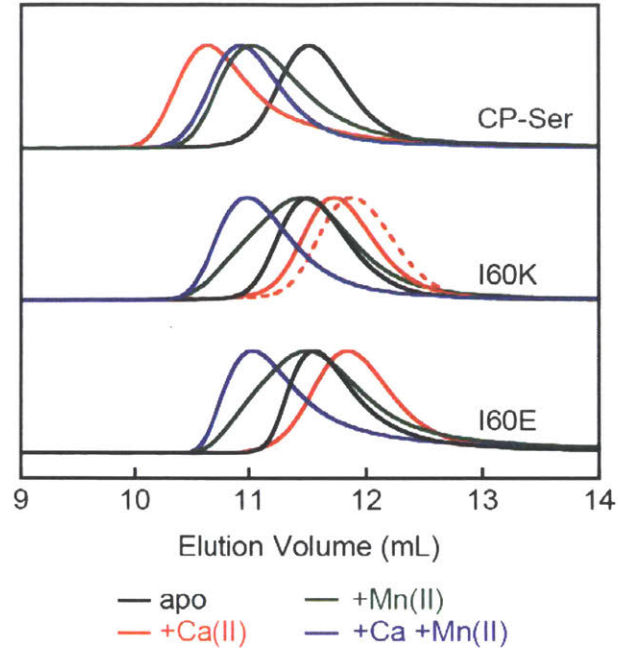


Figure A2.5. Size-exclusion chromatography of CP-Ser, I60K, and I60E (30 μM). Black traces, no metal added. Red traces, 600 μM Ca(II) included in the sample and running buffer. Green traces, 300 μM Mn(II) included in the sample only. Blue traces, 600 μM Ca(II) included in the sample and running buffer, and 33 μM Mn(II) included in the sample only. The black, red and blue traces correspond to the data in Figure 2.2A. All chromatograms were normalized to a maximum absorption of 1. Experiments were performed in 75 mM HEPES, 100 mM NaCl, pH 7.5 at 4 $^{\circ}\text{C}$. The dashed trace represents data from an experiment performed with 500 μM I60K in 75 mM HEPES, 100 mM NaCl, pH 7.5, 10 mM CaCl_2 .

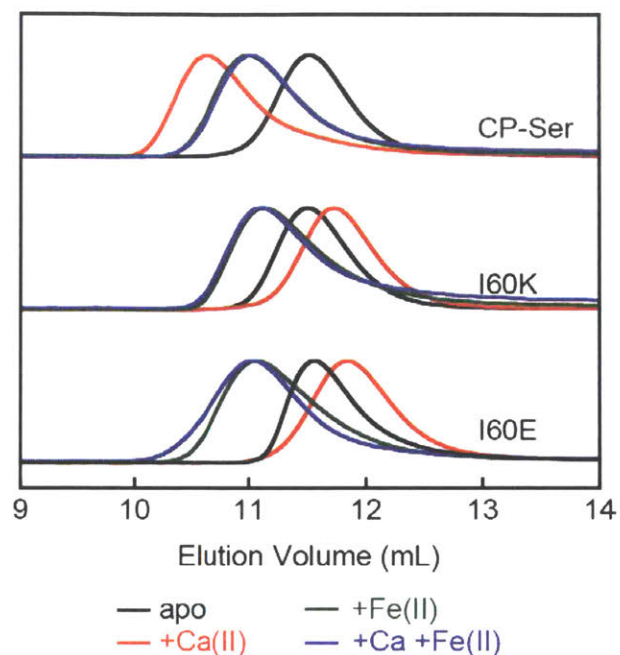


Figure A2.6. Size-exclusion chromatography of CP-Ser, I60K, and I60E (30 μM). Black traces, no metal added. Red traces, 600 μM Ca(II) included in the sample and running buffer. Green traces, 300 μM Fe(II) included in the sample only. Blue traces, 600 μM Ca(II) included in the sample and running buffer, and 30 μM Fe(II) included in the sample only. The black and red traces correspond to the data in Figure 2.2B. All chromatograms were normalized to a maximum absorption of 1. Experiments were performed in 75 mM HEPES, 100 mM NaCl, pH 7.5 at 4 $^{\circ}\text{C}$.

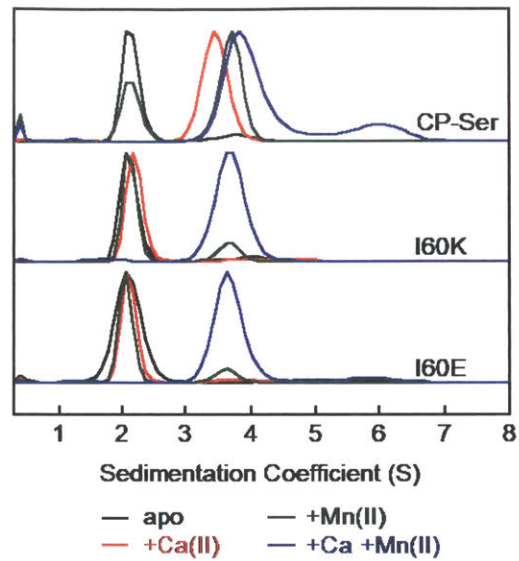


Figure A2.7. Normalized sedimentation coefficient distributions of CP-Ser, I60K, and I60E (27.5 μ M) obtained with the $c(s)$ model in SEDFIT. Buffer: 75 mM HEPES, 100 mM NaCl, \pm 540 μ M CaCl₂, \pm 27.5 μ M MnCl₂, pH 7.5 at 20 °C. For apo CP-Ser, 1.35 mM EDTA was included and no metals were added.

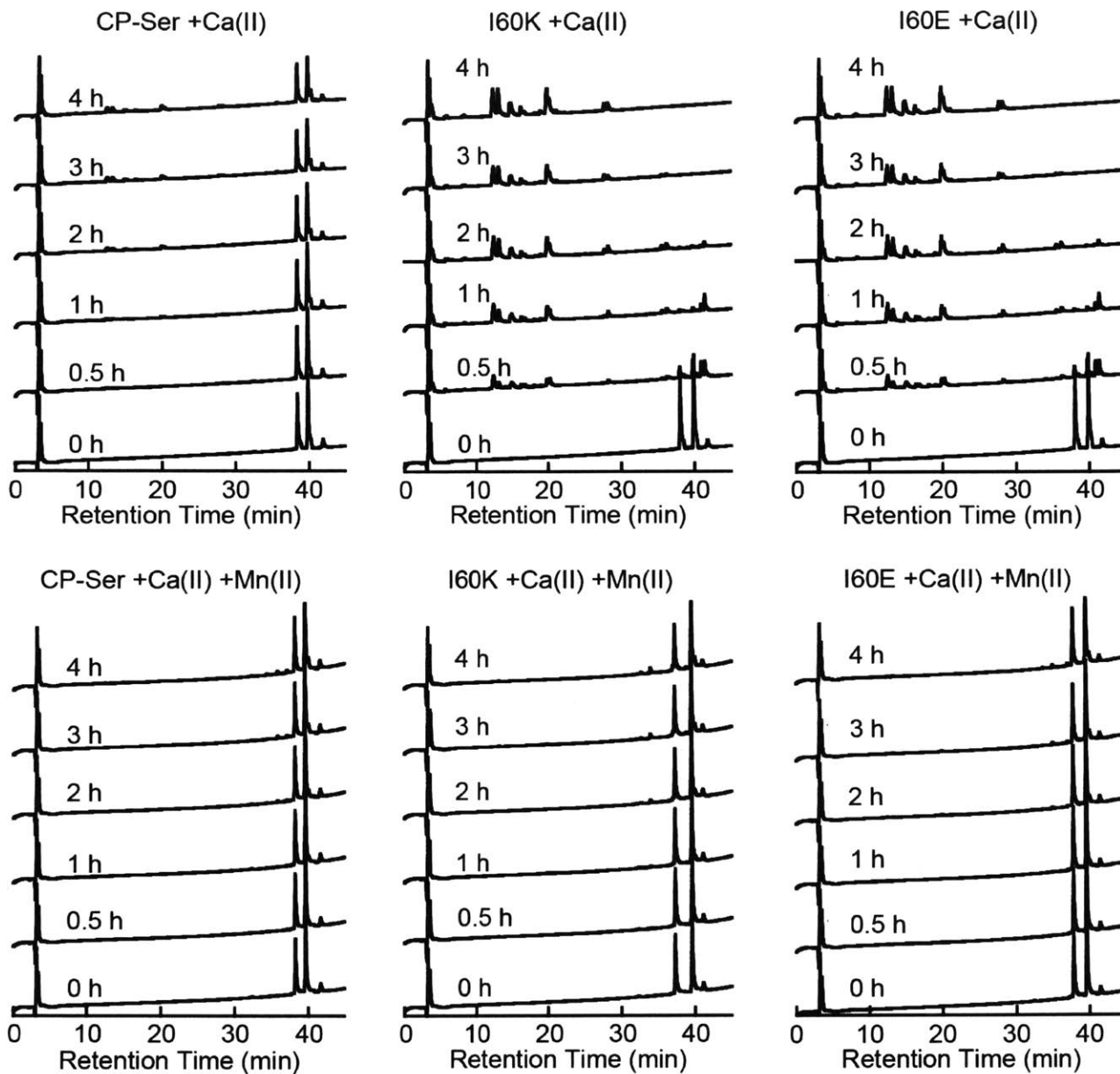


Figure A2.8. Full HPLC chromatograms of trypsin ($0.45 \mu\text{M}$) digestions of CP-Ser, I60E, and I60K ($30 \mu\text{M}$) in 75 mM HEPES, 100 mM NaCl, 1.5 mM CaCl_2 , $\pm 30 \mu\text{M}$ MnCl_2 , pH 7.5 performed at 37°C . These chromatograms correspond to the data presented in Figure 2.5.

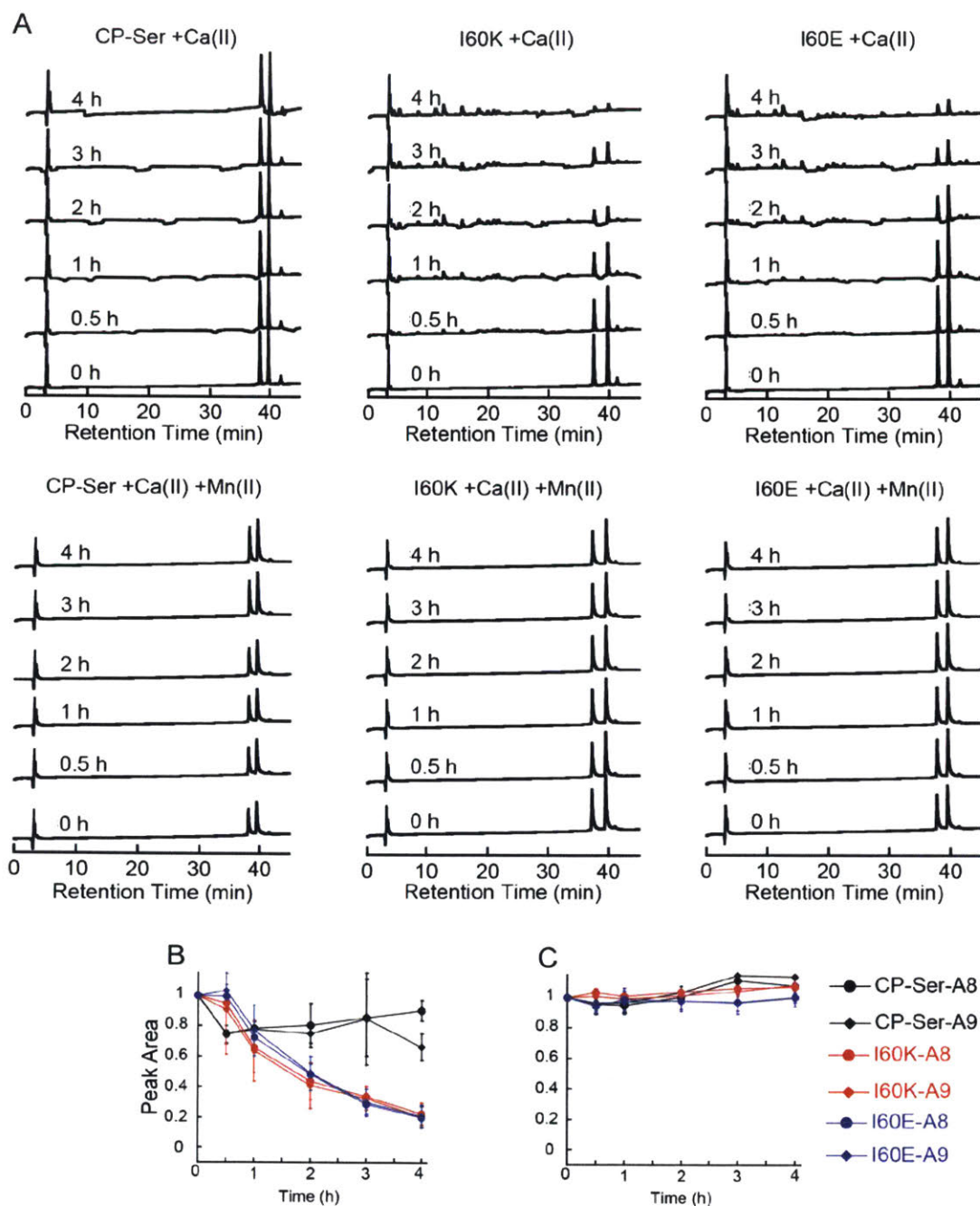


Figure A2.9. Susceptibility of Ca(II)-bound CP-Ser, I60E and I60K to degradation by chymotrypsin (0.3 μ M). (A) Representative full HPLC traces illustrating the S100A8 and S100A9 subunits following incubation with chymotrypsin for 0–4 h at 37 $^{\circ}$ C. Digestions were carried out in 75 mM HEPES, 100 mM NaCl, pH 7.5, 1.5 mM CaCl₂, \pm 30 μ M MnCl₂. (B) S100A8 and S100A9 integrated peak areas as a function of time in the presence of Ca(II) (mean \pm SDM, $n=3$). (C) S100A8 and S100A9 integrated peak areas as a function of time in the presence of Ca(II) and Mn(II) (mean \pm SDM, $n=3$). The area for each $t=0$ peak was normalized to 1.

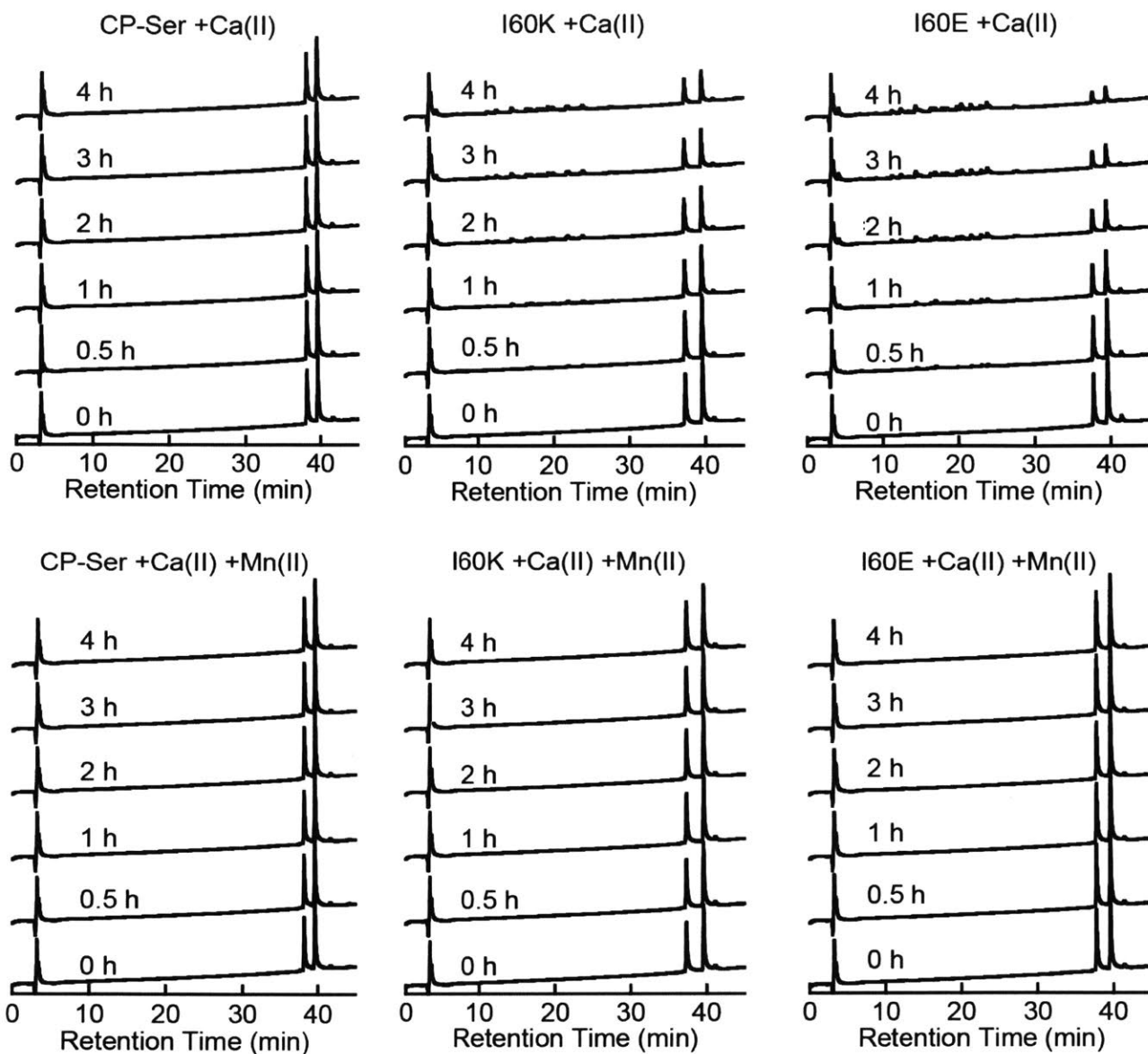


Figure. A2.10. Full HPLC chromatograms of human neutrophil elastase ($0.3 \mu\text{M}$) digestions of CP-Ser, I60K, I60E ($30 \mu\text{M}$) in 75 mM HEPES, 100 mM NaCl, 1.5 mM CaCl_2 , $\pm 30 \mu\text{M}$ MnCl_2 , pH 7.5 performed at $37 \text{ }^\circ\text{C}$. These chromatograms correspond to the data presented in Figure 2.6.

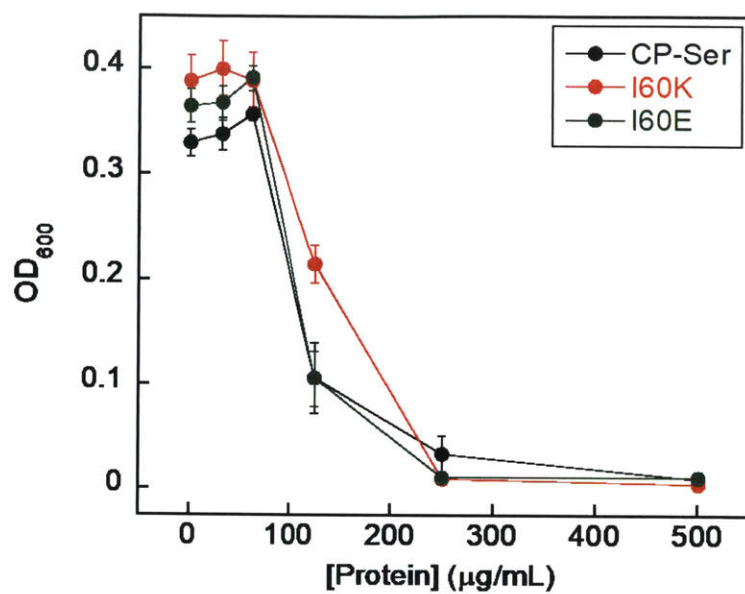


Figure A2.11. Antibacterial activity of CP-Ser, I60K, and I60E against *E. coli* ATCC 25922 in the presence of ≈ 2 mM CaCl_2 in the AMA medium. The OD₆₀₀ values were recorded at $t = 20$ h (mean $\pm n=9$).

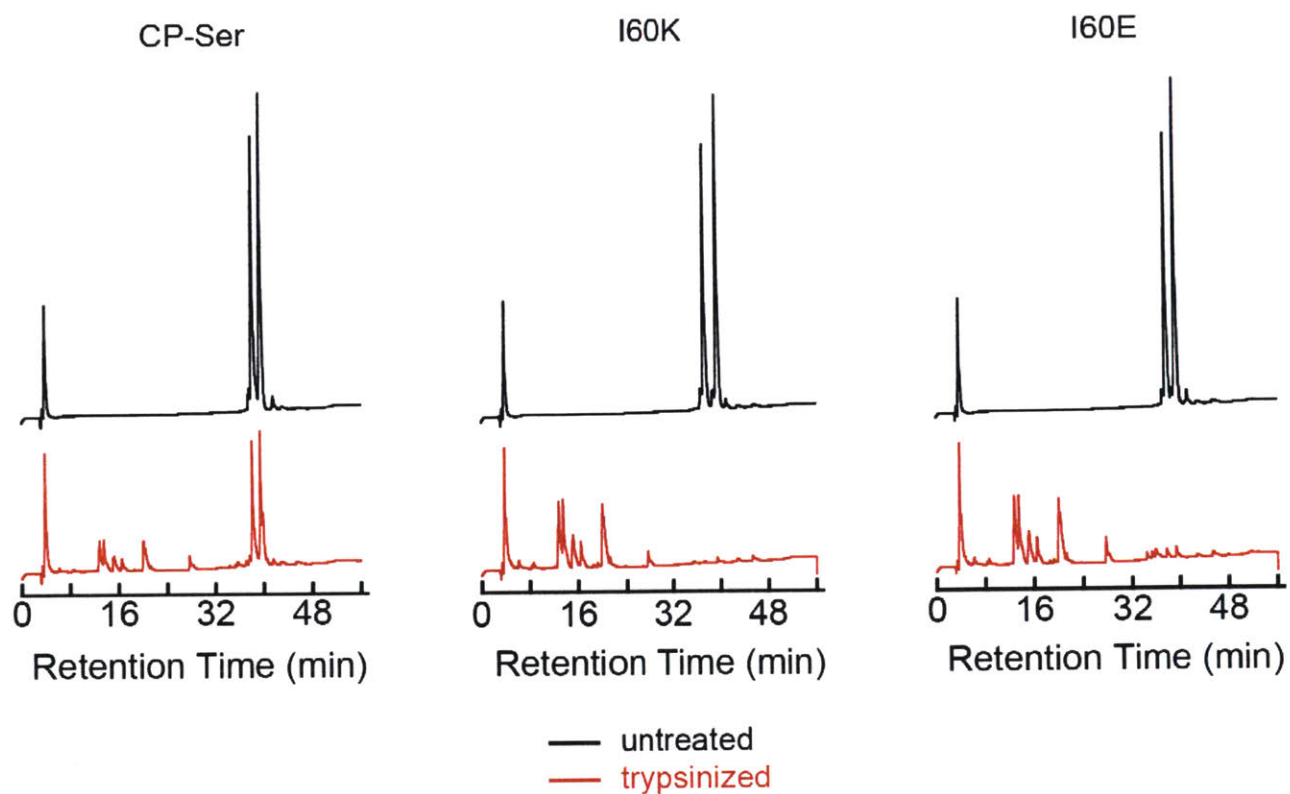


Figure A2.12. HPLC chromatograms (10–60% B over 50 min, 1 mL/min) of proteins employed in the antibacterial activity assays evaluating the effect of pre-incubation with trypsin. The proteins (210 μ M) were incubated at 37 $^{\circ}$ C in 20 mM Tris, 100 mM NaCl, 3 mM CaCl₂, pH 7.5, \pm 0.45 μ M trypsin for \approx 20 h prior to the antimicrobial activity assays. The HPLC traces were acquired following the \approx 20 h incubation. The data for the antimicrobial activity assays are presented in Figure 2.6.

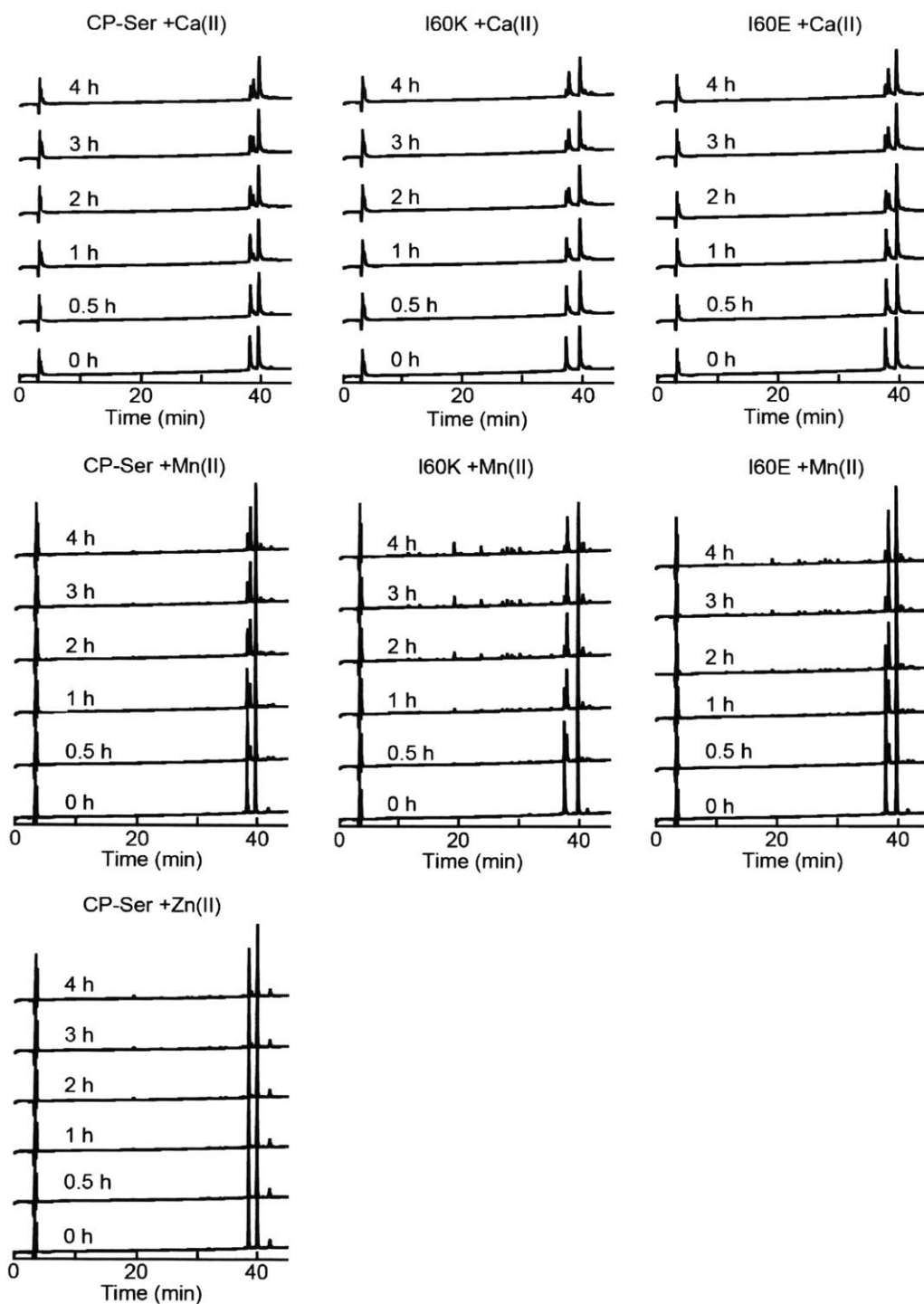


Figure A2.13. Full HPLC chromatograms of GluC ($0.3 \mu\text{M}$) digestions of CP-Ser, I60K, I60E ($30 \mu\text{M}$) in 75 mM HEPES, 100 mM NaCl, $\pm 1.5 \text{ mM}$ CaCl_2 , $\pm 30 \mu\text{M}$ MnCl_2 , pH 7.5. A digestion of CP-Ser with $60 \mu\text{M}$ ZnCl_2 is also shown. All experiments were performed at $37 \text{ }^\circ\text{C}$. These chromatograms correspond to the data presented in Figure 2.7.

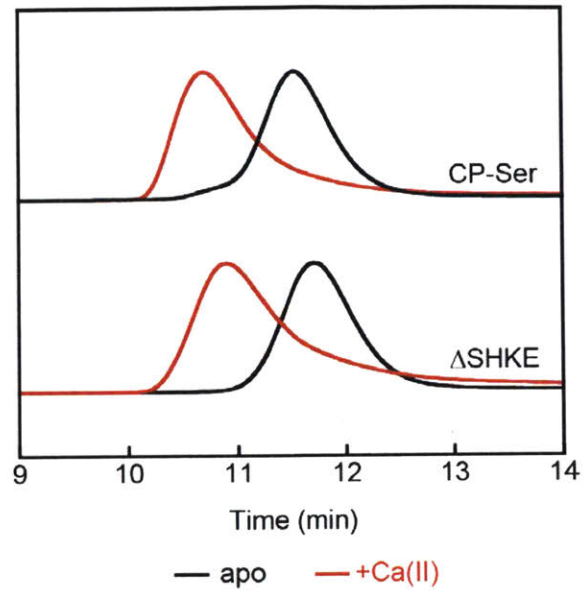


Figure A2.14. Size-exclusion chromatography of CP-Ser and Δ SHKE (30 μ M) performed with no metal added (black trace) and 600 μ M Ca(II) included in the sample and running buffer (red trace). The chromatograms were normalized to a maximum absorption of 1. Experiments were performed in 75 mM HEPES, 100 mM NaCl, pH 7.5 at 4 °C.

A2.2. Additional Characterization for Chapter 3

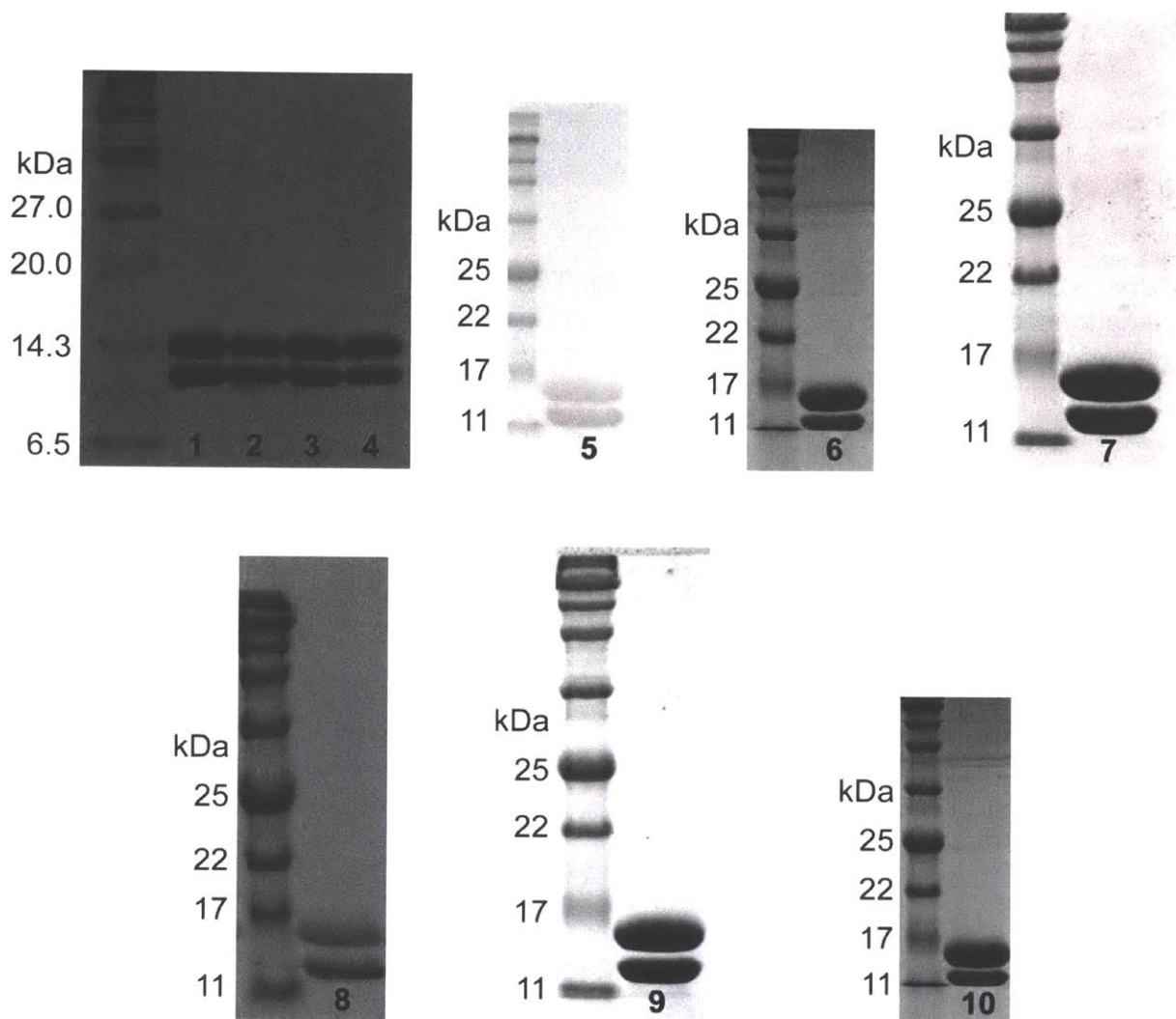


Figure A2.15. SDS-PAGE (15% acrylamide Tris-HCl, glycine) of representative protein purifications of I60K with a single subunit uniformly ^{15}N - or ^{13}C , ^{15}N -, or ^2H , ^{13}C , ^{15}N -labeled. **1**, [^{15}N]-A8-I60K; **2**, [^{15}N]-A9-I60K; **3**, [^{13}C , ^{15}N]-A8-I60K; **4**, [^{13}C , ^{15}N]-A9-I60K; **5**, [^{15}N]-A9-I60K(H103A); **6**, [^{15}N]-A9-I60K(H105A); **7**, [^2H , ^{13}C , ^{15}N]-A8-I60K; **8**, [^2H , ^{13}C , ^{15}N]-A9-I60K; **9**, [^{15}N]-A9-I60K(P107A); **10**, [^{15}N]-A9-I60K(P114A). The ladder was P7702S or P7712S from New England Biolabs.

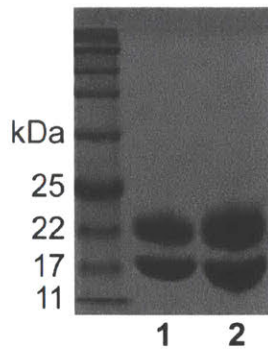


Figure. A2.16. SDS-PAGE (15% acrylamide Tris-HCl, glycine) of representative protein purifications of I60K with a single subunit uniformly ^{13}C -, ^{15}N -, and random fractional deuteration. **1**, [$^1\text{H}/^2\text{H}$, ^{13}C , ^{15}N]-A8-I60K; **2**, [$^1\text{H}/^2\text{H}$, ^{13}C , ^{15}N]-A9-I60K. The ladder was P7712S from New England Biolabs.

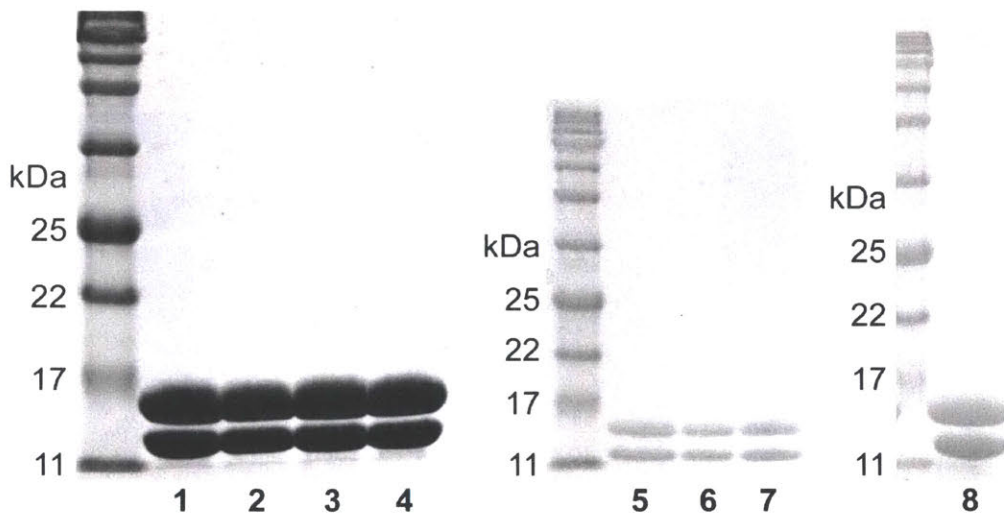


Figure. A2.17. SDS-PAGE (15% acrylamide Tris-HCl, glycine) of I60K with either the S100A8 or S100A9 subunit selectively ^{15}N labeled. **1**, [^{15}N (Phe)]-A8-I60K; **2**, [^{15}N (Leu)]-A8-I60K; **3**, [^{15}N (Ile)]-A8-I60K; **4**, [^{15}N (Val)]-A8-I60K; **5**, [^{15}N (Val)]-A9-I60K; **6**, [^{15}N (Ile)]-A9-I60K; **7**, [^{15}N (Phe)]-A9-I60K; **8**, [^{15}N (Leu)]-A9-I60K. The ladder was P7712S from New England Biolabs.

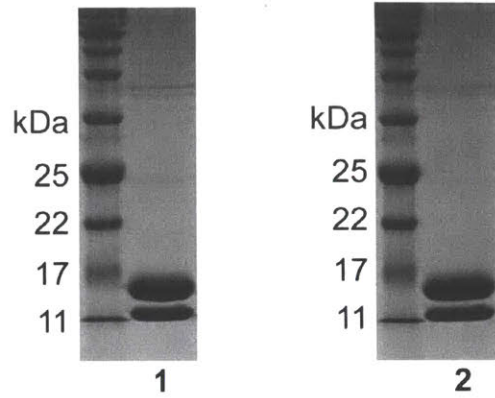


Figure. A2.18. SDS-PAGE (15% acrylamide Tris-HCl, glycine) of CP-Ser with a single subunit uniformly ^{15}N labeled. **1**, [^{15}N]-A8-CP-Ser and **2**, [^{15}N]-A9-CP-Ser. The ladder was P7712S from New England Biolabs.

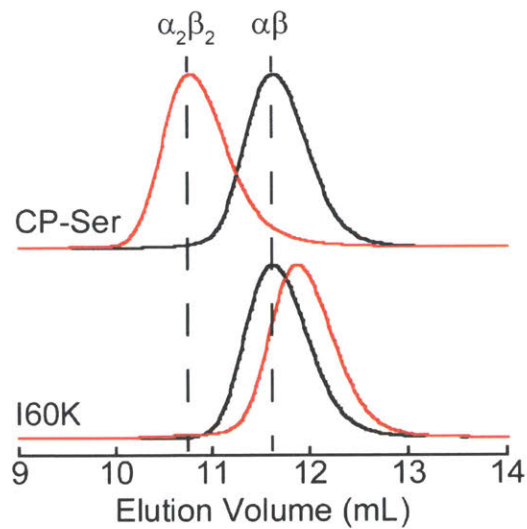


Figure A2.19. Analytical size exclusion chromatography of 500 μM CP-Ser or I60K in the absence (black traces) or presence (red traces) of 10 mM Ca(II) in the running buffer. Conditions: 75 mM HEPES, 100 mM NaCl, ± 10 mM Ca(II), pH 7.5, 4 $^{\circ}\text{C}$. Each chromatogram was normalized to a maximum value of 1.

A2.3. Additional Characterization for Chapter 4

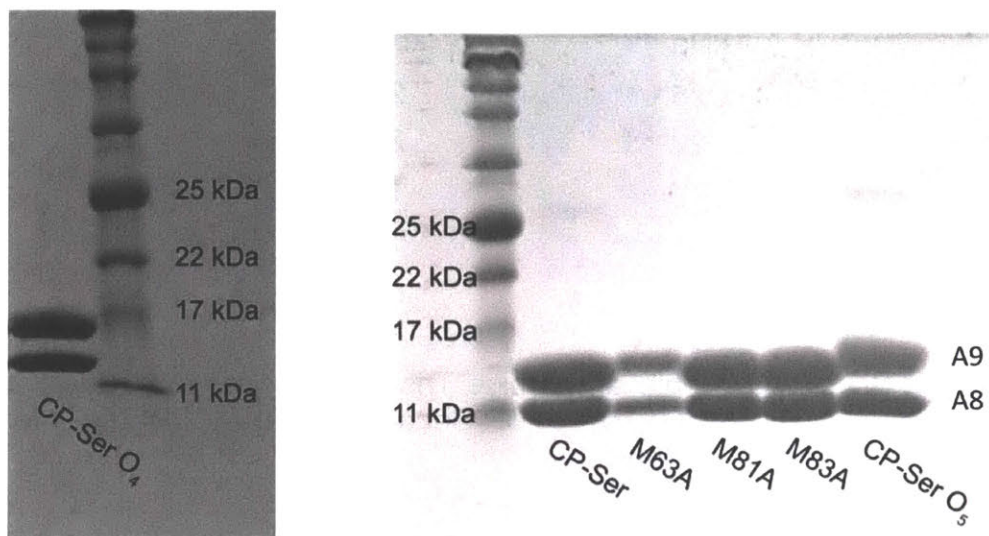


Figure. A2.20. SDS-PAGE (15% acrylamide Tris-HCl, glycine gels) visualized with Coomassie Blue of CP variants used in this study. The ladder is P7712S from New England Biolabs.

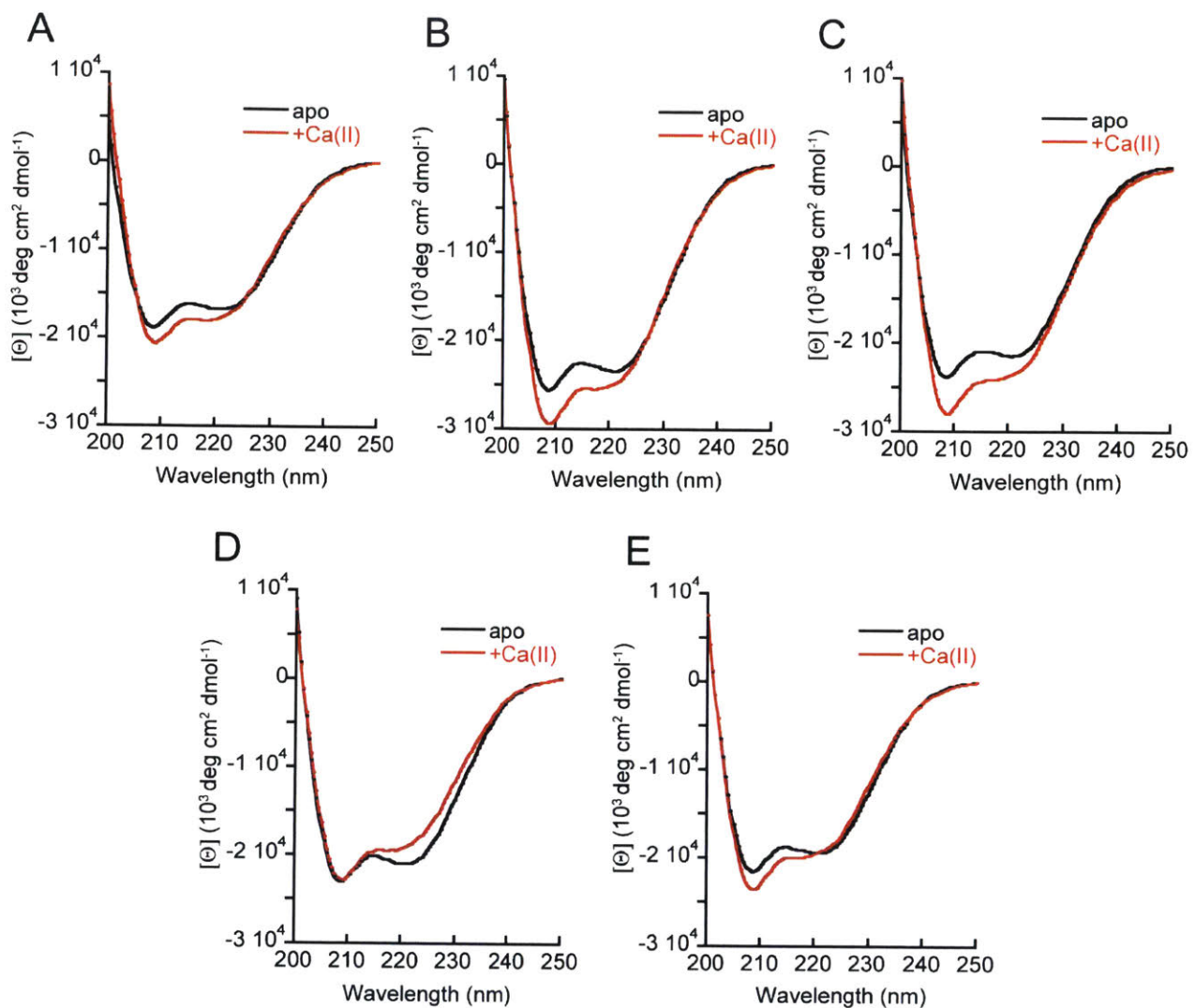


Figure A2.21. Circular dichroism spectra of Met to Ala variants and oxidized CP-Ser. (A) CP-Ser(A9-M63A). (B) CP-Ser(A9-M81A). (C) CP-Ser(A9-M83A). (D) CP-Ser O₄. (E) CP-Ser O₅. Conditions: 10 μ M protein, 300 μ L, 1 mM Tris, \pm 2 mM CaCl₂, pH 8.5, 25 $^{\circ}$ C.

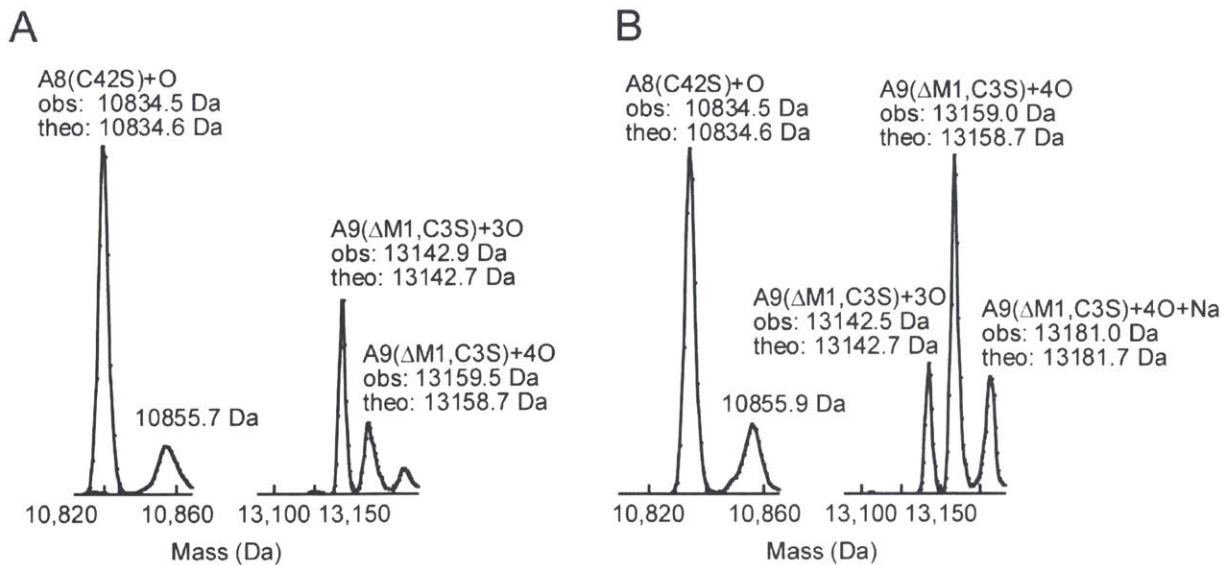


Figure A2.22. Representative deconvoluted mass spectra of (A) CP-Ser O₄ and (B) CP-Ser O₅ after purification.

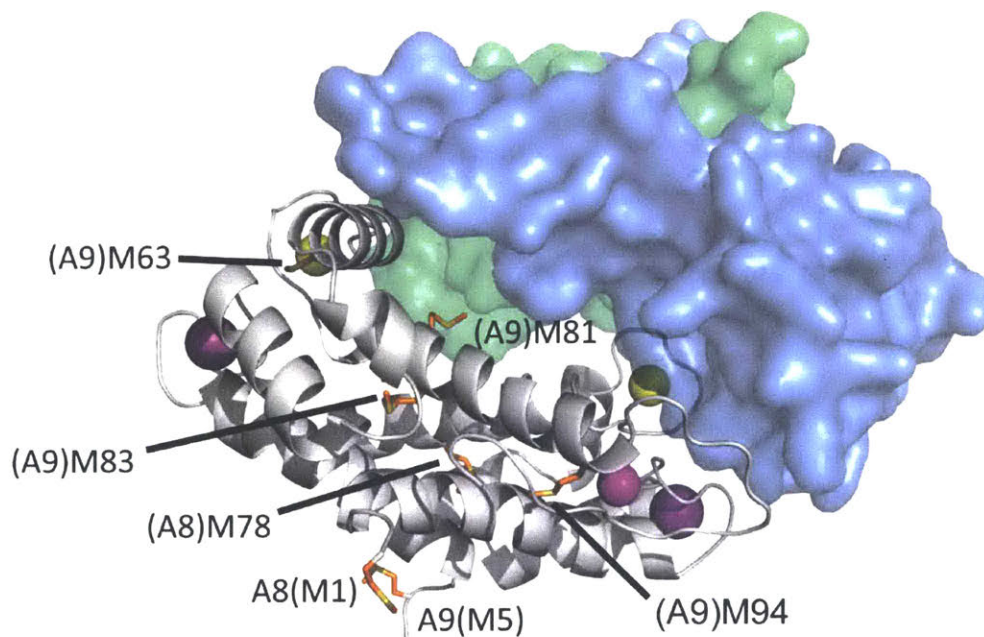


Figure A2.23. Crystal structure of the Ca(II)-, Na(I)- and Mn(II)-bound CP-Ser heterotetramer with all Met residues shown as sticks (PDB: 4XJK). The surface of one dimer unit is shown with S100A8 in green and S100A9 in blue. Both subunits of the other dimer are shown in silver with secondary structure depicted. The yellow spheres are Ca(II) ions, the purple spheres are Na(I) ions, and the pink sphere is a Mn(II) ion. The only Met residue at the dimer-dimer interface is (A9)M81. The N-terminus of A9 is disordered in this structure, and (A9)M1 is cleaved during overexpression, and thus not observed in this structure.

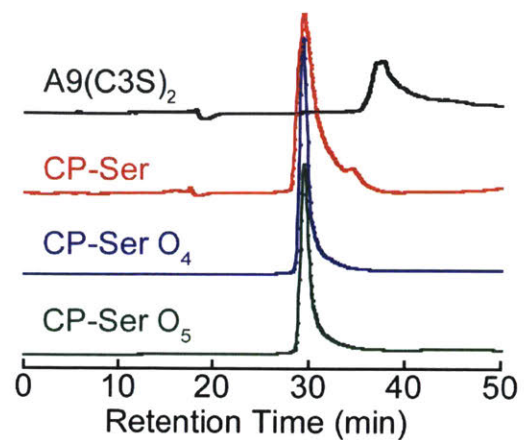


Figure A2.24. Anion exchange chromatography of the S100A9(C3S) homodimer, CP-Ser, CP-Ser O₄, and CP-Ser O₅. Conditions: 20 mM HEPES, 100 μ M protein, pH 8.0. Mobile phase A: 20 mM HEPES, pH 8.0. Mobile phase B: 20 mM HEPES, 1 M NaCl, pH 8.0.

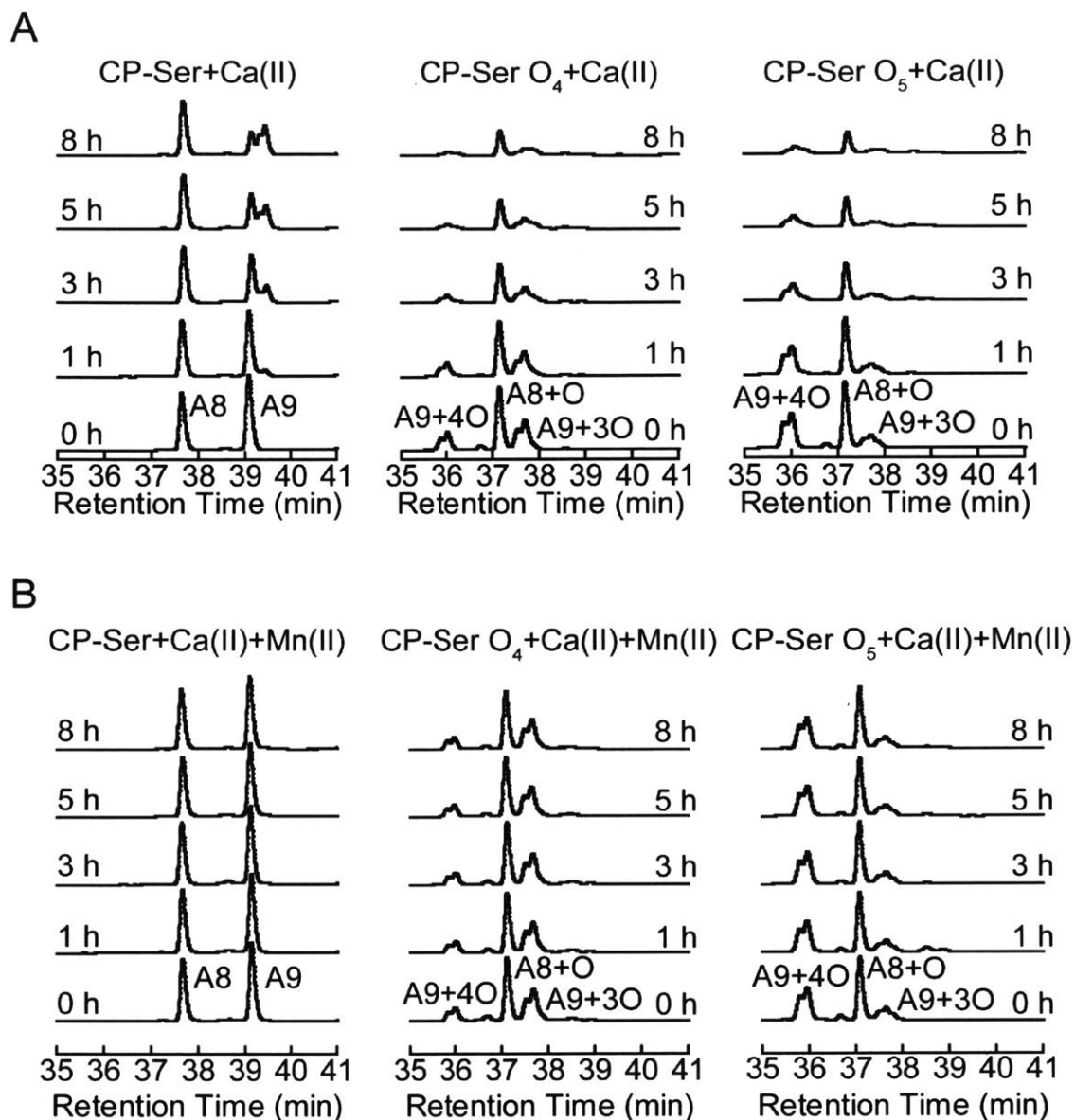


Figure A2.25. Digestions of CP-Ser, CP-Ser O₄ and CP-Ser O₅ by chymotrypsin. (A) Digestions in the presence of Ca(II). (B) Digestions in the presence of Ca(II) and Mn(II). Conditions: 75 M HEPES, 100 mM NaCl, 30 μ M CP, 1.5 mM Ca(II), \pm 30 μ M Mn(II), 1 μ M chymotrypsin, pH 7.5, 37 $^{\circ}$ C.

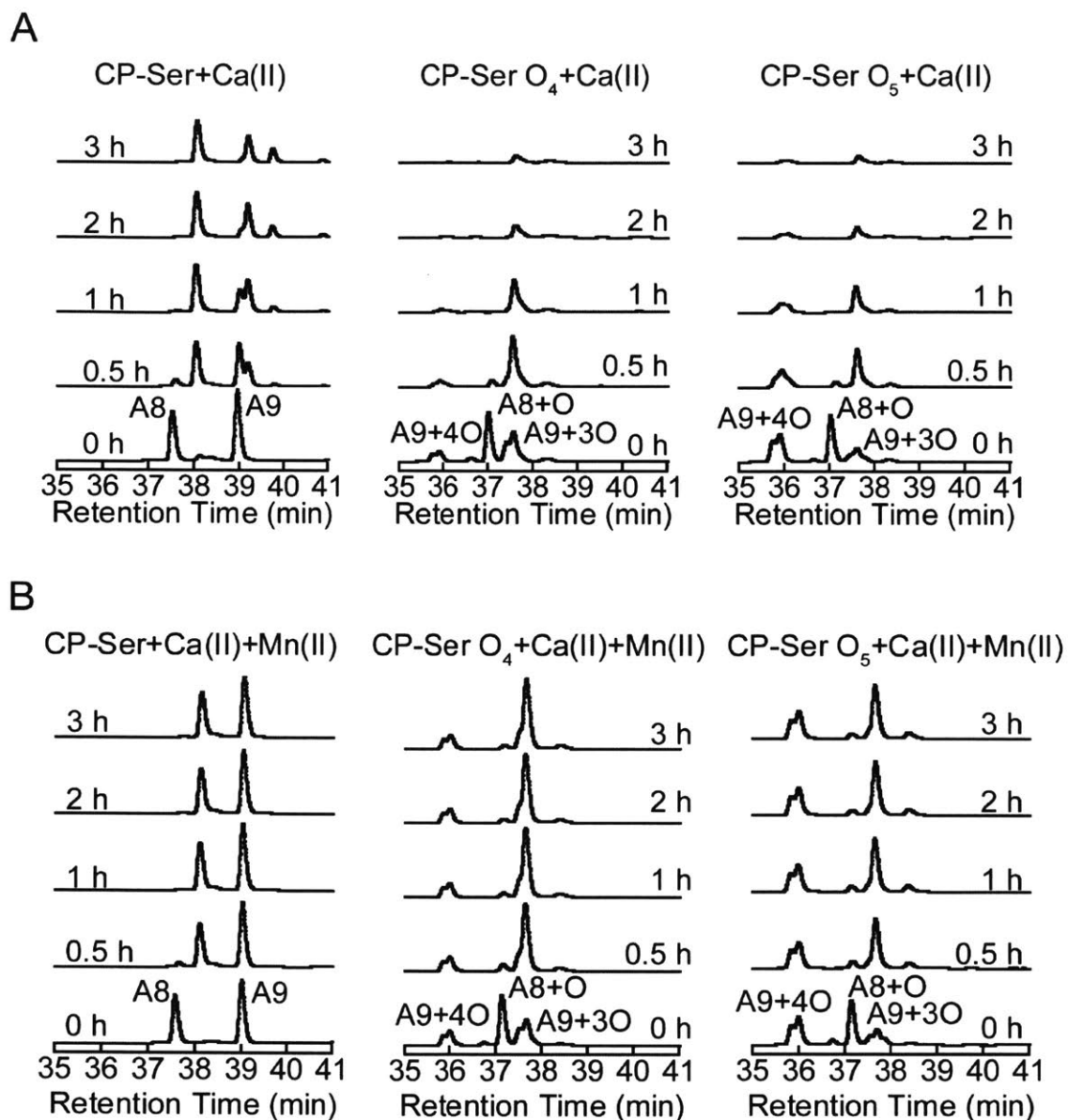


Figure A2.26. Digestions of CP-Ser, CP-Ser O₄ and CP-Ser O₅ by proteinase K. (A) Digestions in the presence of Ca(II). (B) Digestions in the presence of Ca(II) and Mn(II). Conditions: 75 M HEPES, 100 mM NaCl, 30 μM CP, 1.5 mM Ca(II), ±30 μM Mn(II), 1 μM proteinase K, pH 7.5, 37 °C.

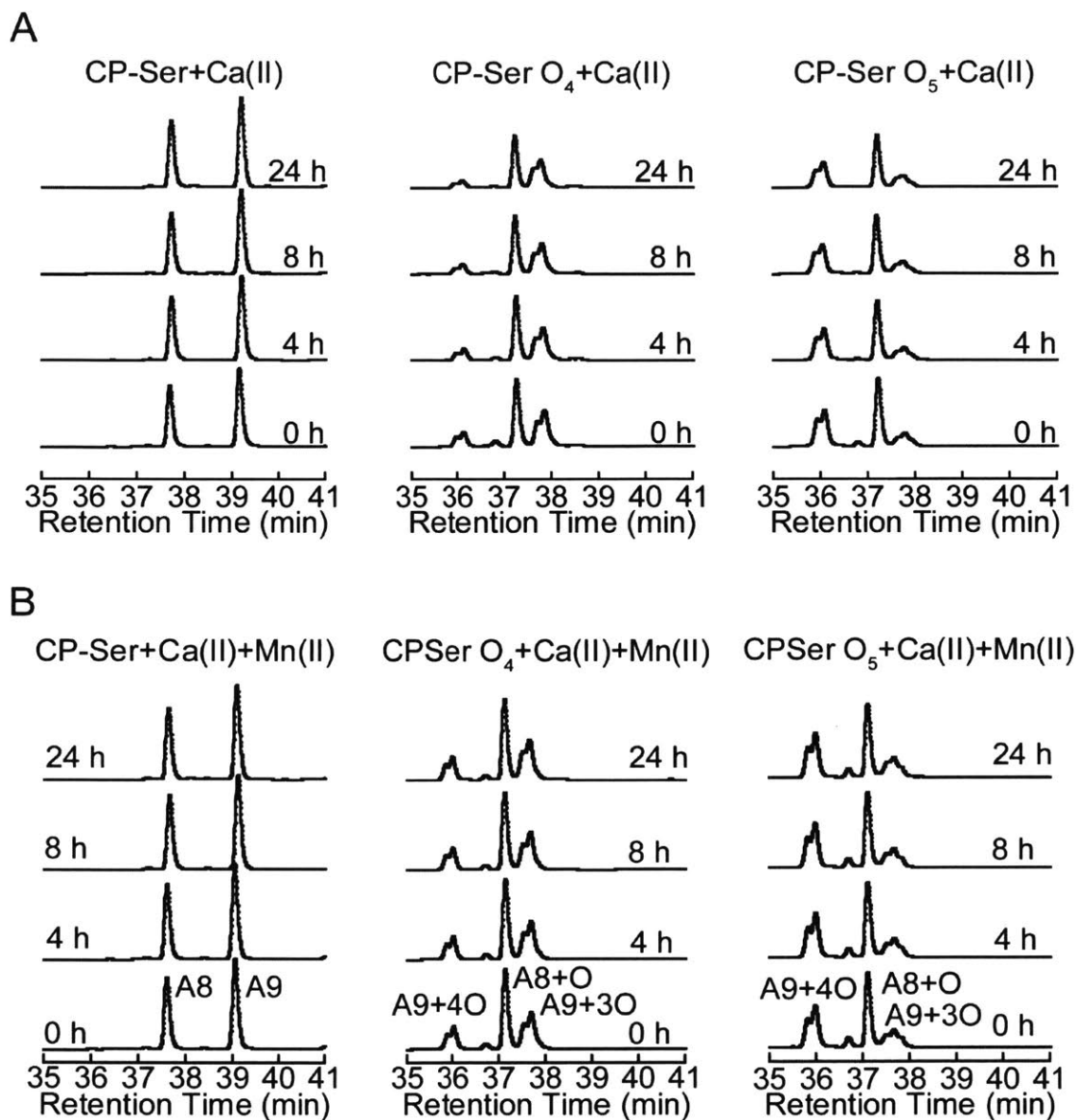


Figure A2.27. Digestions of CP-Ser, CP-Ser O₄ and CP-Ser O₅ by HNE. (A) Digestions in the presence of Ca(II) (reproduced Figure 4.11). (B) Digestions in the presence of Ca(II) and Mn(II). Conditions: 75 M HEPES, 100 mM NaCl, 30 μM CP, 1.5 mM Ca(II), ±30 μM Mn(II), 1 μM HNE, pH 7.5, 37 °C.

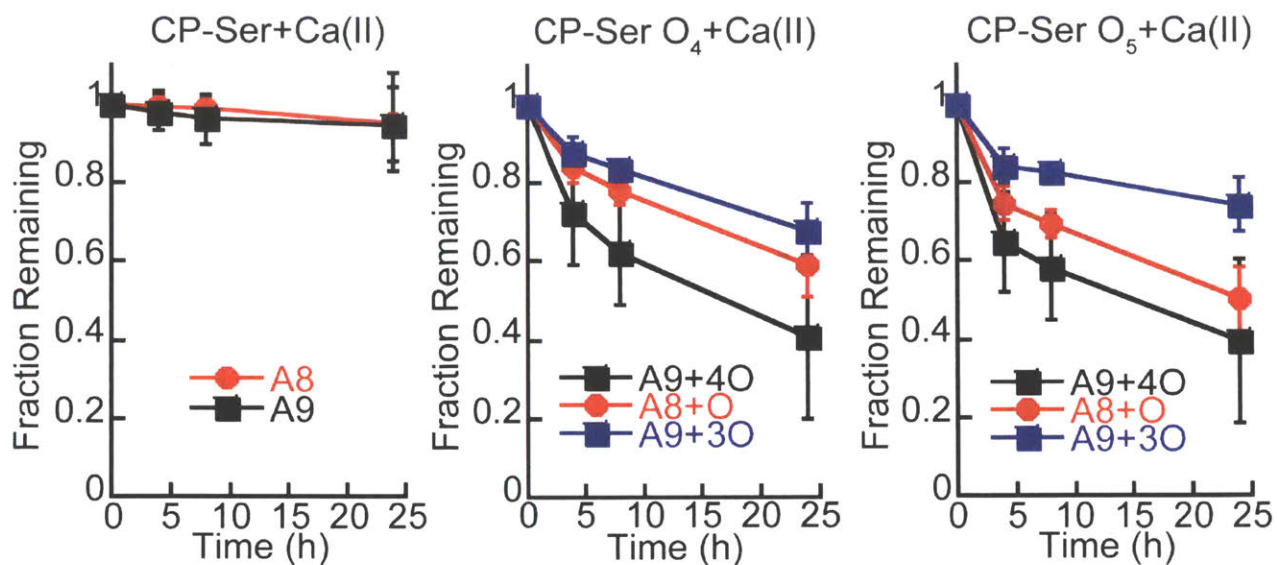
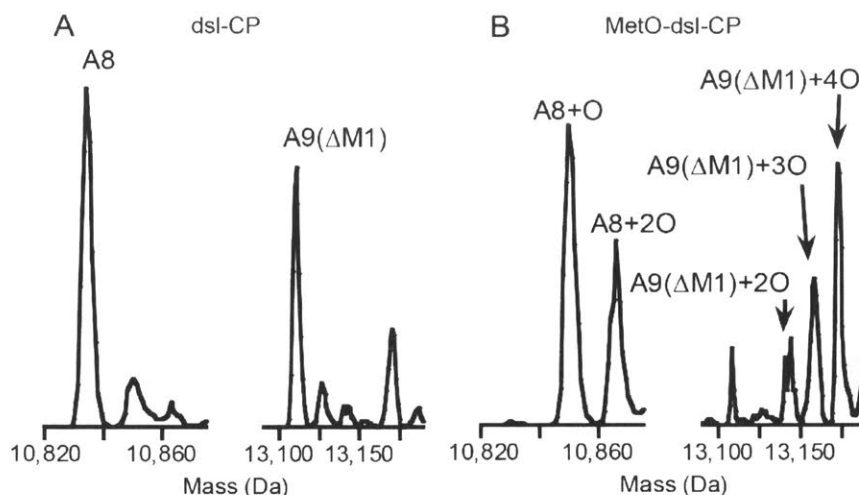


Figure A2.28. Plots of peak area from HPLC chromatograms of HNE digestions in the presence of Ca(II). The areas were normalized to the values obtained from the 0 h chromatograms (mean \pm SDM, $n=3$). Conditions: 75 mM HEPES, 100 mM NaCl, 1.5 mM CaCl₂, pH 7.5, 30 μ M CP, 1 μ M HNE at 37 $^{\circ}$ C.



Protein	Mass
S100A8	Theo: 10 834.5 Da Obs: 10 834.4 Da
S100A8+O	Theo: 10 850.5 Da Obs: 10 850.5 Da
S100A8+2O	Theo: 10 866.5 Da Obs: 10 865.6 Da
S100A9	Theo: 13 110.8 Da Obs: 13 110.4 Da
S100A9+2O	Theo: 13 143.8 Da Obs: 13 142.1 Da
S100A9+3O	Theo: 13 158.8 Da Obs: 13 159.0 Da
S100A9+4O	Theo: 13 174.8 Da Obs: 13 174.0 Da

Figure A2.29. Mass spectra data from oxidation of wild-type CP. (A) Deconvoluted mass spectrum of dsl-CP. (B) Deconvoluted mass spectrum of MetO-dsl-CP (C) Table of theoretical and representative observed masses of oxidized CP. dsl-CP conditions: 75 mM HEPES, 100 mM NaCl, 30 μ M CP, 1.5 mM Ca(II), 100 μ M H₂O₂, pH 7.5, 37 °C, 23 h. MetO-dsl-CP conditions: 75 mM HEPES, 100 mM NaCl, 30 μ M CP, 1.5 mM Ca(II), 100 mM H₂O₂, pH 7.5, 37 °C, 7 h. Prior to mass spectrometry analysis, the protein was combined with an equal volume of 75 mM HEPES, 100 mM NaCl, 20 mM TCEP, pH 7.5 and incubated for 10 min at ambient temperature.

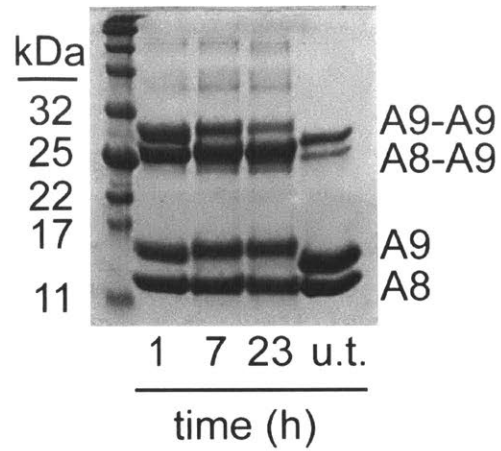


Figure A2.30. SDS-PAGE gel (Tris-HCl glycine, 15% acrylamide) of 30 μ M dsl-CP. Conditions: 75 mM HEPES, 100 mM NaCl, 30 μ M dsl-CP, 1.5 mM Ca(II), pH 7.5, 37 $^{\circ}$ C, 100 mM H₂O₂. Prior to this experiment, CP was treated with 100 μ M H₂O₂ in the same buffer for 23 h at 37 $^{\circ}$ C. The u.t. (untreated) lane contained CP that was on the benchtop for 46 h at 37 $^{\circ}$ C in the assay buffer without H₂O₂. The gel was visualized with Coomassie Blue. The ladder is P7712S from New England Biolabs.

Appendix 3: Additional Spectra and Parameters for NMR Spectroscopy

Table A3.1. NMR acquisition parameters for A8-I60K

Experiment	Labeling	T [K]	B ₀ [T]	B ₀ [MHz]	ns	d1 [s]	t ₁	sw ₁ [Hz]	o ₁ [Hz]	t ₂	sw ₂ [Hz]	o ₂ [Hz]	t ₃	sw ₃ [Hz]	o ₃ [Hz]
[¹ H, ¹⁵ N]-HSQC	U-[¹⁵ N]	298	14.1	600.5	48	1.5	2048	9615.385	2823.70	512	1694.915	7179.72	-	-	-
[¹ H, ¹⁵ N]-HSQC	[¹⁵ N]-Ile	298	14.1	600.5	16	1.0	2048	9615.385	2852.09	135	1936.535	6997.47	-	-	-
[¹ H, ¹⁵ N]-HSQC	[¹⁵ N]-Val	298	14.1	600.5	16	1.0	2048	9615.385	2818.00	164	1694.915	7179.72	-	-	-
[¹ H, ¹⁵ N]-HSQC	[¹⁵ N]-Phe	298	14.1	600.5	128	2.0	2048	9615.385	2825.00	248	1694.915	7179.72	-	-	-
[¹ H, ¹⁵ N]-TROSY	U-[² H, ¹³ C, ¹⁵ N]	298	21.1	900.1	64	1.0	1512	12626.263	4233.15	256	3283.725	10762.05	-	-	-

Table A3.2. NMR processing parameters for A8-I60K

Experiment	Labeling	SI ₁	WDW ₁	LB ₁ [Hz]	GB ₁	SSB ₁	SI ₂	WDW ₂	LB ₂ [Hz]	GB ₂	SSB ₁	SI ₃	WDW ₃	LB ₃ [Hz]	GB ₃	SSB ₃
[¹ H, ¹⁵ N]-HSQC	U-[¹⁵ N]	8192	GM	-5.0	0.05	-	1024	GM	-5.0	0.03	-	-	-	-	-	-
[¹ H, ¹⁵ N]-HSQC	[¹⁵ N]-Ile	4096	GM	-20.0	0.03	-	512	QSINE	-	-	3.5	-	-	-	-	-
[¹ H, ¹⁵ N]-HSQC	[¹⁵ N]-Val	4096	GM	-10.0	0.03	-	1024	QSINE	-	-	3.5	-	-	-	-	-
[¹ H, ¹⁵ N]-HSQC	[¹⁵ N]-Phe	4096	GM	-10.0	0.03	-	1024	QSINE	-	-	3.5	-	-	-	-	-
[¹ H, ¹⁵ N]-TROSY	U-[² H, ¹³ C, ¹⁵ N]	4096	QSINE	-	-	3.5	512	QSINE	-	-	3.5	-	-	-	-	-

Table A3.3. NMR acquisition parameters A8-I60K+Ca(II)

Experiment	Labeling	T [K]	B ₀ [T]	B ₀ [MHz]	ns	d1 [s]	t ₁	sw ₁ [Hz]	o ₁ [Hz]	t ₂	sw ₂ [Hz]	o ₂ [Hz]	t ₃	sw ₃ [Hz]	o ₃ [Hz]
[¹ H, ¹⁵ N]-HSQC	U-[¹⁵ N]	298	14.1	600.5	80	1.5	2048	9615.385	2822.70	512	1694.915	7179.72	-	-	-
[¹ H, ¹⁵ N]-HSQC	[¹⁵ N]-Ile	298	14.1	600.5	32	1.0	2048	9615.385	2852.09	142	1936.535	6997.47	-	-	-
[¹ H, ¹⁵ N]-HSQC	[¹⁵ N]-Leu	298	14.1	600.5	64	1.0	2048	9615.385	2818.00	86	1694.915	7179.72	-	-	-
[¹ H, ¹⁵ N]-HSQC	[¹⁵ N]-Val	298	14.1	600.5	32	1.0	2048	9615.385	2818.00	102	1694.915	7179.72	-	-	-
[¹ H, ¹⁵ N]-HSQC	[¹⁵ N]-Phe	298	14.1	600.5	256	1.0	2048	9615.385	2825.00	128	1694.915	7179.72	-	-	-
[¹ H, ¹⁵ N]-TROSY	U-[² H, ¹³ C, ¹⁵ N]	298	21.1	900.1	64	1.0	1512	12626.263	4233.15	208	2375.297	10762.05	-	-	-
[¹ H, ¹⁵ N, ¹³ C]-HNCACB	U-[² H, ¹³ C, ¹⁵ N]	298	21.1	900.1	64	1.5	2048	15243.902	4233.20	64	2375.297	10762.05	66	13513.514	9279.30
[¹ H, ¹⁵ N]-T ₂ -HSQC	U-[¹⁵ N]	298	21.1	900.1	32	1.5	2048	12626.263	4231.12	128	2827.650	10716.45	10	-	-
[¹ H, ¹⁵ N]-T ₁ -HSQC	U-[¹⁵ N]	298	21.1	900.1	32	1.5	2048	12626.263	4231.12	128	2827.650	10716.45	10	-	-
[¹ H, ¹⁵ N]-hetNOE	U-[¹⁵ N]	298	21.1	900.1	16	5.0	2048	14423.077	4231.12	512	2832.868	10716.45	-	-	-

Table A3.4. NMR processing parameters for A8-I60K+Ca(II)

Experiment	Labeling	SI ₁	WDW ₁	LB ₁ [Hz]	GB ₁	SS B ₁	SI ₂	WDW ₂	LB ₂ [Hz]	GB ₂	SSB ₁	SI ₃	WDW ₃	LB ₃ [Hz]	GB ₃	SSB ₃
[¹ H, ¹⁵ N]-HSQC	U-[¹⁵ N]	8192	GM	-5.0	0.05	-	1024	GM	-5.0	0.03	-	-	-	-	-	-
[¹ H, ¹⁵ N]-HSQC	[¹⁵ N]-Ile	4096	GM	-20.0	0.03	-	512	QSINE	-	-	3.5	-	-	-	-	-
[¹ H, ¹⁵ N]-HSQC	[¹⁵ N]-Leu	4096	GM	-2.0	0.03	-	1024	QSINE	-	-	3	-	-	-	-	-
[¹ H, ¹⁵ N]-HSQC	[¹⁵ N]-Val	4096	GM	-10.0	0.03	-	1024	QSINE	-	-	3.5	-	-	-	-	-
[¹ H, ¹⁵ N]-HSQC	[¹⁵ N]-Phe	4096	GM	-10.0	0.03	-	1024	QSINE	-	-	3.5	-	-	-	-	-
[¹ H, ¹⁵ N]-TROSY	U-[² H, ¹³ C, ¹⁵ N]	4096	QSINE	-	-	3.5	512	QSINE	-	-	3.5	-	-	-	-	-
[¹ H, ¹⁵ N, ¹³ C]-HNCACB	U-[² H, ¹³ C, ¹⁵ N]	4096	QSINE	-	-	3.0	256	QSINE	-	-	3.0	256	QSINE	-	-	3.0
[¹ H, ¹⁵ N]-T ₂ -HSQC	U-[¹⁵ N]	4096	QSINE	-	-	3.0	1024	QSINE	-	-	3.0	-	-	-	-	-
[¹ H, ¹⁵ N]-T ₁ -HSQC	U-[¹⁵ N]	4096	QSINE	-	-	3.0	1024	QSINE	-	-	3.0	-	-	-	-	-
[¹ H, ¹⁵ N]-hetNOE	U-[¹⁵ N]	4096	QSINE	-	-	3.0	1024	QSINE	-	-	3.0	-	-	-	-	-

Table A3.5. NMR acquisition parameters for variant proteins

Variant	Ca(II)	Experiment	Labeling	T [K]	B ₀ [T]	B ₀ [MHz]	ns	d1 [s]	t ₁	sw ₁ [Hz]	o ₁ [Hz]	t ₂	sw ₂ [Hz]	o ₂ [Hz]
A9(H103A)	-	[¹ H, ¹⁵ N]-HSQC	U-[¹⁵ N]	298	13.9	590.9	32	1.0	8192	10000.000	2836.17	1024	2394.6	7184.64
A9(H103A)	+	[¹ H, ¹⁵ N]-HSQC	U-[¹⁵ N]	298	13.9	590.9	32	1.0	8192	10000.000	2836.17	1024	2394.6	7184.64
A9(H105A)	-	[¹ H, ¹⁵ N]-HSQC	U-[¹⁵ N]	298	13.9	590.9	32	1.0	8192	10000.000	2836.17	512	2155.2	7184.64
A9(H105A)	+	[¹ H, ¹⁵ N]-HSQC	U-[¹⁵ N]	298	13.9	590.9	32	1.0	8192	10000.000	2836.17	512	2155.2	7184.64
A9(P107A)	-	[¹ H, ¹⁵ N]-HSQC	U-[¹⁵ N]	298	14.1	600.5	16	1.5	2048	9615.385	2824.00	184	1936.674	7179.72
A9(P107A)	+	[¹ H, ¹⁵ N]-HSQC	U-[¹⁵ N]	298	14.1	600.5	32	1.5	2048	9615.385	2824.00	195	1936.674	7179.72
A9(P114A)	-	[¹ H, ¹⁵ N]-HSQC	U-[¹⁵ N]	298	14.1	600.5	8	1.5	2048	9615.385	2823.70	180	2129.830	7179.72
A9(P114A)	+	[¹ H, ¹⁵ N]-HSQC	U-[¹⁵ N]	298	14.1	600.5	16	1.5	2048	9615.385	2823.70	512	2129.830	7179.72

Table A3.6. NMR processing parameters for variant proteins

Variant	Ca(II)	Experiment	Labeling	SI ₁	WDW ₁	LB ₁ [Hz]	GB ₁	SSB ₁	SI ₂	WDW ₂	LB ₂ [Hz]	GB ₂	SSB ₁
A9(H103A)	-	[¹ H, ¹⁵ N]-HSQC	U-[¹⁵ N]	16384	GM	-10	0.05	-	2048	GM	-10	0.05	-
A9(H103A)	+	[¹ H, ¹⁵ N]-HSQC	U-[¹⁵ N]	16384	GM	-10	0.05	-	2048	GM	-10	0.05	-
A9(H105A)	-	[¹ H, ¹⁵ N]-HSQC	U-[¹⁵ N]	16384	GM	-10	0.05	-	2048	GM	-10	0.05	-
A9(H105A)	+	[¹ H, ¹⁵ N]-HSQC	U-[¹⁵ N]	16384	GM	-10	0.05	-	2048	GM	-10	0.05	-
A9(P107A)	-	[¹ H, ¹⁵ N]-HSQC	U-[¹⁵ N]	8192	GM	-5.0	0.07	-	1024	GM	-5.0	0.07	-
A9(P107A)	+	[¹ H, ¹⁵ N]-HSQC	U-[¹⁵ N]	8192	GM	-5.0	0.07	-	1024	QSINE	-	-	3.0
A9(P114A)	-	[¹ H, ¹⁵ N]-HSQC	U-[¹⁵ N]	8192	GM	-5.0	0.05	-	1024	QSINE	-	-	3.5
A9(P114A)	+	[¹ H, ¹⁵ N]-HSQC	U-[¹⁵ N]	8192	GM	-5.0	0.05	-	1024	QSINE	-	-	3.5

Table A3.7. NMR acquisition parameters for CP-Ser

Variant	Ca(II)	Experiment	Labeling	T [K]	B ₀ [T]	B ₀ [MHz]	ns	d1 [s]	t ₁	sw ₁ [Hz]	o ₁ [Hz]	t ₂	sw ₂ [Hz]	o ₂ [Hz]
CP-Ser A8	-	[¹ H, ¹⁵ N]-HSQC	U-[¹⁵ N]	298	13.9	600.5	32	1.5	2048	9615.385	2825.20	512	1694.915	7179.72
CP-Ser A8	+	[¹ H, ¹⁵ N]-HSQC	U-[¹⁵ N]	298	13.9	600.5	80	1.5	2048	9615.385	2825.20	80	1694.915	7179.72
CP-Ser A9	-	[¹ H, ¹⁵ N]-HSQC	U-[¹⁵ N]	298	13.9	600.5	32	1.5	2048	9615.385	2825.20	444	1886.792	7179.72
CP-Ser A9	+	[¹ H, ¹⁵ N]-HSQC	U-[¹⁵ N]	298	13.9	600.5	32	1.5	2048	9615.385	2825.00	512	1886.792	7179.72

Table A3.8. NMR processing parameters for CP-Ser

Variant	Ca(II)	Experiment	Labeling	SI ₁	WDW ₁	LB ₁ [Hz]	GB ₁	SSB ₁	SI ₂	WDW ₂	LB ₂ [Hz]	GB ₂	SSB ₁
CP-Ser A8	-	[¹ H, ¹⁵ N]-HSQC	U-[¹⁵ N]	8192	GM	-5.0	0.05	-	1024	GM	-5.0	0.03	-
CP-Ser A8	+	[¹ H, ¹⁵ N]-HSQC	U-[¹⁵ N]	8192	GM	-5.0	0.05	-	1024	GM	-5.0	0.03	-
CP-Ser A9	-	[¹ H, ¹⁵ N]-HSQC	U-[¹⁵ N]	8192	GM	-5.0	0.05	-	1024	GM	-5.0	0.03	-
CP-Ser A9	+	[¹ H, ¹⁵ N]-HSQC	U-[¹⁵ N]	8192	GM	-10.0	0.05	-	1024	GM	-10.0	0.03	-

Table A3.9. Chemical shifts (ppm) of assigned A8-I60K-Ca(II) resonances

Res Num	Res Type	N	H	CA	CB
1	M				
2	L			51.597	39.969
3	T	114.646	9.924	58.156	67.522
4	E	119.132	8.837	56.56	25.377
5	L	120.885	8.482	54.819	38.083
6	E	119.073	7.698	56.037	27.576
7	K	117.76	8.768	57.108	29.163
8	A	122.083	7.752	52.152	14.848
9	L				
10	N				
11	S				
12	I				
13	I				
14	D				
15	V				
16	Y				
17	H				
18	K				
19	Y				
20	S				
21	L				
22	I				
23	K				
24	G				
25	N				
26	F				
27	H				
28	A				
29	V				
30	Y				
31	R				
32	D				
33	D				
34	L				
35	K				
36	K				
37	L				
38	L				
39	E				
40	T				

Res Num	Res Type	N	H	CA	CB
41	E				
42	S				
43	P				
44	Q				
45	Y				
46	I				
47	R				
48	K				
49	K				
50	G				
51	A				
52	D				
53	V				
54	W				
55	F				
56	K				
57	E				
58	L				
59	D				
60	K				
61	N				
62	T				
63	D				
64	G				
65	A				
66	V				
67	N				
68	F				
69	Q				
70	E				
71	F				
72	L				
73	I				
74	L				
75	V				
76	I				
77	K				
78	M				
79	G				
80	V				
81	A				

Res Num	Res Type	N	H	CA	CB
82	A				
83	H				
84	K				
85	K				
86	S				
87	H				
88	E				
89	E				
90	S			55.481	60.343
91	H	121.024	8.182	53.657	26.901
92	K	123.353	8.101	52.88	29.614
93	E	127.234	7.984	54.837	27.522

Table A3.10. Chemical shifts (ppm) of assigned A8-I60K+Ca(II) resonances

Res Num	Res Type	N	H	CA	CB
1	M				26.997
2	L	123.777	8.072	51.885	39.307
3	T	114.177	9.35	57.695	67.094
4	E	119.749	8.848	56.883	25.253
5	L	121.76	8.816	55.073	37.785
6	E	119.464	7.542	56.128	26.708
7	K	116.352	8.674	56.988	29.159
8	A	124.405	7.962	52.249	14.441
9	L	117.057	7.768	54.891	35.055
10	N	116.929	8.014	52.01	34.134
11	S	117.407	8.29	56.733	58.638
12	I	122.856	7.751	63.528	33.949
13	I	118.509	7.091	62.607	34.283
14	D	119.87	7.443	54.791	37.748
15	V	120.206	8.591	63.873	27.57
16	Y	118.497	7.477	59.371	34.934
17	H	114.913	8.136	54.987	26.097
18	K				
19	Y				
20	S	113.845	7.187	55.072	61.335
21	L	122.562	8.917	51.307	41.24
22	I	122.83	8.233	58.014	34.901
23	K				
24	G				
25	N			50.3	35.512
26	F	119.189	7.877	53.677	37.807
27	H			53.041	28.927
28	A	123.987	8.6	48.737	19.307
29	V	117.983	7.672	58.2	29.889
30	Y	127.803	9.356	55.029	34.67
31	R	122.301	8.59	58.623	26.064
32	D	117.561	8.997	54.287	36.651
33	D	120.232	7.29	53.826	38.408
34	L	121.26	8.541	53.916	36.961
35	K	118.841	7.707	57.523	28.415
36	K				
37	L				
38	L				
39	E			56.094	26.113
40	T	112.17	7.678	62.144	67.151

Res Num	Res Type	N	H	CA	CB
41	E				
42	S				
43	P				
44	Q				
45	Y				
46	I				
47	R				
48	K				
49	K				
50	G				
51	A				
52	D			54.454	36.645
53	V	122.864	7.489	62.767	27.709
54	W				
55	F			60.243	35.527
56	K	115.842	7.463	55.801	28.782
57	E	117.986	7.732	55.791	26.286
58	L	115.865	8.239	52.305	39.621
59	D	117.339	7.803	49.773	34.644
60	K	127.889	8.148	55.09	29.096
61	N	113.614	7.781	48.562	33.346
62	T	110.909	7.569	58.776	65.85
63	D	118.812	8.485	49.602	37.577
64	G	112.942	10.253	42.894	
65	A	121.75	7.947	47.603	19.512
66	V	125.734	9.374	58.115	28.617
67	N	130.085	9.06	48.81	35.24
68	F	120.638	8.906	59.759	35.281
69	Q	117.104	8.299	56.508	24.538
70	E	118.981	8.195	55.139	26.305
71	F	121.387	8.471	57.248	36.006
72	L	118.217	7.622	54.236	37.532
73	I	117.762	7.096	60.787	32.251
74	L	120.763	6.875	54.796	36.778
75	V	118.097	6.658	63.59	27.183
76	I	119.601	8.156	62.7	34.705
77	K				
78	M				
79	G	109.465	8.98	44.532	
80	V	122.272	8.877	64.279	28.52
81	A	121.619	8.02	52.231	15.442

Res Num	Res Type	N	H	CA	CB
82	A	121.415	8.407	51.742	14.869
83	H	120.947	8.309	57.294	26.732
84	K	120.44	7.932	55.905	28.697
85	K	118.527	7.66	54.894	28.63
86	S	113.827	7.725	57.261	60.054
87	H	119.858	7.746	54.083	26.992
88	E	120.863	7.879	54.226	26.811
89	E	120.855	8.243	53.794	26.561
90	S	116.028	8.067	55.572	60.39
91	H	121.445	8.197	56.33	38.142
92	K	123.989	8.082	53.115	29.54
93	E	127.723	7.983	54.893	27.474

Table A3.11. Chemical shifts (ppm) of assigned A9-I60K-Ca(II) resonances

Res Number	Res Type	N	H	CO	CA	CB
1	M					
2	T					
3	S					
4	K					
5	M			173.601	52.629	31.598
6	S	121.302	9.428	171.482	54.16	62.212
7	Q	120.784	8.982	175.178	56.5	25.144
8	L	118.974	8.933	175.829	55.752	37.784
9	E	116.008	7.469	176.941	56.002	25.956
10	R	119.384	8.435	176.261	56.221	26.389
11	N	118.708	8.546	174.534	53.49	35.88
12	I	120.688	8.518	175.236	61.484	33.184
13	E	119.855	8.13	175.526	57.019	25.738
14	T	115.827	8.391	174.706	63.59	65.023
15	I	122.946	7.747	174.694	63.307	33.992
16	I	118.646	8.348	176.102	63.41	35.218
17	N	115.195	8.906	174.613	52.385	34.91
18	T	117.003	8.112	172.207	64.279	65.441
19	F	119.109	7.134	173.995	58.757	35.52
20	H	116.221	7.877	175.008	56.596	26.323
21	Q	117.124	8.935	176.357	56.098	24.822
22	Y	119.283	8.48	174.273	56.198	34.423
23	S	112.284	7.39	172.921	58.795	
24	V	122.337	7.666	177.585	63.23	28.108
25	K	123.29	8.205	175.625	55.974	28.063
26	L	115.424	7.144	174.11	51.569	38.638
27	G	104.996	7.671	171.263	42.111	
28	H	111.607	7.593		48.728	24.336
29	P			173.536	60.95	28.44
30	D	115.027	9.077	171.824	53.469	36.534
31	T	109.468	7.936	169.822	57.938	68.613
32	L	120.178	8.362	171.76	52.245	42.946
33	N	120.409	9.242	173.739	47.612	36.635
34	Q	117.566	8.297	175.324	59.133	24.055
35	G	109.873	9.743	174.847	43.861	
36	E	122.67	8.72	177.615	55.462	26.253
37	F	119.976	8.857	173.022	58.364	36.215
38	K	119.22	8.716	174.697	56.966	28.371
39	E	114.755	7.345	176.278	55.6	25.837
40	L	119.533	7.524	176.625	54.878	37.221

Res Number	Res Type	N	H	CO	CA	CB
41	V	118.328	8.544	174.624	62.172	27.111
42	R	117.183	7.743	174.909	55.997	26.419
43	K	115.112	7.046	175.873	54.808	29.48
44	D	118.578	8.427	173.334	53.595	38.446
45	L	117.103	8.045	175.197	50.995	37.253
46	Q	113.402	6.607	175.176	55.956	25.976
47	N	119.443	10.357	176.746	53.948	34.901
48	F	123.687	8.745	175.296	54.734	32.685
49	L	112.353	8.177	175.084	53.653	37.21
50	K	116.454	7.329	174.164	52.544	29.745
51	K	121.286	7.358	173.94	54.862	28.929
52	E	121.096	8.673	173.912	54.255	26.762
53	N	116.614	8.599		50.496	34.516
54	K			172.705		
55	N	116.92	8.304	172.362	49.154	33.221
56	E	122.914	8.008	175.741	55.771	26.27
57	K	117.423	8.493	176.502	55.743	27.821
58	V	118.424	7.208	175.599	63.13	28.594
59	I	118.417	7.36	174.6	62.632	34.221
60	E	117.987	8.677	176.538	56.389	25.968
61	H	117.027	7.964	175.029	56.21	25.629
62	I	119.849	8.107	175.588	62.404	34.773
63	M	115.716	8.499	176.248	54.565	27.7
64	E	119.33	8.337	176.566	55.89	26.127
65	D	121.277	8.098	176.134	54.904	37.523
66	L	117.703	8.018	175.498	54.623	37.878
67	D	114.45	7.363	176.71	53.541	37.693
68	T	116.743	8.526	172.283	62.489	65.852
69	N	117.622	7.822	173.01	49.433	35.256
70	A	121.829	7.151	175.696	52.327	16.328
71	D	110.782	8.307	174.009	50.892	37.567
72	K	121.546	7.941	173.999	53.636	29.599
73	Q	123.079	8.769	173.225	53.316	26.066
74	L	124.583	9.082	173.536	50.478	41.05
75	S	119.177	8.894	172.111	53.906	62.436
76	F	121.511	9.173	174.022	57.898	35.092
77	E	116.146	8.724	176.247	57.795	25.328
78	E	118.962	7.769	175.967	56.019	27.255
79	F	120.363	8.377	173.162	58.09	35.145
80	I	117.878	7.942	174.976	59.46	31.584
81	M	118.974	7.958	175.923	56.215	27.925

Res Number	Res Type	N	H	CO	CA	CB
82	L	118.661	8.249	176.972	55.648	39.282
83	M	117.144	8.256	177.561	55.103	28.112
84	A	123.295	8.994	176.57	52.511	15.293
85	R	117.88	8.574	177.605	56.926	27.923
86	L	118.307	8.833	176.782	55.094	39.117
87	T	116.927	8.3	173.563	65.281	
88	W	121.946	8.932	175.217	57.566	26.037
89	A	116.604	8.275	176.459	51.303	15.348
90	S	109.172	7.534	170.204	57.352	60.184
91	H	117.566	7.265	172.583	54.176	27.249
92	E	120.531	8.186	174.039	52.528	29.208
93	K	120.079	8.159	172.222	52.569	29.387
94	M	121.894	8.423		53.499	26.923
95	H					
96	E					
97	G					
98	D			173.577	51.36	38.217
99	E	120.284	8.526	174.053	53.531	26.782
100	G	108.929	8.323		41.503	
101	P			175.043	60.63	28.518
102	G	108.173	8.517	171.309	42.354	
103	H	118.219	8.078	171.94	53.213	27.275
104	H	124.188	8.337	171.517	51.072	28.939
105	H	121.716	8.146		50.85	30.062
106	K					
107	P			174.756	60.245	28.701
108	G	108.863	8.555	171.466	42.264	
109	L	121.201	8.218	175.382	52.395	38.704
110	G	109.405	8.543	171.33	42.398	
111	E	119.855	8.275	174.26	53.54	26.86
112	G	109.286	8.502	171.062	42.306	
113	T	115.859	8.09		56.639	66.72
114	P					
107*	P			174.04	59.776	30.864
108*	G	109.594	8.644	171.182	42.311	
109*	L	121.318	8.417		52.539	38.701
111*	E			174.17		
112*	G	109.582	8.517	170.212	42.408	
113*	T	113.002	7.76		55.82	67.295

Table A3.12. Chemical shifts (ppm) of assigned A9-I60K+Ca(II) resonances

Res Number	Res Type	N	H	CO	CA	CB
1	M					
2	T					
3	S					
4	K	123.067	8.55	173.506		33.064
5	M	121.554	8.296		54.088	30.514
6	S			171.282	55.661	63.633
7	Q	121.532	9.386	175.193	57.612	26.476
8	L	117.171	8.541	176.316	56.15	40.159
9	E	116.26	8.26	177.4	58.448	28.474
10	R	120.102	8.664	176.251	57.645	27.474
11	N	119.004	8.364	174.405	54.68	36.895
12	I	119.062	8.234	174.96	62.657	34.435
13	E	121.093	8.471	175.644	58.051	27.049
14	T	116.467	8.503	175.014	65.204	66.358
15	I	123.907	7.942	174.743	65.147	36.051
16	I	119.54	8.475	175.395	64.392	35.957
17	N	117.92	9.385	176.307	54.113	35.652
18	T	117.509	8.501	172.422	65.99	79.285
19	F	120.043	8.263	174.442	61.062	36.849
20	H	115.912	8.597	173.621	55.688	27.444
21	Q	118.261	8.029	174.037	56.314	25.776
22	Y	111.213	6.978	174.319	58.018	37.951
23	S	114.337	8.809	174.454	60.575	58.889
24	V	114.724	6.987	174.299	60.439	30.37
25	K	121.683	7.412	174.767	59.43	30.796
26	L	117.36	9.995		51.253	43.688
27	G					
28	H					
29	P			174.141	62.424	29.392
30	D	121.847	10.828	172.396	51.587	40.843
31	T	105.002	7.516	171.614	56.963	70.961
32	L	123.597	9.364	173.896	50.645	41.65
33	N	123.265	10.029	172.292	48.618	35.477
34	Q	116.724	8.878	175.116	58.6	27.271
35	G	105.921	8.257	174.642	45.335	
36	E	122.391	8.481	175.449	57.143	28.959
37	F	116.926	8.855	173.583	59.419	37.563
38	K	115.518	8.51	175.755	58.514	30.372
39	E	118.038	7.474	174.072	57.88	27.115
40	L	120.876	7.311	177.493	57.218	39.538

Res Number	Res Type	N	H	CO	CA	CB
41	V	115.711	8.167	175.552	63.953	28.798
42	R	117.306	7.646	174.815	56.568	28.068
43	K	115.843	7.757	175.338	56.057	30.747
44	D	117.496	8.708	174.255	55.776	40.98
45	L	119.4	7.085	174.041	51.957	38.808
46	Q	111.767	6.154	173.202	55.926	27.565
47	N	118.104	10.279	175.212	54.11	37.345
48	F	123.492	9.803	174.632	56.282	35.16
49	L	117.082	8.035	173.119	51.406	37.647
50	K	120.61	6.867	176.084	58.593	30.447
51	K	117.78	8.571	177.044	57.585	29.73
52	E	122.914	9.943	174.325	59.523	25.714
53	N	112.125	8.291	174.058	53.096	37.691
54	K	115.798	7.304	173.32	55.549	30.157
55	N	116.988	7.885	171.703	50.106	38.424
56	E	124.951	9.056	175.15	58.238	27.748
57	K	115.73	8.135	177.013	56.441	29.142
58	V	120.65	7.699	176.041	64.31	28.682
59	I	118.298	7.317	175.892	61.535	33.39
60	E	117.995	8.213	176.437	57.918	26.505
61	H	118.727	8.123	174.691	56.98	26.599
62	I	120.837	8.373	175.385	63.751	35.769
63	M	117.527	7.916	174.325	58.168	28.138
64	E	116.507	7.985	176.525	57.506	27.198
65	D	118.138	7.978	175.488	54.787	39.223
66	L	116.384	7.585	174.888	53.165	41.282
67	D	118.567	7.579	174.63	50.929	36.888
68	T	119.617	8.407	173.131	63.13	66.911
69	N	115.327	7.839	171.694	50.095	34.951
70	A	120.168	7.928	173.362	51.538	14.829
71	D	117.113	8.292	174.636	51.196	38.438
72	K	116.356	10.355	171.996	55.231	25.986
73	Q	113	7.854	172.122	51.401	29.429
74	L	122.599	10.254	174.745	50.794	40.916
75	S	119.393	9.091	172.404	54.605	63.079
76	F	123.896	9.956	173.779	61.578	35.429
77	E	116.639	9.052	175.098	57.956	26.655
78	E	116.329	7.343	177.143	55.993	28.085
79	F	119.289	8.659	174.934	59.431	38.335
80	I	118.834	8.898	173.308	60.858	34.432
81	M	117.934	6.944	177.207	54.589	26.847

Res Number	Res Type	N	H	CO	CA	CB
82	L	119.711	7.498	175.288	55.358	37.55
83	M	114.105	6.891	176.493	55.048	31.095
84	A	121.915	8.191	175.625	53.813	15.655
85	R	117.845	8.034	176.988	58.052	27.867
86	L	117.767	8.572		55.384	39.639
87	T			173.689	65.861	79.988
88	W	121.931	8.576	174.126	58.768	26.906
89	A	118.732	8.292	177.56	53.122	15.586
90	S	112.632	7.837	173.893	58.546	60.807
91	H	120.597	8.256	174.499	58.596	27.385
92	E	117.016	8.195	175.706	56.082	27.312
93	K	118.016	7.605	175.567	55.923	29.492
94	M	117.157	7.808	174.04	55.778	30.379
95	H	115.886	7.683	172.335	54.335	27.748
96	E	120.942	7.871	174.35	55.499	27.769
97	G	108.976	8.412	171.366	43.465	
98	D	120.048	8.191	173.602	52.775	39.181
99	E	119.986	8.498	174.004	54.703	27.976
100	G	108.922	8.291		42.759	
101	P			175.014	61.689	29.74
102	G	108.24	8.537	171.302	43.453	
103	H	118.243	8.083	171.965	54.355	28.496
104	H	124.055	8.336	171.525	52.055	30.191
105	H	121.642	8.139		54.621	31.247
106	K					
107	P			174.723	61.44	29.849
108	G	108.822	8.546	171.517	43.353	
109	L	121.2	8.218	175.323	53.549	39.776
110	G	109.241	8.557	171.469	43.528	
111	E	119.743	8.259	174.267	54.635	28.131
112	G	109.229	8.513	171.068	43.404	
113	T	115.754	8.093		57.81	67.876
114	P					
E60*		118.247	8.21			
P107*				174.018		
G108*		109.617	8.649	171.191	43.454	
L109*		121.26	8.41		53.6	39.854
G112*		109.623	8.534		43.52	
T113*		113.231	7.807		56.974	68.575

Table A3.13. Model-free analysis parameters for A8-I60K+Ca(II)

Res Num	R2 (Hz)	R2err	R1 (Hz)	R1err	hetNOE	err	S2	errS2	Te (ns)	errTe	Kex (Hz)	errKex	S2f	errS2f
1														
2	4.88	0.16	0.93	0.04	0.26	0.03	0.22	0.01	0.73	0.02			0.62	0.03
3	27.26	0.83	0.50	0.02	0.78	0.08	0.95	0.02						
4	28.69	0.21	0.53	0.01	0.88	0.09	0.98	0.01						
5	28.61	0.19	0.48	0.01	0.86	0.09	0.93	0.02			1.89	0.48		
6	28.11	0.62	0.47	0.01	0.96	0.10	0.95	0.02						
7	30.18	0.44	0.48	0.01	0.96	0.10	0.94	0.03			2.36	0.91		
8	28.89	0.26	0.50	0.01	0.88	0.09	0.99	0.01						
9	29.79	0.58	0.48	0.01	0.89	0.09	0.93	0.02			2.94	0.73		
10	30.30	0.72	0.47	0.02	0.95	0.09	0.93	0.04			3.30	1.32		
11	32.27	0.29	0.47	0.02	0.84	0.08	0.92	0.03			5.30	0.94		
12	29.27	0.45	0.49	0.02	0.87	0.09	1.00	0.01						
13	32.23	0.42	0.49	0.01	0.94	0.09	0.96	0.02			4.61	0.78		
14														
15	29.17	0.83	0.48	0.02	0.93	0.09	0.97	0.02						
16	30.73	0.78	0.49	0.02	0.95	0.09	0.95	0.04			3.72	1.48		
17			0.55	0.06										
18														
19														
20														
21														
22			0.64	0.04	0.69	0.07								
23														
24														
25														
26	45.77	2.20	0.70	0.04	0.70	0.07	0.88	0.03	0.87	1.92	20.23	2.20		
27														
28			0.46	0.06	0.91	0.09								

Res Num	R2 (Hz)	R2err	R1 (Hz)	R1err	hetNOE	err	S2	errS2	Te (ns)	errTe	Kex (Hz)	errKex	S2f	errS2f
29	30.98	1.23	0.46	0.03	0.80	0.08	0.85	0.06			7.87	1.99		
30	24.76	0.92	0.49	0.03	0.99	0.10	0.91	0.03						
31	27.54	4.09	0.46	0.04	1.11	0.11	0.92	0.07						
32	29.79	0.17	0.55	0.03	0.94	0.09	0.92	0.04	15.51	7.10	1.60	0.65		
33	33.67	0.75	0.53	0.02	0.78	0.08	1.00	0.02			3.50	1.39		
34	30.52	1.18	0.52	0.02	0.86	0.09	1.00	0.02						
35	34.46	10.01	0.60	0.02										
36														
37														
38														
39														
40	27.89	0.45	0.49	0.03	0.79	0.08	0.96	0.01						
41														
42														
43														
44														
45														
46														
47														
48														
49														
50														
51														
52														
53	28.29	0.48	0.51	0.02	0.85	0.08	0.99	0.01						
54														
55														
56	28.79	0.78	0.51	0.01	0.88	0.09	0.99	0.01						
57	31.06	0.34	0.51	0.01	0.79	0.08	0.97	0.02			3.90	0.66		

Res Num	R2 (Hz)	R2err	R1 (Hz)	R1err	hetNOE	err	S2	errS2	Te (ns)	errTe	Kex (Hz)	errKex	S2f	errS2f
58			0.39	0.08										
59	33.48	3.10	0.46	0.02	0.83	0.08	0.88	0.03			8.85	3.23		
60	34.35	3.78												
61	27.46	0.20	0.53	0.02	0.88	0.09	0.96	0.03			1.55	0.76		
62	33.30	0.67	0.51	0.01	0.85	0.08	1.00	0.02			3.41	1.14		
63	29.80	0.61	0.47	0.02	0.90	0.09	0.99	0.01						
64	30.25	1.40	0.46	0.02	0.79	0.08	0.85	0.03			7.00	1.50		
65	27.26	0.12	0.52	0.01	0.93	0.09	1.00	0.00						
66	28.73	1.39	0.45	0.02	0.83	0.08	0.83	0.04			6.22	1.86		
67	30.50	0.78	0.52	0.03	0.79	0.08	0.95	0.05			5.23	1.77		
68	30.89	7.44	0.44	0.08	0.66	0.07	0.88	0.10	0.03	0.20				
69	32.21	0.82	0.49	0.01	0.86	0.09	0.96	0.02			4.35	1.03		
70	40.18	1.87	0.49	0.02	0.90	0.09	0.89	0.03			16.63	2.26		
71	30.49	1.12	0.49	0.02	0.93	0.09	0.94	0.03			3.81	1.43		
72	33.27	1.94	0.51	0.03	1.05	0.11	1.00	0.02						
73	33.13	1.26	0.49	0.01	0.94	0.09	0.98	0.02			4.41	1.50		
74	30.68	0.58	0.49	0.01	0.91	0.09	0.94	0.02			3.61	0.93		
75	31.64	0.60	0.49	0.01	0.89	0.09	0.96	0.02			3.66	0.85		
76	28.17	3.02	0.51	0.02	0.87	0.09	1.00	0.02						
77														
78														
79														
80	30.43	0.51	0.50	0.01	0.80	0.08	1.00	0.01						
81	30.84	0.67	0.51	0.01	0.82	0.08	1.00	0.01						
82	30.85	2.00	0.47	0.02	0.68	0.07	0.87	0.04	0.03	0.08	5.63	2.47		
83	30.01	1.02	0.54	0.01	0.83	0.08	1.00	0.01						
84	29.27	0.16	0.53	0.02	0.83	0.08	0.99	0.00						
85	29.99	0.54	0.60	0.02	0.75	0.07	0.94	0.03	0.75	3.74	3.09	0.72		
86	24.00	0.67	0.68	0.03	0.74	0.07	0.67	0.05	15.51	2.69				

Res Num	R2 (Hz)	R2err	R1 (Hz)	R1err	hetNOE	err	S2	errS2	Te (ns)	errTe	Kex (Hz)	errKex	S2f	errS2f
87	23.19	2.14	0.67	0.05	0.56	0.06	0.84	0.03	0.61	0.09				
88	16.08	0.40	0.79	0.03	0.70	0.07	0.70	0.07	1.27	1.96			0.75	0.03
89	11.80	0.30	1.01	0.05	0.54	0.05	0.49	0.02	0.95	0.10			0.78	0.03
90	7.52	0.19	1.03	0.06	0.45	0.05	0.33	0.02	0.89	0.06			0.69	0.03
91	7.17	0.51	0.89	0.07	0.35	0.03	0.36	0.03	0.76	0.03			0.65	0.04
92	4.88	0.11	0.93	0.05										
93	2.52	0.03	1.13	0.01	-0.22	-0.02	0.05	0.00	0.52	0.01			0.80	0.01

Table A3.14. Model-free analysis parameters for A9-I60K-Ca(II)

Res Num	R2 (Hz)	R2err	R1 (Hz)	R1err	hetNOE	err	S2	errS2	Te (ns)	errTe	Kex (Hz)	errKex	S2f	errS2f
1														
2														
3														
4														
5														
6			0.71	0.27										
7	25.18	2.13	0.57	0.04	0.71	0.07	0.94	0.04	1.36	4.39			0.80	0.06
8	27.83	2.33	0.50	0.03	0.85	0.08	0.84	0.04						
9	21.72	2.87	0.54	0.05	0.85	0.09	0.78	0.06						
10	24.89	1.51	0.55	0.02	0.93	0.09	0.84	0.07	23.57	10.50			0.81	0.04
11	25.97	1.05	0.50	0.03	0.78	0.08	0.80	0.03						
12														
13	28.76	0.43	0.63	0.02	0.77	0.08	0.95	0.03	1.75	6.73			0.91	0.02
14	28.78	0.95	0.49	0.02	0.79	0.08	0.85	0.02						
15	29.43	0.67	0.52	0.01	0.83	0.08	0.88	0.01						
16	30.33	1.75	0.55	0.02	1.03	0.10	0.92	0.02						
17	32.52	1.17	0.54	0.03	0.84	0.08	0.96	0.03						
18			0.59	0.01	0.70	0.07								
19	27.69	1.99	0.57	0.04	0.98	0.10	0.89	0.07	23.57	10.68			0.88	0.05
20	35.40	3.66	0.50	0.03	0.86	0.09	0.87	0.04						
21	34.57	1.47	0.54	0.02	0.83	0.08	0.96	0.02						
22	33.11	1.47	0.50	0.02	0.88	0.09	0.85	0.03			4.75	1.66		
23	24.92	0.83	0.51	0.02	0.78	0.08	0.97	0.03	1.78	9.49			0.77	0.02
24	35.56	1.75	0.54	0.02	0.83	0.08	0.89	0.03	0.00	0.00	6.77	1.85		
25	29.46	1.03	0.55	0.02	0.78	0.08	0.66	0.12	7.04	8.19	37.26	5.30		
26	32.79	1.70	0.52	0.03	0.91	0.09	0.93	0.04						
27	29.83	0.78	0.57	0.03	0.89	0.09	0.91	0.02						
28			0.57	0.02	0.90	0.09								

Res Num	R2 (Hz)	R2err	R1 (Hz)	R1err	hetNOE	err	S2	errS2	Te (ns)	errTe	Kex (Hz)	errKex	S2f	errS2f
29														
30	33.58	3.88	0.64	0.06	1.00	0.10	1.00	0.06						
31	27.26	1.15	0.54	0.03	0.73	0.07	0.85	0.03						
32	24.50	0.82	0.56	0.02	0.82	0.08	0.94	0.06	5.24	10.21			0.78	0.02
33	32.35	1.00	0.56	0.02	0.82	0.08	0.90	0.03			3.70	1.39		
34	29.21	1.16	0.58	0.02	0.93	0.09	0.93	0.02						
35	30.51	0.60	0.55	0.01	0.73	0.07	0.92	0.01						
36	28.60	1.26	0.55	0.02	0.78	0.08	0.89	0.03						
37	36.22	1.23	0.53	0.02	0.82	0.08	0.86	0.03			8.45	1.65		
38	29.25	0.59	0.53	0.01	0.81	0.08	0.89	0.01						
39	25.80	0.69	0.50	0.02	0.92	0.09	0.80	0.02						
40	31.28	0.54	0.54	0.01	0.85	0.08	0.88	0.02			2.66	0.86		
41	28.06	6.68	0.48	0.05										
42	29.95	1.49	0.58	0.03	0.74	0.07	0.94	0.03						
43	22.36	0.93	0.55	0.02	0.79	0.08	0.94	0.05	2.57	9.40			0.73	0.03
44	29.23	0.78	0.44	0.03	1.04	0.10	0.72	0.05			5.89	1.73		
45	31.51	0.50	0.50	0.01	0.81	0.08	0.85	0.02			3.20	0.83		
46	29.74	0.42	0.49	0.01	0.81	0.08	0.81	0.02			3.19	0.89		
47	31.76	1.71	0.53	0.02	0.87	0.09	0.91	0.03						
48	40.13	3.45	0.49	0.04	0.85	0.09	0.83	0.08			12.76	4.26		
49	34.60	3.30	0.49	0.02	0.87	0.09	0.82	0.03						
50	32.09	0.78	0.50	0.01	0.79	0.08	0.84	0.02			4.02	1.09		
51	33.47	10.54	0.46	0.06										
52	26.95	1.35	0.61	0.03	0.70	0.07	0.94	0.03	1.25	3.95			0.86	0.04
53			0.47	0.03	0.79	0.08								
54														
55			0.55	0.02										
56	47.66	2.54	0.52	0.02	0.79	0.08	0.87	0.04			19.14	3.15		
57	27.14	1.19	0.58	0.01	0.74	0.07	0.95	0.03	1.38	7.33			0.86	0.03

Res Num	R2 (Hz)	R2err	R1 (Hz)	R1err	hetNOE	err	S2	errS2	Te (ns)	errTe	Kex (Hz)	errKex	S2f	errS2f
58	31.13	5.01	0.50	0.04	0.85	0.09	0.83	0.06						
59			0.45											
60	32.24	0.74	0.51	0.01	0.68	0.07	0.82	0.03	0.02	0.01	5.22	1.25		
61	34.51	1.44	0.52	0.01	1.03	0.10	0.86	0.02			6.51	1.46		
62	43.18	5.11	0.49	0.01	0.85	0.09	0.80	0.02			17.31	4.80		
63	31.06	0.90	0.49	0.01	0.98	0.10	0.81	0.02			4.56	1.03		
64	26.82	0.48	0.52	0.01	0.76	0.08	0.98	0.02	0.96	6.39			0.83	0.02
65	28.17	0.33	0.53	0.01	0.76	0.08	0.87	0.01						
66	26.96	0.62	0.52	0.01	0.83	0.08	0.84	0.02						
67	26.38	0.40	0.49	0.01	0.81	0.08	0.81	0.01						
68			0.60	0.08	0.66	0.07								
69	25.07	0.57	0.55	0.01	0.71	0.07	0.97	0.03	0.77	3.64			0.82	0.04
70	27.25	0.57	0.59	0.01	0.68	0.07	0.95	0.01	0.96	2.83			0.88	0.02
71	29.68	0.66	0.50	0.01	0.70	0.07	0.83	0.01			2.43	0.70		
72	30.12	0.47	0.52	0.01	0.78	0.08	0.89	0.01						
73	26.16	0.51	0.53	0.01	0.73	0.07	0.84	0.01						
74	27.01	0.68	0.52	0.01	0.71	0.07	0.84	0.01						
75	32.33	1.29	0.52	0.02	0.77	0.08	0.84	0.04			5.77	1.66		
76	26.49	1.40	0.57	0.02	0.72	0.07	0.95	0.03	1.34	4.20			0.83	0.03
77	28.69	1.04	0.52	0.02	0.70	0.07	0.87	0.02						
78	30.81	1.05	0.49	0.02	0.77	0.08	0.87	0.02						
79	23.35	0.95	0.53	0.02	0.88	0.09	0.82	0.07	23.57	10.47			0.76	0.02
80	32.18	1.27	0.56	0.02	0.84	0.08	0.95	0.02						
81	35.78	0.97	0.57	0.01	0.76	0.08	0.96	0.02			4.06	1.21		
82	36.28	1.96	0.40	0.02	0.84	0.08	0.68	0.03			13.48	2.33		
83			0.45	0.02	0.86	0.09								
84	29.67	0.63	0.53	0.01	0.83	0.08	0.89	0.01						
85	31.27	1.12	0.53	0.01	0.85	0.09	0.90	0.01						
86	29.59	1.15	0.49	0.02	0.81	0.08	0.85	0.02						

Res Num	R2 (Hz)	R2err	R1 (Hz)	R1err	hetNOE	err	S2	errS2	Te (ns)	errTe	Kex (Hz)	errKex	S2f	errS2f
87														
88	31.53	1.60	0.53	0.02	0.91	0.09	0.91	0.04						
89	32.36	1.27	0.49	0.02	0.77	0.08	0.70	0.12	5.98	8.62	41.52	5.53		
90	31.89	1.71	0.51	0.03	0.85	0.09	0.91	0.04						
91	33.12	1.76	0.56	0.03	0.76	0.08	0.97	0.03						
92														
93	13.28	1.76	0.69	0.04	0.50	0.05	0.66	0.05	1.50	0.13			0.57	0.04
94	13.85	0.93	0.91	0.07	0.50	0.05	0.59	0.03	1.58	0.16			0.66	0.03
95														
96														
97														
98														
99	6.13	0.50	1.17	0.04	0.33	0.03	0.25	0.02	1.40	0.05			0.60	0.02
100	5.45	0.57	1.27	0.04	0.32	0.03	0.19	0.03	1.41	0.05			0.62	0.02
101														
102	4.66	0.66	1.11	0.07	0.38	0.04	0.20	0.03	1.52	0.08			0.52	0.04
103	3.90	0.71	1.17	0.07	0.52	0.05	0.14	0.04	1.89	0.17			0.49	0.03
104	4.24	0.84	1.20	0.06	0.31	0.03	0.15	0.04	1.41	0.05			0.57	0.03
105	3.72	0.71	1.16	0.09	0.37	0.04	0.14	0.05	1.53	0.07			0.52	0.04
106														
107														
108	3.84	0.78	1.20	0.05	0.27	0.03	0.13	0.04	1.35	0.04			0.56	0.03
109	2.44	0.62	1.28	0.04	0.26	0.03	0.04	0.03	1.35	0.04			0.56	0.02
110	3.15	0.70	1.09	0.06	0.13	0.01	0.11	0.04	1.18	0.02			0.54	0.03
111	1.89	0.54	1.17	0.05	0.14	0.01	0.03	0.03	1.22	0.02			0.53	0.02
112	1.91	0.61	0.97	0.05	-0.19	-0.02	0.05	0.03	0.94	0.01			0.51	0.03
113	0.64	0.55	0.96	0.05	-0.29	-0.03	0.00	0.02	0.89	0.01			0.50	0.02

Res Num	R2 (Hz)	R2err	R1 (Hz)	R1err	hetNOE	err	S2	errS2	Te (ns)	errTe	Kex (Hz)	errKex	S2f	errS2f
108	3.59	0.78	1.38	0.07	0.37	0.04								
112	3.99	0.77	1.01	0.06	0.17	0.02								
113	1.16	0.23	1.03	0.03	-0.16	-0.02								

Table A3.15. Model-free analysis parameters for A9-I60K+Ca(II)

Res Num	R2 (Hz)	R2err	R1 (Hz)	R1err	hetNOE	err	S2	errS2	Te (ns)	errTe	Kex (Hz)	errKex	S2f	errS2f
1														
2														
3														
4														
5														
6			0.71	0.27										
7	25.18	2.13	0.57	0.04	0.71	0.07	0.94	0.04	1.36	4.39			0.80	0.06
8	27.83	2.33	0.50	0.03	0.85	0.08	0.84	0.04						
9	21.72	2.87	0.54	0.05	0.85	0.09	0.78	0.06						
10	24.89	1.51	0.55	0.02	0.93	0.09	0.84	0.07	23.57	10.50			0.81	0.04
11	25.97	1.05	0.50	0.03	0.78	0.08	0.80	0.03						
12														
13	28.76	0.43	0.63	0.02	0.77	0.08	0.95	0.03	1.75	6.73			0.91	0.02
14	28.78	0.95	0.49	0.02	0.79	0.08	0.85	0.02						
15	29.43	0.67	0.52	0.01	0.83	0.08	0.88	0.01						
16	30.33	1.75	0.55	0.02	1.03	0.10	0.92	0.02						
17	32.52	1.17	0.54	0.03	0.84	0.08	0.96	0.03						
18			0.59	0.01	0.70	0.07								
19	27.69	1.99	0.57	0.04	0.98	0.10	0.89	0.07	23.57	10.68			0.88	0.05
20	35.40	3.66	0.50	0.03	0.86	0.09	0.87	0.04						
21	34.57	1.47	0.54	0.02	0.83	0.08	0.96	0.02						
22	33.11	1.47	0.50	0.02	0.88	0.09	0.85	0.03			4.75	1.66		
23	24.92	0.83	0.51	0.02	0.78	0.08	0.97	0.03	1.78	9.49			0.77	0.02
24	35.56	1.75	0.54	0.02	0.83	0.08	0.89	0.03			6.77	1.85		
25	29.46	1.03	0.55	0.02	0.78	0.08	0.66	0.12	7.04	8.19	37.26	5.30		
26	32.79	1.70	0.52	0.03	0.91	0.09	0.93	0.04						
27	29.83	0.78	0.57	0.03	0.89	0.09	0.91	0.02						
28			0.57	0.02	0.90	0.09								

Res Num	R2 (Hz)	R2err	R1 (Hz)	R1err	hetNOE	err	S2	errS2	Te (ns)	errTe	Kex (Hz)	errKex	S2f	errS2f
29														
30	33.58	3.88	0.64	0.06	1.00	0.10	1.00	0.06						
31	27.26	1.15	0.54	0.03	0.73	0.07	0.85	0.03						
32	24.50	0.82	0.56	0.02	0.82	0.08	0.94	0.06	5.24	10.21			0.78	0.02
33	32.35	1.00	0.56	0.02	0.82	0.08	0.90	0.03			3.70	1.39		
34	29.21	1.16	0.58	0.02	0.93	0.09	0.93	0.02						
35	30.51	0.60	0.55	0.01	0.73	0.07	0.92	0.01						
36	28.60	1.26	0.55	0.02	0.78	0.08	0.89	0.03						
37	36.22	1.23	0.53	0.02	0.82	0.08	0.86	0.03			8.45	1.65		
38	29.25	0.59	0.53	0.01	0.81	0.08	0.89	0.01						
39	25.80	0.69	0.50	0.02	0.92	0.09	0.80	0.02						
40	31.28	0.54	0.54	0.01	0.85	0.08	0.88	0.02			2.66	0.86		
41	28.06	6.68	0.48	0.05										
42	29.95	1.49	0.58	0.03	0.74	0.07	0.94	0.03						
43	22.36	0.93	0.55	0.02	0.79	0.08	0.94	0.05	2.57	9.40			0.73	0.03
44	29.23	0.78	0.44	0.03	1.04	0.10	0.72	0.05			5.89	1.73		
45	31.51	0.50	0.50	0.01	0.81	0.08	0.85	0.02			3.20	0.83		
46	29.74	0.42	0.49	0.01	0.81	0.08	0.81	0.02			3.19	0.89		
47	31.76	1.71	0.53	0.02	0.87	0.09	0.91	0.03						
48	40.13	3.45	0.49	0.04	0.85	0.09	0.83	0.08			12.76	4.26		
49	34.60	3.30	0.49	0.02	0.87	0.09	0.82	0.03						
50	32.09	0.78	0.50	0.01	0.79	0.08	0.84	0.02			4.02	1.09		
51	33.47	10.54	0.46	0.06										
52	26.95	1.35	0.61	0.03	0.70	0.07	0.94	0.03	1.25	3.95			0.86	0.04
53			0.47	0.03	0.79	0.08								
54														
55			0.55	0.02										
56	47.66	2.54	0.52	0.02	0.79	0.08	0.87	0.04			19.14	3.15		
57	27.14	1.19	0.58	0.01	0.74	0.07	0.95	0.03	1.38	7.33			0.86	0.03

Res Num	R2 (Hz)	R2err	R1 (Hz)	R1err	hetNOE	err	S2	errS2	Te (ns)	errTe	Kex (Hz)	errKex	S2f	errS2f
58	31.13	5.01	0.50	0.04	0.85	0.09	0.83	0.06						
59			0.45											
60	32.24	0.74	0.51	0.01	0.68	0.07	0.82	0.03	0.02	0.01	5.22	1.25		
61	34.51	1.44	0.52	0.01	1.03	0.10	0.86	0.02			6.51	1.46		
62	43.18	5.11	0.49	0.01	0.85	0.09	0.80	0.02			17.31	4.80		
63	31.06	0.90	0.49	0.01	0.98	0.10	0.81	0.02			4.56	1.03		
64	26.82	0.48	0.52	0.01	0.76	0.08	0.98	0.02	0.96	6.39			0.83	0.02
65	28.17	0.33	0.53	0.01	0.76	0.08	0.87	0.01						
66	26.96	0.62	0.52	0.01	0.83	0.08	0.84	0.02						
67	26.38	0.40	0.49	0.01	0.81	0.08	0.81	0.01						
68			0.60	0.08	0.66	0.07								
69	25.07	0.57	0.55	0.01	0.71	0.07	0.97	0.03	0.77	3.64			0.82	0.04
70	27.25	0.57	0.59	0.01	0.68	0.07	0.95	0.01	0.96	2.83			0.88	0.02
71	29.68	0.66	0.50	0.01	0.70	0.07	0.83	0.01			2.43	0.70		
72	30.12	0.47	0.52	0.01	0.78	0.08	0.89	0.01						
73	26.16	0.51	0.53	0.01	0.73	0.07	0.84	0.01						
74	27.01	0.68	0.52	0.01	0.71	0.07	0.84	0.01						
75	32.33	1.29	0.52	0.02	0.77	0.08	0.84	0.04			5.77	1.66		
76	26.49	1.40	0.57	0.02	0.72	0.07	0.95	0.03	1.34	4.20			0.83	0.03
77	28.69	1.04	0.52	0.02	0.70	0.07	0.87	0.02						
78	30.81	1.05	0.49	0.02	0.77	0.08	0.87	0.02						
79	23.35	0.95	0.53	0.02	0.88	0.09	0.82	0.07	23.57	10.47			0.76	0.02
80	32.18	1.27	0.56	0.02	0.84	0.08	0.95	0.02						
81	35.78	0.97	0.57	0.01	0.76	0.08	0.96	0.02			4.06	1.21		
82	36.28	1.96	0.40	0.02	0.84	0.08	0.68	0.03			13.48	2.33		
83			0.45	0.02	0.86	0.09								
84	29.67	0.63	0.53	0.01	0.83	0.08	0.89	0.01						
85	31.27	1.12	0.53	0.01	0.85	0.09	0.90	0.01						
86	29.59	1.15	0.49	0.02	0.81	0.08	0.85	0.02						

Res Num	R2 (Hz)	R2err	R1 (Hz)	R1err	hetNOE	err	S2	errS2	Te (ns)	errTe	Kex (Hz)	errKex	S2f	errS2f
87														
88	31.53	1.60	0.53	0.02	0.91	0.09	0.91	0.04						
89	32.36	1.27	0.49	0.02	0.77	0.08	0.70	0.12	5.98	8.62	41.52	5.53		
90	31.89	1.71	0.51	0.03	0.85	0.09	0.91	0.04						
91	33.12	1.76	0.56	0.03	0.76	0.08	0.97	0.03						
92														
93	13.28	1.76	0.69	0.04	0.50	0.05	0.66	0.05	1.50	0.13			0.57	0.04
94	13.85	0.93	0.91	0.07	0.50	0.05	0.59	0.03	1.58	0.16			0.66	0.03
95														
96														
97														
98														
99	6.13	0.50	1.17	0.04	0.33	0.03	0.25	0.02	1.40	0.05			0.60	0.02
100	5.45	0.57	1.27	0.04	0.32	0.03	0.19	0.03	1.41	0.05			0.62	0.02
101														
102	4.66	0.66	1.11	0.07	0.38	0.04	0.20	0.03	1.52	0.08			0.52	0.04
103	3.90	0.71	1.17	0.07	0.52	0.05	0.14	0.04	1.89	0.17			0.49	0.03
104	4.24	0.84	1.20	0.06	0.31	0.03	0.15	0.04	1.41	0.05			0.57	0.03
105	3.72	0.71	1.16	0.09	0.37	0.04	0.14	0.05	1.53	0.07			0.52	0.04
106														
107														
108	3.84	0.78	1.20	0.05	0.27	0.03	0.13	0.04	1.35	0.04			0.56	0.03
109	2.44	0.62	1.28	0.04	0.26	0.03	0.04	0.03	1.35	0.04			0.56	0.02
110	3.15	0.70	1.09	0.06	0.13	0.01	0.11	0.04	1.18	0.02			0.54	0.03
111	1.89	0.54	1.17	0.05	0.14	0.01	0.03	0.03	1.22	0.02			0.53	0.02
112	1.91	0.61	0.97	0.05	-0.19	-0.02	0.05	0.03	0.94	0.01			0.51	0.03
113	0.64	0.55	0.96	0.05	-0.29	-0.03	0.00	0.02	0.89	0.01			0.50	0.02

Res Num	R2 (Hz)	R2err	R1 (Hz)	R1err	hetNOE	err	S2	errS2	Te (ns)	errTe	Kex (Hz)	errKex	S2f	errS2f
108	3.59	0.78	1.38	0.07	0.37	0.04								
112	3.99	0.77	1.01	0.06	0.17	0.02								
113	1.16	0.23	1.03	0.03	-0.16	-0.02								

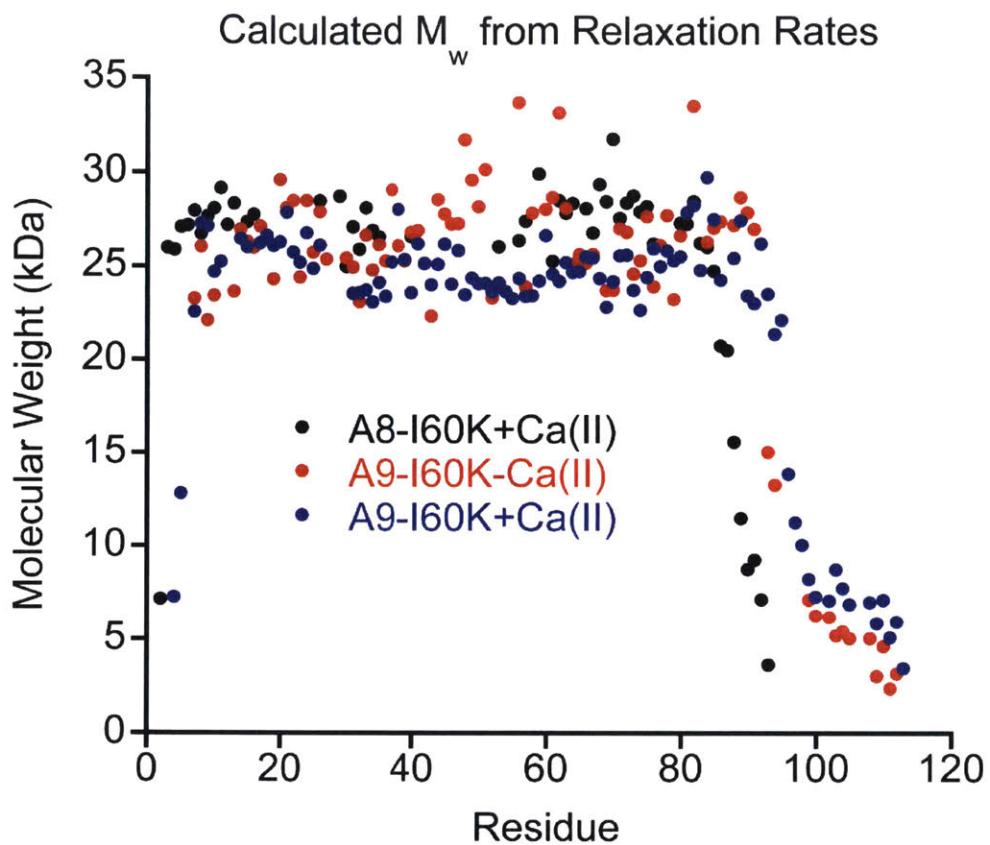


Figure A3.1. Calculated molecular weight based on the T_1/T_2 ratio for ^{15}N -A8-I60K in the presence of Ca(II) and ^{15}N -A9-I60K in the absence and presence of Ca(II).

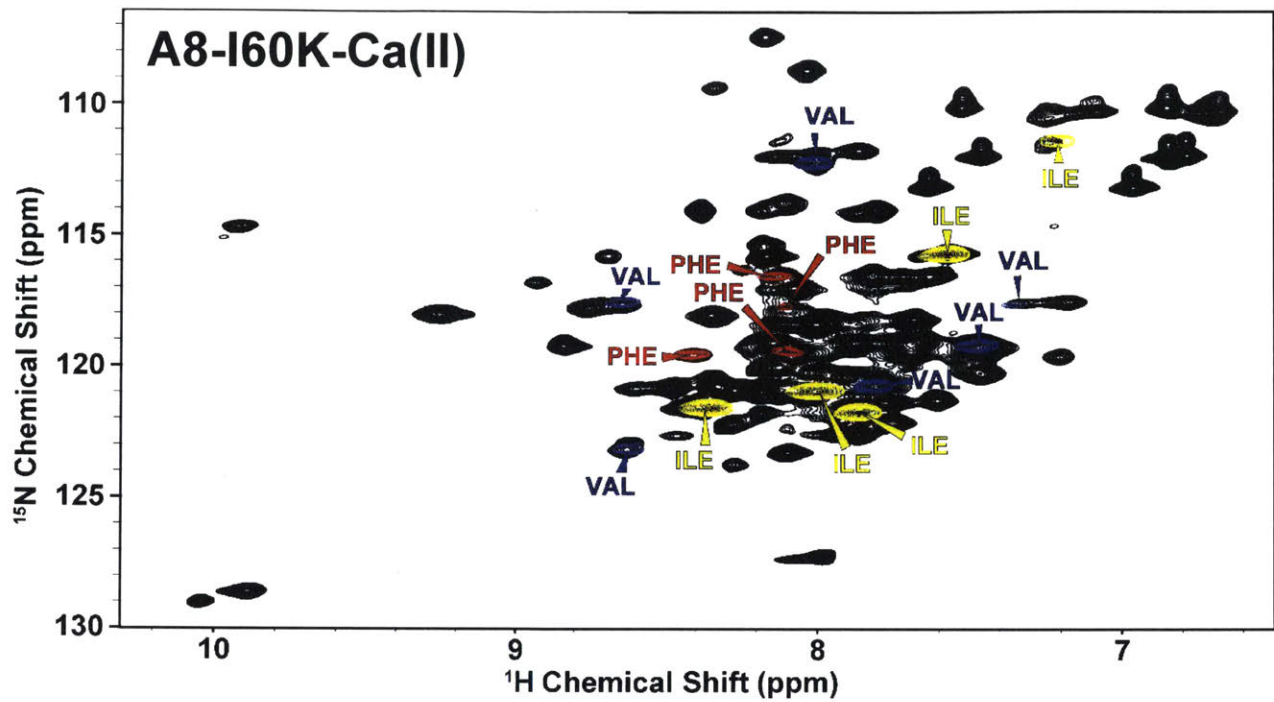


Figure A3.2. $[^1\text{H}-^{15}\text{N}]$ -HSQCs of A8-I60K with selective ^{15}N labeling (colored) overlaid onto a $[^1\text{H}-^{15}\text{N}]$ -HSQC from a uniformly labeled sample (black) in the absence of Ca(II). Note the twin $\text{W54N}^{\epsilon 1}$ peaks.

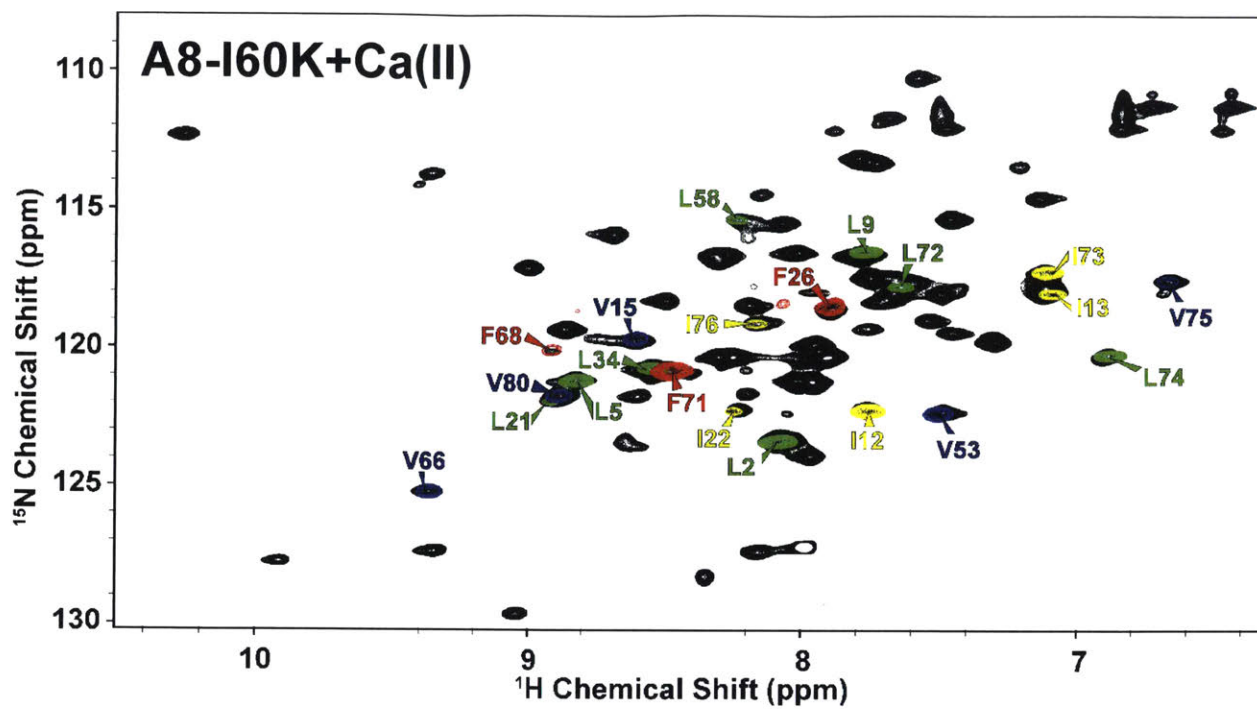


Figure A3.3. [^1H - ^{15}N]-HSQCs of A8-I60K with selective ^{15}N labeling (colored) overlaid onto a [^1H - ^{15}N]-HSQC from a uniformly labeled sample (black) in the presence of Ca(II).

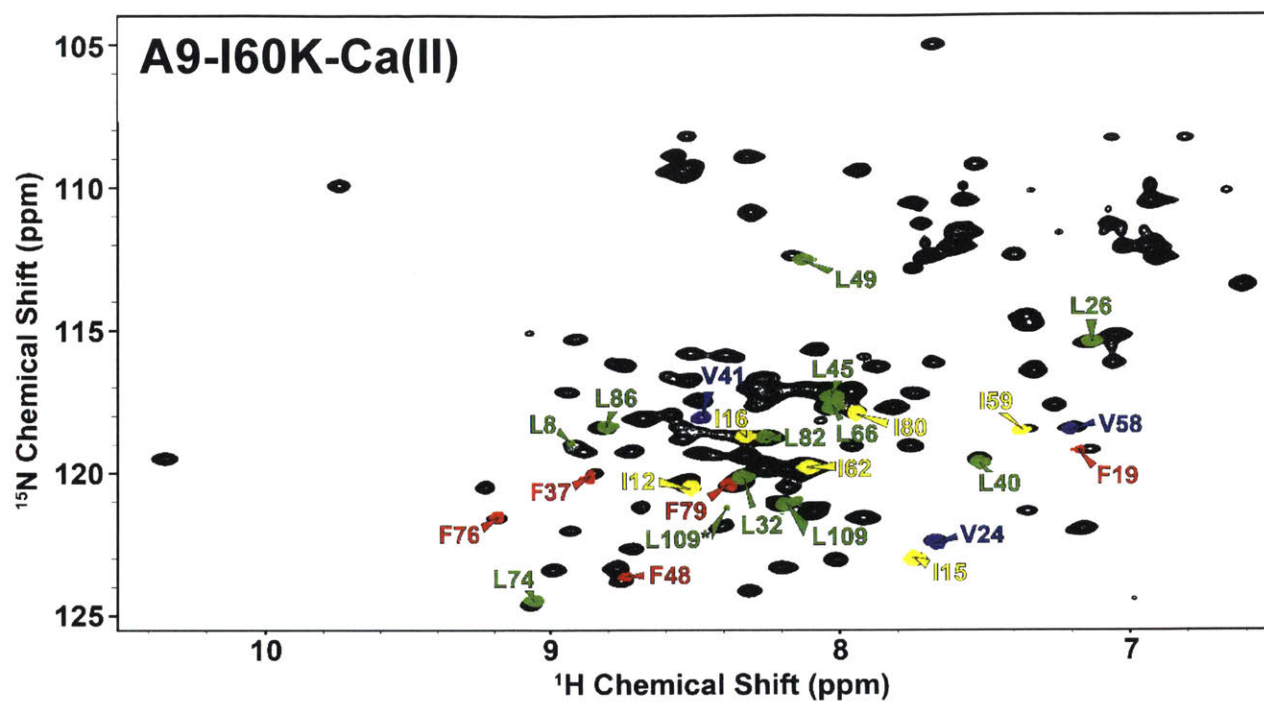


Figure A3.4. [^1H - ^{15}N]-HSQCs of A9-I60K with selective ^{15}N labeling (colored) overlaid onto a [^1H - ^{15}N]-HSQC from a uniformly labeled sample (black) in the absence of Ca(II).

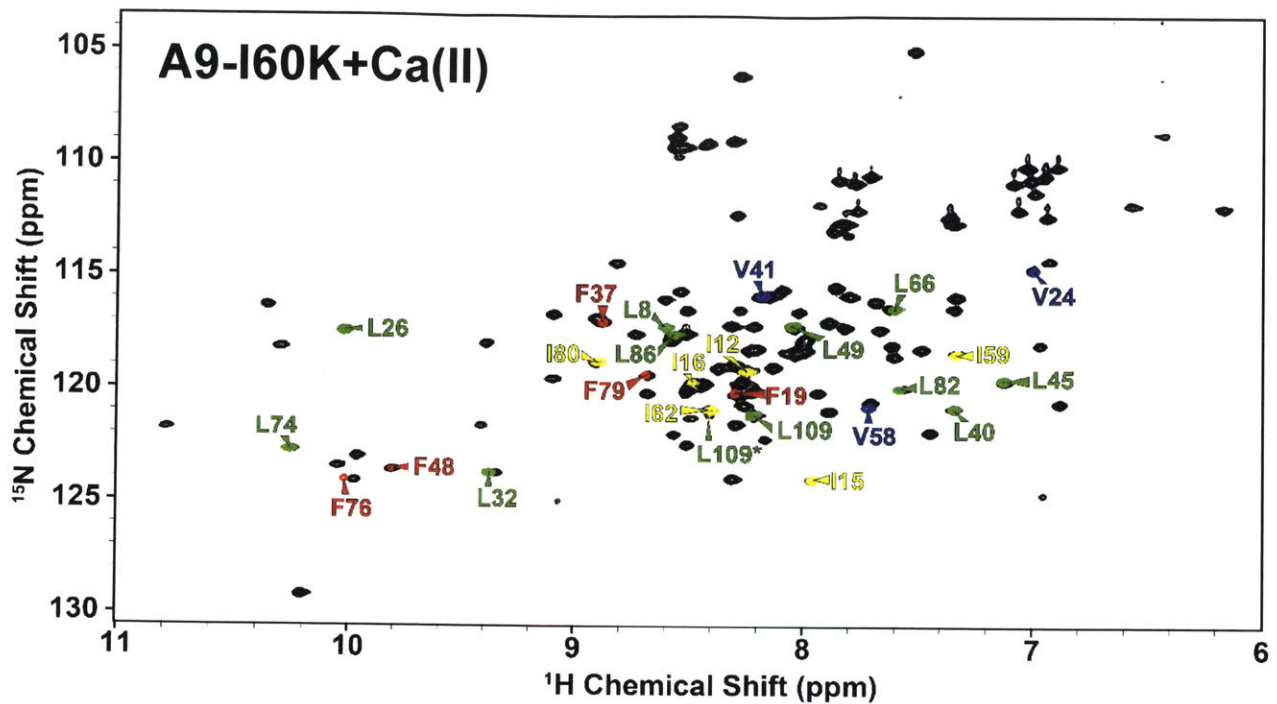


Figure A3.5. $[^1\text{H}-^{15}\text{N}]$ -HSQCs of A9-I60K with selective ^{15}N labeling (colored) overlaid onto a $[^1\text{H}-^{15}\text{N}]$ -HSQC from a uniformly labeled sample (black) in the presence of Ca(II).

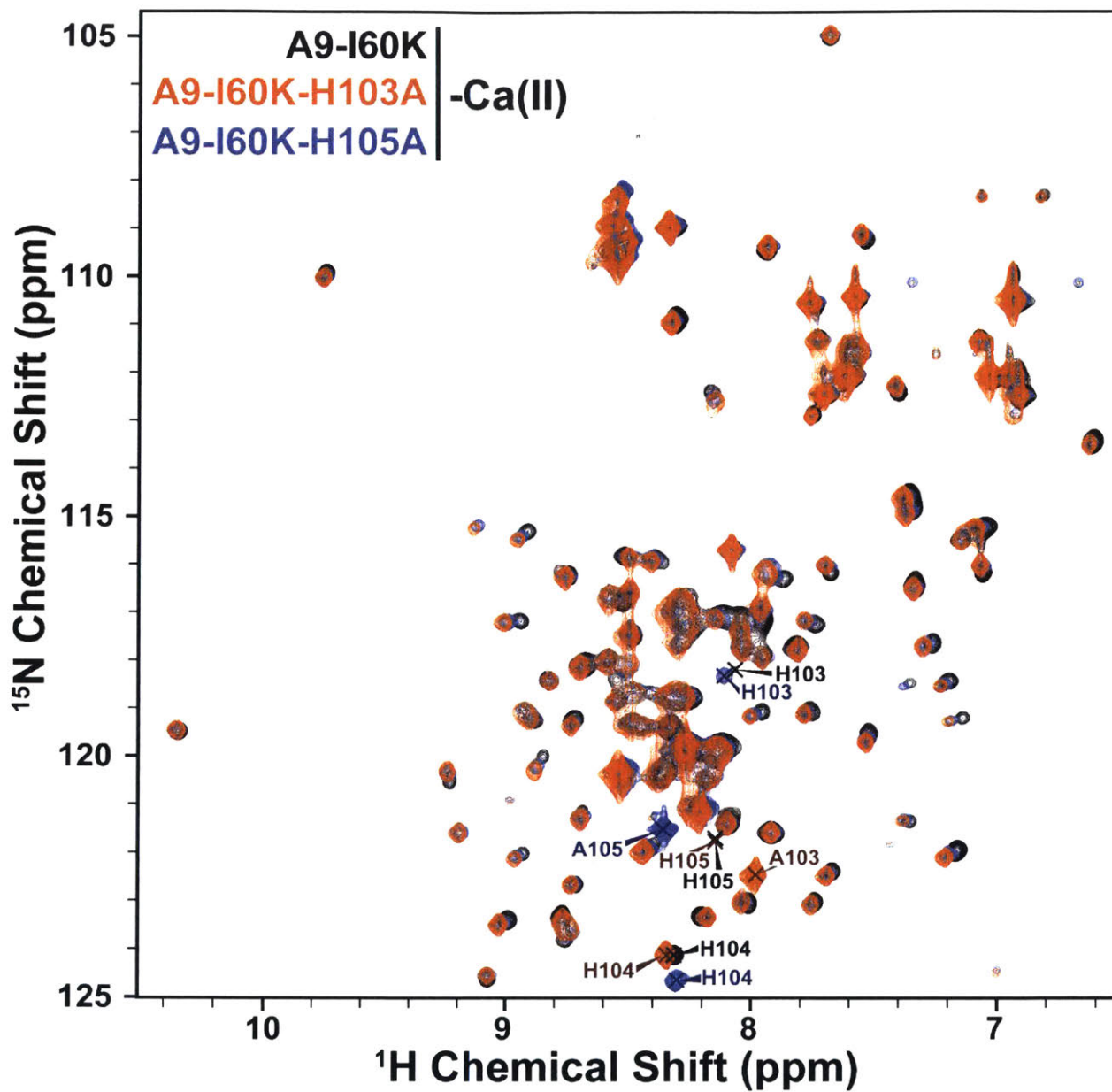


Figure A3.6. [^1H - ^{15}N]-HSQCs of [^{15}N]-A9-I60K (black), [^{15}N]-A9-I60K(H103A) (blue), and [^{15}N]-A9-I60K(H105A) (orange) absence of Ca(II).

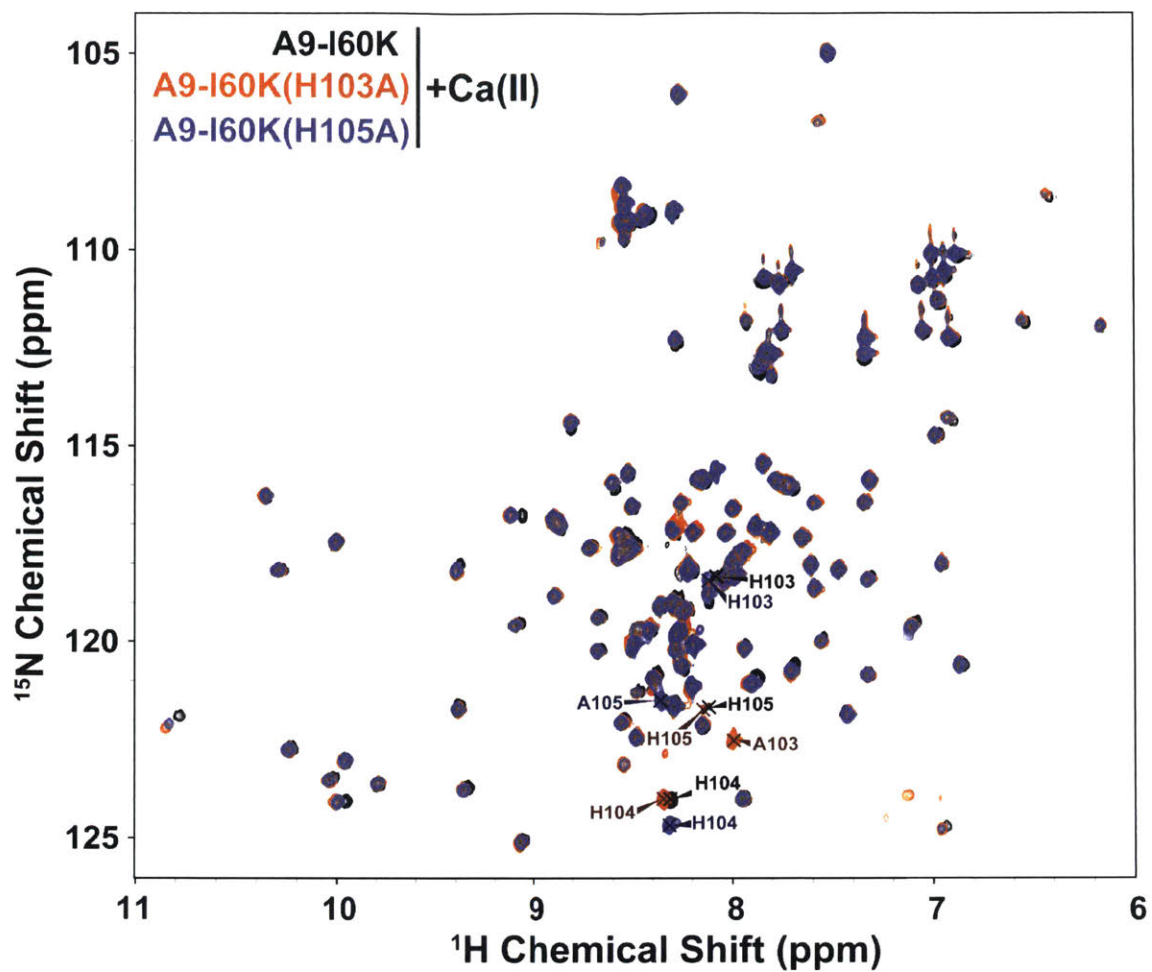


Figure A3.7. [^1H - ^{15}N]-HSQCs of [^{15}N]-A9-I60K (black), [^{15}N]-A9-I60K(H103A) (blue), and [^{15}N]-A9-I60K(H105A) (orange) presence of $\text{Ca}(\text{II})$.

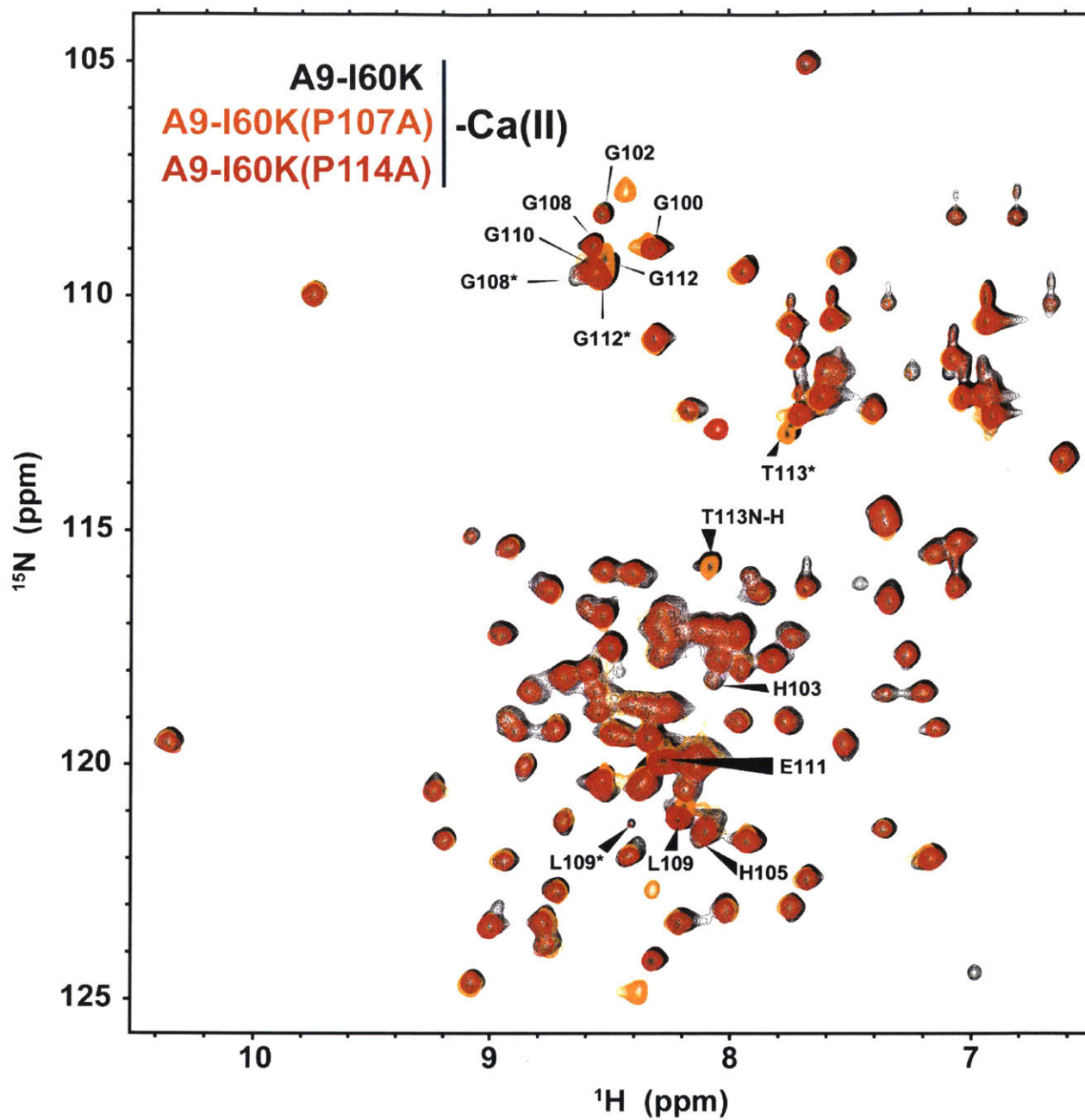


Figure A3.8. $[^1\text{H}-^{15}\text{N}]$ -HSQCs of $[^{15}\text{N}]$ -A9-I60K (black), $[^{15}\text{N}]$ -A9-I60K(P107A) (orange), and $[^{15}\text{N}]$ -A9-I60K(P114A) (red) in the absence of Ca(II).

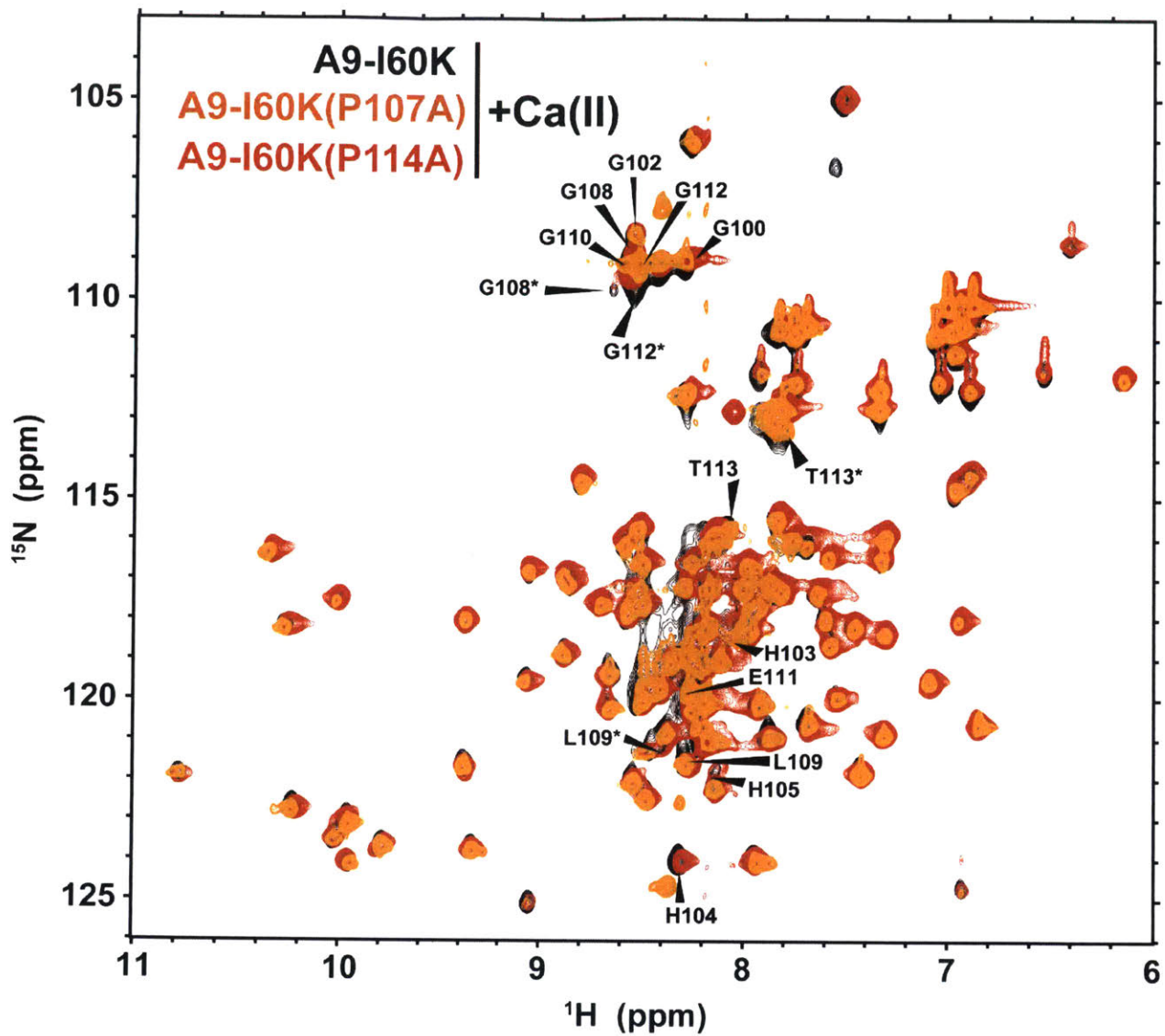


Figure A3.9. $[^1\text{H}-^{15}\text{N}]$ -HSQCs of $[^{15}\text{N}]$ -A9-I60K (black), $[^{15}\text{N}]$ -A9-I60K(P107A) (orange), and $[^{15}\text{N}]$ -A9-I60K(P114A) (red) in the presence of Ca(II).

A8-I60K+Ca(II)

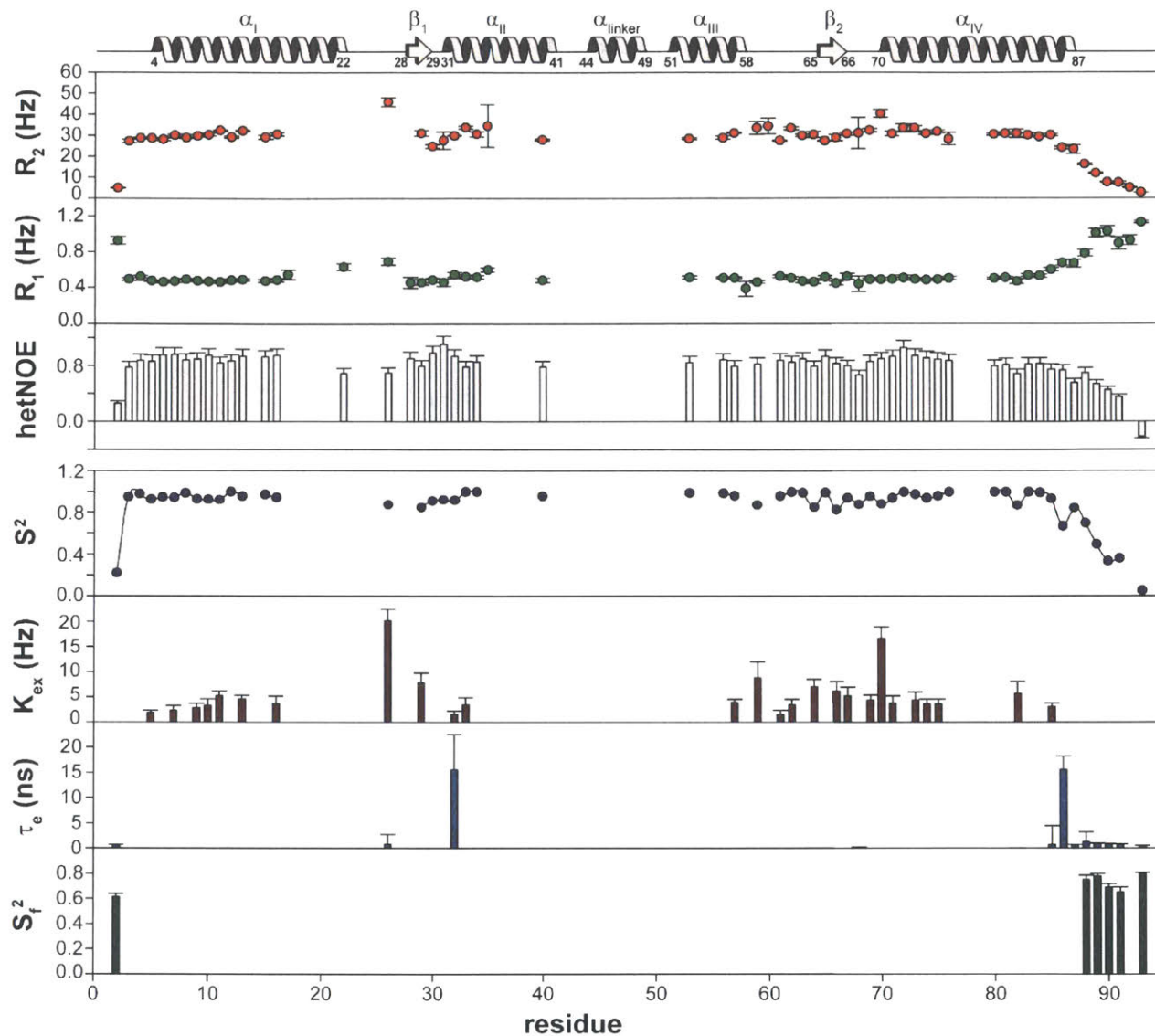


Figure A3.10. Relaxation and model-free analysis of A8-I60K in the presence of Ca(II).

Appendix 4: Several Dimer-Dimer Interface Variants of CP Exhibit Ca(II)-Induced Tetramerization

A4.1. Introduction

In the course of our work to discover tetramer-deficient variants of human CP, we tested several variant proteins that did not display the desired oligomeric properties. These variants have charged or polar residues in place of native hydrophobic residues at or near the tetramer interface. In this Appendix, we report the methods used to generate the plasmids encoding these variants, SDS-PAGE (Figure A4.1), and SEC chromatograms (Figures A4.2-A4.5). For a small subset of proteins, we also report velocity AUC (Figure A4.6). The I60S, I73R, I73S variants are all single mutants of the S100A8 subunit in CP-Ser. The CP-Ser(E57A)(I73R) and CP-Ser(E57K)(I73R) variants are double mutants of the S100A8 subunit of CP-Ser because unpublished diffraction data obtained by Dr. T. Nakashige in collaboration with the Drennan laboratory indicated that there was a hydrogen bond between (A8)E57 and (A8)R73, which may have assisted in tetramerization in the presence of Ca(II) and Mn(II). The W88R variant is a single mutant of the S100A9 subunit of CP-Ser. The CP-Ser(Δ Hb) and CP-Ser(Δ Hb)(Q69A) variants have many hydrophobic to hydrophilic mutations in the S100A8 subunit of CP-Ser along the tetramer interface. The specific mutations are detailed below. We chose (A8)Q69 for mutation because it appears to make a hydrogen bond between the dimers of the tetramer. Most of these variants did not display any perturbations to Ca(II)- or Mn(II)-induced tetramerization. The I73R variant was found to dynamically interconvert between the heterodimer and heterotetramer states by ultracentrifugation, and the I60S variant displayed incomplete tetramerization as determined by SEC.

A4.2. Generation of DNA for Variant Proteins

A modified Quick-Change site-directed mutagenesis protocol was employed to generate plasmids encoding S100A8(C42S)(I60S), S100A8(C42S)(E57A)(I73R),

S100A8(C42S)(E57K)(I73R), and S100A9(C3S)(W88R). The template plasmids and primers are listed in Table 2.3. PCR amplification was carried out using PfuTurbo DNA polymerase. For the I60K and I60E variants, the PCR protocol was: 95 °C for 30 sec, 55 °C for 1 min, 68 °C for 15 min, (25 cycles), and 4 °C hold. After PCR amplification, the template DNA was digested by DpnI (New England Biolabs) by adding 1 μL of the restriction enzyme to a 25-μL PCR reaction at 0 h and 1.5 h with incubation at 37 °C. The digestion products were transformed into chemically competent *E. coli* TOP10 cells. Overnight cultures (5 mL, 50 μg/mL kanamycin) were grown from single colonies. The plasmids were isolated using a miniprep kit (Qiagen). The presence of the mutations and fidelity of the protein coding sequences were verified by DNA sequencing (Quintara Biosciences).

For the ΔHb and ΔHb(Q69A) variants, genes encoding S100A8(I60S)(I73S)(V80T)(I76S) and S100A8(I60S)(I73S)(V80T)(I76S)(Q69A), respectively, were employed. The DNA for these variants was ordered from DNA 2.0 with *NdeI* and *XhoI* restriction sites flanking the gene sequence. The gene was excised from the amplification plasmid using *NdeI* and *XhoI* enzymes, and then ligated into the *NdeI* and *XhoI* sites of pET41a vectors using T4 ligase. After expression, these S100A8 variants were paired with S100A9(C3S).

***E. coli* optimized nucleotide sequence for S100A8(ΔHb):**

```
CATATGCTGACCGAACTGGAGAAAGCTCTGAATAGCATCATTGACGTGTATCACAA
GTACAGCTTGATTAAGGGTAACTTCCACGCGGTCTACCGTGATGACCTGAAAAAGT
TGCTGGAAACGGAGAGCCCGCAGTATATCCGCAAGAAAGGCGCGGATGTGTGGTT
TAAAGAACTGGACAGCAATACCGATGGCGCCGTTAACTTTCAAGAGTTCCTGAGCC
TGGTTAGCAAGATGGGTACCGCAGCGCATAAGAAATCCCACGAAGAGTCTCATAA
AGAGTAACTCGAG
```

Translated sequence for S100A8(ΔHb):

```
MLTELEKALNSIIDVYHKYSLIKGNFHAVYRDDLKKLLETESPQYIRKKGADVWFKELD
SNTDGA VNFQEFSLVSKMGTA AHKKSHEESHKE
```


***E. coli* optimized nucleotide sequence for S100A8(Δ Hb)(Q69A):**

CATATGCTGACCGAGCTGGAGAAAGCGCTGAACAGCATCATTGACGTCTACCACA
AGTACAGCTTGATTAAGGGCAATTTCCACGCCGTGTATCGTGACGATTTGAAAAAG
CTGCTGGAAACCGAGAGCCCGCAGTATATCCGCAAGAAAGGTGCGGACGTTTGGT
TCAAAGAACTGGATTCCAATACGGATGGCGCGGTTAACTTTGCCGAGTTTCTGAGC
CTGGTGTCTAAGATGGGTACCGCAGCTCATAAGAAAAGCCATGAAGAGAGCCACA
AAGAGTAACTCGAG

Translated sequence for S100A8(Δ Hb)(Q69A):

MLTELEKALNSIIDVYHKYSLIKGNFHAVYRDDLKKLLETESPQYIRKKGADVWFKELDS
NTDGAVNFAEFLSLVSKMGTAAHKKSHEESHKE

Table A4.1. Primers employed for site-directed mutagenesis.

Primer	Sequence ^a
I60S-1	5'-GTTTAAGGAGTTGGAC <u>AGT</u> AACACGGATGGCGCTG-3'
I60S-2	5'-CAGCGCCATCCGTGTT <u>ACT</u> GTCCAACCTCTTAAAC-3'
E57A-1	5'-GACGTGTGGTTTAAG <u>GCG</u> TTGGACATTAACACG-3'
E57A-2	5'-CGTGTTAATGTCCAA <u>CGC</u> CTTAAACCACACGTC-3'
E57K-1	5'-GACGTGTGGTTTAAG <u>AAG</u> TTGGACATTAACACG-3'
E57K-2	5'-CGTGTTAATGTCCAA <u>CTT</u> CTTAAACCACACGTC-3'
W88R-1	5'-GGCCCGTCTGAC <u>GCG</u> GGCGAGCCACGAG-3'
W88R-2	5'-CTCGTGGCTCGCC <u>CGC</u> GTCAGACGGGCC-3'

^aThe codons containing mutations are underlined and colored red. The genes had been ligated into the *Nde*I and *Xho*I restriction sites of pET41a plasmids for over expression.

A4.3. Analytical Size-Exclusion Chromatography

An ÄKTA purifier (GE Lifesciences) housed in a 4 °C cold room and outfitted with a 100- μ L sample loop was used to perform all analytical size exclusion chromatography (SEC) experiments.¹ A Superdex 75 10/300 GL column (GE Lifesciences) equilibrated in running buffer was calibrated with a low-molecular-weight calibration mixture (GE

Lifesciences) as described previously.¹ The protein of interest was thawed at room temperature and buffer exchanged from the storage buffer into the running buffer using a filter (0.5-mL, 10-kDa MWCO, Amicon), and the protein concentration was adjusted to 30 μM , unless noted otherwise, by diluting with the running buffer. For the experiments with Ca(II), 600 μM CaCl_2 was included in the running buffer and protein sample. For experiments with Mn(II), 300 μM MnCl_2 was added to the sample only. For experiments with both Ca(II) and Mn(II), the running buffer and sample contained 600 μM CaCl_2 and 33 μM MnCl_2 was included in the sample only. Samples were incubated for 15 min at 4 $^\circ\text{C}$ after adding metals and then centrifuged at 13 000 rpm for 10 min. The entire volume of each sample (30 μM protein, 300 μL) was loaded onto the 100- μL sample loop. The loop was emptied with 0.5 mL of running buffer, and the protein was eluted over one column volume at a flow rate of 0.5 mL/min at 4 $^\circ\text{C}$.

A4.4. Results

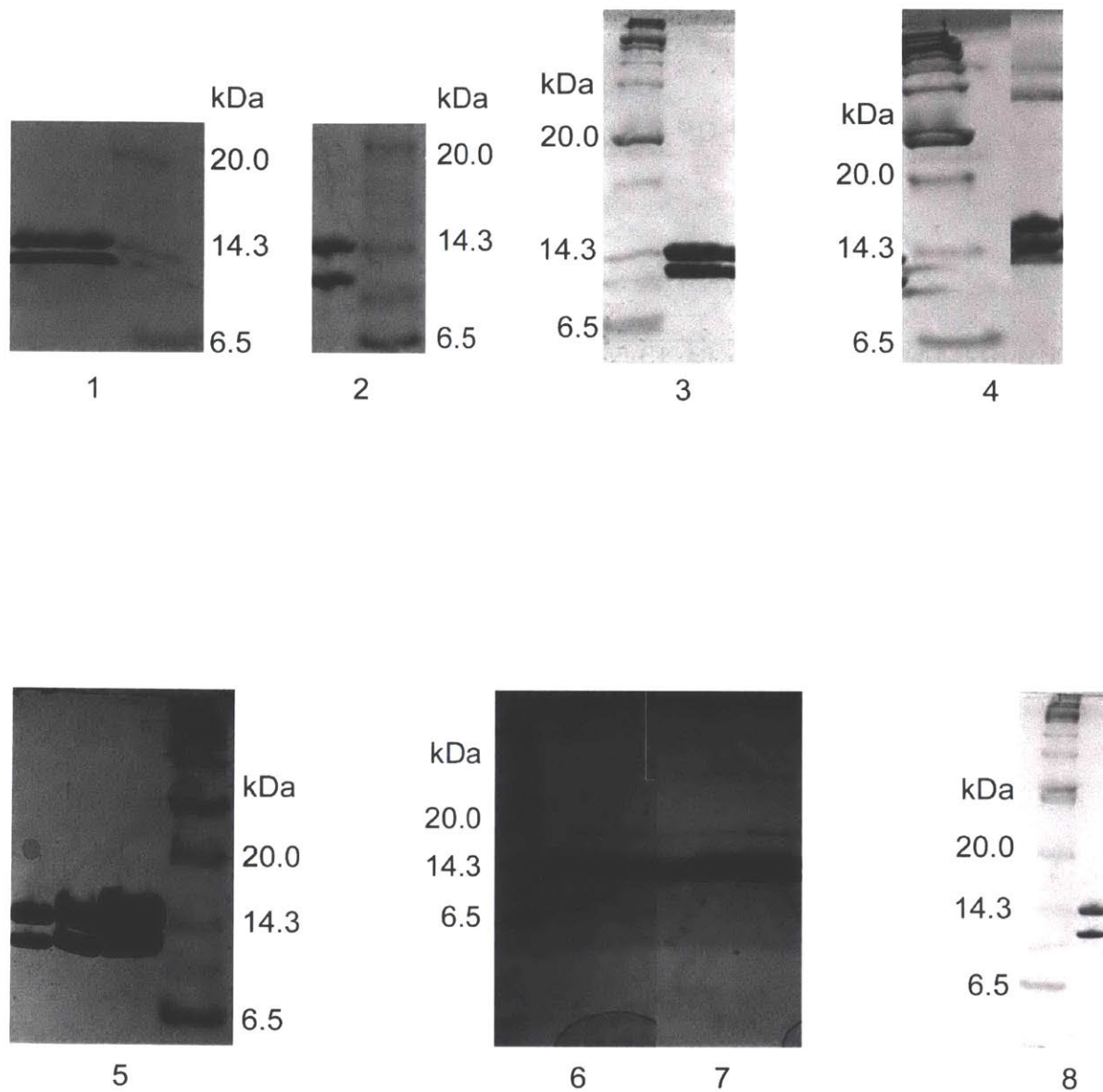


Figure A4.1. SDS-PAGE analysis of proteins in this Appendix. (1) I73R, (2) I73S, (3) CP-Ser(Δ Hb), (4) CP-Ser(Δ Hb)(Q69A), (5) I60S, (6) CP-Ser(E57A)(I73R), (7) CP-Ser(E57K)(I73R), (8) CP-Ser(W88R).

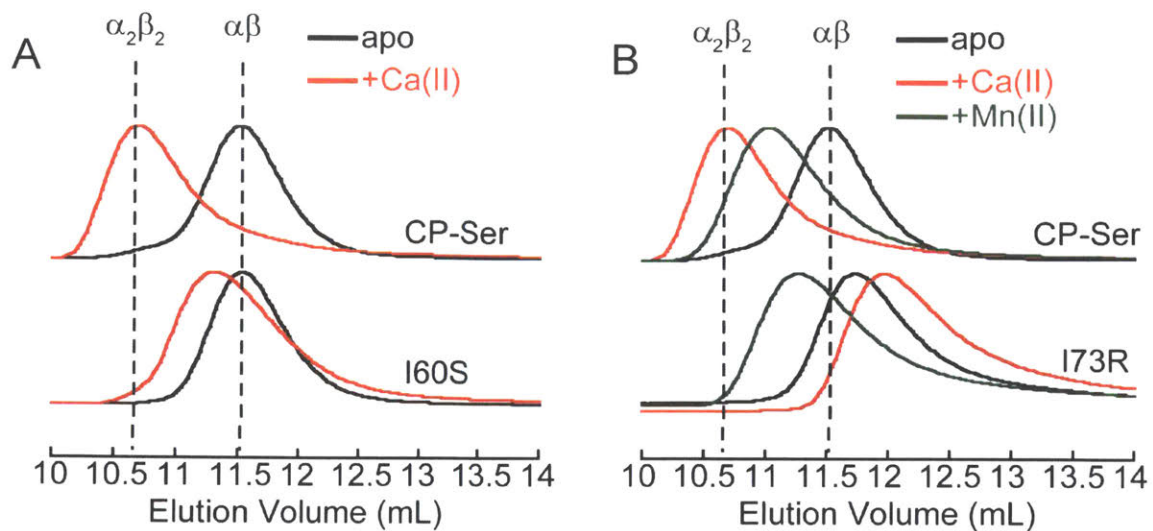


Figure A4.2. Analytical SEC of CP-Ser(I60S) and CP-Ser(I73R). The mutations are in the S100A8 subunit. The dashed vertical lines represent the elution volumes of the dimer ($\alpha\beta$) and Ca(II)-tetramer ($\alpha_2\beta_2$). (A) Comparison of CP-Ser and CP-Ser(I60S) chromatograms. (B) Comparison of CP-Ser and CP-Ser(I73R) chromatograms. Conditions: 75 mM HEPES, 100 mM NaCl, pH 7.5, 4 °C, 30 μ M CP, \pm 600 μ M CaCl₂, \pm 300 μ M MnCl₂.

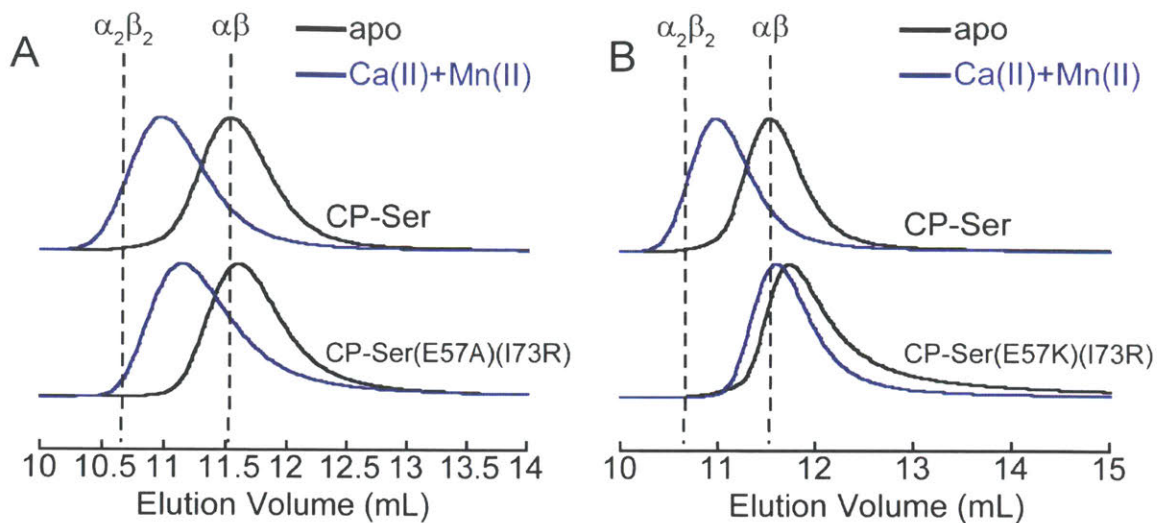


Figure A4.3. Analytical SEC of CP-Ser(E57A)(I73R) and CP-Ser(E57K)(I73R). The mutations are in the S100A8 subunit. The dashed vertical lines represent the elution volumes of the dimer ($\alpha\beta$) and Ca(II)-tetramer ($\alpha_2\beta_2$). (A) Comparison of CP-Ser and CP-Ser(E57A)(I73R) chromatograms. (B) Comparison of CP-Ser and I73R chromatograms. Conditions for CP-Ser: 75 mM HEPES, 100 mM NaCl, pH 7.5, 30 μ M CP, \pm 600 μ M CaCl₂, \pm 33 μ M MnCl₂. Conditions for CP-Ser(E57A)(I73R) and CP-Ser(E57K)(I73R): 75 mM HEPES, 100 mM NaCl, pH 7.5, 4 °C, 100 μ M CP, \pm 2 mM CaCl₂, \pm 110 μ M MnCl₂. Note: The variants with mutation of (A8)E57 did not give a reliable signal when the experiment was performed with 30 μ M protein.

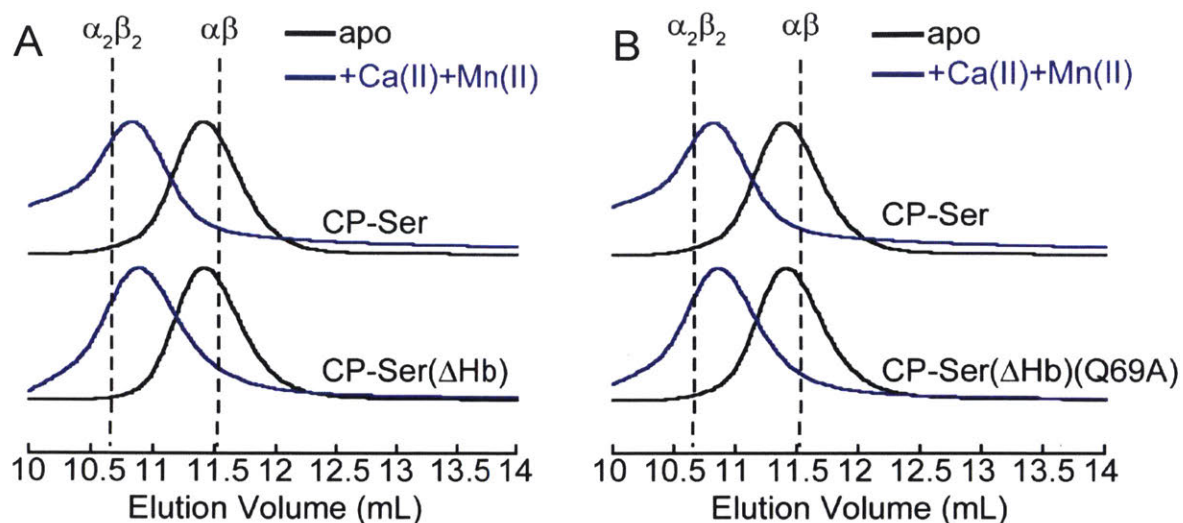


Figure A4.4. Analytical SEC of CP-Ser(Δ Hb) and CP-Ser(Δ Hb)(Q69A). The Δ Hb notation represents the following mutations of S100A8: (I60S)(I73S)(V80T)(I76S). The Q69A mutation is also on S100A8. The dashed vertical lines represent the elution volumes of the dimer ($\alpha\beta$) and Ca(II)-tetramer ($\alpha_2\beta_2$). (A) Comparison of CP-Ser and CP-Ser(Δ Hb) chromatograms. (B) Comparison of CP-Ser and CP-Ser(Δ Hb)(Q69A) chromatograms. Conditions: 75 mM HEPES, 100 mM NaCl, pH 7.5, 4 °C, 30 μ M CP, \pm 600 μ M CaCl₂, \pm 33 μ M MnCl₂.

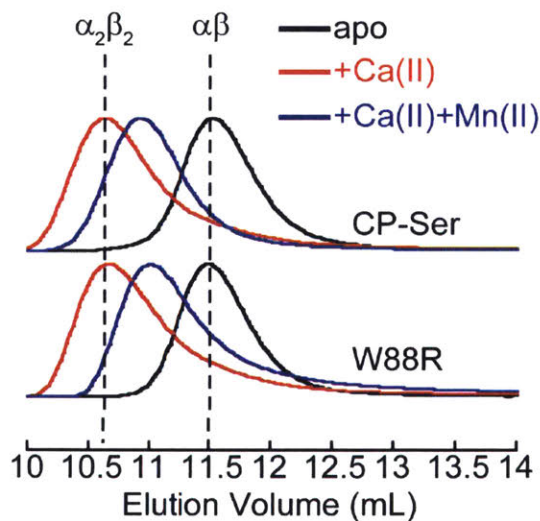


Figure A4.5. Analytical SEC of CP-Ser(W88R) compared to CP-Ser. The mutation is in the S100A9 subunit. The dashed vertical lines represent the elution volumes of the dimer ($\alpha\beta$) and Ca(II)-tetramer ($\alpha_2\beta_2$). Conditions: 75 mM HEPES, 100 mM NaCl, pH 7.5, 4 °C, 30 μ M CP, \pm 600 μ M CaCl₂, \pm 33 μ M MnCl₂.

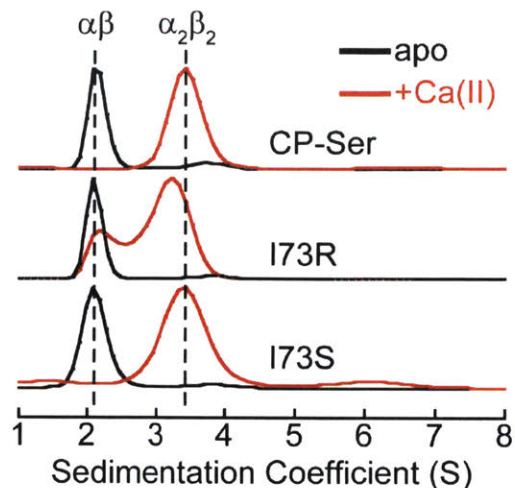


Figure A4.6. Sedimentation velocity AUC analysis of CP-Ser, I73R, and I73S. The mutations were in the S100A8 subunit. The data were fit with SEDFIT. The dashed vertical lines represent the sedimentation coefficients of the dimer ($\alpha\beta$) and Ca(II)-tetramer ($\alpha_2\beta_2$). Conditions: 75 mM HEPES, 100 mM NaCl, pH 7.5, 27 μ M CP, \pm 30 μ M EDTA, \pm 540 μ M CaCl₂, 20 °C, 42000 rpm. More complete experimental details can be found in section 2.2.6. The theoretical S-values ($s_{20,w}$) are 2.1 S and 3.7 S for the dimer and tetramer, respectively.

A4.5. References

1. Brophy, M. B.; Hayden, J. A.; Nolan, E. M., Calcium ion gradients modulate the zinc affinity and antibacterial activity of human calprotectin. *J. Am. Chem. Soc.* **2012**, *134* (43), 18089-18100.

Biographical Note

Jules Stephan was born to Drs. Rabie and Eugena Stephan in Buffalo, New York. He attended high school at The Nichols School where he graduated as a member of the National Cum Laude Society. He attended The University of Chicago for his undergraduate education where he earned B. S. degrees in Biological Chemistry with honors and Chemistry. He trained under Professor Stephen B. H. Kent where he participated in research on anti-freeze proteins, ice-nucleation peptides, and methods to use triflic acid for deprotection after Boc-solid-phase-peptide synthesis. Jules was named an Institute of Biophysical Dynamics fellow for his research in the Kent laboratory. After graduation, he pursued a Ph.D. at Massachusetts Institute of Technology where he worked in the laboratory of Professor Elizabeth M. Nolan. During graduate school, he studied the interplay between oligomerization, Ca(II) binding, and the biological fate of a human innate immune protein named calprotectin.

Jules R. Stephan

Education

Ph.D. Biological Chemistry
2013-2018

Massachusetts Institute of Technology
Advisor: Professor Elizabeth M. Nolan

B.S. Biological Chemistry
B.S. Chemistry
2009-2013

The University of Chicago
Advisor: Professor Stephen B. H. Kent

Publications

Nakashige, T. G.; Stephan, J. R.; Cunden, L. S.; Brophy, M. B.; Wommack, A. J.; Keegan, B. C.; Shearer, J. M.; Nolan, E. M., The hexahistidine motif of host-defense protein human calprotectin contributes to zinc withholding and its functional versatility. *J. Am. Chem. Soc.* **2016**, *138* (37), 12243-12251.

Stephan, J. R.; Nolan, E. M., Calcium-induced tetramerization and zinc chelation shield human calprotectin from degradation by host and bacterial extracellular proteases. *Chem. Sci.* **2016**, *7* (3), 1962-1975.

Gates, Z. P.; Stephan, J. R.; Lee, D. J.; Kent, S. B. H., Rapid formal hydrolysis of peptide- α thioesters. *Chem. Commun.* **2013**, *49* (8), 786-788.